

KfK 3228  
November 1981

**Proceedings of the Workshop  
on High Intensity Accelerators  
and Compressor Rings**

**Karlsruhe, Federal Republic of Germany  
June 25-26, 1981**

**Editor: M. Kuntze  
Institut für Kernphysik**

**Kernforschungszentrum Karlsruhe**



Kernforschungszentrum Karlsruhe

Institut für Kernphysik

KfK 3228

Proceedings of  
the workshop on high intensity accelerators  
and compressor rings

Karlsruhe, Federal Republic of Germany

June 25 - 26, 1981

Editor: M. Kuntze

Kernforschungszentrum Karlsruhe GmbH, Karlsruhe

Als Manuskript vervielfältigt  
Für diesen Bericht behalten wir uns alle Rechte vor

Kernforschungszentrum Karlsruhe GmbH  
ISSN 0303-4003

## P r e f a c e

The International Collaboration on Advanced Neutron Sources ICANS held its V. Meeting in Germany on June 25 - 26, 1981.

The meeting was sponsored by the KFA and KfK laboratories and was subdivided into a plenary session and a target workshop held at Jülich \* and the accelerator workshop located at KfK, Karlsruhe.

These proceedings are a compilation of the written contributions to the workshop on "High Intensity Accelerators and Compressor Rings".

The major part of the papers documented consists of status reports and discussions of technical problems contributed from the ICANS laboratories.

Two invited papers are contained in these proceedings. B. Macek reviewed the experience of intense beam operation (p. 123) and D. Keefe developed the prospects of induction linear accelerators as future spallation neutron sources (p. 63). Aside from the sessions, a poster show demonstrated experimental results and design activities in more detail as could be summarized in the talks.

The discussions of this workshop were of particular help for the preparation of a following expert meeting, which was held to review the SNQ project study on June 29, at Heidelberg.

The assistance of all who participated in the workshop and who contributed to these proceedings is appreciated. We would like to thank M. Kuntze and the KfK staff for the organization of the meeting and for their work of preparing these proceedings for publication.

A. Citron

K. Reich

J.E. Vetter

Organizing Committee

---

\* Jül-Conf-45 (1981)

## Institutions represented

1. ANL, Argonne, USA
2. BNL, Brookhaven, USA
3. CERN, Geneva, Switzerland
4. CRNL, Chalk River, Canada
5. GSI, Darmstadt
6. KEK, Japan
7. KFA, Jülich
8. LANL, Los Alamos, USA
9. LBL, Berkeley, USA
10. MPI, Heidelberg
11. NEN, Billerica, USA
12. Rutherford-Appleton-Laboratories, Chilton, Didcot, England
13. SIN, Villigen, Switzerland
14. University of Eindhoven, The Netherlands
15. University of Dorchester, UK
16. University of Maryland, USA
17. TU München
18. Bruker Physik, Karlsruhe (manufacturer of magnets)
19. Herfurth, Hamburg (manufacturer of rf equipment)
20. KfK, Karlsruhe

<u>Content</u>		page
1. Improvements in the Rapid Cycling Synchrotron	C.W. Potts (ANL, Argonne)	3
2. Status of the Los Alamos Proton Storage Ring	R.K. Cooper and G. Spalek (LANL, Los Alamos)	13
3. SNQ Compressor Ring IKOR: Isochronous Operation, Why and How?	K.H. Reich (CERN, Genf)	33
4. SNQ Linear Accelerator Beam Dynamics	K. Mittag (KfK, Karlsruhe)	45
5. Injection System for the Proton Storage Ring at LASL	D.W. Hudgings and A.J. Jason (LANL, Los Alamos)	57
6. Proton Induction Linacs as High-Intensity Neutron Sources	D. Keefe and E. Hoyer (LBL, Berkeley)	63
7. Foils for Negative Ion Charge-Exchange Injection	C.W. Planner (Rutherford- Appleton-Laboratories)	75
8. Rapid Beam Switching Techniques	G. Schaffer (KfK, Karlsruhe)	79
9. Rf Power System for SNQ	G. Hochschild (KfK, Karlsruhe)	101
10. New Methods of Rf-Control for the SNQ	D. Schulze (KfK, Karlsruhe)	111
11. Operating Experience with the Meson Factory	R.J. Macek (LANL, Los Alamos)	123
12. Status of the New England Nuclear 45 MeV Proton Linac	W.E. Jule (NEN, Billerica)	143

		page
13.	Accelerator Development Work at CRNL	B.G. Chidley (CRNL, Chalk River) 149
14.	Radiation Problems Expected for the German Spallation Neutron Source	K. Goebel (CERN, Genf) 159
15.	Remote Handling Systems	G.W. Köhler (KfK, Karlsruhe) 197
16.	Appendix: Papers from the poster session	
	Self field effects on the beam in storage rings	K. Mika, L. Stanco, V.G. Vaccaro, G. Wüstefeld (KfA, Jülich ) 229
	Present status of the Rutherford H <sup>-</sup> -ion source	P.E. Gear, R. Sidlow (Rutherford-Appleton-Laboratories) 235
	The control of $\gamma_{tr}$ by sextupole magnets in IKOR	C.J.A. Corsten (Univ. Eindhoven) 245
17.	Workshop summary	A. Citron (KfK, Karlsruhe) 251
18.	List of participants	253

Improvements in the Rapid Cycling Synchrotron\*

Charles W. Potts  
Argonne National Laboratory  
Argonne, Illinois 60439 USA

Abstract

The Rapid Cycling Synchrotron<sup>1</sup> (RCS), originally designed as an injection energy booster for the Zero Gradient Synchrotron (ZGS), operated under constraints imposed by ZGS operation until December 1979. Once these restraints were removed, the RCS made rapid strides toward its near-term goals of 8  $\mu$ A of protons for Argonne National Laboratory's (ANL) Intense Pulsed Neutron Source (IPNS) program. Reliable 30 Hz operation was achieved in the spring of 1980 with beams as high as  $2 \times 10^{12}$  protons per pulse and weekly average intensities of over 6  $\mu$ A on target. These gains resulted from better injection matching, more efficient RF turn-on and dynamic chromaticity control. A high intensity small diameter synchrotron, such as the RCS, has special problems with loss control which dictate prudence during intensity improvement activities. Additional improvements were made to the machine starting in August of 1980 while the extraction magnets were relocated for operation with the IPNS-I target. These improvements have now been completed. Startup of the accelerator is now underway, and it is clear that these modifications have resulted in a radioactively cleaner operation. It is too early to evaluate the effects of the improvements on intensity and reliability, but a single pulse extracted intensity of  $2.4 \times 10^{12}$  protons has been achieved, a 20% increase. The studies and equipment leading to the intensity gains are discussed.

---

\*Work supported by the U.S. Department of Energy.

## Introduction

Figure 1 shows the configuration of the IPNS-I spallation neutron facility.<sup>2</sup> It will come into operation in July of 1981 as a national user-oriented facility intended to be used for neutron scattering studies 75% of the time and radiation effect studies 25% of the time. A high energy physics test beam is also provided. In this facility, a fast burst (90 ns) of 500 MeV protons from the RCS is slammed into a uranium target 30 times per second. Resulting spallation and fission neutrons travel down 12 neutron beam lines to users' instruments. A prototype target (ZING-P'), Fig. 1, was the recipient of the protons in 1979 and 1980. The neutrons from ZING-P' were used for target yield studies, moderator material and arrangement studies as well as neutron science. Some 55 publishable neutron scattering measurements were made after the RCS came into a production mode in the summer of 1980.

The trials of turning-on and improving a new machine with scientific users waiting with high expectations is old hat to most of the readers. Normally, however, the users have some previous accelerator user experience and are, therefore, somewhat tolerant of the foibles of synchrotrons. In the case of the RCS, however, the users are reactor oriented and become somewhat irate when the published intensity, energy, and reliability are not available within a few months after startup. Fortunately, the accelerator made dramatic progress in intensity and reliability during the summer 1980 run and the needed rapport was developed between users and operators, and a viable scientific program seems to be on the horizon.

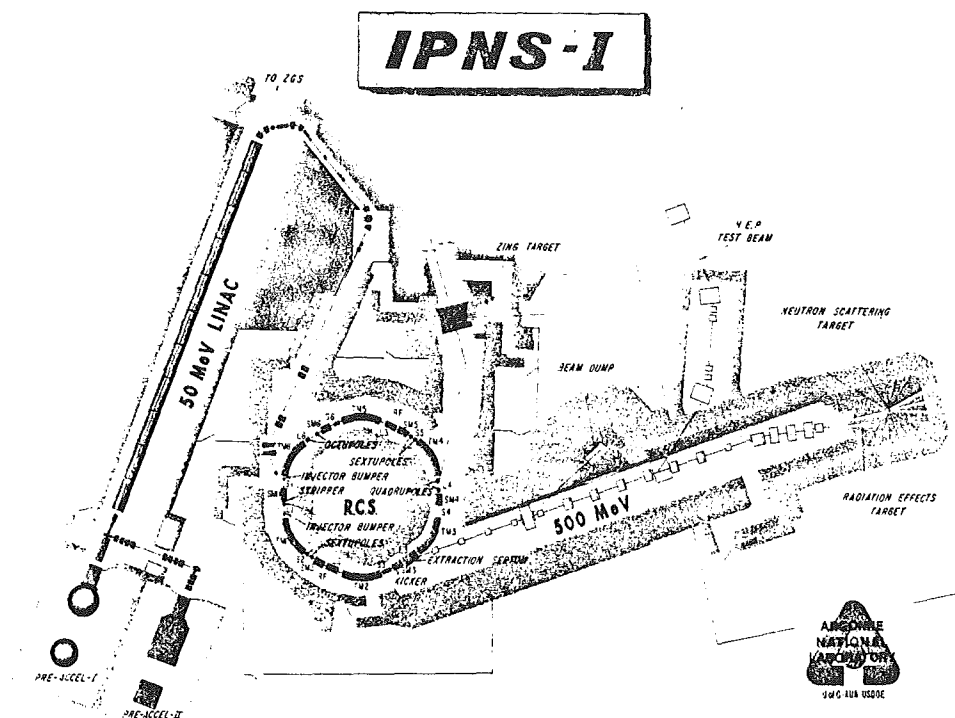


Fig. 1. IPNS-I Accelerator System

The goals of the RCS have long been to deliver 20  $\mu\text{A}$  of 500 MeV protons to a target with 90% operating reliability. Numerous review panels have not seriously questioned the ability of the RCS to meet the 20  $\mu\text{A}$  goal. Neutron science reviews have, however, questioned whether the national neutron science budget can support a dedicated facility like IPNS-I. This is a complicated, many-faceted question which may take quite awhile to answer. Lower goals are compatible with a lower budget and the goals have now been changed to 8 to 10  $\mu\text{A}$ . As Table I indicates, the RCS has made tremendous progress since 1978 and the new lower goals will be achieved in 1981.

Table I

	<u>1978</u>	<u>1979</u>	<u>1980</u>
Scheduled Operating Time	2681 hours	3976 hours	2569.2 hours
Actual Operating Time	1796 hours	2928 hours	2187.8 hours
Operating Efficiency	67%	73.6%	85.2%
Total Protons on Target	$0.294 \times 10^{20}$	$1.06 \times 10^{20}$	$2.25 \times 10^{20}$
Total Pulses on Target	$0.43 \times 10^8$	$1.13 \times 10^8$	$1.98 \times 10^8$
Average Beam Current	0.73 $\mu\text{A}$	1.61 $\mu\text{A}$	4.72 $\mu\text{A}$

The remainder of this paper will present, in chronological order, what improvements were made to achieve these results. It is of great importance to realize that in some of 1979 and most of 1980, the beam intensity was limited somewhat by fears concerning heating and thermal cycling of the prototype uranium target. One certainly must not be fooled into thinking that the target was the only limit. The operators of a small radius fast-cycling synchrotron, without extensively prepared remote handling apparatus, must always consider beam loss control as a prime goal if the synchrotron is to be kept repairable. The gentle positive slope of the beam current vs. time in Fig. 2 was planned as accelerator problems and uranium target worries were slowly worked out in unison. Some of the peak numbers such as 10  $\mu\text{A}$  and  $2.4 \times 10^{12}$  protons per pulse were short-term accomplishments that could not be sustained over long periods because of beam losses, but they do provide input as to the synchrotron's overall capability.

#### Operation in 1979

The RCS time-shared the 50 MeV linac with the ZGS, usually in a mode of 3 seconds RCS to 1 second ZGS. Programmable bending and focussing magnets made the ZGS  $\text{H}^+$  polarized proton operation and the  $\text{H}^-$  operation of the linac compatible. The operating frequency of the RCS was limited to 15 Hz due to possible damage to the linac when operated at 30 Hz. No one expected major damage, but even two or three weeks of lost operation was considered vital to the high energy polarized beam which was shutting down permanently at ANL in October.

This was a very productive period for the RCS physicists. Approximately 20 hours per week were dedicated to machine studies. Many of the

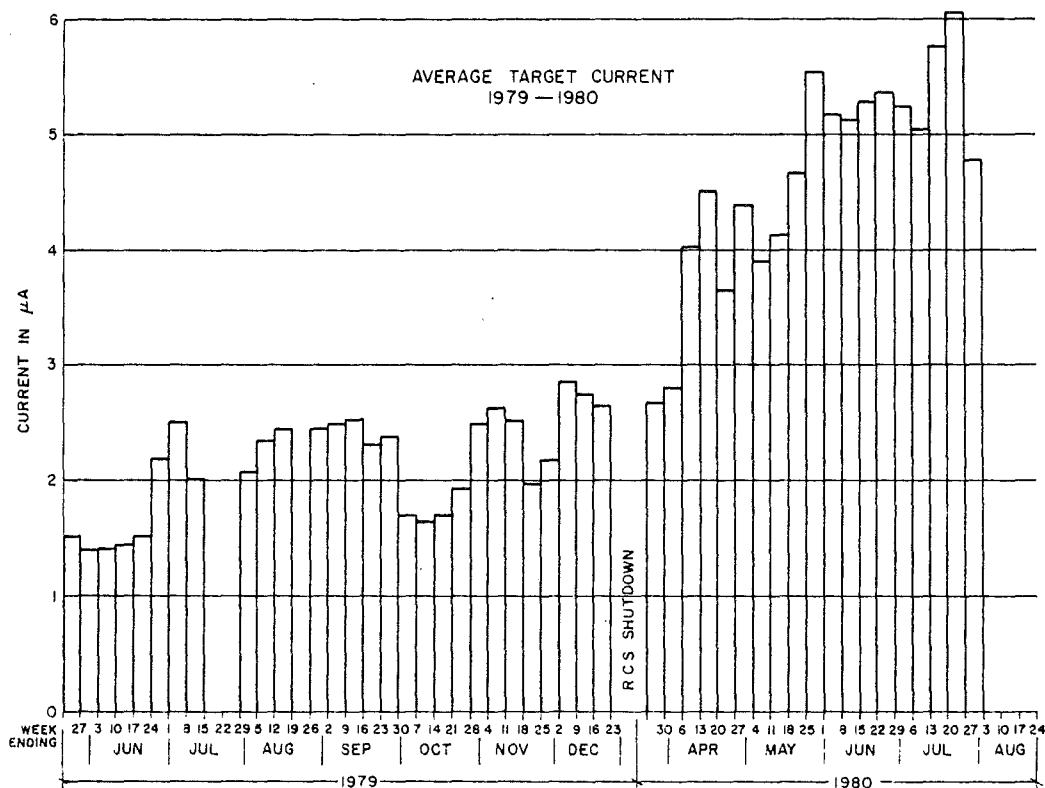


Fig. 2. Weekly Average Beam Current on Target

beam problems uncovered during this period are still being addressed although some were corrected in the spring of 1980 with gratifying results. Studies found that the 500 MeV beam was too large for efficient extraction due to "head-tail" instability.<sup>3</sup> Tune measurements disclosed dynamic reversal of the chromaticity at 350 MeV. Extraction was studied at 200 MeV, and it was noted that 100% of the accelerated beam could be extracted. The extraction kick was insufficient to kick out the wide 500 MeV beam created by the "head-tail" instability. The 500 MeV extraction efficiency was about 65%. A temporary compromise of 300 MeV operation was chosen to get fairly good neutron yield while still providing a radioactively clean extraction efficiency of over 90%.

High radiation levels were detected at the 50 MeV end of the linac. This resulted from gas stripped  $H^0$  and  $H^+$  particles. Appropriate shielding was added. Quantitative measurements were made later of  $H^0$  and  $H^+$  production as a function of linac tank pressure.<sup>4</sup> These measurements show that  $H^0$  and  $H^+$  production is proportional to residual gas pressure as expected.

This was a beneficial time for the users also as neutron yield measurements were made in tungsten, tantalum, and uranium targets. The results agreed fairly well with computer predictions, and uranium was chosen as the target material in the IPNS-I monolith for neutron scattering and radiation damage work. Tantalum backup targets were also built. A uranium target was then installed in the ZING-P monolith for operation

until August of 1980. While this target was only a few pounds of uranium, numerous safety reviews, ad hoc committees, and some 30 target interlocks gave the accelerator operators some new concerns.

One of the more ambitious accomplishments was phase locking the accelerator to a crystal controlled neutron chopper.<sup>5</sup> From the accelerator standpoint this is like the "tail wagging the dog," but it works! Extensive modifications were made in the controls and capacitor bank of the ring magnet power supply of the synchrotron to automatically keep the parallel tuned portion of the system in resonance as the chopper clock forced the system slightly off the power main's frequency. This kept the magnet field stable as it drifted in respect to the power line frequency. An added modification allowed the chopper to control the extraction time of the beam as early as 100  $\mu$ s before the peak energy and as late as 100  $\mu$ s after. If the chopper did not call for extraction by the later time, the beam was extracted for the benefit of the other users while the chopper missed that particular pulse. It was found that the chopper and machine were synched within this 200  $\mu$ s window over 95% of the time. The size of the 200  $\mu$ s window was chosen experimentally by studying extraction and transport losses for off-nominal energy extraction.

. Reliability during this period was not good. The pulsed septum magnet was the real Achilles' heel. It was a 30-inch long conventional 4-turn thin septum magnet. Several different versions of this magnet failed with the best lasting  $10^8$  pulses. Failure required a lengthy cool-down before repair. The extraction kicker magnet system provided more than its share of failures through high voltage cable breakdowns which often destroyed low level electronics as well.

Once the ZGS was shut down in October of 1979 restrictions on linac operating frequency were lifted, but insufficient data existed to begin 30 Hz operation at once. The ZGS authorities graciously allowed use of half the ZGS main ring magnet system and its beam diagnostics as a spectrometer for analysis of behavior in the linac beam running at 30 Hz. At the same time the linac tank was instrumented for temperature measurements at various points. When the linac was run at 30 Hz with RF on for long enough to accommodate 120  $\mu$ s beam pulses, some hot spots were noted on un-cooled tuning balls. These had grown leaky over the years and the water was shut off, which was acceptable during low power operation. A very clever design provided cooling for these leaky units, but construction and installation of these cooling adapters took over two months. Thirty-hertz operation was tried again in mid-December, but because of kicker magnet power supply problems it was not successful, although short-term currents of 5  $\mu$ A were achieved.

#### 1980 Modification and Operation

From January until the third week of March the machine was off for improvement. The most extensive was the installation of a new transformer septum magnet<sup>6</sup> that provided one-half the bend of the old magnet. A more standard dc septum provided the remainder. In addition, two small vertical and one small horizontal trimming magnets were designed and built to better

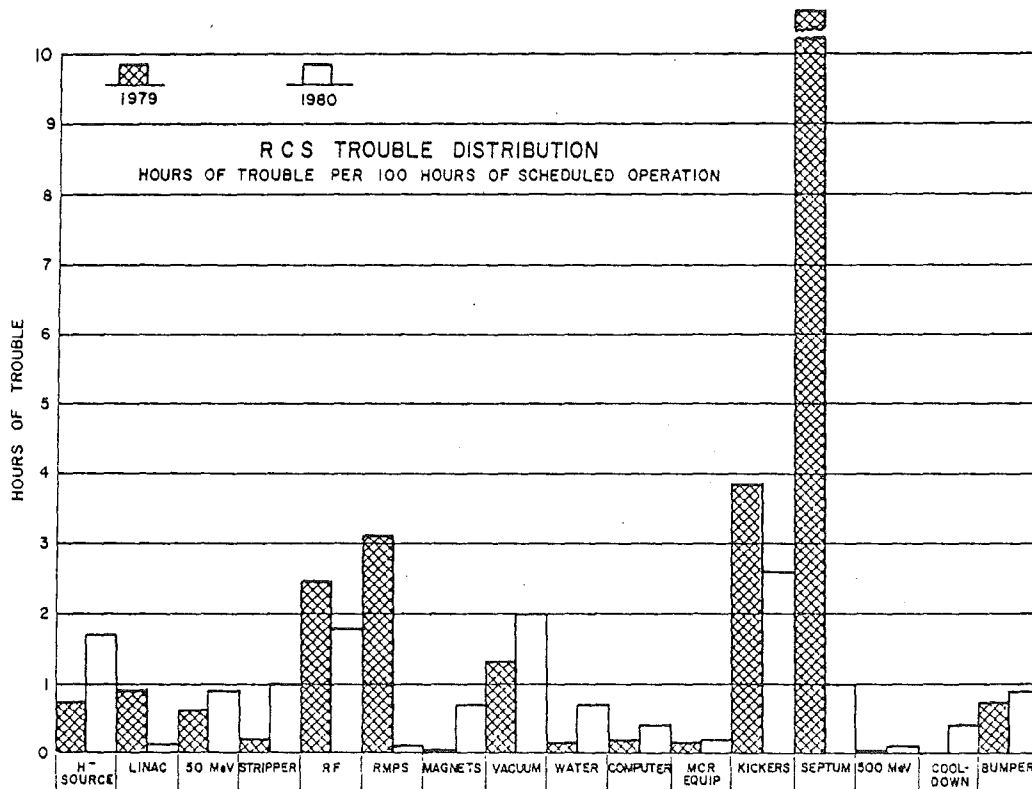


Fig. 3. Comparison of RCS Trouble Distribution for 1979 and 1980

match the machine to the target transport line. Significant improvements were made in protecting the low level electronics in the kicker magnet power supplies, and cable termination problems were solved. These two efforts made great improvements in the operating reliability of these systems, as can be seen from comparing the 1979 and 1980 system reliability data in Fig. 3. Several other modifications were added to improve beam output and beam handling efficiency. Programmable linear amplifier power supplies were provided for dynamic chromaticity adjustment. Pre-amplifier improvements were made in the RF system to improve dynamic range and automatic gain control (AGC) response. Ninety percent of the complicated 50 MeV transport line from the linac to synchrotron was wire orbited, and the beam diagnostics were realigned for better injection matching. A 750 keV proton beam chopper was constructed to give the machine synchronous injection capability. One look at Fig. 2 from April through July 1980 should convince the reader that these modifications were, on the whole, quite successful. It was during this running period that 30 Hz operation became routine. The reader should bear in mind that this running was carried out with the ratio of beam on target to 50 MeV beam delivered to the synchrotron at 70% or better.

Machine physics studies continued during this running period, more problems noted, some corrections made and some longer range plans formulated. A disturbing coupling between proton beam noise and the ring magnet power supply was discovered and partially corrected. This was particularly troublesome when the accelerator was running in synchronism

with a neutron beam chopper. Two-turn extraction, 500 MeV acceleration, and the effects of space charge distribution were among the more common topics. The most troublesome aspect of beam acceleration was, and remains, an instability which occurs at intensities of over  $1.5 \times 10^{12}$  protons per pulse for about the last 6 ms of the acceleration cycle. It seems to be longitudinal in nature since there is a great deal of bucket size modulation. A "head-tail" instability has been noted at this time in the acceleration cycle. This instability causes about 3% amplitude modulation in the RF amplitude envelope. Several theories have been considered concerning this instability: (1) Oscillation in the AGC loops of the RF system; (2) Oscillations in the loop that phase locks the two RF cavities together; (3) Coupling between the dc position feedback loop and the band-pass beam phase compensation loop; (4) A microwave instability generated by beam coupling to the eddy current shields in the accelerator; (5) A microwave instability caused by the lack of symmetry in the straight sections. This instability has been controlled during 300 MeV operation with extracted beams up to  $2.4 \times 10^{12}$  protons by very judicious injection and careful chromaticity adjustment, but it cannot be said to be operational at 30 Hz at these intensities due to extensive beam losses.

#### Conversion for Operation into IPNS-I Target Monolith

The accelerator was shut down August 4, 1980, to begin the attachment of a new proton transport system (PTS) to carry the beam to the IPNS-I target monolith. From the accelerator standpoint, additional work was required as may be seen in Fig. 4. The extraction straight section containing the septum magnets has been moved from the L-4 to L-3 straight section; a set of quadrupoles was moved from the L-3 to L-4 straight section; a longer fast kicker magnet has been installed in the S-3 straight section; extensive shielding additions totaling 450 tons of concrete have been added over the extraction straight section.

Several system modifications and additions were completed during the time of IPNS-I conversion. These items should improve beam handling, beam intensity and operating reliability. The most ambitious of these has been complete reconstruction of the fast kicker extraction system. A new magnet and power supply<sup>7</sup> have been designed and constructed to provide efficient 500 MeV extraction. Four separate thyatron switching power supplies each drive 1/4 turn of a 75 cm long ferrite magnet. Each 1/4 turn is terminated in  $7 \Omega$  and the system is operated at 62 kV. The peak switched power is over 0.5 gigawatts. The four supplies must fire within 2 ns of each other. So far, the system works quite well. Measurements with the proton beam indicate the kick angles are as predicted.

Octupole magnets<sup>8</sup> driven by programmable 30 kW linear transistor amplifiers have been added to the synchrotron. Betatron tune measurements indicate that these magnets perform as predicted; however, they have not as yet shown the ability to control beam instabilities. Less than four hours of machine time has been spent in applying them to instability correction studies, so prospects for their success are still bright. The injection bumper power supply was modified extensively to up its duty

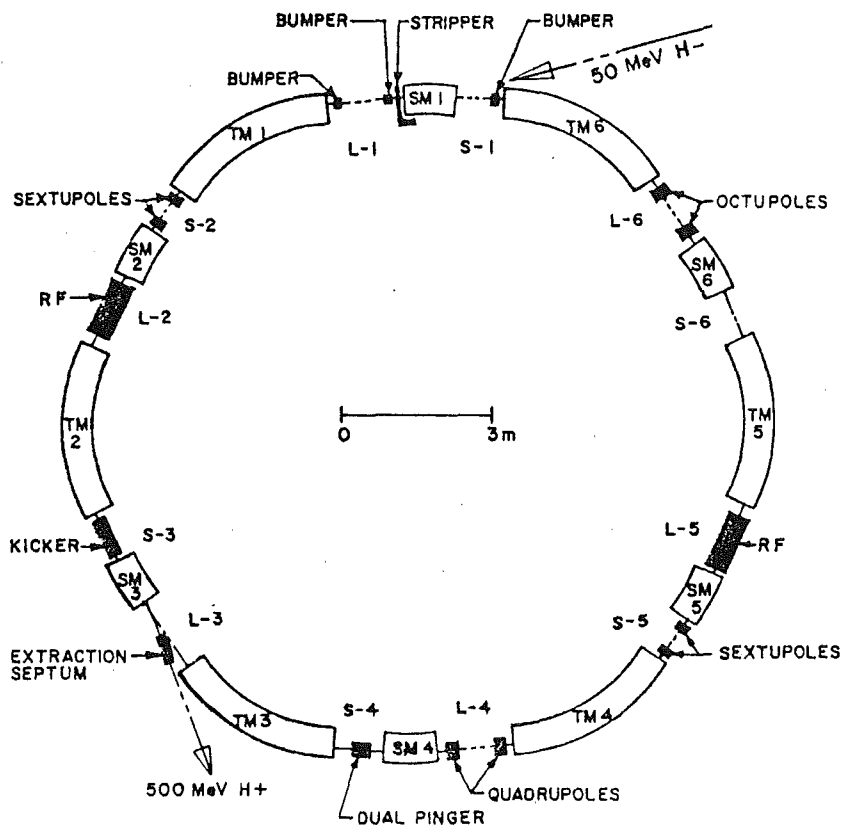


Fig. 4. RCS Component Arrangement

cycle by 50%, provide faster injection slewing and greater waveform flexibility, as well as improved accessibility for repair.

Linear transistor amplifiers control the dynamic impedance of the RF cavities by magnetically modulating the inductance as the RF frequency sweeps from 2 to 5 MHz during the beam acceleration cycle. These amplifiers are part of the cavity bias system (CBS). New CBS amplifiers have been constructed and installed which increase the corner frequency of this system from 800 Hz to 10 kHz. It is hoped that better cavity impedance control will improve many aspects of the dynamic RF performance, in particular, better cavity-to-cavity tracking and better AGC control, since both the phase and magnitude of the load impedance seen by the amplifier are more constant. The synchrotron oscillation frequency of the beam varies from 4 to 7 kHz during the machine cycle. The potential problem of having the CBS response span this frequency was recognized. In fact, studies have shown that beam losses do increase when CBS response corners above 3 kHz, so the response is limited there.

Extensive changes have been completed on the RCS computer control system with an Eclipse AP-130 replacing a NOVA 210. The greatly augmented capacity is used to interact with machine studies,<sup>9</sup> provide more flexible parameter monitoring and readout to control and monitor the new proton transport line to the IPNS-I target. It also monitors all the parameters required for cooling and radioactivity control of both the neutron

scattering and radiation effect targets and is part of the protective shutdown system.

The accelerator physics team remeasured both the injection and extraction orbits during the IPNS-I installation shutdown. They recommended changes in nominal injection angle and extraction apertures. These changes were carried out with what seems, at this time, to be excellent results. Beam output to input ratios have improved from 70% to 85%. Radiation outside shielded areas has decreased by factors of at least 5 and in some places by a factor as high as 20. Of course, shielding improvements and improved extraction kick have also helped.

#### Linac and Ion Source

One does not expect that a 1 Hz linac and a 1 Hz  $H^-$  ion source will easily operate at 30 Hz, but they have performed surprisingly well. The linac, with the beam pulse width restricted to 70  $\mu s$  or less, has performed flawlessly thus far. Modifications in tank water flow, tuning ball cooling and oscillator cavity cooling have been necessary. The ion source, with similar power restrictions, has done well with grid life being the limiting factor. With pulse widths under 60  $\mu s$ , grids last about six weeks.

The previously mentioned fiscal problem has brought a two-year program of ion source development to a halt. A Penning discharge type  $H^-$  ion source was beginning to show promise.<sup>10</sup> This work has completely stopped. Linac operating personnel are working to adapt a 15 Hz magnetron type source to 30 Hz operation. This will be a very modestly financed program and does not have a high probability of success for that reason. A new or improved ion source is generally regarded as one of the easiest ways to improve RCS beam intensity.

#### Foil Life

The stripping foils used in the RCS are made of poly-paraxylene.<sup>11</sup> They are 3000 to 4500  $\text{\AA}$  ( $60 \mu g/cm^2$ ) thick with a 400  $\text{\AA}$  coating of aluminum deposited on them. Considerable work has been done on nonstressed mounting of these foils with satisfying results, but the aluminum coating has been the most effective factor in extending their life to millions of beam pulses. The aluminum coating allows a bleed-off of charge and also allows for an even distribution of charge. Noncoated foils tend to contract when protons pass through them.

The injected current on the RCS is typically 5 mA for 60  $\mu s$ . The way this beam is injected determines the number of passes the recirculating beam makes through a foil. This obviously has a significant, but unquantified, effect on foil life. The RCS has a remotely controlled foil changer, which can hold 50 foils in its magazine. For reasons that are unclear, a new foil survives best if it is "conditioned" for an hour or so at 5 Hz before applying beam at 30 Hz. Foils usually last about 10 million pulses.

### Conclusions

Great strides have been made since the 1978 commissioning. Weekly average beam currents have gone from less than 1  $\mu\text{A}$  to over 6  $\mu\text{A}$ , weeks with over 15 million extracted pulses have been recorded and reliability has jumped from 67% to 85%. Peak intensities of  $2.4 \times 10^{12}$  protons per pulse and a 24-hour average of 7.6  $\mu\text{A}$  has been attained. Much remains to be done. Five-hundred MeV operation must be reliably demonstrated. Firm control of beam losses must be maintained and stable financing would help.

### Acknowledgments

In a survey paper of this type the work of many must be acknowledged. To acknowledge some would slight others. Thanks to everybody who helped. You know who you are.

### References

1. Rauchas, A. V., Brumwell, F. R., and Volk, G. J., "Commissioning of the Argonne Intense Pulsed Neutron Source (IPNS-I) Accelerator," IEEE Trans. Nucl. Sci., Vol. NS-26, No. 3, p. 3006 (June 1979).
2. Carpenter, J. M., Blewitt, T. H., Price, D. L., and Werner, S. A., "Pulsed Spallation Neutron Sources," Physics Today, Vol. 32, No. 12, p. 42 (December 1979).
3. Cho, Y. and Rauchas, A. V., "Observations and Cure of Head-Tail Effect in the Argonne Rapid Cycling Synchrotron," IEEE Trans. Nucl. Sci., Vol. NS-28, No. 3, p. 2585 (June 1981).
4. Cho, Y., Madsen, J., Shin, S.-A., and Stipp, V., "Measurements of  $\text{H}^0$  and  $\text{H}^+$  Ion Yields During  $\text{H}^-$  Acceleration in a 50-MeV Linac," IEEE Trans. Nucl. Sci., Vol. NS-28, No. 3, p. 2888 (June 1981).
5. Praeg, W., McGhee, D., and Volk, G., "Phase Lock of Rapid Cycling Synchrotron and Neutron Choppers," IEEE Trans. Nucl. Sci., Vol. NS-28, No. 3, p. 2171 (June 1981).
6. Foss, M., Thompson, K., and Praeg, W., "A Transformer Septum Magnet," IEEE Trans. Nucl. Sci., Vol. NS-26, No. 3, p. 4024 (June 1979).
7. Suddeth, D. E. and Volk, G. J., "The Rapid Cycling Synchrotron Extraction Kicker Magnet Drive System," IEEE Trans. Nucl. Sci., Vol. NS-28, No. 3, p. 3017 (June 1981).
8. Potts, C., Faber, M., Gunderson, G., Knott, M., and Voss, D., "Tune Control Improvements on the Rapid Cycling Synchrotron," IEEE Trans. Nucl. Sci., Vol. NS-28, No. 3, p. 3020 (June 1981).
9. Rauchas, A. V., Brumwell, F. R., Cho, Y., Czyz, W. S., Gunderson, G.R., Knott, M. J., Suddeth, D. E., and Volk, G. J., "Betatron Tune Measurement at the Argonne Rapid Cycling Synchrotron," IEEE Trans. Nucl. Sci., Vol. NS-28, No. 3, p. 2331 (June 1981).
10. Moffett, D. R. and Barner, R. L., "An Intense  $\text{H}^-$  Source for the IPNS-I Rapid Cycling Synchrotron," IEEE Trans. Nucl. Sci., Vol. NS-28, No. 3, p. 2678 (June 1981).
11. Poly-paraxylene film developed by Carbide Chemicals and Plastics, Research and Development Department, Bound Brook, New Jersey.

Status of the Los Alamos Proton Storage Ring\*

Richard K. Cooper and George Spalek

Accelerator Technology Division, Los Alamos National Laboratory

Los Alamos, New Mexico

Abstract

The Proton Storage Ring for the Weapons Neutron Research Facility of the Los Alamos National Laboratory is reviewed as a construction project. The current status of construction and design is outlined.

Introduction

The purpose of this paper is not to describe the design features of the Los Alamos Proton Storage Ring (Ref. 1), but to describe the present status of the Ring as a construction project. To that end we will start by describing the status of the design and construction of the buildings, followed by the status of procurement actions, and finally we will indicate the design status of various components of the Ring.

Building Construction

A 12,500 square foot (1160 square metre) staging building is presently under construction and is scheduled for completion by July 15, 1981. This building will provide room for component fabrication and testing, as well as magnet assembly and mapping. Areas have been allocated for such activities as vacuum, low-level electronics, fast-kicker development, and 600 MHz and 3 MHz rf research and development. There will also be a machine shop in the building.

The Architect-Engineer for the project, Randy Holt and Associates of Albuquerque, New Mexico, is currently making detailed construction drawings of the Ring tunnel and the equipment building. These drawings should be complete by October 1, so that construction bids will be requested about October 15. The bids should be received by December 1 and opened December 15, so that construction of the Ring tunnel should begin in early 1982.

The Ring tunnel will be 18.5 feet (5.6 metres) wide and 12 feet (3.7 metres) high. The equipment building, which will house the power

---

\*Work performed under the auspices of US Department of Energy.

supplies, rf sources, and general electronics, will be 90 feet square (27 metres square) and will be located above the Ring tunnel. The vertical separation from the roof of the tunnel to the floor of the equipment building will be 23.5 feet (7.2 metres) of earth and steel shielding.

### Equipment Procurements

In this section we will indicate what major items have been purchased or have been put out for bids. In general those items which have been completely specified and for which complete design drawings are in hand have either been purchased or bids requested; we are not holding back any orders.

A Digital Equipment Company VAX 11/750 has been purchased as the control computer; it should arrive by July 1, 1981. Approximately 60% of all the vacuum equipment has been purchased. This percentage includes all the vacuum pumps and their controllers, valves, ion gauges, and pumping tees. The five injection line quadrupole magnets have been purchased; the power supplies for these magnets are out for bid. The bids for the Ring dipole magnets are due to be received June 15; the copper conductor for the prototype magnet coil has been purchased. The power supply specifications for the Ring dipoles are being written at this time and shortly will go out for bid. The power triodes for the transverse damper distributed amplifiers are on order. Finally, the 603.75 MHz transmitter is out for bids.

### Design Status

The injection and extraction line optics, to be reported on at this conference by A. Jason, have been developed to the point where the location and size of the skew dipole magnets and the quadrupole magnets can be specified. As a result, these magnets are now in the process of being designed. The Ring focusing quadrupoles are also being designed, as are the septum magnets. The beam dump for the unstripped neutral injected beam is being designed.

### Research and Development

Areas of significant research and development effort in the PSR project tend to be centered about those items which are expected to have a long lead time. Principal among these items is the fast extraction kicker, the power supply (ferrite-isolated Blumlein line) for which has recently achieved its rated voltage and repetition rate ( $\pm 50$  kV, 1 kA, 720 Hz). The active damper high-power electronics have been under development for several years (Ref. 2). A prototype beam position monitor (stripline electrodes) has been developed and installed in Line D for testing purposes. With an eye toward solving or alleviating the beam loading problem in the 603.75 MHz rf system some effort has been spent in developing rapid cavity detuning techniques.

Areas which have received little research effort to the present time include principally the rf bunching systems (an area of considerable concern), the beam scraper system, and the multipole magnet system. These areas are now starting to be addressed in a significant way, although our efforts could benefit greatly by the addition of experienced personnel.

References 3 through 6 are papers on PSR research and development published in the proceedings of the March 1981 National Accelerator Conference in Washington, DC.

### Schedule

Presented here in tabular form is the projected schedule for the PSR:

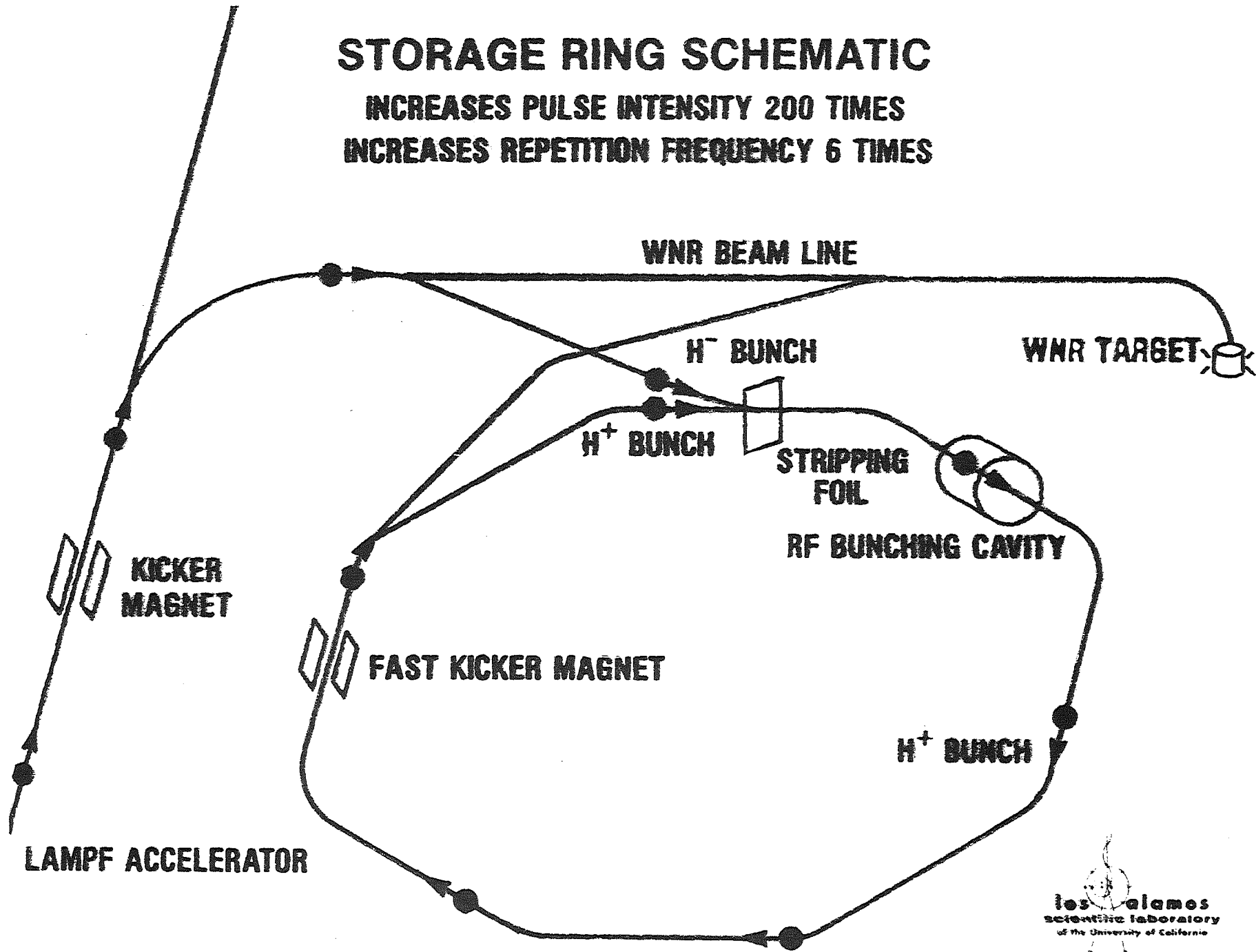
3/83	Beneficial occupancy of Ring tunnel
6/83	Beneficial occupancy of equipment building
3/84	Line D modifications complete
6/84	PSR equipment installation complete
10/84 thru	
3/85	LAMPF/Line D/WNR shutdown
3/85	PSR ready to accept beam

### References

1. George P. Lawrence et al., "LASL High-Current Proton Storage Ring," Proc. of the XI Int. Conf. on High Energy Accelerators, p. 103, Geneva, Switzerland, July 1980.
2. James S. Lunsford, "Design of a Power Amplifier for the LAMPF Proton Storage Ring Transverse Damper System," IEEE Trans. on Nucl. Sci., NS-28, p. 2952, 1981.
3. E. Higgins and F. Wells, "A Beam Position Monitor System for the Proton Storage Ring at LAMPF," IEEE Trans. on Nucl. Sci., NS-28, p. 2308, 1981.
4. B. Sandberg, "A Novel Current Monitor for DC and Modulated Magnets in the Proton Storage Ring," IEEE Trans. on Nucl. Sci., NS-28, p. 2314, 1981.
5. Andrew J. Jason et al., "Neutralization of H<sup>-</sup> Beams by Magnetic Stripping," IEEE Trans. on Nucl. Sci., NS-28, p. 2704, 1981.
6. Daniel W. Hudgings and Andrew J. Jason, "Los Alamos Proton Storage Ring Extraction System," IEEE Trans. on Nucl. Sci., NS-28, p. 2791, 1981.

# STORAGE RING SCHEMATIC

INCREASES PULSE INTENSITY 200 TIMES  
INCREASES REPETITION FREQUENCY 6 TIMES



# PSR STRUCTURAL PARAMETERS

ORBIT CIRCUMFERENCE	90.2 m
FOCUSING STRUCTURE	D-O-F-O
LATTICE TYPE	SEPARATED FUNCTION
NUMBER OF PERIODS	10
FREE STRAIGHT SECTION LENGTH	4.7 m/cell
DIPOLE FIELD STRENGTH	1.2 T
DIPOLE APERTURE	10.5 cm x 28 cm



# PSR DYNAMICAL PARAMETERS

CIRCULATION TIME	357.7 ns
PROTON KINETIC ENERGY/ $\gamma$	797 MeV/1.85
PROTON RIGIDITY	4.869 Tm
TRANSITION GAMMA	3.02
TUNES (NOMINAL)	$\nu_H = 3.25, \nu_V = 2.25$
EMITTANCE (INJECTION/EXTRACTION)	.05 cm-mrad/2.0 cm-mrad
$\Delta p/p$ (INJECTION/EXTRACTION)	$\pm 0.001/\pm 0.003$

# LONG BUNCH MODE

## UTILIZATION

NO. BUNCHES IN RING

BUNCH LENGTH

BUNCHING FREQUENCY

PROTONS/BUNCH

INJECTION RATE

INJECTION TIME

EXTRACTION RATE

ACCUMULATED TURNS

AVERAGE CURRENT

## NEUTRON SCATTERING

1

270 ns

2.795 MHz

$5 \times 10^{13}$

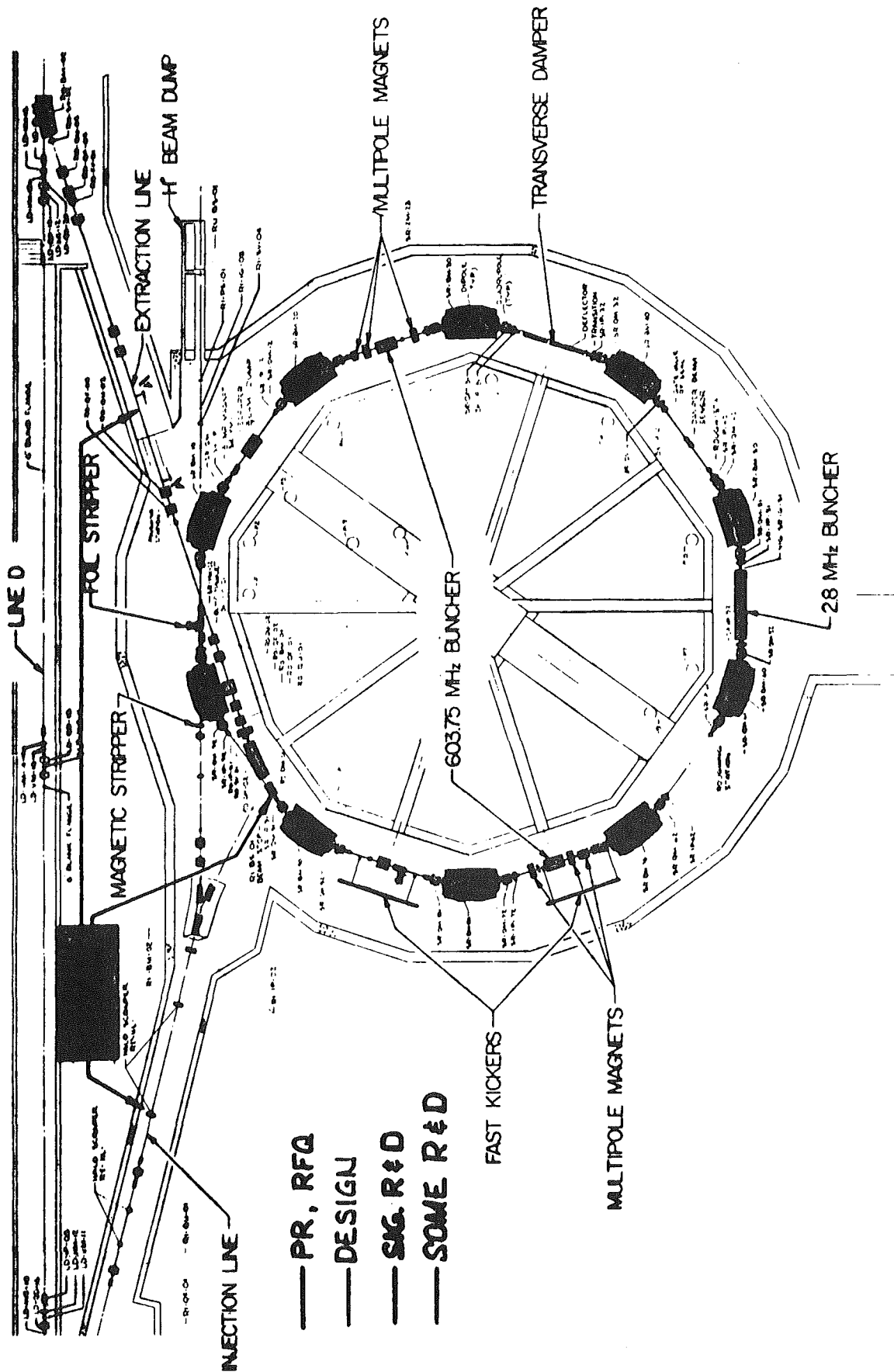
12 pps

750  $\mu$ s

12 pps

2100

100  $\mu$ A



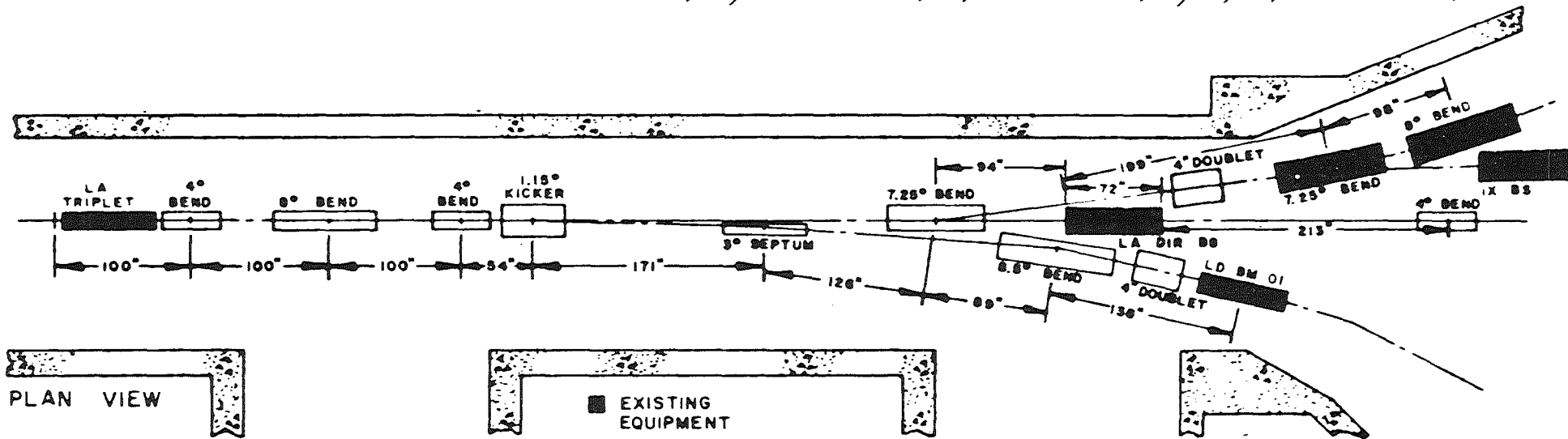
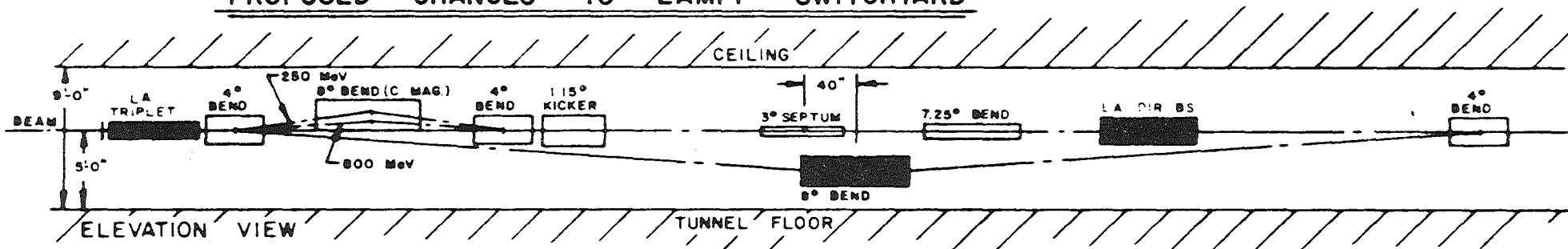
# Design and Development

- \* Short-bunch extraction kicker modulator tested at full voltage and repetition rate.
- \* Beam centroid monitor prototype demonstrated.
- \* Active damper distributed amplifier under development.
- \* 603.75 MHz buncher fast tuning scheme.

# Design and Development

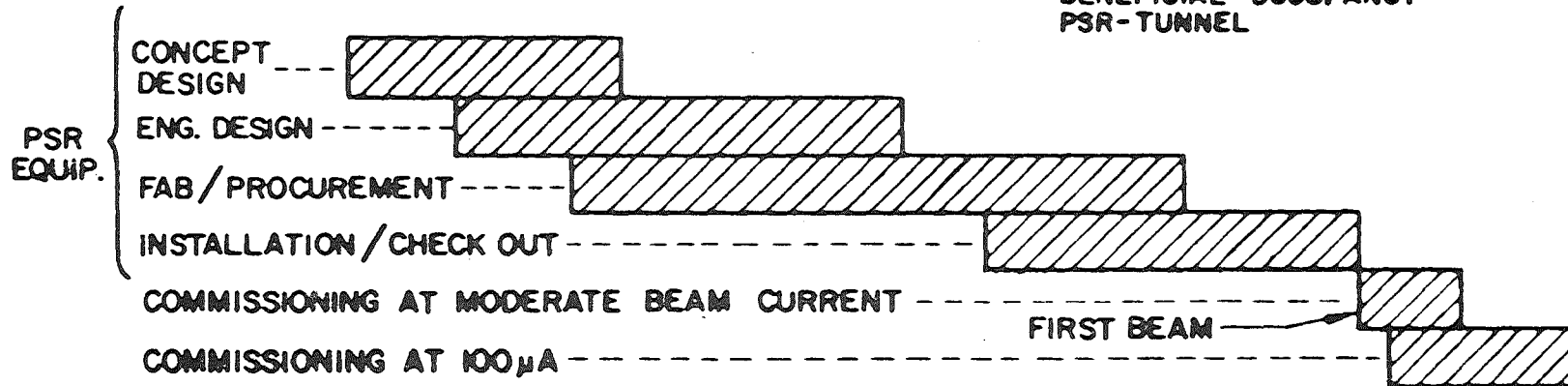
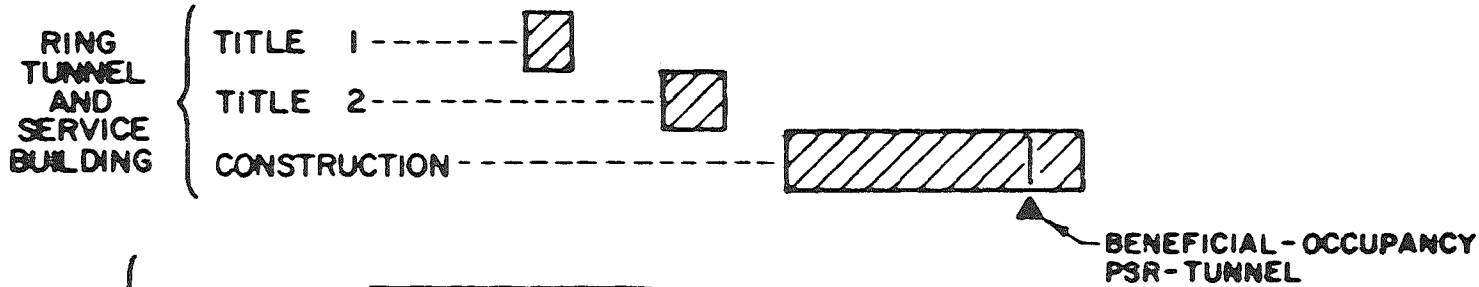
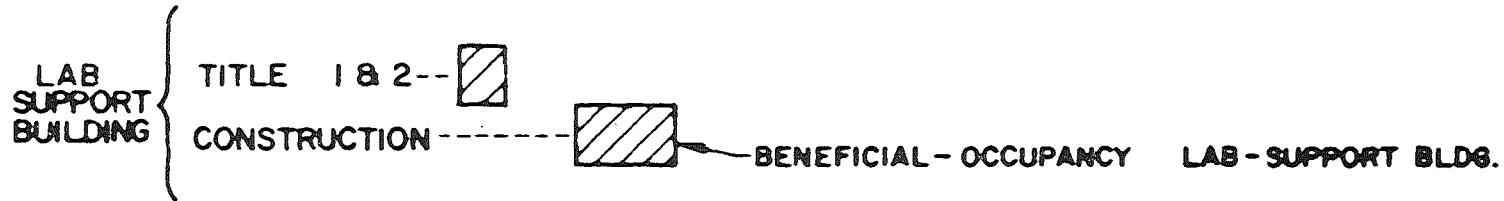
- \* Injection optics complete.
- \* Extraction optics complete (to WNR target). Includes option for future neutrino line.
- \* Magnetic stripping expt. confirms 2-step  $H^-$  injection scheme.
- \* New switchyard kicker conceptual design.

# PROPOSED CHANGES TO LAMPF SWITCHYARD



# PROTON STORAGE RING SCHEDULE

CY | 1979 | 1980 | 1981 | 1982 | 1983 | 1984 | 1985 | 1986 |



# Extraction System

Beam deflection provided by:

- a) 2 kicker magnets, 100 MW pulsers, . . .
- b) PSR lattice elements

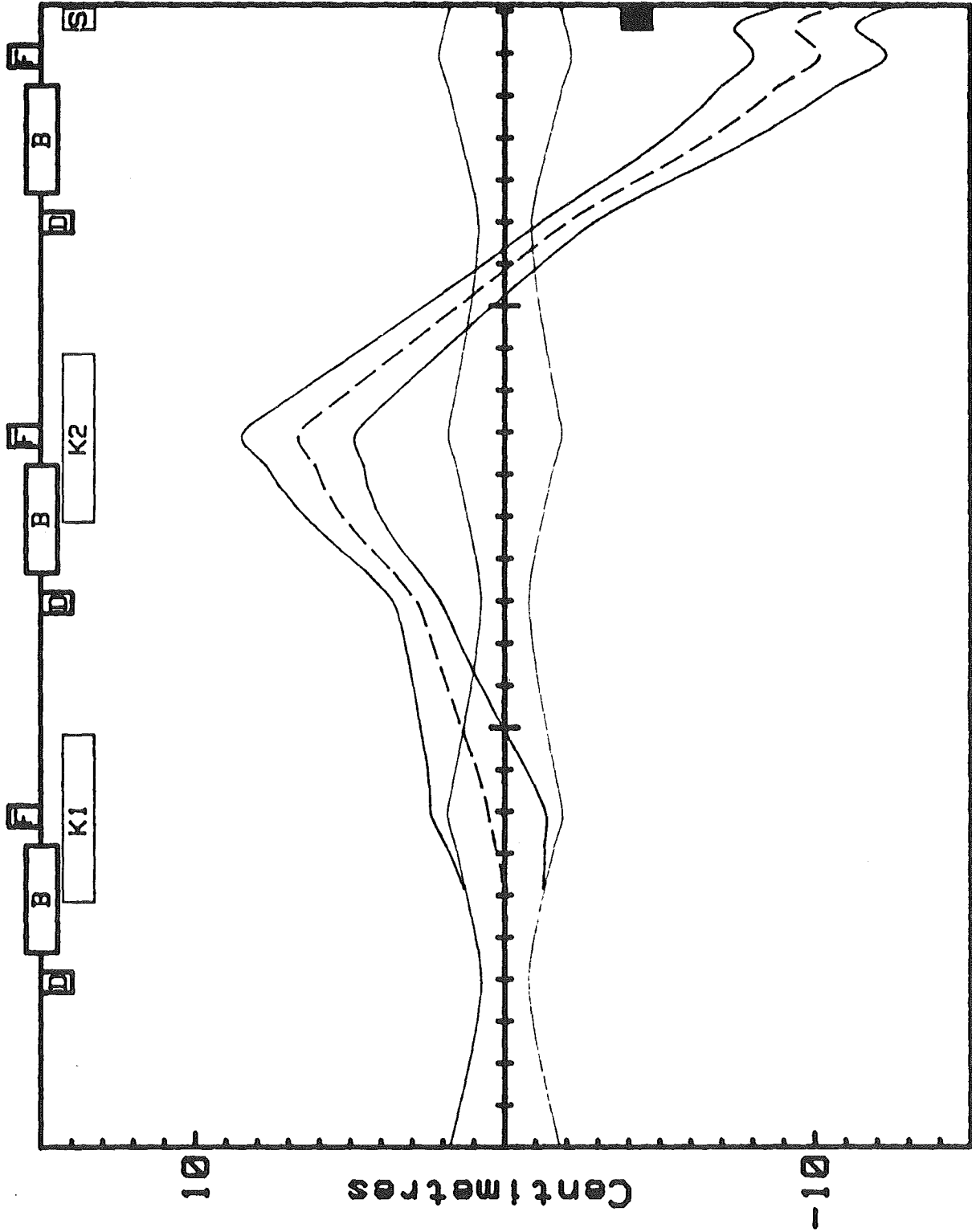
Septa:

- a) current sheet between PSR, extraction channel
- b) 1.2 T iron septum magnet

Extraction Line:

- a) transports beam to line D re-insertion or  
to tuneup beam dump
- b) cancels PSR dispersion

# BEAM ENVELOPES



Metres

# Design for Low Beam Loss

- \* Large extraction kick - 9 cm.
- \* Injection line phase space trimming.
- \* Beam edge scraping in ring.
- \* Large apertures  $> 10$  cm.

## Beam Loss Objectives

- \*  $< 50$  nA in complex equipment areas.
- \* High losses only at shielded scrapers.

# Shielding

- \* External shield O.K. for 4  $\mu$ A point loss.
- \* Buried steel over hot areas.
- \* Extra-large tunnel for local shielding of beam scrapers, etc.

# Activation / Handling

- \* Bridge crane and manipulator designed into ring tunnel.
- \* Equipment transport vehicle adaptable to remote operation.
- \* Remotely demountable flanges.
- \* Borated concrete in tunnel walls.

# *PSR FEATURES (I)*

- *2-Mode operation: short bunch/long bunch*
- *1 ns/720 pps in short bunch mode*
- *12 pps/100  $\mu\text{A}(\text{av})/5 \times 10^{13}$  ppp in long bunch mode*
- *2-Step  $\text{H}^-$  stripping injection; phase space control*
- *High space charge limit: large aperture, 800 MeV injection*
- *Potential for upgrade to higher current*

## *PSR FEATURES (II)*

- \* Separated function lattice: tune flexibility*
- \* Extra room in straight sections*
- \* Short accumulation time; no acceleration*
- \* Chopped injection into rf buckets*
- \* Extraction on demand; mechanical chopper phasing*
- \* Active feedback damper for instability control*



SNQ COMPRESSOR RING IKOR :

ISOCHRONOUS OPERATION, WHY AND HOW ?

K.H. Reich, CERN, CH-1211 Geneva 23

Summary

A one-year study and a machine experiment at the CERN PS have shown how isochronous operation of an otherwise classical AG compressor ring would lead to the absence of an RF system and to rise times of longitudinal instability modes an order of magnitude longer than the ring filling time. Further studies aimed at making this attractive approach fully transparent are pointed out.

SNQ COMPRESSOR RING IKOR :

ISOCHRONOUS OPERATION, WHY AND HOW ?

K.H. Reich<sup>\*</sup>, CERN, CH-1211 Geneva 23

Introduction

The IKOR /1/ design proton intensity of  $2.7 \cdot 10^{14}$  protons per pulse (ppp) is five times higher, and the design flux of  $2.7 \times 10^{16}$  p/s twenty times higher, than proton intensities and fluxes of comparable machines at present under construction.

Under these conditions beam dynamics considerations practically dominate almost all aspects of ring design. On the one hand, this design must ensure that beams of such very high intensities can be injected, kept stably in the ring, and ejected. On the other hand, relative beam losses must be kept far below what is currently admissible; the maximum tolerable operational loss is assumed to be  $5 \cdot 10^{-3}$ . The major beam dynamics implications for the IKOR design are described. (The very important implications for machine components, radiation protection, remote handling etc. are dealt with elsewhere in this workshop.)

Injection : The minimum IKOR beam emittances ( $\epsilon_H = 150\pi \cdot 10^{-6}$  rad m,  $\epsilon_V = 50\pi \cdot 10^{-6}$  rad m at 1.1 GeV) are determined by the need to limit the space-charge detuning to reasonable values ( $\Delta Q_H \leq 0.2$ ,  $\Delta Q_V \leq 0.4$ ). Hence the minimum four-dimensional phase-space volume (which one would not like to increase in order to keep the IKOR cost down) is  $7500\pi^2 \cdot 10^{-12}$  rad<sup>2</sup> m<sup>2</sup>. The four-dimensional volume occupied by the linac beam is  $25\pi^2 \cdot 10^{-12}$  rad<sup>2</sup> m<sup>2</sup>, i.e. a three hundredth of the former. However, to reach the IKOR design intensity by multiturn injection of the design linac beam, more than six hundred turns have to be injected (without losses). Hence, to stay within the minimum beam emittances, the phase-space density has to be increased in both planes by at least a factor slightly over two. (To obtain the desirable uniform distribution in geometrical space, a much larger factor is required.)

---

<sup>\*</sup>) Standing in for Dr. H. Willax, the unforgotten IKOR study project leader, who so untimely passed away on 17th April, 1981.

As RF stacking and stochastic beam "cooling" are much too slow for the present filling rate of 100 Hz, only charge-exchange injection offers itself as a proven technique for achieving such an increase of phase-space density. It is also noted that losses on a (thin) stripping foil are much smaller than those on a magnet septum, indispensable for proton injection. Finally, because of the relative independence of the phase-spaces before and after charge-exchange, it should be easier to obtain the desired uniform filling in geometrical space by starting with a  $H^-$  beam.

Keeping the beam stably in IKOR : Transverse instabilities of the resistive wall type are potentially unavoidable. In the case of a copper vacuum chamber, the computed rise times of the fastest vertical modes /1/ are shorter than the filling time of 500  $\mu s$ , and in the case of a (stainless) steel vacuum chamber this is true for practically all modes. Rise times for longitudinal instabilities (basically of the negative mass type) depend even more on the details of a particular machine design. Anyway, it is clear that the entire beam should be ejected as soon as the filling process is terminated in order to minimize build-up of instabilities. In addition various beam-stabilizing measures will be required.

Ejection : The requirement to keep the beam loss at very low values advocates use of the proven fast ejection scheme consisting of kicker and septum magnet. One has then to provide an azimuthal void in the beam to ensure that no beam loss occurs during the rise of the kicker magnet field. (An alternative attractive in principle would be to have a highly effective ejection scheme not requiring a void in the beam /1/ and thus to get rid of the undesirable space-charge fields near the edges facing the void.)

#### Why isochronous operation /2/ ?

Debunching : The azimuthal void required for nearly loss-free beam ejection is assumed to be created by appropriate chopping of the linac beam. In the absence of longitudinal RF or space-charge fields the void will shrink, because off-momentum particles at both beam edges will drift into the void (Fig. 1) according to

$$\int \Delta T_{\text{rev}} = - \eta T_F \Delta p/p \quad (1)$$

where

- $\int \Delta T_{\text{rev}}$  = Total difference in revolution time of off-momentum particle with respect to particle with nominal momentum
- $\eta = \gamma_0^{-2} - \gamma_{\text{tr}}^{-2}$  ( $\gamma_{\text{tr}}$  = normalized transition energy of alternating gradient magnet ring;  $\gamma_0 = 2.172$ )
- $T_F$  = filling time (= nominal total revolution time of first turn injected)
- $\Delta p/p$  = relative beam momentum spread.

Hence, by making  $\eta$  sufficiently small, i.e. approaching closely isochronous operation,  $\int \Delta T_{\text{rev}}$  can be reduced to an acceptable value (Fig. 2). Experiments at the CERN PS have notably shown /3/ that at least in beams with relatively lesser space-charge fields shrinking of the void during 500  $\mu\text{s}$  can be reduced to  $2 \times \int \Delta T_{\text{rev}} = 5 \text{ ns}$  (while even 30 ns would not be entirely unacceptable in the IKOR case).

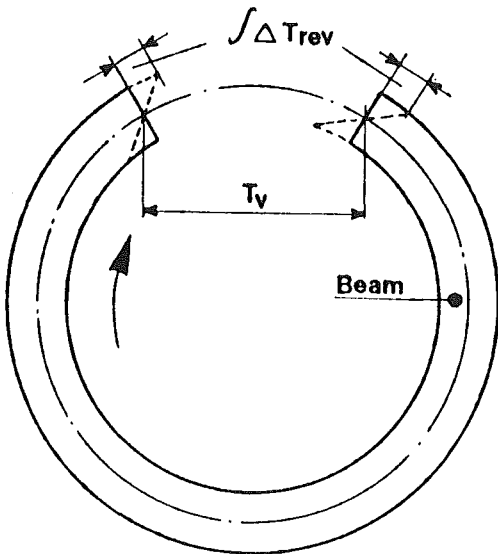


Fig. 1 In the absence of longitudinal RF or space-charge fields, the azimuthal beam void of duration  $T_v$  (= 100 ns in IKOR) shrinks by  $2 \times \int \Delta T_{\text{rev}}$  due to the drifting caused by the beam momentum spread. (Not to scale)

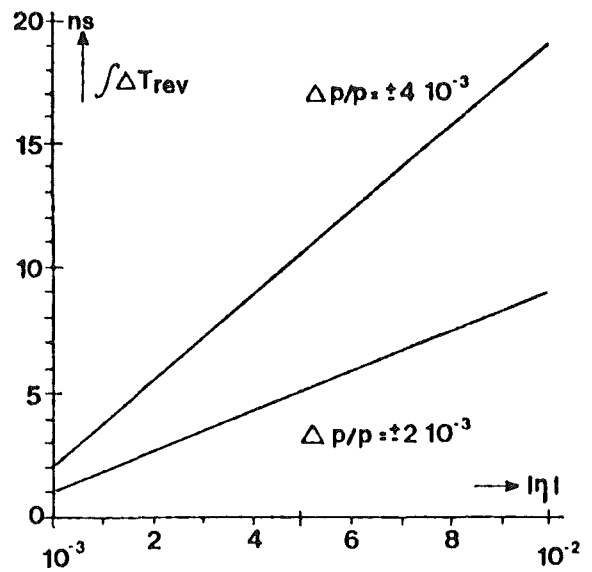


Fig. 2 Total revolution time difference  $\int \Delta T_{\text{rev}}$  in IKOR at the end of filling ( $T_F = 500 \mu\text{s}$ ) as a function of the values of  $\eta (= \gamma_0^{-2} - \gamma_{\text{tr}}^{-2})$  and momentum spread  $\Delta p/p$ , under the conditions of Fig. 1.

Advantages of the absence of an RF system : Apart from the obvious saving in cost and effort, the absence of an RF system has at least one advantage, even if only a "void keeper" system is used /1/. The absence of an extra contribution to the beam-equipment coupling impedance makes for higher instability thresholds and slower rise times.

Beam dynamics for  $\eta \approx 0$  : As AG synchrotrons are designed to stay away from the region  $\eta \approx 0$ , or, if unavoidable, to cross this region as fast as possible, some specific beam dynamics points of interest here have not been fully studied previously. During the IKOR study, a start was made, but it is too early to come to final conclusions. Tentatively, the following can be said (see also next Section).

There should definitely be a gain as regards longitudinal stability, not only because of the absent undesirable beam-RF system coupling impedance. While the threshold for instabilities ( $\propto \eta$ ) is lowered, their rise times become very much longer for  $\eta \approx 0$ . This is particularly true, if the sign of the effective beam coupling impedance is right (capacitive below  $\gamma_{tr}$ , inductive above) and the impedance value is kept reasonable low even at high frequencies (by specifying a smooth vacuum chamber and designing appropriately the injection and ejection kicker magnets as well as the transverse damping equipment). Calculations have shown /1/ that, given these conditions, the rise times, even for the fastest modes, would be longer than five milliseconds, i.e. an order of magnitude longer than the filling time.

What price is to be paid for the advantages gained ?

Lattice : The condition  $\gamma_{tr} \approx \gamma_0 \approx 2.2$  influenced the lattice design rather strongly, eliminating in fact some otherwise attractive designs. While the bending magnet gap height could practically be kept as small as in any of the eliminated designs, the lens bore diameter had to be increased somewhat on account of the larger amplitude functions. Also, a third lens per cell had to be added for  $\gamma_{tr}$ -tuning independent of Q-tuning. Best operating conditions will probably require  $\gamma_{tr}$ -tuning during filling (to offset the space-charge effect on  $\gamma_{tr}$  while staying close to  $\eta = 0$  but always above  $\gamma_0$ ). While a fast adjustment of the quadrupole currents had already been specified for the control of local beam density during injection /1/, simultaneous control of  $Q_{H,V}$  and  $\gamma_{tr}$

presumably does not represent a simplification. Furthermore, as already mentioned, sextupoles are required for reducing the  $\gamma_{tr}$ -dependence on momentum (radius).

Beam dynamics : As said before, this point needs further study. - The use of sextupoles for reducing the  $\gamma_{tr}(p)$  dependence will reduce the useable working area in the  $Q_H - Q_V$  diagram. In the limit this may lead to specifying somewhat larger transverse emittances so as to reduce the space-charge tune shifts. (Another reason to go in that direction would be the wish to reduce  $\eta$  at the beam edges, see Fig. 4).

More detailed computations of transverse stability limits and growth times are needed, taking into account the definite parameters of the vacuum chamber, the injection and ejection kicker magnets, the beam observation equipment, and of course the transverse feedback damping system as well as the strength of reasonably achievable Landau damping. The latter is presumably smaller than at  $\eta \neq 0$  and hence the bandwidth of the damping system may have to be larger.

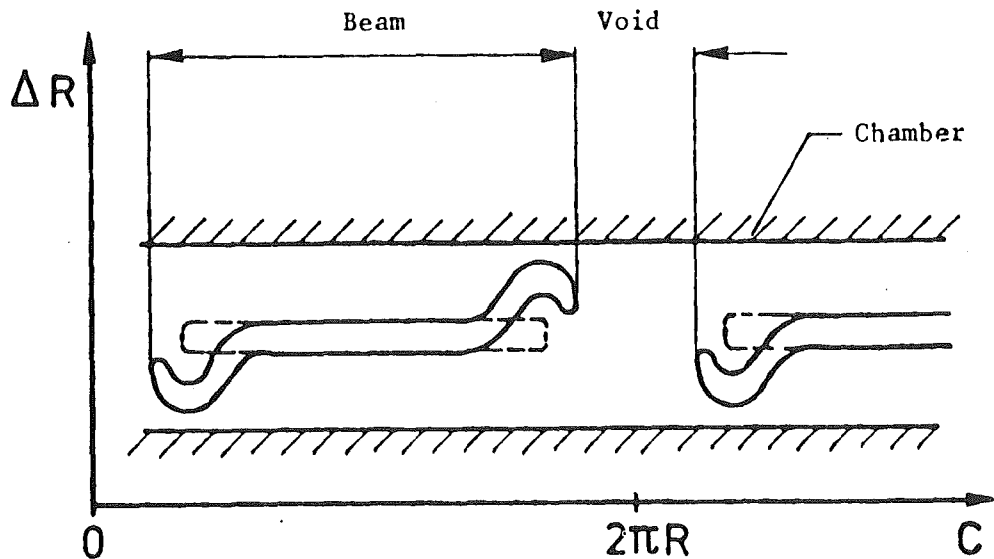


Fig. 3 Radial and longitudinal distortions at the beam edges near the void (full lines) at  $\eta \approx 0$  due to longitudinal space-charge fields resulting from longitudinal density gradients /1/. (Not to scale)

Another point needing further clarification concerns the extra momentum spread due to longitudinal space-charge forces, particularly near the beam edges facing the void /1/. For  $\eta \approx 0$  this extra spread leads to local radial beam distortions (Fig. 3), requiring somewhat wider horizontal machine and ejection septum magnet apertures. To reduce these space-charge forces as much as possible already in the micro-pulses, these pulses should be lengthened by a factor of three to five on leaving the linac.

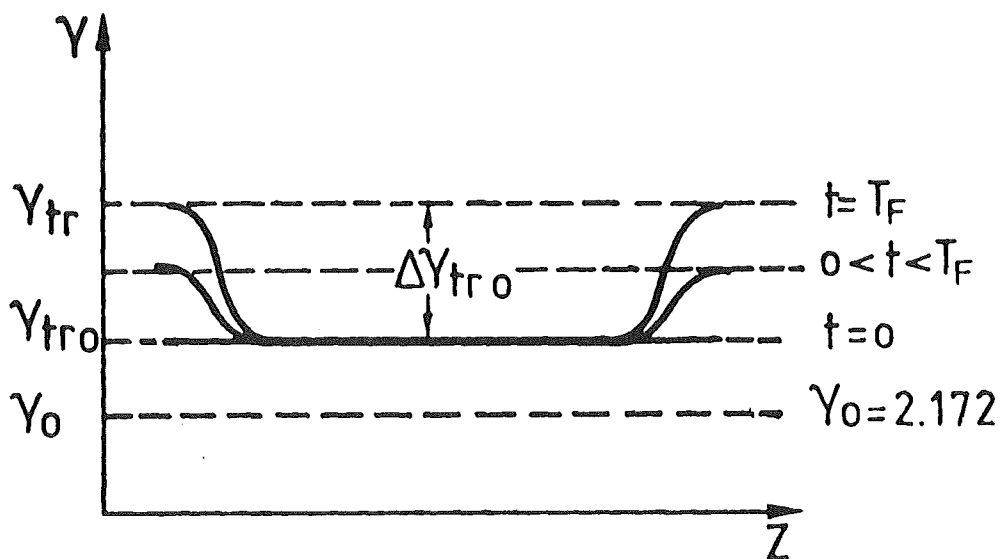


Fig. 4 Programmed adjustment of nominal transition energy during filling (dashed lines) to compensate the  $\gamma_{tr}$  depression caused by transverse space-charge forces /1/. The full lines show the azimuthal dependence of the resulting effective  $\gamma_{tr}$ -values for three times (at the beginning, during, and at the end of the filling time  $T_F$ ). The lesser  $\gamma_{tr}$ -depression at the beam edges is due to the gradual reduction of the line density towards these edges. Choice of  $\gamma_{tr0}$  and  $\Delta\gamma_{tr0}$  will require careful balancing between on the one hand the stability requirement to keep always  $\gamma_{tr} > \gamma_0$  and on the other hand the need to keep  $\Delta\gamma_{tr}$  (and hence  $\eta$ ) small enough at the beam edges to avoid excessive drifting. (Not to scale)



With a mean radius of 32.18 m, eleven 1.3 T bending magnets with apertures 10 cm x 20 cm, thirty-three 3.5 T/m quadrupole lenses with 21 cm diameter bore, and eleven correction multipoles (located between  $Q_F$  and QD1), lattice parameters are nevertheless very reasonable for a ring containing  $2.7 \cdot 10^{14}$  ppp.

Another nice feature of this lattice is the ejection arrangement. As the beam to be ejected practically fills the vacuum chamber (no adiabatic damping of betatron amplitudes), efficient ejection is particularly important. A kicker magnet located immediately downstream of QD1 horizontally deflects the beam outwards by 11 mrad. The defocusing quadrupole QD2 increases this angle to 20.6 mrad. A further bend by 130.6 mrad ( $7.48^\circ$ ) in the septum magnet located upstream of the first bending magnet steers the beam out of the machine (leaving it between the coils of the C-shaped bending magnet). As the deflected beam does not cross neither a bending magnet nor an F-lens, their apertures need not be increased. As the beam has a horizontal waist in the D-lens, only slightly more aperture is required (+ 5%) for the deflected beam (assuming equal bores diameter in D and F lenses). Increasing also the bore diameter of the F-lenses to the new D-value leads to a single, reasonable lens design.

Commissioning : Starting from the computed values, notably the quadrupole and sextupole currents will need to be optimized, to give optimum (programmed) settings of  $Q_H(t)$ ,  $Q_V(t)$  and  $\gamma_{tr}(t,p)$ . As stated before, the aims are (i) uniform particle distribution in geometrical space at injection and hence minimum space-charge detuning (leading to minimum beam blow up caused by stop-band penetration), and (ii)  $n \approx 0$  (but  $\gamma_{tr} > \gamma_0$  for all particles) to prevent excessive shrinking of the void and maintain long rise times of longitudinal instabilities while allowing some decrease of longitudinal space-charge fields through debunching of the micro-pulses.

A related optimisation concerns the programmed chopping of the linac beam on successive turns so as to shape the beam edges facing the void. For instance, to allow (partially) for the shrinking (which takes time), one could make the void a little longer during the first part of the filling, and shorter than the nominal value during the latter part. More generally, one could experiment with the detailed decrease of the line density towards the beam edge so as to

decrease the strength of the longitudinal space-charge fields (and, unfortunately, of the azimuthal uniformity of the transverse fields) or vice-versa. The aim would be to maintain the local radial beam distortions as well as the spread in space-charge depression of  $\gamma_{tr}$  and  $Q_{H,V}$  within reasonable bounds.

### Conclusions

While not yet a proven method, isochronous operation of an otherwise classical AG compressor ring looks sufficiently attractive to study this approach further. A one-year study and a machine experiment at the CERN PS have brought out the following interesting features : (i) absence of an RF system (which, with a beam current of 66A, would not be straightforward to build and operate) leading to a reduced beam-equipment coupling impedance and hence higher instability thresholds, and (ii) for  $\gamma_{tr} > \gamma_0$  lengthening of the rise times of longitudinal instability modes to values an order of magnitude longer than the filling time. The price to be paid for these advantages is essentially one extra lens per lattice cell and probably fast programming of all lens currents, besides of course the general extra risk to adopt a novel approach not yet fully transparent, particularly as regards beam dynamics. But then, how can one expect to build a ring with a performance about an order of magnitude beyond the (yet to be demonstrated) state of the art without taking some risks ?

### Acknowledgements

The work reported here was done by the (part-time) members of a Study group<sup>\*</sup> meeting periodically at the KFA Jülich from October 1979 to November 1980 under the leadership of the late Dr. H. Willax. As regards isochronous operation, particular acknowledgements are due to Professor Schatz, Dipl.-Ing. H. Fischer and Dr. H.G. Hereward for launching, respectively examining, this suggestion, to Drs. R. Cappi and J.P. Delahaye for their collaboration on the CERN PS experiment, to Dr. L. Palumbo, Professor V. Vaccaro and Dr. G. Wüstefeld for tackling the novel beam dynamics problems at  $\eta \approx 0$ , and last but not least, to Miss H. Lindqvist for optimizing the lattice notably with a view to  $\gamma_{tr}$ -tuning, and to Dr. C.J.A. Corsten for studying the  $\gamma_{tr}(p)$  correction with sextupoles.

<sup>\*</sup>) J. Ahlbäck, W. Busse, R. Cappi, C.J.A. Corsten, J.S. Colonias, W. Davies, J.P. Delahaye, H. Fischer, K. Goebel, H.L. Hagedoorn, M. Höfert, W. van Kampen, H. Lindqvist, P.F. Meads, L. Palumbo, K.H. Reich, G. Schaffer, V. Vaccaro, H. Willax, R. Wolgast, G. Wüstefeld.

References

- /1/ IKOR study report, Institute for Solid State Physics, KFA Jülich, 1981, and references quoted (in German and English). Some knowledge of that work is assumed in this presentation.
- /2/ H. Fischer, K.H. Reich, private communication
- /3/ R. Cappi, J.P. Delahaye, K.H. Reich,  
IEEE Trans. Nucl. Sci., Vol. 28, No. 3, June 1981 p.2389



SNQ Linear Accelerator Beam Dynamics

K. Mittag

Kernforschungszentrum Karlsruhe, Institut für Kernphysik,  
Postfach 3640, D-7500 Karlsruhe, Federal Republic of Germany

Summary

The main arguments leading to the SNQ linear accelerator parameters are summarized. Relatively low rf frequencies were chosen mainly because of availability and cost minimization of rf power sources. The beam dynamics is discussed as to its relevance with respect to beam spill. Special parameter choices and measures leading to minimal beam spill are outlined.

Main Accelerator Parameters

The linear accelerator based neutron spallation source SNQ<sup>1</sup> has the objective to produce an average thermal neutron flux of  $7 \times 10^{14} \text{ cm}^{-2}\text{s}^{-1}$ , pulsed at about 100 Hz repetition rate with about 500  $\mu\text{s}$  pulse length. The particles to be accelerated are protons at first, H<sup>-</sup>-ions are planned for a later option. The final proton energy is 1.1 GeV. From these specifications there results the requirement of 5 mA average, and 100 mA pulse beam current.

These parameters are summarized in Table 1 and compared with those achieved with the proton linear accelerator at LANL. While the final energy, the pulse length, and the repetition rate are not so much different in both machines, the average beam current is about a factor of 8 higher than achieved at present at LANL. Although the SNQ pulse beam current is a factor of about 10 higher than realized at LANL, it is about a factor of 2 smaller than routinely achieved in low duty cycle Alvarez accelerators used as injectors to synchrotrons.

Main Accelerator Parameters		
	SNQ design reference - option	LAMPF achieved
particles	H <sup>+</sup> (H <sup>-</sup> )	H <sup>+</sup> , H <sup>-</sup>
final energy	1100 MeV	800 MeV
beam current		
-average	5 mA - 10 mA	0.6 mA
-pulse	100 mA	12 mA
pulse length	0.5 ms - 1 ms	0.75 ms
repetition rate	≤100 Hz	120 Hz

Table 1 Main SNQ accelerator parameters in comparison with those achieved at LANL.

The combination of high average and high pulse beam current in the SNQ accelerator calls for special attention to the beam spill problem. Hence a major guide line for the beam dynamics design is the minimization of proton loss at high energies, which, in turn, is largely effected by the beam dynamics in the space charge dominated regime at small energies.

Having the basic accelerator parameters final energy, beam current, and pulse characteristics fixed, the choice of the accelerator operating frequency is the most important one to make. It has a large impact on the rf system, on the accelerator structures, and also on the beam dynamics. The high beam current both on the average and during the pulse has led to the relatively low frequencies chosen: 108 MHz for the

Alvarez low energy accelerator as compared to 200 MHz in other proton linear accelerators, and 324 MHz for the high energy accelerator part as to 800 MHz of the side coupled linac at LANL. For the SNQ frequency choice the cost of the rf power system is minimized, because rf power sources with high power output for high duty cycle operation will be available. Even though the accelerator structures are slightly more expensive at the lower frequencies than at higher ones, the total machine cost is dominated by that of the rf system, hence less for the lower frequency. For the beam dynamics<sup>1</sup> the lower frequencies insure larger longitudinal and transverse acceptances, from which comparatively less beam spill can be expected.

A general layout of the SNQ linear accelerator is shown in Fig. 1. For the reference design a 450 keV dc preacceleration has been proposed

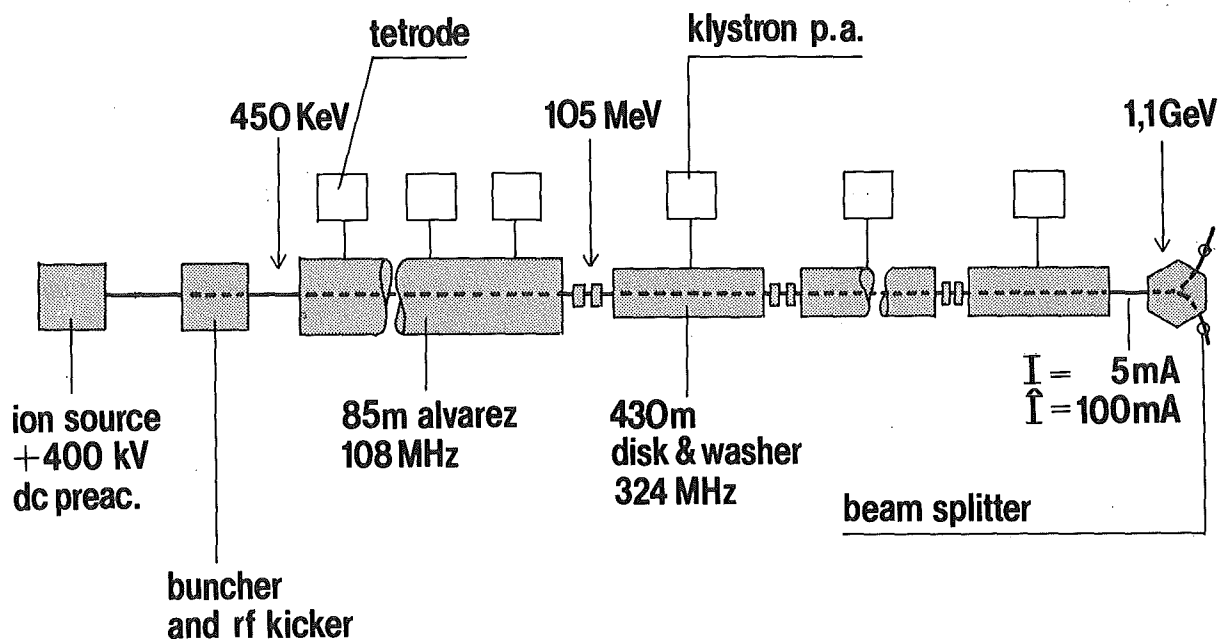


Fig. 1 SNQ linear accelerator, general layout

which is low compared to the conventional 750 keV in 200 MHz proton linacs. Although from beam dynamics arguments a higher injection energy into the Alvarez accelerator would have been preferred (as is indicated by Fig. 2), this choice of dc voltage insures a reliable, sparkfree operation of the dc injector for the high average and high peak beam current to be accelerated. This requirement has been another reason to choose the relatively low 108 MHz Alvarez accelerator frequency. Then, the beam dynamics problems at injection into the Alvarez accelerator are similar as in a 750 keV, 200 MHz solution<sup>2</sup>.

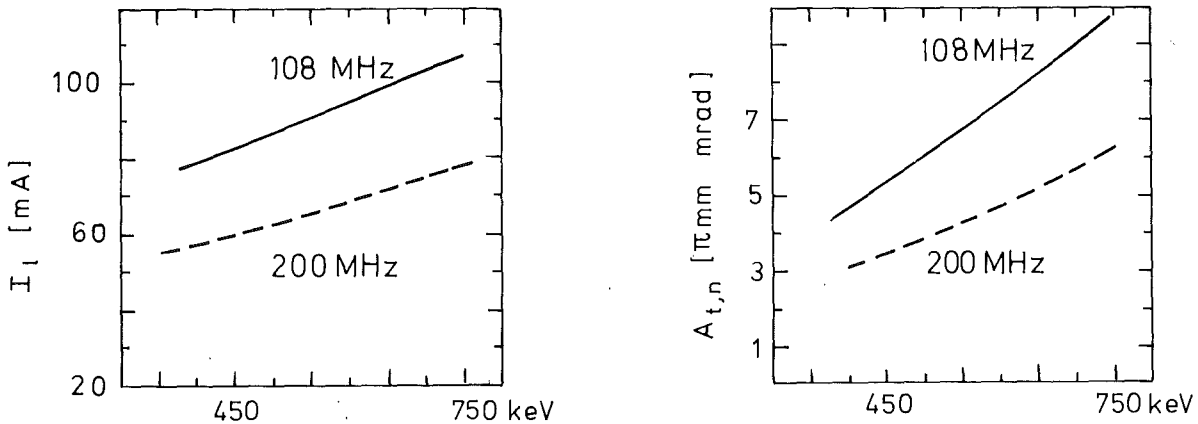


Fig. 2 Longitudinally accepted beam current  $I_1$  and normalized transverse acceptance  $A_{t,n}$  as a function of the injection energy into the Alvarez accelerator  $E_{kin}$  (analytical estimate for  $3 \pi$  mm mrad normalized emittance; parameter is the Alvarez accelerator frequency; higher beam currents can be accelerated in practice)

The dc preacceleration is followed by the low energy beam transport (LEBT)<sup>3</sup>. Its main components are a fast kicker system to create the desired time structure of the beam pulses, a limiting aperture system to limit the beam extension transversely, and a matching section to match the beam both longitudinally and transversely to the following Alvarez accelerator. It also contains various beam diagnostic devices like for emittance measurement, such that the beam entering the Alvarez accelerator is well tailored and analyzed.

During the past few years a new concept for preacceleration has been proven to be technical feasible. It is the rf quadrupole structure<sup>4</sup> RFQ which can focus the beam both transversely and longitudinally. By a proper design it is possible to longitudinally bunch the beam and accelerate it from about 50 keV to 2 MeV. Although for 100 mA beam current this can more easily be achieved with a RFQ operating at 108 MHz, this goal could also be realized in a 200 MHz version. As the injection of a well bunched beam at 2 MeV into a 200 MHz Alvarez accelerator does not present major difficulties from a beam dynamics point of view, a higher frequency choice than taken as reference for the RFQ design would be possible, if not the cost optimization arguments indicated above would still lead to the low frequency version. However, independent of the frequency choice the task to shape the macropulse by a fast kicker system looks more complicated than in the reference design.

Returning the attention to the reference design and Fig. 1, the Alvarez accelerator is followed at 105 MeV proton energy by a 324 MHz disk-and-washer accelerator, which is more effective in acceleration at high proton energies. At the transition between the two accelerators there is a beam matching and analyzing section.

### Beam Dynamics Aspects in Relation to Beam Spill

The SNQ beam dynamics has been discussed in detail elsewhere<sup>1</sup>. This contribution concentrates on aspects which are relevant to the beam spill problem<sup>5</sup>.

About 12 % of the beam gets lost at low energies in the early part of the Alvarez accelerator. These losses (see Fig. 3) originate from the

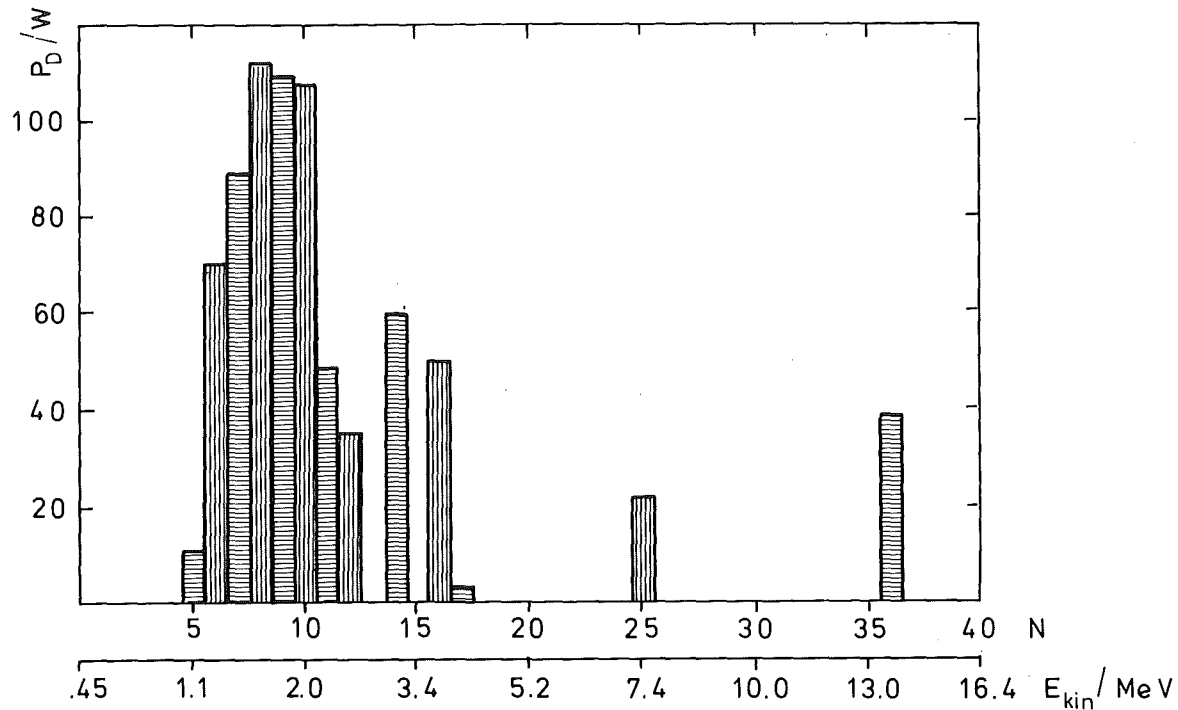


Fig. 3 Beam power load  $P_D$  per drift tube at 5 % duty cycle resulting from particle losses due to incomplete bunching as a function of the drift tube number  $N$  and the proton energy  $E_{kin}$  (multiparticle simulation with 2000 macro particles; large statistical errors above 2.5 MeV)

incomplete bunching inherent to conventional bunching systems. The last macroparticle loss in the multiparticle simulation of Fig. 3 occurred at 13 MeV design energy with a 12 MeV proton energy. An accelerator activation by this kind of particle loss is small. The technical layout of accelerator handling and shielding for this part of the Alvarez accelerator has been for a pessimistic 25 % particle loss in the 0.5 MeV to 10 MeV energy range<sup>6</sup>. The design goal of the double-drift-harmonic bunching system<sup>3</sup> just in front of the Alvarez accelerator has been to minimize these bunching losses. To this end the longitudinal emittance is filled as homogeneously as possible to minimize longitudinal space charge effects. This is achieved by operating the second buncher at 216 MHz, twice the frequency of the first one. Further, the longitudinally non-trapped particles get an additional energy off-set by a third 108 MHz buncher such that the losses occur at low energies already.

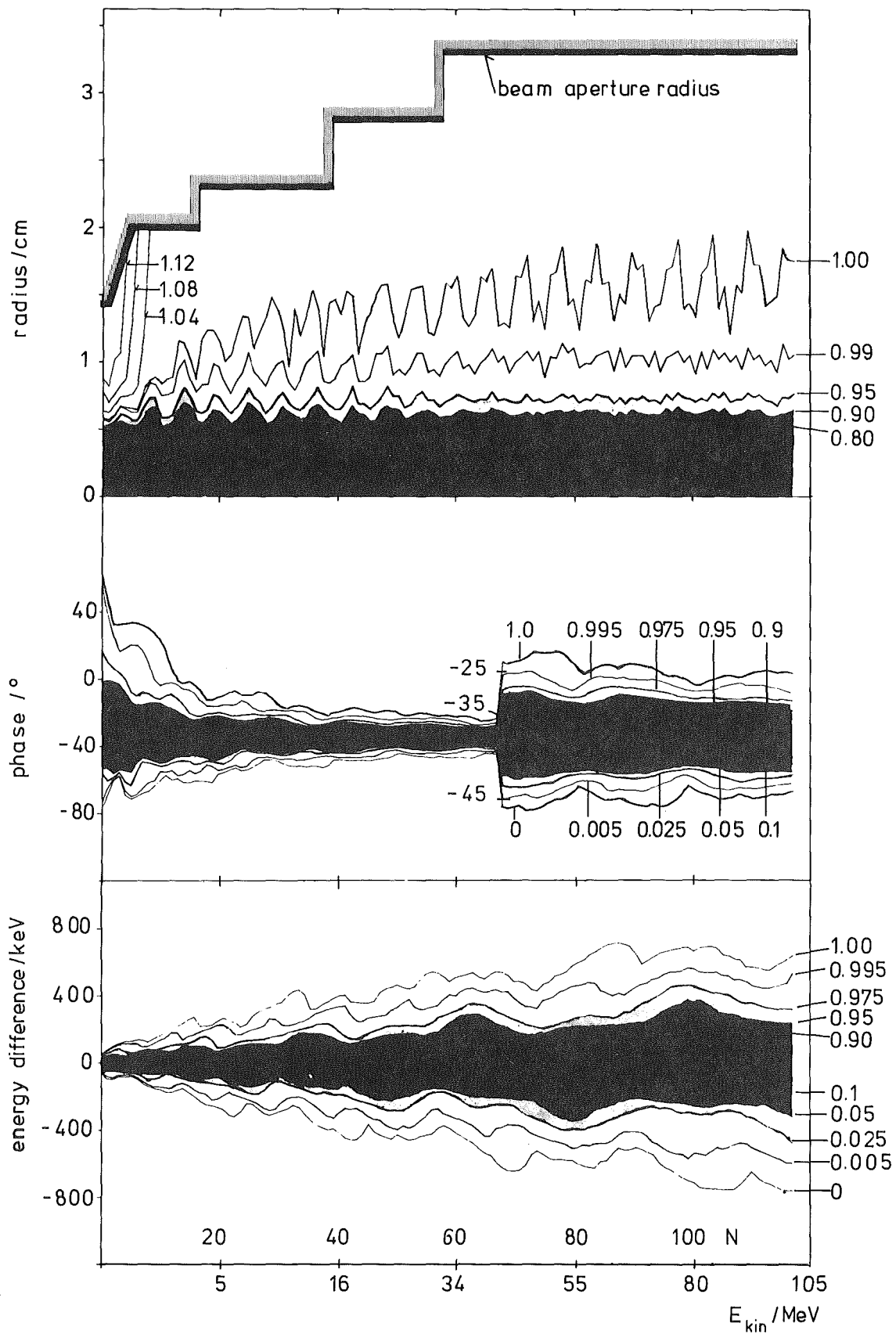


Fig. 4 Transverse (top) and longitudinal (below) density distribution inside the bunch along the Alvarez accelerator. Parameter is that particle fraction having smaller radius, phase or energy than given by a considered curve. In the top diagram the bunching losses are included.  $N$  = drift tube number,  $E_{kin}$  = proton energy (multiparticle simulation, hence the curves labelled with 1.0 or 0.0 are subject to large statistical errors).

Fig. 4 shows the density distribution inside the proton bunch along the Alvarez accelerator as obtained by a multiparticle simulation. At the top the radial dependence is given. The bunching losses cause a rapid initial growth for 12 % of the bunch. At injection the simulated beam was mismatched partly because the matching parameters were chosen for a 100 mA beam current, whereas 125 mA were actually injected into the Alvarez accelerator for this simulation. These mismatches cause the beam envelope to oscillate about the matched solution. In the course of the acceleration the major part of the bunch (95 %) adiabatically matches itself to the accelerator. The outer particles form a slowly expanding halo. The relatively large transverse extension of this halo can be cut down effectively by apertures inside the drift tube beam hole in the energy range from 4 to 8 MeV. The simulation indicates that circular diaphragms with 1.2 cm hole radius would intercept only about 1 % beam current (corresponding to a heat load of about 300 W), but thereby reduce the "maximum" beam radius in the Alvarez accelerator from about 2 cm to about 1.5 cm. Then there remains a large safety margin between the halo particles and the aperture which has a 3.3 cm radius at high energies. The tolerance requirements to be set on the drift tube alignment, quadrupole gradients, accelerating fields, rf phases between tanks, and on the matching parameters are such that this safety margin is sufficient.

The middle of Fig. 3 shows the longitudinal phase damping of the bunch to which a spreading of the proton energies corresponds as can be seen at the bottom. Also longitudinally a halo builds up: at 105 MeV the phase width for "100 %" of the beam is  $18^\circ$ , whereas for 95 % it is only  $11^\circ$ ; the energy width for "100 %" of the beam is 1.4 MeV, whereas for 95 % it is down to 0.8 MeV. Theoretically, the longitudinal tails of the halo decay exponentially with distance from the bunch<sup>7</sup>. The phase acceptance of the 324 MHz disk-and-washer accelerator at 105 MeV is about  $54^\circ$ , which is just equal to the "100 %" - longitudinal bunch extension at the end of the Alvarez accelerator. Taking into account that two rebunchers of the 105 MeV matching section reduce the bunch length, the particles losses resulting from particles longitudinal outside the rf bucket in the disk-and-washer accelerator should be tolerable, although numerical estimates are not available at present. In the technical layout of the accelerator handling and shielding 1 % proton losses have been assumed after the 105 MeV transition section<sup>6</sup>. A reason to choose a frequency ratio of 3 between the Alvarez and disk-and-washer accelerators - and not e.g. 4 as in the LANL proton linac - has been to minimize these "longitudinal" losses.

To choose the optimum parameters the beam dynamics design is concerned to keep the rms emittance growth along the accelerator as small as possible. This ensures a minimization of the beam spill. The rms-emittance development along the Alvarez accelerator is plotted in Fig. 5 as given by the multiparticle simulation. The transverse emittance increase is largest at low energies, being relatively small beyond 20 MeV; longitudinally the situation is reversed. Transversely the increase is roughly a factor 2, longitudinally about 30 %. Several theoretical effects can be correlated to this behavior.

First, there is the longitudinal to transverse coupling due to the phase dependence of the rf defocusing, which decreases as the bunch shrinks in phase due to its increasing velocity. Nevertheless, at injection the transverse focusing has to be so strong that not only the bunch center but also the bunch head is transversely stable, otherwise a large trans-

verse emittance blow-up would occur. This condition sets a lower limit to the average transverse tune  $\sigma$  (defined at the synchronous phase including the space charge defocusing): independent of the transverse emittance  $\sigma$  must not be lower than  $40^\circ$  in the low energy region of the SNQ Alvarez accelerator.

Second, there exists the possibility to excite parametric beam instabilities<sup>8</sup>. The most dangerous one is a transverse envelope oscillation occurring when the coherent tune of the bunch, that is the tune disregarding the space charge defocusing, is  $\sigma_0 = 90^\circ$ . Computer simulations prove that this resonance has to be avoided. Having  $\sigma$  at the operating current of 100 mA fixed to  $40^\circ$ , the tune  $\sigma_0$  at zero current is determined, it gets the larger the smaller the transverse emittance is. In turn, this condition then sets a lower limit to the transverse emittance to be injected into the SNQ Alvarez accelerator; the "100 %" normalized emittance should not be appreciably smaller than  $3 \pi$  mm mrad. The tune depression gets smaller with increasing proton velocity: keeping  $\sigma = 40^\circ$  fixed,  $\sigma_0$  is  $65^\circ$  at 105 MeV compared to  $83^\circ$  at 0.45 MeV for  $3 \pi$  mm mrad emittance, thus the probability to excite transverse instabilities reduces along the accelerator.

Third, transverse emittance increase can stem from temperature transfer from the longitudinal phase space caused by the fact that the longitudinal bunch temperature is about a factor of 8 larger than the transverse one at injection into the SNQ Alvarez accelerator; however at 105 MeV the temperatures have become nearly equal mainly because of kinematic effects. This temperature transfer could be responsible for the tendency of the longitudinal emittance to stay constant in the low energy region (Fig. 5). The increase observed later might be correlated to the decrease of the longitudinal tune from  $28^\circ$  to  $3^\circ$  along the Alvarez accelerator: the longitudinal motion gets more and more space charge dominated and rather close to its stability limit.

Theoretically the causes for beam spill in the disk-and-washer accelerator are mainly limited to effects related to finite tolerances. Especially, these can be matching errors caused by changes in the accelerator periodicity at 105 MeV and once more at 350 MeV, where the transverse focusing period is doubled. Next, there are the alignment errors. To estimate their influence the following assumptions were made for the most important error types:

quadrupole deviation from the doublet axis:  $\leq \pm 0.3$  mm

doublet deviation from the ideal beam axis:  $\leq \pm 0.5$  mm

rf tank deviation from the ideal beam axis:  $\leq \pm 1$  mm

From these errors results<sup>9</sup> an average quadratic beam deviation from the ideal axis of 18 mm at the disk-and-washer accelerator end. For comparison the beam radius is about 20 mm, the aperture radius 40 mm. Thus this intolerably large displacement has to be counteracted by steering magnets in combination with beam position monitors. The calculation indicates that 7 steering magnet pairs are required along the disk-and-washer accelerator to reduce the maximum beam displacement to 5 mm. Another important error type is the setting of the rf phase between disk-and-washer tanks, which is expected to have to be accurate to less than 1 degree. The rf amplitude in the accelerator tanks probably has to be accurate to 0.1 % also during the transients caused by the beam loading<sup>13</sup>.

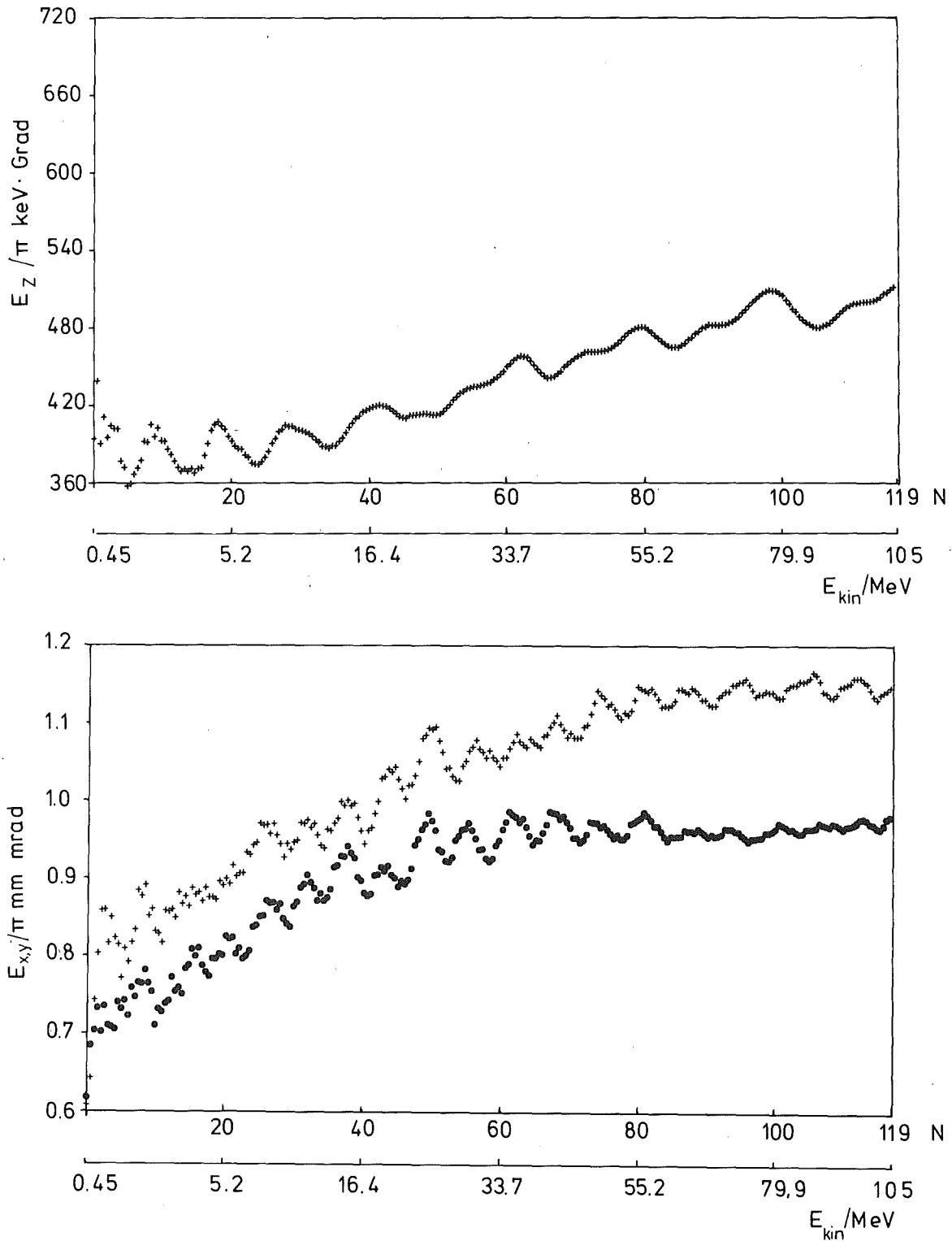


Fig. 5 Normalized rms-emittance along the Alvarez accelerator (at the top the longitudinal  $E_z$ , at the bottom the transverse ones  $E_x$ ,  $E_y$ ;  $N$  = drift tube number,  $E_{kin}$  = proton energy)

Other problems, like the longitudinal to transverse coupling or space charge effects are of less importance in the disk-and-washer beam dynamics. The coupling is appreciably reduced due to the higher proton velocity and due to the higher accelerator frequency. The space charge forces are reduced because the bunch volume has increased due to the longitudinal bunch lengthening correlated to the phase damping and due to transverse emittance growth. In addition, longitudinally the ratio of space charge force to focusing rf force is reduced by the rf frequency ratio of 3.

The disk-and-washer accelerator design was checked by a multiparticle simulation<sup>10</sup>. The matching parameters for this calculation were not optimized as yet. Nevertheless, all macro particles were transported through the disk-and-washer accelerator without any loss. Fig. 6 shows the transverse beam envelope as a function of the proton energy. The beam diameter stays about a factor of 2 smaller than the beam hole up to 350 MeV energy. In the present design the beam was not properly matched to the change of the transverse focusing periodicity at this energy which caused large envelope oscillations thereafter. This can be avoided in an optimized design.

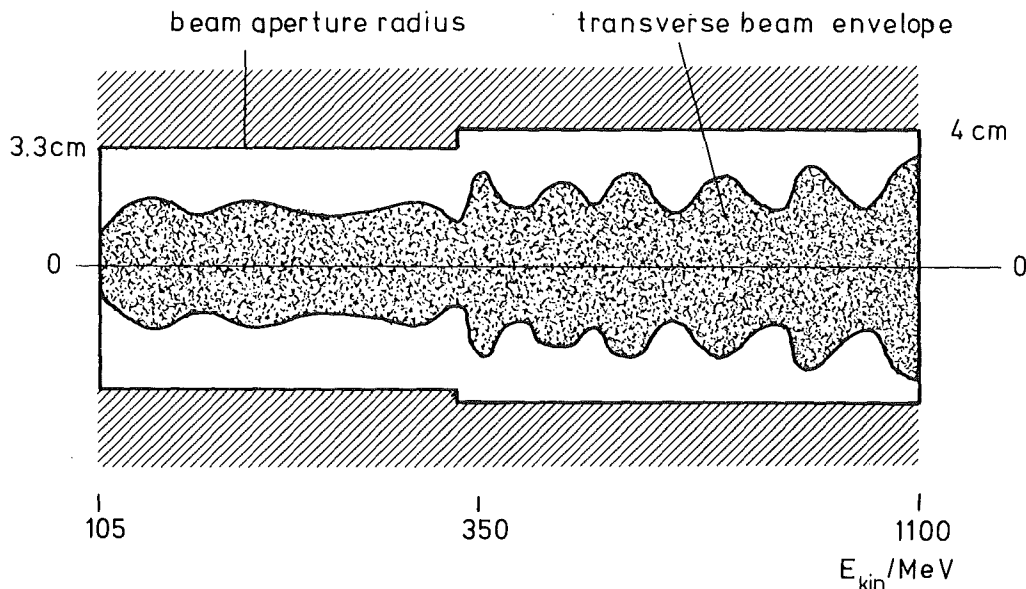


Fig. 6 Transverse beam envelope along the disk-and-washer accelerator,  $E_{kin}$  = proton energy

Having the accelerator properly designed the most important methods to minimize the beam spill are the following. Beam halo scrapers cut the maximum beam size to about half the aperture size, suitable locations being the LEBT, the first Alvarez accelerator tank, and the matching sections at 105 MeV and 350 MeV. Enhancing the action of the third buncher on the LEBT, the longitudinal tails of the bunch can be thrown away at relatively low energies by properly reducing the longitudinal Alvarez acceptance, a method successfully applied at LANL<sup>11</sup>. Further, of utmost importance is the careful diagnostic, control and adjustment of the various accelerator

parameters during the accelerator operation. A prognosis about the beam spill and the resulting activation to be expected for the SNQ accelerator can be guided by the operating experience with the 800 MeV proton linear accelerator in Los Alamos (LAMPF)<sup>12</sup>. At present this accelerator routinely achieves 0.6 mA average beam current. The accelerator tunnel is accessible soon after machine shut-down. Beam spill is no serious problem any more for this linear accelerator. Right now it could accelerate already 1.1 mA average current, the limitation being solely the meson target design<sup>13</sup>.

#### Acknowledgement

This work has benefitted to a large extent from contributions by K. Bongardt, K. Crandall, H.G. Hereward, M. Pabst, D. Sanitz, D. Warner and M. Weiss.

Literature

1. J.E. Vetter, editor, The Basic Concept of the SNQ Linear Accelerator, Kernforschungszentrum Karlsruhe, KfK 3180 B (1981)
2. K. Mittag, Beam Dynamics in a Proton Linear Accelerator for a Neutron Spallation Source, Linear Accelerator Conference, Montauk, USA, BNL 51 134 (1979), 253
3. E. Boltezar, M. Weiss, Low Energy Beam Transport System for the German Spallation Neutron Source, private communication
4. R.H. Stokes, T.P. Wangler, K.R. Crandall, The Radio-Frequency Quadrupole - A New Linear Accelerator, Proc. of the 1981 Part. Acc. Conf., March 11-13, Washington, DC (1981), to be published
5. H.G. Hereward, On Beam Losses in the Linear Accelerator of the Neutron Spallation Source, private communication
6. K. Goebel, private communication
7. H.G. Hereward, Notes on Beam Dynamics in a Linear Accelerator for the Neutron Spallation Source SNQ, Part III, private communication
8. I. Hoffmann, Emittance Growth of Beams Close to the Space Charge Limit. Proc. of the 1981 Part. Acc. Conf., March 11-13, Washington DC (1981), to be published
9. M. Pabst, K. Bongardt, Note on Tolerances in Rf Linear Accelerators, private communication
10. K. Crandall, private communication
11. A. Browman, private communication
12. D.C. Hagerman, private communication
13. R.J. Macek, D. Boehne, private communication

INJECTION SYSTEM FOR THE PROTON STORAGE RING AT LASL\*)

Daniel W. Hudgings and Andrew J. Jason

Los Alamos Scientific Laboratory, Los Alamos, NM 87545 USA

ABSTRACT

The Proton Storage Ring at LAMPF will accumulate a high current of 800-MeV protons by multiturn charge-changing injection. An 800-MeV neutral hydrogen atomic beam, formed by field ionization of H<sup>-</sup> ions in a 1.8 T transverse magnetic field, will be stripped to protons by a carbon foil. To minimize peak proton current on the foil, the beam orbit will be deformed so that the edge of the beam grazes the edge of the foil. As the beam diameter grows, the orbit perturbation is decreased, vanishing at the end of the accumulation cycle. The hardware requirements are simple. Single-turn orbit deformation magnets are pulsed to peak field and switched across power dissipation circuits that control the field decay rate.

Stripping foil requirements and a method of calculating the desired orbit deformation are described.

1. INTRODUCTION

High-current 800-MeV proton beams will be accumulated in the Proton Storage Ring (PSR) at LASL by multiturn charge-changing injection of H<sup>-</sup> ions from the LAMPF linac. Two modes of operation will be used: a short-bunch mode in which six bunches of 10<sup>11</sup> protons are accumulated in 108 μs, and a long-bunch mode in which a 270-ns bunch of 5.2 x 10<sup>13</sup> protons is accumulated in 750 μs<sup>1)</sup>. Peak current in the long-bunch mode is 46.3 A, with the injection and extraction cycle repeated at a 12-pps rate.

A chopper in the low-energy transport between the 750-kV injector and Alvarez linac section at LAMPF prepares the beam in the required temporal format<sup>1)</sup>. After acceleration to 800 MeV the beam is switched into beam line D and deflected from line D into the PSR injection line by a kicker magnet and skewed dipole. Figure 1 shows the rest of the injection system in summary form. Another skewed dipole directs the beam approximately collinearly to the circulating beam in the injection straight section of the PSR. Achromatic transport in the injection line is achieved by focusing elements that cause cancellation of the dispersion of the two bend magnets. Both the horizontal and vertical phase ellipses rotate significantly in the drift space between the third quadrupole and second skewed dipole. This permits us to remove the nominally Gaussian edges of the injected beam to the 3-σ level by stripping on a series of foil apertures. The unwanted stripped beam is deflected into a beam dump by the skewed magnet. Programmed steering magnets adjust the ion beam trajectory through a stripping magnet (which converts H<sup>-</sup> to H<sup>0</sup>) onto the stripping foil (which converts H<sup>0</sup> to H<sup>+</sup>). Unstripped H<sup>0</sup> beam drifts through a dipole magnet into a beam dump. Programmed bump magnets in the PSR radially deform the closed orbit to control the profile of the accumulating beam.

2. CHARGE CHANGING INJECTION

A novel two-step charge-changing scheme will be used for injection into the PSR<sup>2)</sup>. Figure 2 shows the 1/e stripping length of 800-MeV H<sup>-</sup> ions as a function of magnetic field in the laboratory frame of reference, as measured in a recent experiment at LAMPF<sup>3)</sup> and as calculated from the results of Stinson, et al.<sup>4)</sup>.

\*) Work performed under the auspices of the US Department of Energy.

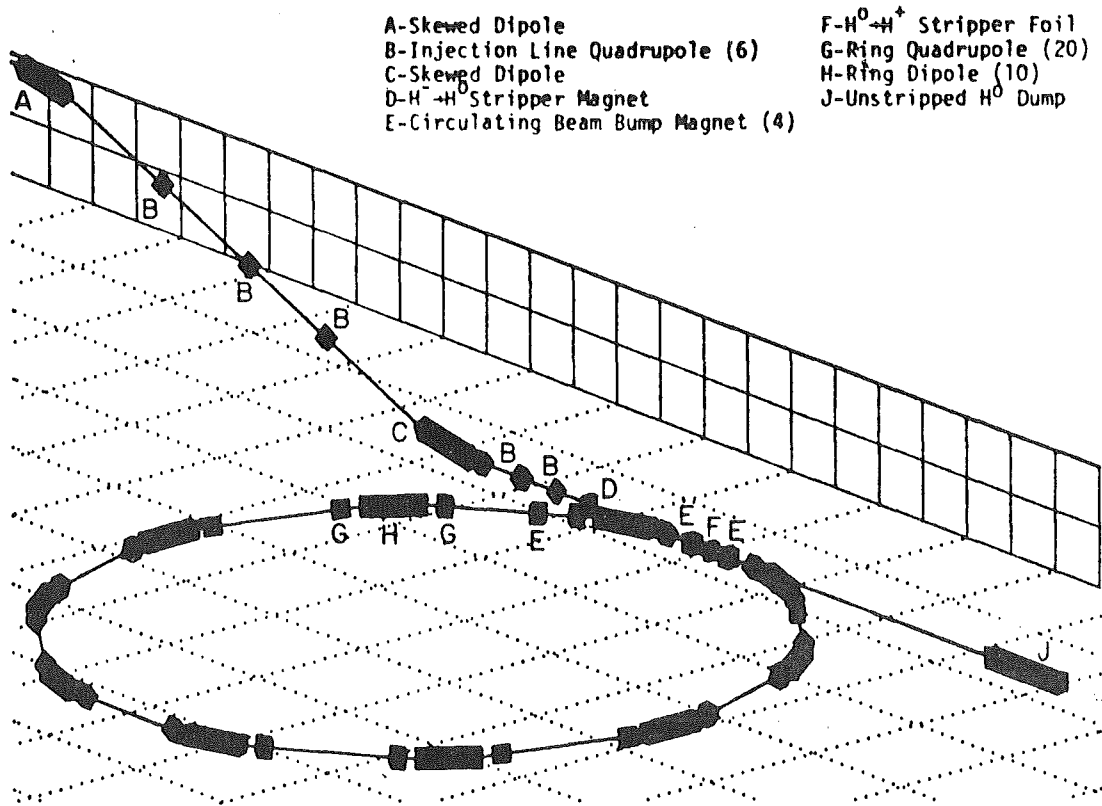


Fig. 1. PSR injection system schematic.

Charge-changing injection is necessary because the accumulation of beam for many (300 to 3000) machine circulation periods requires the brightness of the circulating beam to exceed that of the injected beam. Conventionally, this is done by blending the injected H<sup>-</sup> beam and the circulating H<sup>+</sup> beam in a magnetic field and directing them through a stripping foil.

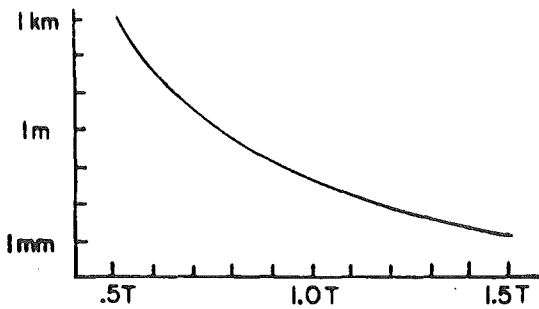


Fig. 2. 1/e Lorentz stripping length H<sup>-</sup> to H<sup>0</sup> for 800-MeV H<sup>-</sup> ions as function of magnetic field.

Because field stripping of 800-MeV H<sup>-</sup> ions is a significant effect for bending radii less than 12.8 m, this method is difficult to implement for the PSR. The ease with which the H<sup>-</sup> ion can be Lorentz stripped is a problem in beam transport, but can be used to great advantage. By stripping the H<sup>-</sup> ion beam to neutral hydrogen in a strong transverse magnetic field, the beam can be passed unperturbed through a ring dipole and focusing quadrupole to the foil, which then strips it to H<sup>+</sup>. The H<sup>0</sup> beam can be "painted" across the stripping foil in the

vertical direction during the injection cycle by pulsed steering magnets that precede the stripping magnet. An increase in beam angular divergence, caused by the stripping process, of  $< 1.6$  mrad was measured in an experiment at LAMPF using a simple dipole magnet<sup>3)</sup>. A smaller divergence increase should be achievable using the specially designed magnet intended for the PSR injection system<sup>2)</sup>.

3. STRIPPING FOIL CONSIDERATIONS

A carbon foil will strip the  $H^0$  beam to protons. The parameters considered in selecting foil thickness were beam emittance growth from multiple scattering in the foil, foil lifetime, stripping efficiency, and the release of radioactive material from the foil. A minimum foil thickness of  $\sim 200 \mu g cm^{-2}$  is required for at least 95% stripping efficiency, to limit the beam absorbed in the neutral beam dump to  $5 \mu A$ . For this foil thickness the other parameters are acceptable. Less than one part in  $10^{12}$  of the circulating beam is lost because of elastic scattering. Inelastic scattering results in losses of  $\sim 30$  nA in the region immediately downstream of the foil. Foil activation in long-pulse service is summarized in Table 1.

Foil heating rate is determined by the circulating beam-current density on the foil. The characteristic time for temperature decrease by thermal radiation, the only significant heat-loss mechanism, is several times the  $750\text{-}\mu s$  beam accumulation period. Thus the foil's peak temperature is largely independent of thickness, and depends only on its specific heat, differential stopping power, and the beam-current density. For the injection programming scheme described below, the peak foil temperature should be  $\sim 1200^\circ C$ .

Radiation damage may be the key factor limiting foil lifetime. Damage estimates predict minimum lifetimes of hours for suitably prepared foils. Foils will be mounted on frames in a device that permits automatic and rapid replacement of damaged units.

4. PHASE-SPACE CONTROL

An advantage of multiturn beam accumulation is that the transverse phase-space distribution of the beam can be controlled by steering the injected beam and the circulating beam on the stripping foil.

Injected beam is accumulated on the surface of the circulating beam. This has the advantage of zero closed orbit perturbation at the end of the injection cycle, when the accumulated beam and resultant tune shifts are greatest. The foil intersects only a fraction of the X-X' phase-space projection of the beam and thus is struck by each stored

proton only in a fraction of its circuits around the ring. This process is illustrated in Fig. 3, which shows the X-X' phase space occupied by the beam near the beginning and at the end of the accumulation period.

Beam accumulation can be described by a Green's function method. Assuming an irrational

Table 1  
Carbon Stripping Foil Activation for 2-hour Service

<u>Isotope</u>	<u>Half-life</u>	<u>2-hr. Activation</u>
C <sup>11</sup>	20 min	0.37 Ci
H <sup>3</sup>	12.3 yrs	3.2 $\mu Ci$
Be <sup>7</sup>	53.4 days	130 $\mu Ci$

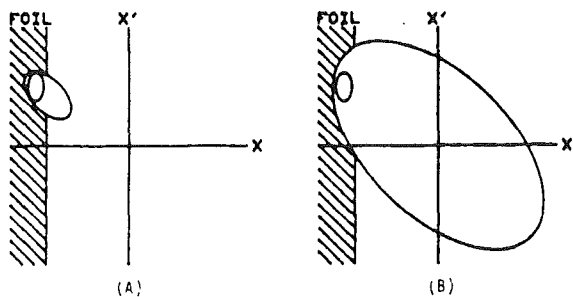


Fig. 3. Beam Accumulation:  
 (A) Near beginning of accumulation period with circulating beam displaced toward foil.  
 (B) End of accumulation period, circulating beam centered on unperturbed equilibrium.

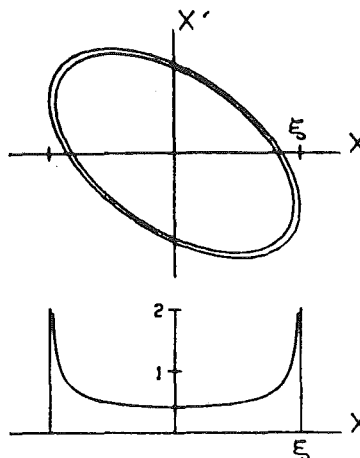


Fig. 4. Green's function for beam accumulation.

horizontal tune so that spatially impulsive injection distributes beam uniformly into a narrow annulus in the X-X' projection of the beam phase space, the appropriate Green's function is

$$G(X, \xi) = (1/\pi)(\xi^2 - X^2)^{-1/2} [H(\xi - X) - H(-\xi - X)] \quad (1)$$

where H is the Heaviside step function and the variable  $\xi$  is the x-component of the injection radius relative to the beam axis. This is illustrated in Fig. 4. The beam distribution shown in Fig. 5 is obtained for

$$\xi(t) = X_{\max} (1-t/t_{\max})^{1/2} H(t) H(t_{\max} - t) \quad (2)$$

where  $X_{\max}$  is the half-width of the fully accumulated beam and  $t_{\max}$  is the accumulation time. Rapid injected beam movement near the center of accumulated beam, as is the case for Eq. 2, is necessary to avoid beam pileup. This type of analysis has been extended to bivariate distributions and finite injection spot size.

Beam profile also can be controlled by programming the vertical size of the injected beam spot on the stripping foil, which, along with the bump magnet system, permits simultaneous control of both transverse components of the distribution. This function is provided by the final quadrupole in the PSR injection line.

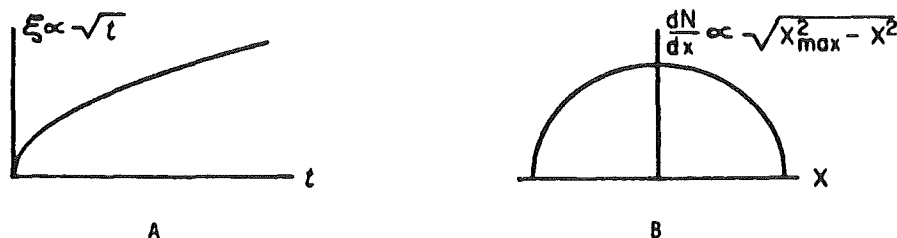


Fig. 5. Beam-bumping program (A) produces beam distribution (B).

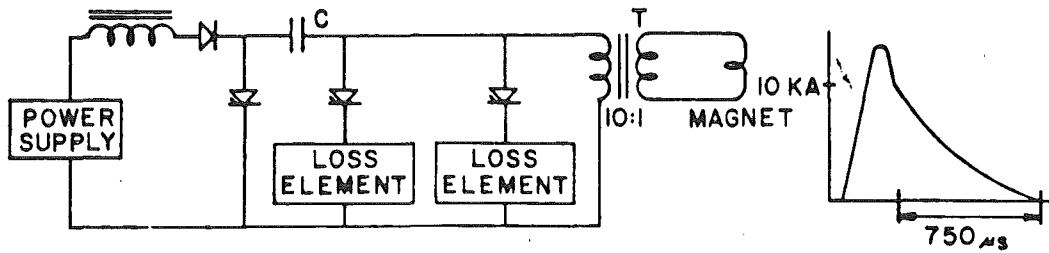


Fig. 6. Pulsed power supply for bump magnets. Loss elements are switched in after peak of field is passed, to control rate of field decay. Thyristor trigger elements are not shown.

Figure 6 shows a schematic of a pulsed power supply for driving the single-turn bump magnets that deform the closed orbit. The energy stored in capacitor C is switched through transformer T into the field of the magnet. Energy dissipation elements are switched across the primary side of the transformer to control the rate of field decay.

The transformer, which permits switch operation at a practical impedance level, is a low inductance type developed for controlling a plasma pinch device<sup>5)</sup>. The switches are thyristors. For energy dissipation elements we have used resistors in series with zener diodes or zener diode/power transistor combinations. A tenth-scale model using an active feedback circuit and power transistors for the dissipative element was tested successfully, but no full-scale actively regulated circuit has yet been tried.

#### 5. CONCLUSION

We have designed an injection system for the PSR that utilizes the best features of a unique asset: an 800-MeV  $H^-$  ion injector. The high beam energy makes possible neutral beam injection. Neutral injection and the low emittance of the injected beam permit multiturn beam accumulation with low loss and precise control of the circulating beam profile. The ability to change easily the beam distribution function in the PSR should make it an attractive test bed for investigating high-current accumulation in a proton storage ring.

\* \* \*

#### REFERENCES

- 1) G. P. Lawrence, R. K. Cooper, D. W. Hudgings, G. Spalek, A. J. Jason, E. F. Higgins, and R. E. Gillis, private communication
- 2) D. W. Hudgings, Trans. IEEE NS-26, p. 3556, (1979).
- 3) A. J. Jason, D. W. Hudgings, W. M. Folkner, O. B. Van Dyck, and D. Clark, to be published.
- 4) G. M. Stinson, S. C. Olsen, W. J. McDonald, P. Ford, D. Axen, and E. W. Blackmore, Nucl. Instrum. Methods, 74, 333 (1969).
- 5) R. T. Buck, J. D. Galbraith, and W. C. Nunnally, Conf. Proc. of 8th Symp. on "Engineering Problems of Fusion Research," San Francisco, CA 1979.



PROTON INDUCTION LINACS AS HIGH-INTENSITY NEUTRON SOURCES\*

Denis Keefe and Egon Hoyer

Lawrence Berkeley Laboratory  
University of California  
Berkeley, California 94720

Abstract

Proton induction linacs are explored as high intensity neutron sources. The induction linac - concept, properties, experience with electrons, and possibilities - and its limitations for accelerating ions are reviewed. A number of proton induction linac designs are examined with the LIACEP program and general conclusions are given. Results suggest that a proton induction accelerator of the lowest voltage, consistent with good neutron flux, is preferred and could well be cost competitive with the usual rf linac/storage ring designs.

---

\*This work was supported by the Assistant Secretary for Defense Programs, Office of Inertial Fusion, Research Division of the U. S. Department of Energy under Contract No. W-7405-ENG-48.

## PROTON INDUCTION LINACS AS HIGH-INTENSITY NEUTRON SOURCES\*

Denis Keefe and Egon Hoyer

Lawrence Berkeley Laboratory  
University of California  
Berkeley, California 94720

### 1. Induction Linac Concept and Properties

An induction linac is composed of a sequence of independent pulse-power modules each of which adds an increment,  $\Delta V$ , to the beam voltage (kinetic energy/charge state of ion). Within or between the modules, focussing elements -- electrostatic or electromagnetic -- are used to transport the beam.

The evolution of the concept in terms of a transmission-line analogy can be seen by reference to Figure 1. Here, a rectangular voltage pulse derived from a pulsed-power source (pulse-forming network or line, or a Marx generator) will provide an accelerating voltage across the gap (Fig. 1(a)) for the duration of the pulse, provided the shorted end of the transmission-line is far enough away that the inverted reflection does not return too soon. For a vacuum transmission line this transit-time isolation makes a satisfactory system for pulses of the order of 10 nanosec since the dimensions can be kept to the order of 1 meter. For much longer pulses, however, the dimensions can be kept manageable (Fig. 1(b)) by changing the propagation speed through the use of ferromagnetic or dielectric loading. The former is preferred because it presents a higher impedance to the generator. Suitable materials include ferrite, thin iron tape ( $\leq 0.1$  mm to reduce eddy-currents), or the new amorphous iron materials now becoming available.

Instead of simply stacking the cores one behind the other to give incremental voltage increases, various geometrical arrangements of the cores can be made to give voltage step-up per gap -- either axially (Fig. 1(c)), or radially (Fig. 1(d)).

The key utility of this device rests on the ability of pulsed-power systems to supply very high peak-power ( $\sim$  gigawatts) for short periods of time.(1) With a typical operating voltage per module in the range 0.1 - 1.0 MV, beam currents anywhere in the range  $10^2$  to  $10^5$  amperes can be efficiently accelerated. Note that this far exceeds the capability of rf linacs for which a typical beam current is about 1 ampere or less.

### 2. Experience with Induction Linacs for Electrons

The first induction linac was conceived by N. Christofilos and built at Livermore more than twenty years ago as an injector for the Astron experiment.(2) After successive modifications, it operated reliably for many years with a beam current of about 1 kA, a pulse-length of 300 nanosec., a voltage of 6 MeV, and a repetition rate capability of 30 Hz. A simpler and more elegant machine based on

---

\*This work was supported by the Assistant Secretary for Defense Programs, Office of Inertial Fusion, Research Division of the U. S. Department of Energy under Contract No. W-7405-ENG-48.

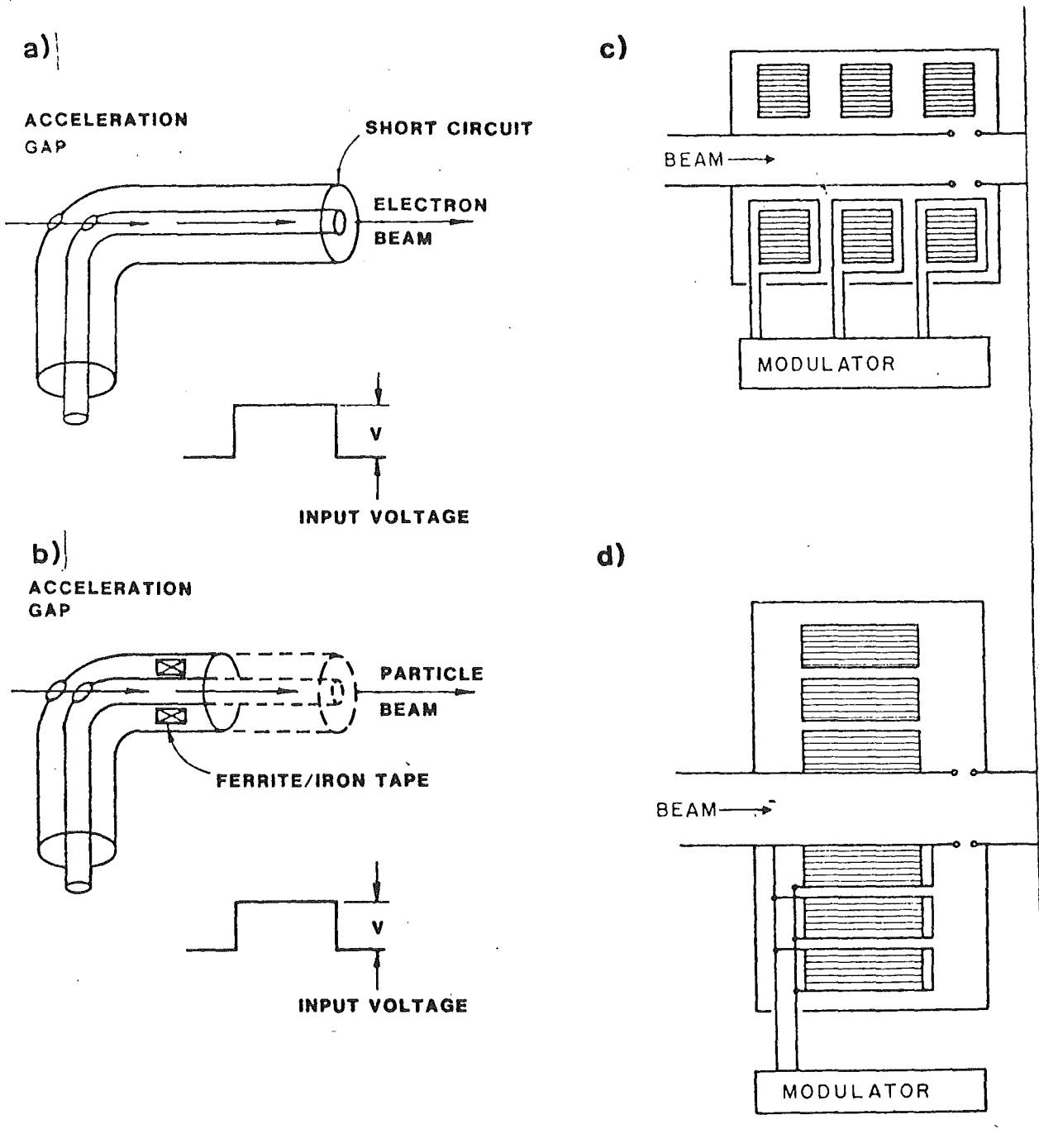


Fig. 1: Evolution of the induction linac geometry. In (a) it can be seen that a shorted transmission line with a hollow center conductor can accelerate particles across the gap shown; the voltage disappears, however, when the inverted reflection returns, from the shorted end to the gap. For pulses much longer than a few nanoseconds this would provide a very low accelerating gradient. In (b) ferromagnetic material increases the electrical line-length and thus allows long pulse-length without sacrificing gradient. Several cores driven in parallel can provide increased gap voltage; they may be stacked axially (c) or radially (d). The latter was the choice for the NBS 2  $\mu$ sec induction linac.

TABLE 1: SOME ELECTRON INDUCTION LINACS

Accelerator	Astron Injector Livermore, 1963	ERA Berkeley, 1971	NEP 2 Injector Dubna, 1971	ATA Livermore, 1976	NBS Proposed, 1971
Kinetic					
Energy, MeV	3.7	4.0	30	50	100
Current, Amps	350	900	250	10,000	2,000
Pulse					
Duration, ns	300	2-45	500	50	2,000
Pulse					
Energy, J	0.4	0.1	3.8	25	400
Rep Rate,					
pps	60	0-5	50	5	1
Number of					
Switches	300	17	750	200	250

ferrite cores, better matched to a shorter pulse length requirement, was operated for many years at Berkeley.(3) The U. S. National Bureau of Standards pioneered the development of long pulse (2  $\mu$ sec) modules.(4) A selection of induction linacs for electrons is included in Table 1 which shows some of their important parameters. The reader is referred to Reference 5 for a description of some other classes of induction linac that do not use ferromagnetic loading.

It will be seen from Table 1 that the pulse length has typically ranged from several nanoseconds to several microseconds. Applications have normally demanded high peak power and low average power. Below a repetition rate of several tens of Hertz, spark gaps offer the least expensive switch solution; higher repetition rates are achievable, if desired, by the use of more expensive thyratrons or vacuum tubes.

Finally, it should be noted that an advanced technology accelerator (ATA) under construction at present will advance the voltage and current achievements by an order of magnitude apiece beyond those of the earlier accelerators, namely, to 50 MV and 10,000 A respectively.

A common feature of electron induction linacs is that, because the particles are launched from the gun area with relativistic speeds, it is not possible to accomplish any significant bunching thereafter. Thus the current and the bunch length remain the same throughout the accelerator. The design of an electron machine is thus rather simple since it requires the sequential placement of identical modules each with the appropriate number of volt-seconds of core. Solenoid lenses are adequate to handle the beam focussing.

### 3. Induction Linacs for Ions

When the possibility of using short pulses of high-intensity heavy ions to drive the implosion of small deuterium-tritium pellets to achieve inertial-confinement fusion was first proposed,(6) it seemed a natural choice to examine the induction linac as a candidate.(7) An immediate apparent difficulty is that at low energies currents of only several

amperes can be transported whereas a current of 10-20 kA is needed at the target. A striking new feature in this application, however, was recognized,(7) in that the ions travel, by and large, with sub-relativistic speeds ( $\beta \approx 0.3$ ); thus bunching and consequent current amplification becomes a new degree of freedom not available in electron devices.

In any linac, if the accelerating fields have been established prior to entry of the bunch of charge, the head of the bunch will experience acceleration at the moment of its entry, and earlier in time, than the remaining parts of the beam. In this case the bunch becomes extended in length and continues to do so in such a way that the beam-current remains constant throughout the entire linac. If, instead, in an induction linac, the entire bunch length (perhaps 20-30 m long) is inserted into the linac structures and then the fields are pulsed on, the head and tail of the bunch (and parts between) can all observe the same acceleration at the same time and the bunch length will remain a constant throughout the whole acceleration process. In this case the bunch duration,  $\tau = L/\beta c$ , decreases directly as  $1/\beta$  and the current increases proportional to  $\beta$  during the acceleration process. Because the voltage waveforms applied to the induction modules can be chosen to have a variety of shapes, a further strategy becomes possible, viz., by introducing a modest ramp on the voltage the rear portions of the bunch can be accelerated somewhat more than the front. Thus, the bunch length can in fact be gradually compressed and the current amplified during acceleration at a rate proportional to  $\beta^k$ , where  $k > 1$ .

A major consideration in the design of an ion induction linac is that the beam current is limited to inconveniently low values by the inability of the quadrupole transport system to handle large amounts of space-charge. As pointed out by Maschke,(8) for magnetic quadrupoles the current limit is

$$I_M = 1.7 \times 10^6 (A/Z)^{1/3} (\epsilon_N \eta B)^{2/3} (\beta\gamma)^{5/3} \text{ amps} \quad \text{Eq. (1)}$$

where  $A, Z$ , are the atomic weight, number, of the ion,  
 $\epsilon_N$  = normalized emittance (meters),  
 $B$  = quadrupole "pole-tip" field (maximum  $\approx 5T$ ),  
 $\eta$  = fraction of length occupied by quadrupoles.

For a heavy ion fusion driver ( $A \approx 200$ ),  $I_M$  varies from a few amperes at injection, to a few thousand amperes at full energy ( $\beta \approx 0.3$ ). To make best use of the induction linac it is important to choose a design that can handle a current as high as possible (within reason) at all points along the accelerator. Thus it is advantageous to arrange for some pulse-length compression so that the current amplification exponent,  $k$ , defined in the previous paragraph, can approach the value 5/3 (see Eq. 1). Other constraints, however, can enter; for example, the bunch compression must be halted if the longitudinally defocussing self-fields at the bunch ends become too strong.

A procedure has been developed at LBL to examine at any given point along the accelerator how one can choose the design of accelerator modules and associated transport system to minimize the cost,  $\Delta C/\Delta V$ , to add a further unit increment in voltage.(9) In brief, one can see from

Eq. 1 that one would tend to choose values for  $n$  close to unity in order to achieve high current, but that would result in leaving no space for accelerating modules. On the other hand, making  $n$  small decreases the current and, for a given charge,  $[I\tau]$ , in the beam, leads to a long pulse duration,  $\tau$ , thereby necessitating a large investment in volt-seconds of core to achieve the next increment of voltage. Thus, one can see how a reasonable optimum solution must exist between these extremes. In the computer program, LIACEP, one specifies, to begin with, the ion mass and charge state, the emittance, the allowed betatron tune depression (usually from  $60^\circ$  to  $24^\circ$  in terms of phase advance per period), the pulse repetition rate, and proceeds with optimization at each voltage point along the machine for a wide variety of assumed total beam charge,  $[I\tau] = 30 \mu\text{C}, 60 \mu\text{C}, \dots, \text{etc.}$  A pre-chosen set of engineering design options and a variety of ferromagnetic material are cycled through to find the most suitable solutions at each point.

The region of parameter space that has been most explored has been centered on  $A > 200$ ,  $Z < 6$ ,  $\epsilon_N = 3 \times 10^{-5}$  rad-m,  $Z_eV = 10$  GeV, final energy  $\approx 1-10$  MJ,  $[I\tau] \approx 200-600 \mu\text{C}$ , pulse rate 1-10 Hz. Almost all of these are quite far from the parameters of interest for a proton induction linac to produce neutrons but the procedure is still applicable even if the results need more caution in interpretation. Three important differences between the heavy-ion driver and proton INS cases should be borne in mind:

(i) The heavy ions are in essence non-relativistic throughout the course of acceleration ( $\beta < 0.3$ ). Bunch length compression is accomplished at quite low speeds ( $\beta < 0.1$ ) and the bunch-length held at a constant value thereafter until a final impulsive compression stage in the final transport system to the target. By contrast, protons can be considered as non-relativistic when their kinetic energy is less than 100-200 MeV for bunch-length compression purposes. Thereafter, if one assumes a final energy of 1 GeV, current amplification can occur significantly only through the  $\beta$ -factor which saturates as  $\beta$  tends towards unity.

(ii) Creation and preservation of a low-emittance beam is crucial in the design of a heavy-ion driver for which it is essential that the beam ultimately be focussed, at a stand-off distance of some 10 m, to a spot a few millimeters in radius. Taking into account the difference in  $\beta\gamma$  and the relaxed target conditions, it would seem to us that, perhaps, two-orders-of-magnitude greater normalized emittance could be tolerated for a proton induction linac for an INS. Since the normalized emittance,  $\epsilon_N$ , occurs to the 2/3 power in Eq. 1 this could alter the space charge limit by a factor of twenty!

(iii) The zero-th order cost-determining factor in our heavy-ion driver studies turned out to be simply the beam energy in joules,  $[I\tau]V$ . There is a weak dependence upon emittance within the narrow range allowed (bigger  $\epsilon_N$  is better), weak dependence on charge-state -- within a narrow range -- (higher  $Z$  is better), and substantial gains observed by incorporating several independently focussed beams within a single induction-linac accelerator structure. For reasons we do not yet fully understand, the result for the example proton linacs examined had quite dramatically different indications, namely, that the cost seemed to be more significantly related to the final beam voltage and not to the final joules in the beam. This is probably because of the significantly lower charge accelerated.

Finally, it should be remarked that a major program element in the LBL efforts towards heavy-ion fusion has been research and development on long-pulse (several micro-second) induction modules suitable for the front-end of an ICF driver. Despite support and encouragement from the U. S. Department of Energy, financial support for this basic R D has not been forthcoming and we have been able to pursue only small-scale model tests to seek out the more prospective candidates for ferromagnetic core material. Part of that low-level program has included a cooperation with Allied Chemical who are the producers of the amorphous-iron material registered as Met-Glas.

To conclude this section, it should be recorded that Nation has reported accelerating several hundred amperes of protons with an induction linac module.(10) The beam probably had a large component of electrons, which, while supplying space-charge neutralization, also provided a drain on the generator and a backward bombardment of the ion source.

#### 4. Induction Linacs for Intense Neutron Sources

To our knowledge, the first person to draw attention to the possibility of using the very large current, short pulse capability of the induction linac for neutron production was C. Bowman.(11) He proposed that a 10 MeV, 1000 ampere electron induction linac with a 30 nanosecond pulse could produce an average neutron rate of  $3 \times 10^{14}$  per second by bombarding a suitable target containing beryllium or deuterium. To achieve this rate would require a pulse repetition frequency of 1000 Hz; except in this one respect his suggested parameters are well within past and tried technology. At 1000 Hz, spark-gap switches are probably inappropriate but thyratrons and vacuum tubes are viable alternatives.

From studies for heavy-ion fusion drivers the two major candidates have been identified as the low-current rf linac followed by a current-amplifying storage ring, on the one hand, or the single-pass induction linac in which current amplification is accomplished during acceleration. Recognizing the correspondence between the similar - if less demanding - requirements for a spallation source and, also, that only the former candidate has so far been considered, Foss has recently looked at the induction linac as a possible design concept alternative.(12) His goal was not to develop dimensions, gradients or any engineering features of a design but rather to establish the feasibility of bunching the proton beam in a "buncher" section - in which the current is kept just below the space charge limit and then to enter a purely "accelerating" section in which the current remains more or less constant throughout. His single-particle bunching calculations parallel those done by Laslett (13) for a heavy ion test bed - which, in addition, included longitudinal space-charge effects - but have the advantage of being explicitly for protons.

Our approach taken in this early examination of the problem is different, however, and starts from an engineering evaluation of how the beam can be most economically accelerated and transported from point to point down the length of the accelerator (see previous section regarding LIACEP program). Whether the physics of the implied bunching process to meet the minimum-cost goals is reasonable or not must be examined as a separate issue. While we are confident in knowing that solutions exist

for the heavy ion driver case ( $\beta=0.3$ ,  $\gamma=1.05$ ), some caution is needed in accepting the results for the present examples where  $\beta=0.875$  and  $\gamma=2.07$ . As noted earlier, ultra-relativistic electrons cannot, in practice, be bunched whereas non-relativistic ions can; for a proton accelerator of 1 GeV we are dealing with an intermediate case. Most of the bunching by modestly ramping the voltage pulses is carried out at low velocities. Later, the degree of difficulty - in terms of the magnitude of the ramp - is essentially determined by the relativistic increase in longitudinal mass,  $m\gamma^3$ ; one could thus assume that any voltage ramps needed would still be of reasonably modest proportions up to  $\beta$  between 0.6 and 0.7 ( $T \sim 230 - 370$  MeV) where the  $\gamma^3$  factor is about 2. Beyond that, however, current amplification of more than a factor of two becomes very difficult.

We were gratified to note that the economically most advantageous strategy of pulse-time compression by a factor of 1/10, between 1 and 10 MeV, is in agreement with the physics-based estimates by Foss. Since this is well within the non-relativistic domain, which had been examined for various heavy-ion scenarios in detail, it is not surprising.

## 5. Results

Some parameters proposed for neutron sources appear in Table 2. It would be nice to report that we can present cost estimates for a variety of induction linac scenarios. Unfortunately, we can not, but have arrived at the important conclusion that the proton induction linac is a candidate worthy of careful scrutiny for the pulsed neutron source application. Major uncertainties in cost stem from several main reasons:

TABLE 2: PARAMETERS OF SOME OPERATING OR PROPOSED NEUTRON SOURCES

Neutron Spallation Source	Kinetic Energy (MeV)	Repeti- tion Rate (Hz)	Pulse Length ( $\mu$ sec)	Charge per Pulse ( $\mu$ C)	Normalized Emittance mm-mrad.	Average Beam Power (MW)
IPNS-1	500	30	01.00	0.5		0.01
KENS	500	20	< 1	0.1	20 $\pi$	0.001
SNS	800	50	0.100	4	80 $\pi$	0.17
PSR	800	12	0.250	8	30 $\pi$	0.1
		(720)	(0.001)	(0.01)		
SNQ	1,100	100	500	50	15 $\pi$	5.5
			(< 1)	(45)		

a) No very large induction linac system has been built which one can use as a calibration point. The largest in the U.S. is the ATA, still under construction; it will provide a 500 $\mu$ C beam at 10kA and 50 MeV.

b) The level of effort in exploring this question for ions has been confined to the part-time activity of two or three people at Berkeley.

c) We have used two quite different cost bases for exploring a cost-minimum optimization routine;

(A) Assume you must proceed immediately with a low-energy accelerator on the basis of conservative assumptions and proven technology. Examples: (i) assume 250kV per Marx generator—a proven technology of more than a decade ago for rep-rated induction linacs; (ii) Silicon steel tape in 0.001 ins thickness is not immediately an economic choice; use 0.002 in. thick material at current prices. The origin of this cost basis, labelled "conservative" or C, derives from the urging by the U.S. DOE Office of Inertial Fusion in 1979 to proceed rapidly to a 10-50 MeV test bed for Heavy Ions.

(B) Estimate the future(F) cost of a heavy ion driver in the megajoule range — an accelerator that will cost several hundred million dollars. Here, one must assume some years of research, development, and prototyping to develop cheaper insulators, better ways of fabricating and packaging cores, development of better ferromagnetic materials, e.g. amorphous iron materials, and higher voltage for reliable and rep-rateable pulse-power generators. (In the last case, the present rep-rated performance is regularly in the 350 kV — 400 kV range at LBL).

For the purposes of this discussion, unfortunately, the differences between Cost Basis C and Cost Basis F are too far apart to allow us to give any really meaningful cost estimates. We have run several examples with the following parameters:

$I \uparrow (\mu C) =$	5	10	20	80
$T(\text{GeV}) =$	1 and 2	1	0.5	0.125

with a variety of values of  $\epsilon_N$  in the range 20 to  $80\pi$  mm-mrad. We have assumed that only a single-beam is transported through the accelerator (multiple beams would be cheaper). We adopt a reference repetition rate of 20 Hz (spark-gap switches can be used up to  $\approx 100$  Hz if that is desirable — beyond that thyratrons would be better).

Some general conclusions were:

- Whether the "Conservative(C)" or "Future(F)" cost basis was used the derived prescriptions for how the beam current (and pulse duration), the magnet occupancy factor, quadrupole field and beam size turned out to be very similar (see figure 2, for one example). The biggest difference was that the final pulse-length for the F-basis, i.e. using amorphous iron, was at most a factor of two larger than with the C-basis.

- While the initial pulse was several microseconds long it could be dropped to 1/10 of this by the 10 MeV point

- Increase in  $\epsilon_N$  reduced costs some ( $\approx 10\%$  between  $40$  and  $80\pi$  mm-mrad).

- The F-costed accelerators always turned out to be about one-half the length of the corresponding C-costed cases — a direct reflection of the higher module voltage assumed. The corresponding gradients were about 2 MV/m and 1 MV/m, respectively.

- The most dramatic difference between the two cost bases showed up when the beam energy was fixed at 10kJ/pulse and the charge varied from  $5\mu C$  to  $80\mu C$ . On the C-basis the cost decreased sharply to

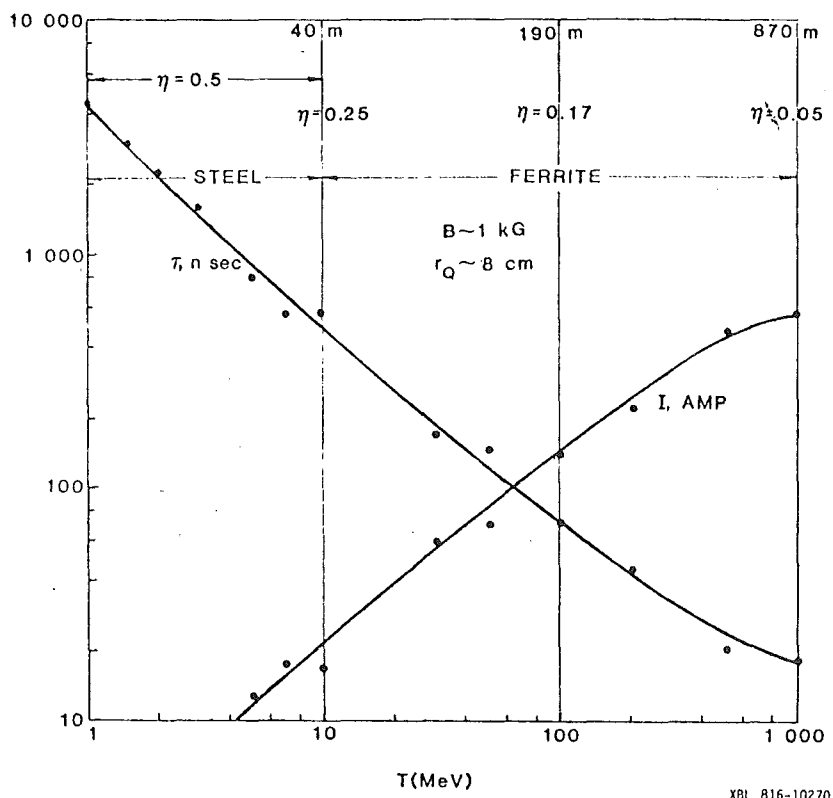


Figure 2: An example of how the current and pulse duration should vary to minimize the overall cost (on the conservative (C) basis). The fraction of space occupied by magnets,  $\eta$ , is indicated and can be seen to be small over most of the length. With the F cost-basis the length is halved.

one quarter with increasing charge. On the F-basis the change was less - to one half. This suggests strongly that choice of the lowest voltage machine, consistent with a good neutron flux, is preferred.

- If we fix our attention on a particular beam voltage, e.g. 500 MeV, we find for both the C and F scenarios that whether one accelerates  $5\mu\text{C}$  or  $10\mu\text{C}$  the cost is the same (a "single-particle" approximation), and to accelerate  $80\mu\text{C}$  is less than a factor of two more in cost.

Table 3 gives some representative results.

TABLE 3 - Proton Induction Linacs ( $f=20\text{Hz}$ )

$I\tau$ ( $\mu\text{C}$ )	T (MeV)	L (m)	$eN$ $\pi\text{mm mrad}$	$\tau_j$ $\mu\text{sec}$	$\tau_f$ $\mu\text{sec}$	$I_f$ amps
5	1000	470-890	25	5	.014	200-350
10	1000	460-870	80	5	.018	300-550
20	500	360-700	40	14	.05	375
80	125	235-365	80	33	0.3	250-280

Our final guess, based on a cursory survey, is that a 500 MV accelerator delivering 50 kJ per pulse can be built for significantly less than 100 M\$, given a serious design study and some aggressive research, development, and prototype work.

#### References

1. A. Faltens and D. Keefe: Proc. Xth Int. Conf. on High Energy Accelerators (Serpukhov), p. 358 (1977).
2. N. C. Christofilos, R. E. Hester, W. A. S. Lamb, D. D. Reagan, W. A. Sherwood and R. E. Wright: Rev. Sci. Inst., 35, 886 (1964).
3. R. Avery, G. Behrsing, W. W. Chupp, A. Faltens, E. C. Hartwig, H. P. Hernandez, C. MacDonald, J. R. Meneghetti, R. G. Nemetz, W. Popenuck, W. Salsig and D. Vanecek: IEEE Trans. Nuc. Sci., NS-18, 479 (1971).
4. J. Leiss, N. Norris and M. Wilson: Particle Accelerators, 10, 223 (1980).
5. D. Keefe: Particle Accelerators, 11, 153 (1981).
6. A. W. Maschke: Brookhaven National Laboratory Report BNL-19008 (1974); R. Arnold and R. Martin: Proc. Int. Conf. on Rad. Test Facil. for CTR, (ed. P. Persiani) (1975).
7. D. Keefe: private communication (1976).
8. A. W. Maschke: unpublished report, July 1976.
9. A. Faltens, E. Hoyer, D. Keefe and L. J. Laslett: IEEE Trans. Nuc. Sci., NS-26, 3106 (1979).
10. J. A. Nation, D. Aster and J. Ivers: Bull. Am. Phys. Soc., 25, 945 (1980)
11. C. D. Bowman: Nuc. Sci. and Eng., 75, 12 (1980)
12. M. Foss: IEEE Trans. Nuc. Sci., NS-28, 3181 (1981).
13. L. J. Laslett: in "50 Joule Induction Linac Proposal" LBL PUB-5039 (1980)

Discussion.

The neutron flux  $n$  is proportional to the charge and the kinetic energy per pulse, that means proportional to  $(I\tau) \cdot T$ . This quantity fixed the induction linac will become cheaper with increasing charge and decreasing energy. An induction linac accelerating an beam of  $80 \mu\text{C}$  to an energy of 125 MeV is cheaper than an induction linac accelerating  $20 \mu\text{C}$  to 500 MeV.

How to handle the first 10 MeV is described in the Proceedings of the Particle Accelerator Conferencies. The current between 1 and 10 MeV increases by about a factor 10.

The sources for protons are available. At LBL a multi-aperture source is developed, delivers a neutralized beam of about 10 Amps and an emittance between 2-10 mm·mrad normalized.

The apertures of an induction linac are determined by the costs. An aperture of 8 cm in radius seems to be a good choice because of the relaxed current densities.

## FOILS FOR NEGATIVE ION CHARGE-EXCHANGE INJECTION

C.W. Planner

Rutherford and Appleton Laboratories

Chilton, Didcot, Oxon, UK

### INTRODUCTION

High intensity neutron sources based on proton storage rings or fast cycling proton synchrotrons use negative hydrogen ion charge-exchange injection as a method of maximising the proton beam brightness.

The electrons are fully stripped from the negative ions at the point of injection and the already stripped ions, protons, are circulated through the stripping device together with the incoming negative ions. In storage rings operating around 1 GeV it is proposed to strip the more loosely bound of the two electrons from the  $H^-$  ion using a high magnetic field. The second electron is then stripped in the storage ring and the protons recirculated through the stripper with the  $H^0$  ions.

Thin foils, gas and liquid jets and lasers have been proposed as possible stripping systems. Thin foils are being used successfully in negative ion charge-exchange injection systems and appear to be the simplest practical system.

### FOIL PARAMETERS

The foils are required to be of a material of low atomic number to minimise angular and momentum scattering. The thickness of the foil is a compromise between maximising the stripping efficiency and minimising the angular and momentum scattering. For injection energies over the range 50 MeV to 1 GeV the optimum foil thickness ranges from 50-250  $\mu\text{g cm}^{-2}$ , varying approximately as  $\beta^{-2}$  ( $\beta = v/c$ ).

The foil thickness and material also determine the total heat deposited in the foil by the protons and electrons. For the SNS the energy loss due to multiple traversals of the protons produces a temperature rise, in a material such as carbon, of 260°C during injection, cooling to 160°C between pulses. Since the foil may be in the field or fringe field of the magnet used to bring the protons and  $H^-$  ions together at the foil the stripped electrons may circulate through the foil losing their total energy. For the SNS this raises the foil temperature to 700°C, cooling to 240°C. Increasing the brightness of the injected beam, the brightness of the circulating beam or the repetition rate increases the foil temperatures. In the WNR and IKOR storage rings, foils will run at temperatures in excess of 1000°C.

The protons and electrons passing through the foil also produce a relatively high current of secondary electrons. For the SNS the secondary electron current is estimated to be  $\sim 50 \mu\text{A}$ . To avoid electrostatic stress, insulating foils will need to be coated with a low resistivity material.

#### FOIL MATERIALS

Foils of poly-para-xylene and carbon are being used successfully in negative ion charge-exchange injection systems<sup>1,2</sup>.

The poly-para-xylene foils used at ANL are made by a proprietary method developed by the Union Carbide Corp<sup>3</sup>. Foils are made by sublimating poly-para-xylene onto a glass substrate coated with a release agent. The foils are subsequently peeled mechanically, in a high humidity atmosphere. The foils are 90% carbon, 10% hydrogen by weight. Large area foils, 125 mm x 50 mm, with thickness ranging from 0.18  $\mu\text{m}$  to 1.4  $\mu\text{m}$  have been made at ANL. They have relatively short exposure lifetimes of the order of  $10^{19} \text{H}^-$  ions<sup>4</sup>. After irradiation the foils shrink and become exceedingly fragile.

FNAL<sup>5</sup> are using foils of carbon made by vapour deposition onto a glass substrate coated with a soap film as release agent. Immersion in water releases the foil to float on the surface from where it is carefully picked up on a three sided frame. The foils have a free edge of  $\sim 50 \text{ mm}$  and are  $200 \mu\text{g cm}^{-2}$  thick. Carbon foils shrink on irradiation but appear to get stronger.

The foils on the glass substrate may be obtained commercially in various sizes and thicknesses. Experiments<sup>6</sup> at FNAL for the Beijing accelerator have shown that it is possible to mount foils  $70 \mu\text{g cm}^{-2}$  thick, with a free edge  $\sim 50 \text{ mm}$ , but were not successful in mounting foils  $50 \mu\text{g cm}^{-2}$ .

Carbon foils have been prepared by cracking hydrocarbon vapour in an ethylene gas discharge<sup>7,9</sup> and in heavy ion accelerators, these foils have been found to shrink less after irradiation and have longer lifetimes. Large area foils have not yet been made by this method. Carbon foil lifetime may also be increased by mounting the foils such that they are slack initially<sup>8,9</sup>.

Experiments on pyrolytic carbon foils have been made at LANL but with foils thicker than  $1000 \mu\text{g cm}^{-2}$ .

For the SNS a foil  $\sim 120 \text{ mm} \times 300 \text{ mm}$  is required with a 120 mm free edge and a thickness  $\sim 50 \mu\text{g cm}^{-2}$ . From mechanical considerations the use of poly-para-xylene

foils or vapour deposited carbon foils did not seem practical. Metal foils of low atomic number were investigated, but the minimum thicknesses available were 10  $\mu\text{m}$  for Beryllium and 0.7  $\mu\text{m}$  for Aluminium.

The Fulmer Research Institute (UK)<sup>11</sup> has performed a preliminary investigation into the manufacture of 50  $\mu\text{g cm}^{-2}$  foils from several, low atomic number, refractory materials viz: Alumina, Aluminium Nitride, Pyrolytic Boron Nitride and Vitreous carbon.

Experiments to form thin films of Aluminium Nitride on Aluminium were not successful.

Pyrolytic Boron Nitride has a similar crystal structure to graphite. Thin films are made by growing BN on polished graphite substrates at a temperature  $\sim 1800^{\circ}\text{C}$ . The foils are subsequently released from the graphite by heating in air at  $\sim 600^{\circ}\text{C}$ . It was found that below about 4  $\mu\text{m}$  the films were not of good integrity and detached in pieces. Examination under an electron microscope showed the graphite substrate to have pits with dimensions of a few microns and these were only bridged by the BN at about a thickness of 4  $\mu\text{m}$ . To obtain integral sub-micron films would require the development of a higher quality substrate and this technique has not been pursued further. Pyrolytic BN is attractive as a foil material as it has a very high thermal shock resistance.

Vitreous carbon is a glassy form of carbon made by slowly pyrolysing organic materials in an inert atmosphere. Vitreous carbon films on copper and aluminium have been formed by pyrolysing phenolic resin films. The metal has been dissolved from the carbon film and the films appear to be continuous and void free. To date only vitreous carbon films 1-2  $\mu\text{m}$  thick have been produced. Metal has been successfully coated with sub-micron films of phenolic resin but further pyrolysing experiments have not taken place.

The most successful results were obtained with Aluminium Oxide. Early work on Aluminium Oxide foils<sup>12</sup> indicate they should have good strength and integrity. Aluminium Oxide foils are made by masking an area of aluminium, anodising the remaining surfaces in a weak electrolyte at constant current (2  $\text{mA/cm}^2$ ). The mask is removed and the aluminium is dissolved from the oxide film in a 3% bromine-methanol solution. The manufacture of the Aluminium Oxide foils is now under development at the Rutherford and Appleton Laboratories. Foils of the required dimensions with a 120 mm free edge have been made successfully. It has

been found necessary to bake the anodised aluminium at 350<sup>0</sup> for several hours before dissolving the aluminium. Without this treatment the foils split, around the vapour pressure of water, when being pumped down. One result of the heating process is that it stretches the foil and the foil becomes slack in the support frame after the aluminium is removed.

#### ACKNOWLEDGEMENTS

I would like to thank Dr C Potts of ANL and Dr C Hojvat of FNAL for the many useful discussions on the work at their Laboratories. I would also like to thank Dr N D West and Mr V T Pugh for assistance with the foil development program and Mr M Yates who is now developing the manufacture of the Aluminium Oxide foils at the Rutherford and Appleton Laboratories.

#### REFERENCES

1. C W Potts, IEEE NS-24 p1385, 1977.
2. C Hojvat et al, IEEE NS 26 No 3 p 3149, 1979.
3. A J Gorkca, IEEE NS-20 No 3 p387-391, 1973.
4. M A Spivack, Rev Sc In LI (II) 1614-1616, 1970.
5. H Huizenga et al, Rev Sc In 52(5) 673-677, 1981.
6. M Joy, FNAL Report TM-699.
7. C Hojvat et al, IEEE NS 26 No 3 p4009, 1979.
8. C Hojvat, private communication.
9. N R S Tait et al, Nucl Inst & Meth 163 (1979) 1-14.
10. B Armitage et al, Nucl Inst & Meth 155 (1979) 565-567.
11. B Armitage et al, Nucl Inst & Meth 163 (1979) 277-278.
12. D J Liska, private communication .
13. RAL Contract N2B 9R 1805, Final Report (in prep).
14. U Hauser & W Kerler, Rev Sc Inst V29 No 5, 1958, 380-382.

#### Discussion:

It is possible to use a hydrochlorid solution for dissolving the Al, but the bromine-methanol solution is more effective.

Rapid Beam Switching Techniques

G. Schaffer

Kernforschungszentrum Karlsruhe

Institut für Kernphysik

P.B. 3640

7500 Karlsruhe

Federal Republic of Germany

Abstract

The report gives a survey on rapid beam switching techniques as they are required for the SNQ project. This includes formation and repartition of the 1.1 GeV linac macropulses for various targets, and ejection from the isochronous compressor ring IKOR. The design of fast kicker magnets and of fast beam choppers required for these purposes is treated in some detail.

## 1. Introduction

Particle accelerator and pulse compressor projects which are of interest for neutron spallation stimulate a continuous development of technology for rapid and reliable beam switching /1-3/. This is essential for proper handling of high beam power levels. A survey on jobs and possible solutions, mainly referring to the SNQ project /4/ should illustrate it.

As major jobs for beam switching we have to consider

- a) linac macropulse repartition
- b) fast ejection from a pulse compressor ring
- c) beam suppression during switching intervals.

The SNQ linear accelerator /5/ will feed, at a maximum repetition rate of 100 Hz, sections of beam macropulses (1.1 GeV protons or, eventually,  $H^-$  ions) into various beam lines as shown by Fig.1. Subdivision of the 0.5 ms macropulses offers a convenient operational flexibility for sharing the available total beam power by different users, according to their individually desired duty cycle or pulse length.

The SNQ beam lines include, as an option, an isochronous compressor ring, IKOR /6/. Designed for stacking full linac macropulses over 90 % of its circumference by charge exchange injection / 1 / the compressor requires fast beam switching each time after filling, within less than 100 ns, for repetitive ejection (100 Hz) /7/.

For our designs we draw great profit from the hard work which has been performed in the past decades on fast ejection from large synchrotrons, on ring-to-ring transfer of particle bunches and on other systems which have been invented and are in operation /8-21/.

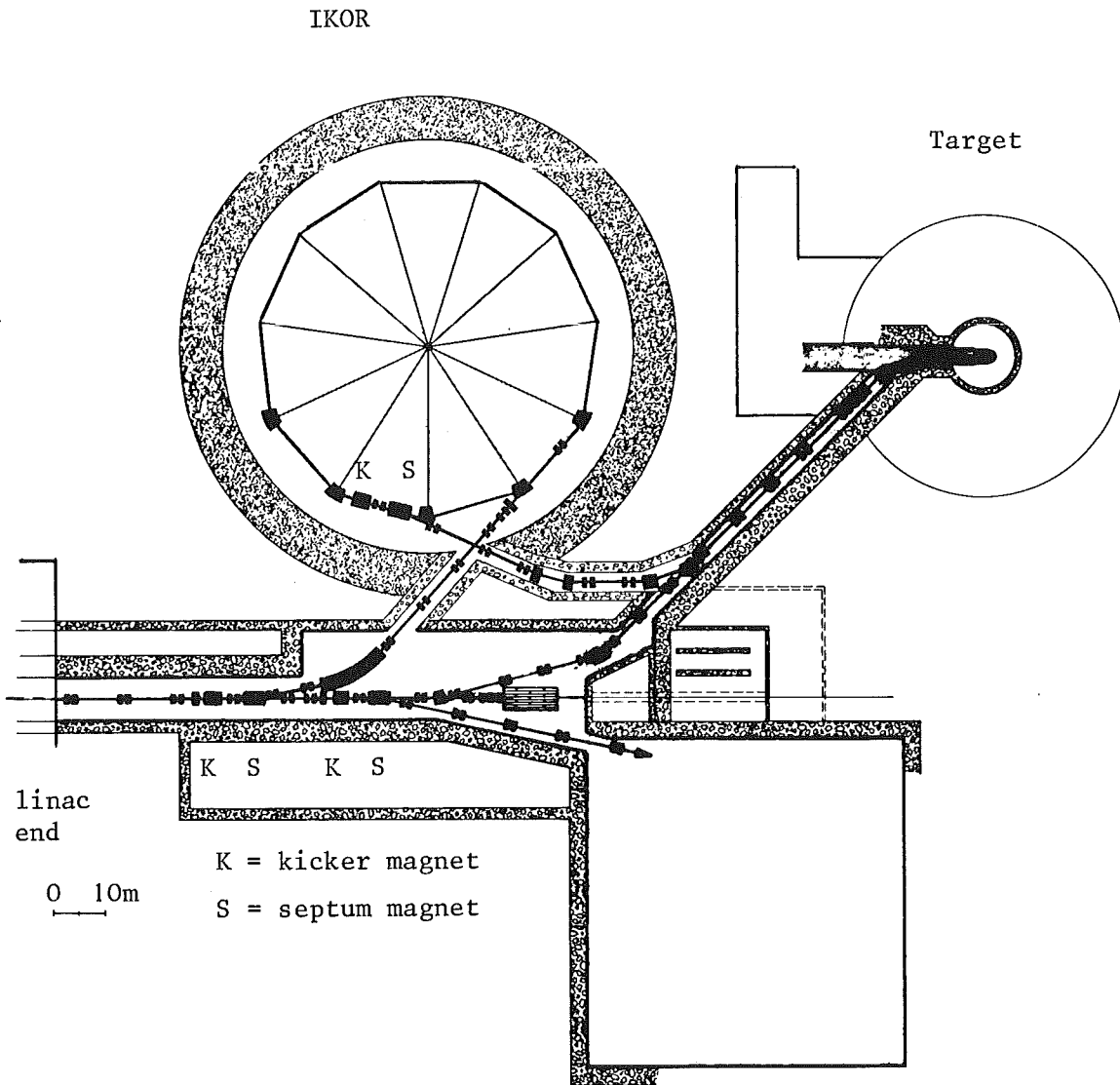


Fig. 1 SNQ linac and IKOR beam transport, general layout

## 2. Beam separation by kicker and septum

A common feature of fast switching systems for high-energy beams of charged particles is the combination of kicker and septum (Fig.2). This permits a minimum investment on apparatus and on switching power for a given deflection angle and a given switching interval. To avoid beam spill, either an existing void between particle bunches is used or it has to be generated by low-energy beam chopping /15,22/.

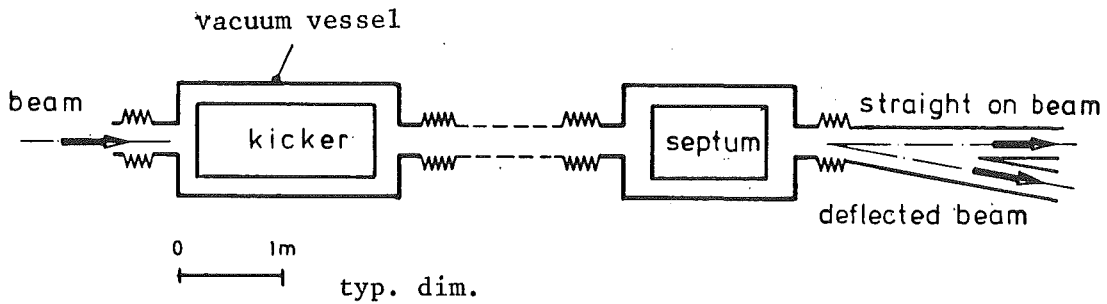


Fig.2 Schematical arrangement of kicker and septum

'Kicker' means a rapidly excited low-field deflector (electric or magnetic), 'septum' means a slowly or permanently excited high-field deflector (electric or magnetic) with a thin metallic separation between the high-field channel and a zero-field (better: low-field) channel. The kicker, situated typically a few meters upstream from the septum, has to deflect the desired beam portion into the high-field channel of the septum.

Both devices, kicker and septum, are operated under high vacuum in order to save on aperture for the deflecting field. After the septum, the beam vacuum chambers are separated.

### 3. Septum magnets

In the IKOR ejection section we find a conventional septum magnet of about 0.8 Tm bending strength, with a copper conductor between circulating beam and ejected beam. The kick given to the ejected beam by the kicker magnet (11 mrad) moves the beam radially outwards, is further enhanced (to 20.6 mrad) by a radially defocusing quadrupole of the IKOR lattice /6,7/, and then leads the beam onto the high-field side of the septum where it is bent out by about 7.5 degrees. A cross-section at the septum entrance is sketched in Fig.3.

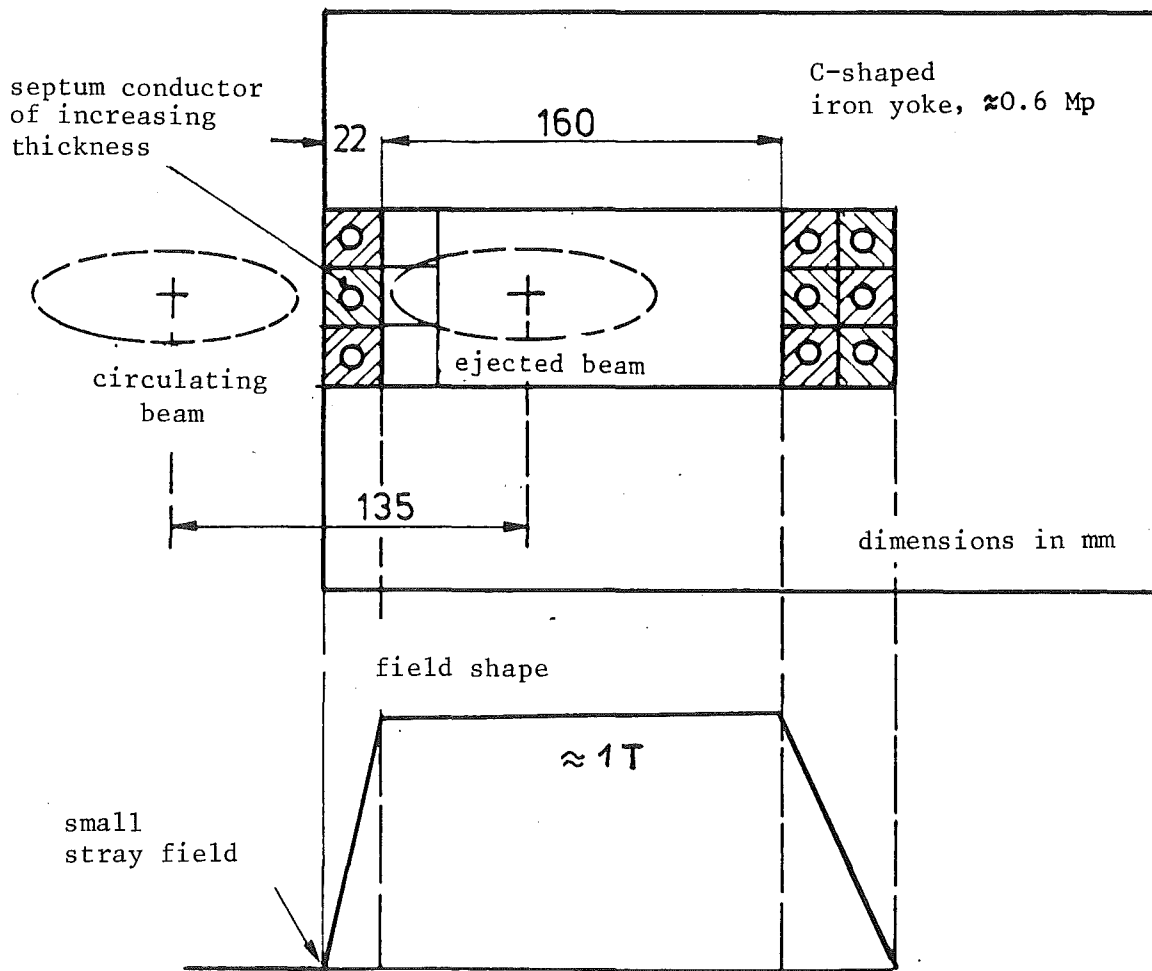


Fig.3 IKOR septum magnet, schematically.  
length 0.8 m  
current 67 kA  
power  $\approx 160$  kW

Another type of magnetic septum, the so-called Lambertson septum (Fig.4) can also frequently be found [23,24]. Here, the beam is switched over an iron separation and not over a high-current copper sheet. The kick to the beam by the kicker and the main deflection by the septum field are orthogonal to each other. We prefer to use this type of septum in the switchyard of the SNQ linac.

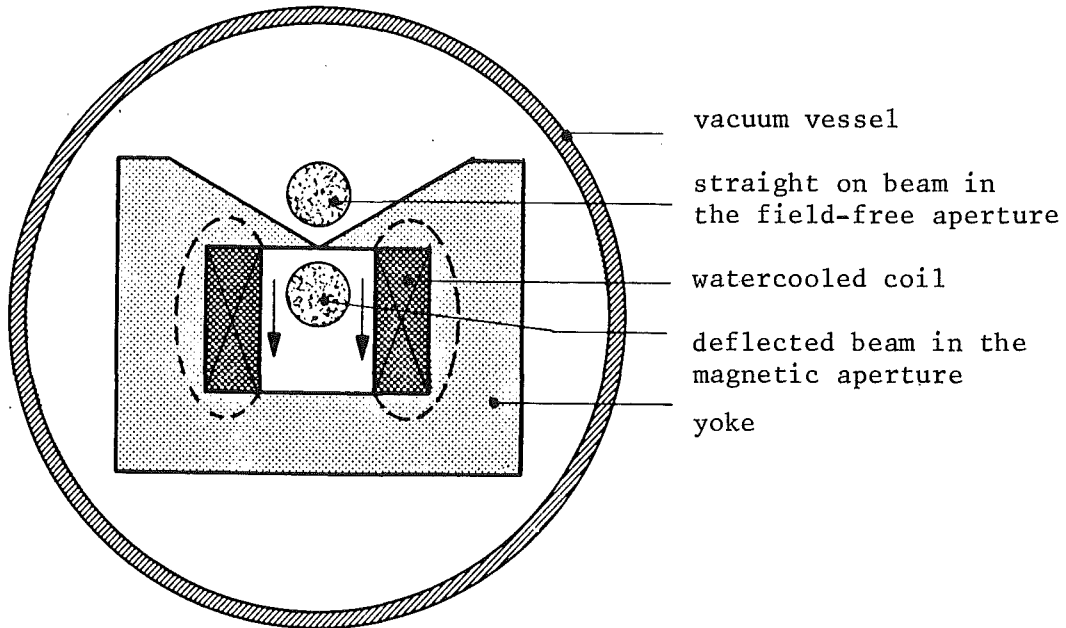


Fig. 4 Lambertson-Septum  
(iron septum, schematically, kick vertical, main deflection horizontal)

#### 4. Kicker requirements

In the following list:

- aperture
- length  $\ell$
- current (voltage) I (U)
- rise time
- pulse duration
- pulse flatness
- repetition frequency
- magnetic vs. electric deflection
- beam coupling impedance

we underline the importance of the repetition frequency for the SNQ project. The beam coupling impedance is of interest for the compressor ring design /6/.

Theoretical minimum  $I l$  ( $U l$ ): For 'short' kickers (small offset of beam at exit), with an aperture matched to the beam envelope, we are able to indicate a theoretical minimum value for the current  $I$  (in ampereturns) or the voltage  $U$  of an idealized magnetic or electric kicker of length  $l$  [25]. These limits are determined by the normalized beam emittance  $\epsilon$ , as follows:

$$\text{mag.} \quad I l = \frac{4W_0}{\pi e / u_0 c} \cdot \epsilon \quad (\text{round beam})$$

$$\text{el.} \quad U l = \frac{4W_0}{\pi e} \cdot \beta \cdot \epsilon$$

with  $W_0 =$  proton rest energy

$$\beta = v/c.$$

These formulated values (reference values) produce the kicker action sketched by Fig.5, i.e. the emittance ellipse is just shifted by its own diameter.

In practice, one has to add a fraction for the offset of the beam at the kicker exit and, also very important for the nerves of the operators, a considerable safety margin for allowable beam mis-steering and emittance blow-up.

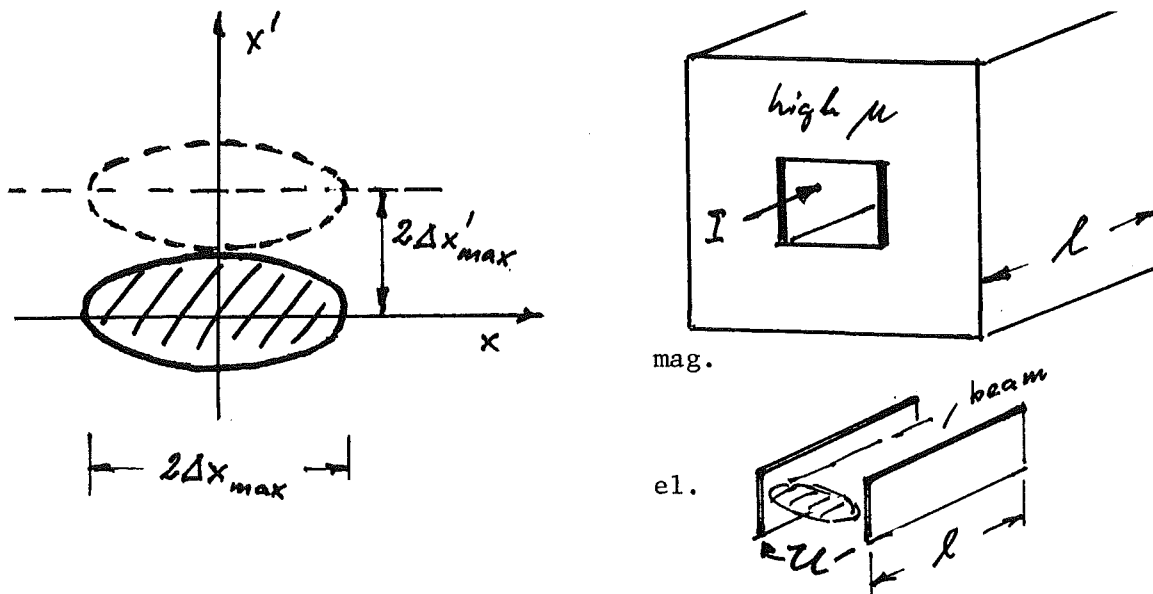


Fig.5 Emittance shift by theoretical minimum  $I l$  ( $U l$ )

5. Practical kicker design

We propose 2 examples for the SNQ layout which should be discussed in the light of experience gained with other projects.

Examples (3 x ... 10 x theor. minimum  $I\ell$ )

	effective kicker length	aperture ratio (b/h)	$I\ell$	rise time $\tau_K$	kicker voltage U	U x I switching power
SNQ linac:	2 m	1	2.2 kAm	10 $\mu$ s	280 V	310 kVA
IKOR:	3.6 m	2	4.3 kAm	50 ns	220 kV	260 MVA

Dominant system parameters are the kicker rise time  $\tau_K$  and the

kicker inductance:

$$L \approx \mu_0 \cdot \ell \cdot (b/h)$$

$\downarrow$   
 $\sim 1.2 \mu\text{H/m}$

in approximation for single turn and a surrounding (ferrite) of high permeability.

The required kicker voltage  $U = \frac{L \cdot I}{\tau_K}$  is independent of the chosen total length  $\ell$  but very dependent on aperture and aperture ratio b/h.

As a consequence, we find the following typical solutions:

- for short rise time (ns-range)

single turn,  
L/C-pulse forming  $\rightarrow$  fractional turn  
several short modules  
powered individually

- for  $\mu$ s rise time

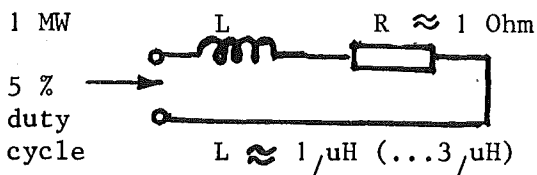
single turn or multiturn magnets

low impedance approach

high/medium impedance systems,

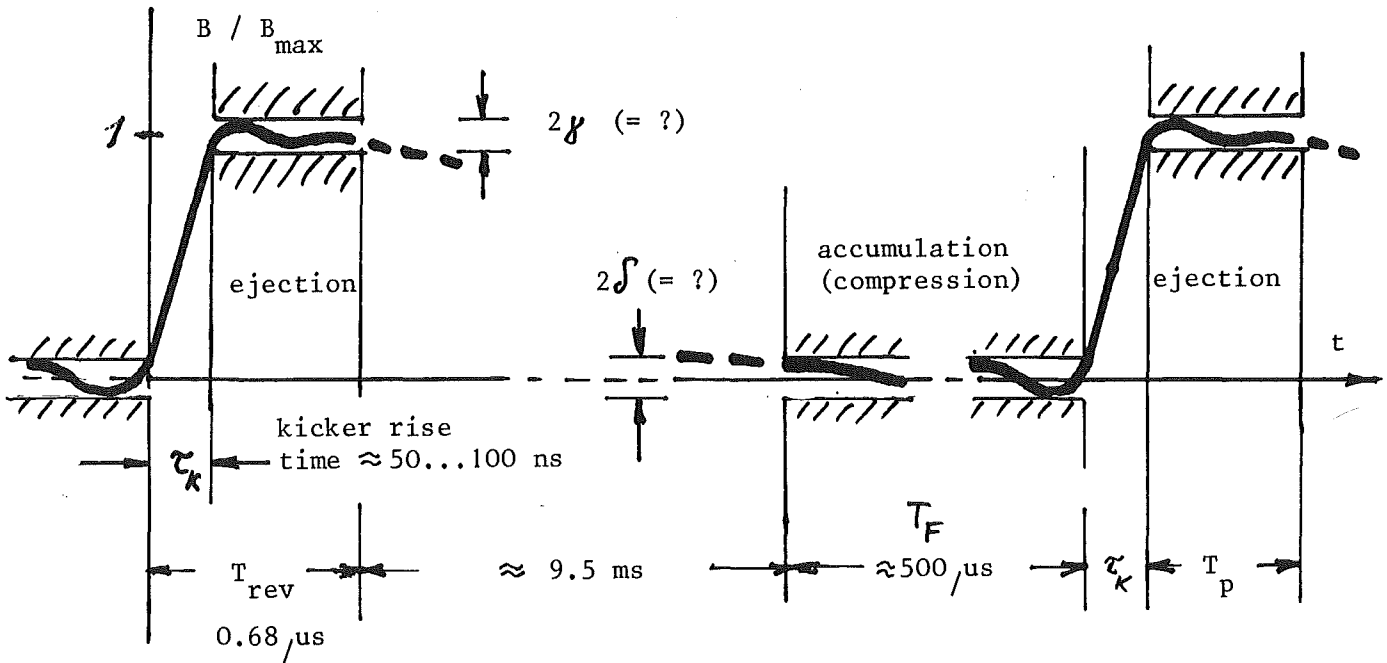
L/R circuit  
e.g. SNQ (LASL)

smaller losses if important



L/C - pulse forming,  
possibly  
with energy recuperation.

The kicker field tolerances, as a function of time (sketched, for example by Fig.6 for IKOR ejection), indicate admissible (mainly systematic) shifts of beam emittances during and before beam deflection. Also, the quality of the dipole field has to be taken into account for second order effects.



upper frequency content of Fourier-spectrum:

$$\tau_K \approx 1/2f_g ; \quad f_g \approx 1/2\tau_K = 10...5 \text{ MHz}$$

Fig.6 Tolerance scheme for kicker field (IKOR ejection)

L/C - pulse forming networks (or cables) are widely used for generating short kicker pulses with good pulse quality. The principle is illustrated by Fig.7. Also, the kicker magnet is then usually constructed in form of a delay line with an (intentionally) low characteristic impedance in order to achieve sufficient current with a reasonable voltage (in case of IKOR-ejection:  $Z=25 \text{ Ohm}$ ). However, capacitive loading increases the filling time  $\tau$ , which must not exceed given limits ( $\tau = \sqrt{LC}$  for unidirectional filling).

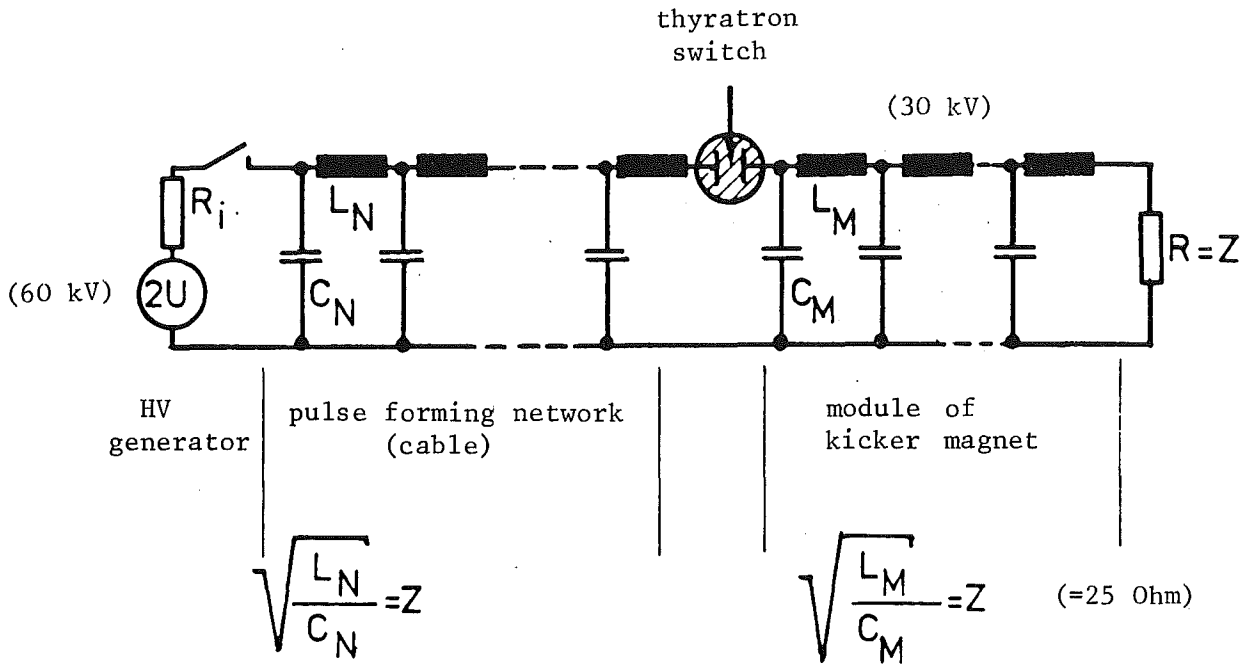


Fig.7 Generation of kicker pulses for beam ejection, schematically. The indicated values are typical for one of the 8 IKOR kicker modules.

Structures of single turn ferrite kicker magnets with capacitive loading are shown in Fig.8.

Also feasible and in use on storage rings are kicker magnets without ferrite insertion /26,27/. The required excitation current increases considerably in these cases.

#### 6. Remote handling of kicker and septum magnets

Kicker and septum magnets of the high energy beam switchyard and of the compressor ring must be designed for remotely handled installation, and particular attention has to be paid to operational reliability and radiation safety. This engineering task requires much care and skill for an appropriate design of vacuum, current, signal, and cooling water connections. Installation and removal must be possible in a narrow, specially radiation shielded area. Good examples exist /28,29/.

For comparison: the aperture of the SNQ disk and washer structure is 70 mm in diameter, the aperture of the linac beam kicker magnet may be as small as 50 mm. This aperture will, of course, be protected by collimators and other devices; nevertheless, the highest level of induced radioactivity has to be expected in the beam transfer lines after the linac /38/.

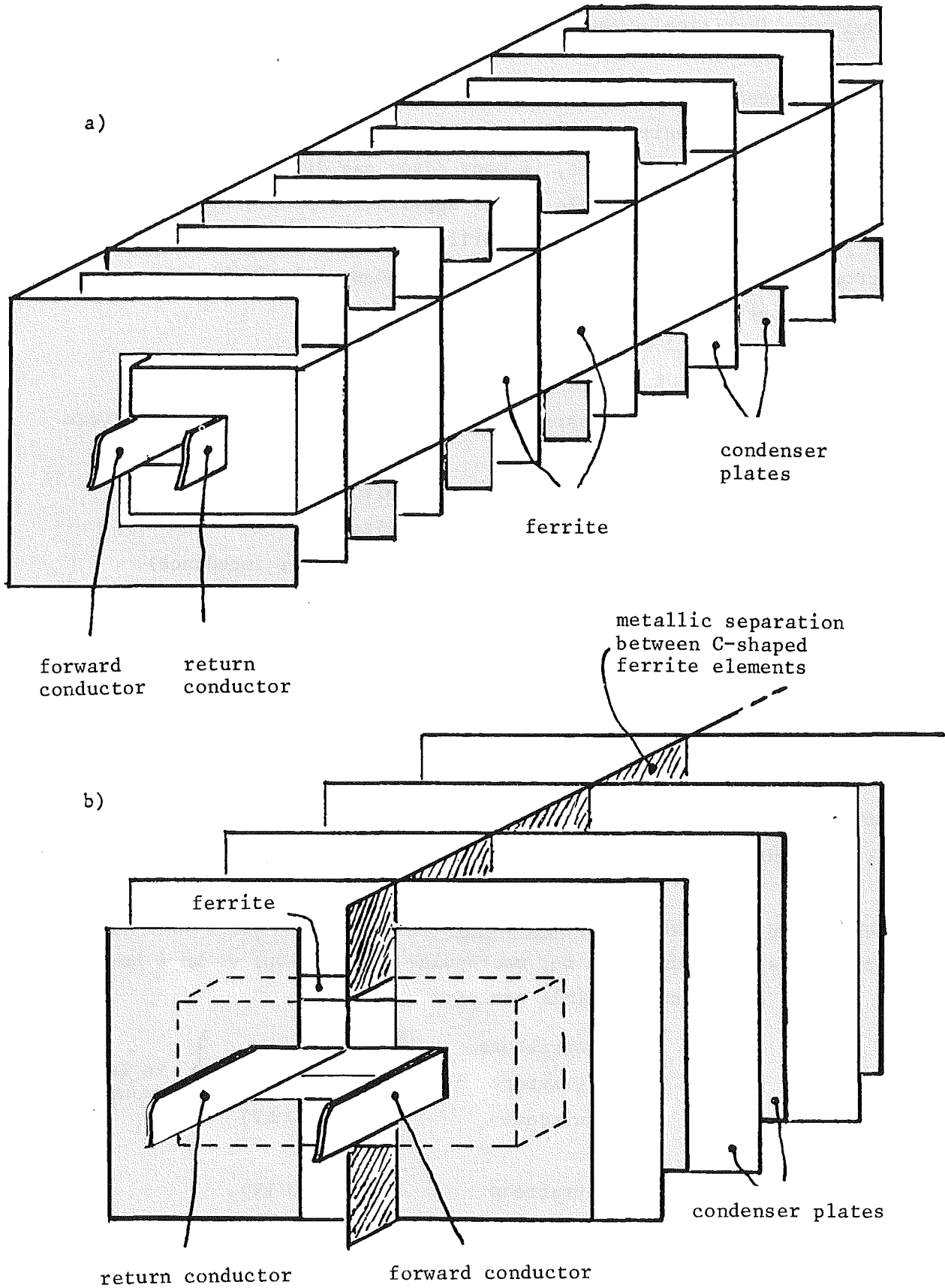


**Fig.8** Typical structure of a kicker module  
a) asymmetric C-shaped magnet (6 cells)  
b) symmetric (double C) magnet with metallic separation.  
The IKOR ejection system would include 8 modules of 0.45 m length,  
 $I = 1200 \text{ A}$ ,  $Z = 25 \text{ Ohm}$ , filling time per module 50 ns.

7. Switches (=critical components)

Little has been said so far on the importance of selecting qualified components such as capacitors, coils, insulation, ferrite etc. The performance limits of high-power switches, in many cases gas discharge switches /30/, play the most outstanding role in our application problems. Without ignoring the fact that sufficient reliability has been achieved in most cases by proper engineering, we note here some fundamental limitations associated with different types:

	<u>problem</u>
- spark gaps	erosion, maintenance
- thyratrons	no long pulse, low duty cycle
- ignitrons	repetition rate, life
- thyristors	voltage
- transistors	voltage
- etc (hard tubes)	(high inner impedance).

The combination of thyatron (fast rise) and ignitron (long pulse) has been introduced by CERN for the SPS beam dumping system /31/, with great success ('thyragitron'). However, this is a typical low-repetition rate application ( $\leq 1$  Hz).

Modern hydrogen or deuterium filled thyratrons /32/ achieve 100 kA/ $\mu$ s, thyristors may be manufactured for kA/ $\mu$ s typical rise of current.

For switching the high-energy SNQ linac beam (up to 10  $\mu$ s rise time and up to 250  $\mu$ s pulse duration for macropulse repartition) we have to investigate in more detail the possible use of:

- transistors	$\leq 300$ V	} in larger quantities;
- thyristors	( $\sim$ kV)	
- ignitrons	(25 ... 30 kV)	

for the compressor ring: thyratrons (60 ... 80 kV).

8. Pulse energy recuperation

Whereas for short kicker pulses and low duty cycle the question of average power consumption is normally less important, energy recuperation becomes attractive for long pulses and elevated duty factors. This condition is typical for the SNQ beam switchyard kicker magnets.

With some speculative optimism we may consider schemes for PFN operation with pulse reflection /33,34/. Representing pulse lines in a simplified manner as indicated by Fig.9, a few examples are shown by the successive Figures 10 to 14. The way leads from the simplest circuit (kicker magnet with short-circuited end, Fig.10), over a twin wave system (kicker excitation from both sides, Fig.11), addition of empty line sections for the deionization time of gas-discharge switches (Fig.12), to a ring circuit (Fig.13) and, finally, to a twin wave ring system (Fig.14) /34/.

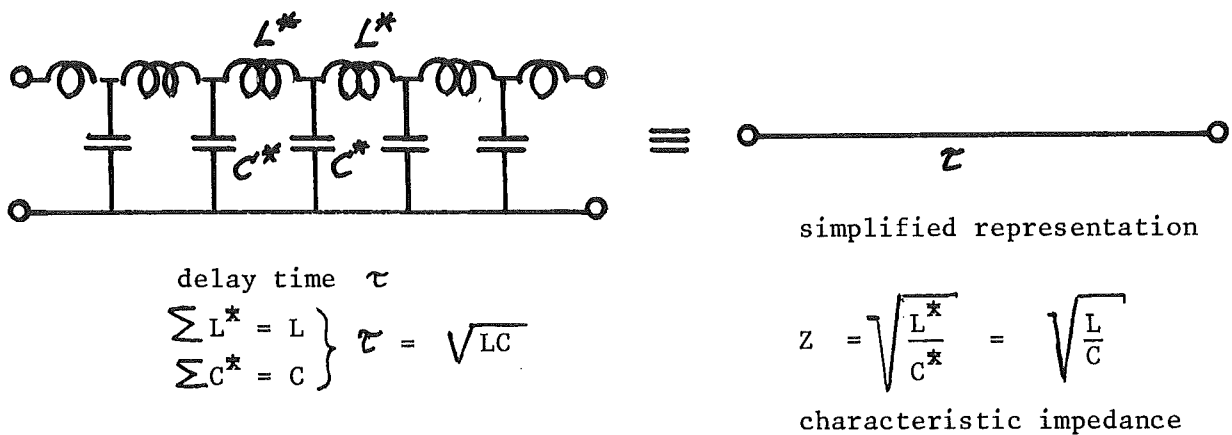
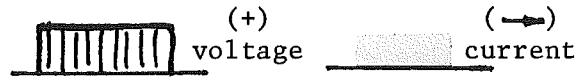


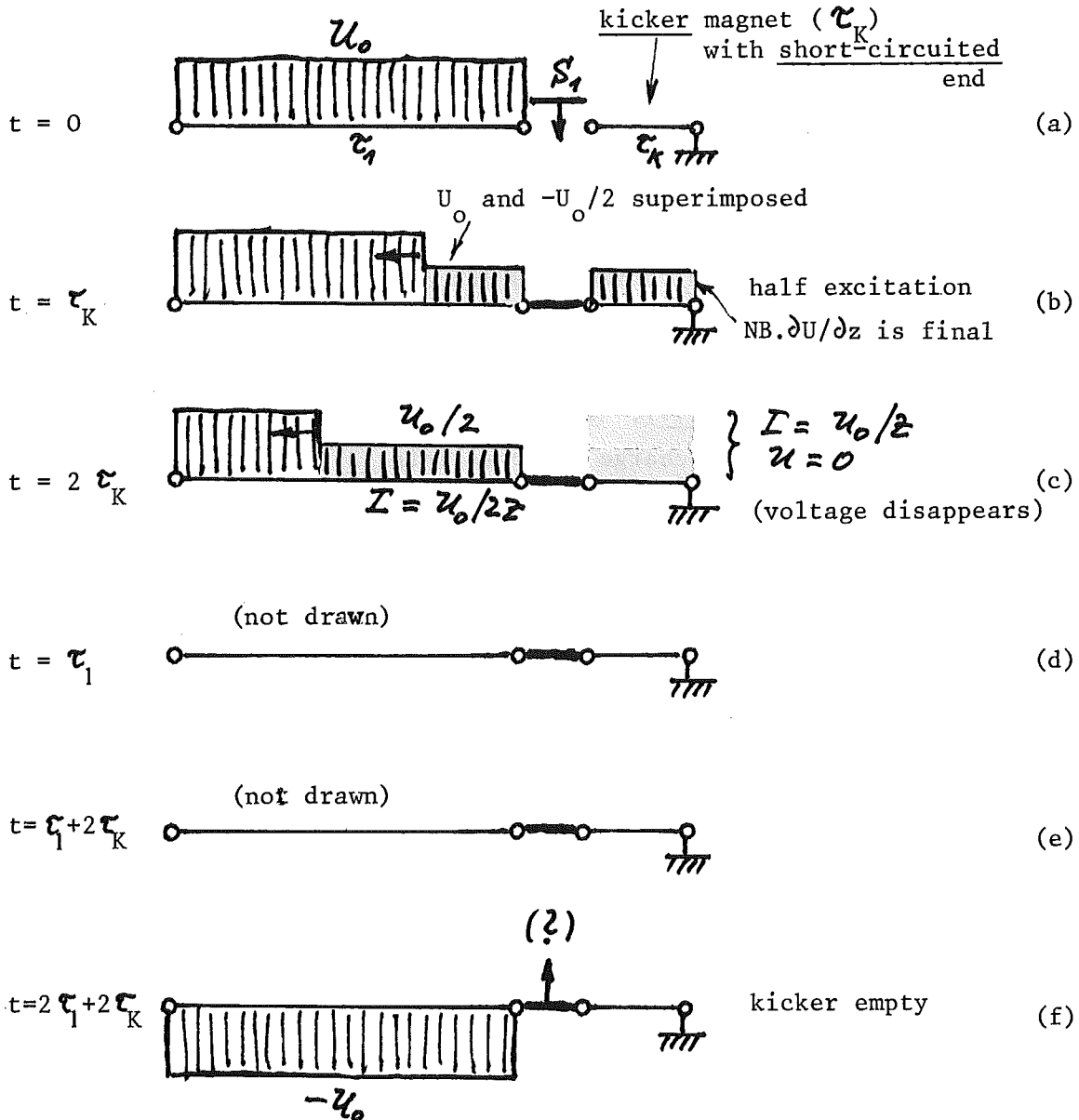
Fig.9 Representation of a pulse line of delay time  $\tau$ , open input and output

These circuits and methods may be applicable if low resistive losses (low attenuation  $R/2Z$ ) can be achieved and if compatible types of switches exist. Low partial reflexion on the various transition points is also essential. The compensation of losses must be done by distributed valves along the pulse lines during the time between successive kicker pulses /33/.

Example for PFN operation with pulse reflexion:



pulse forming network  
charged to voltage  $U_0$



NB. always check that  $\sum L I^2 + \sum C U^2 = C_1 U_0^2 = \text{constant}$

$\tau = \sqrt{LC} = ZC = \frac{L}{Z}; \quad C_1 = \frac{\tau_1}{Z}$

Fig.10 Pulsed excitation of a shortcircuited kicker magnet (delay time  $\tau_k$ ). The kicker is filled after  $2\tau_k$ . Phase f shows that the PFN has received its previous energy when the kicker is empty again, but the PFN voltage has reverse sign.

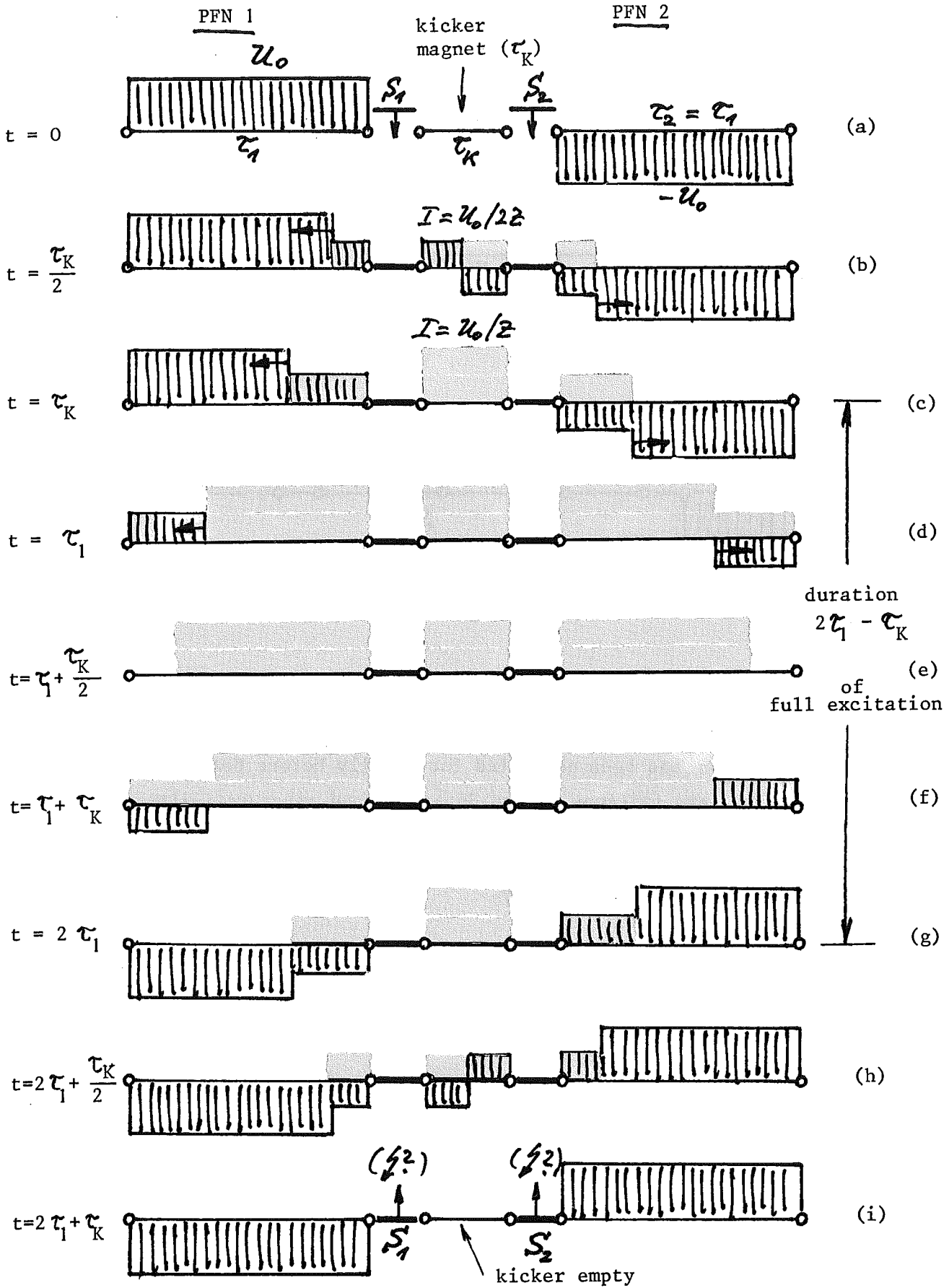
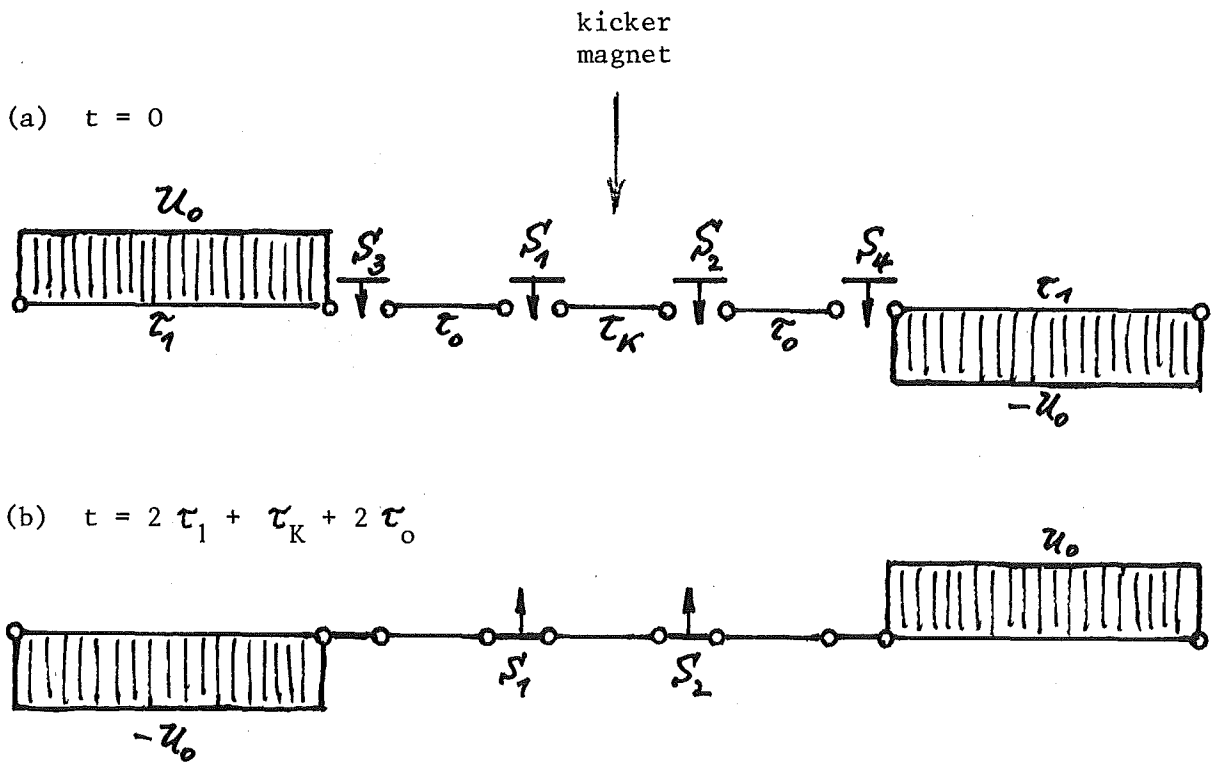


Fig.11 Twin wave system: kicker excitation from both sides by 2 PFN's of opposite polarity



**Fig. 12** Modified twin wave system: the addition of empty line sections ( $\tau_0$ ) permits an opening of the gas discharge switches S1 and S2 at zero voltage and zero current after the charge exchange between the 2 PFN's has been completed (or shortly before that).

The auxiliary switches S3 and S4 are opened after refilling and smoothing (by distributed valves and damping resistors which are not shown in the scheme). After this procedure, the auxiliary line sections can be discharged. The next kicker pulse, however, would have negative polarity.

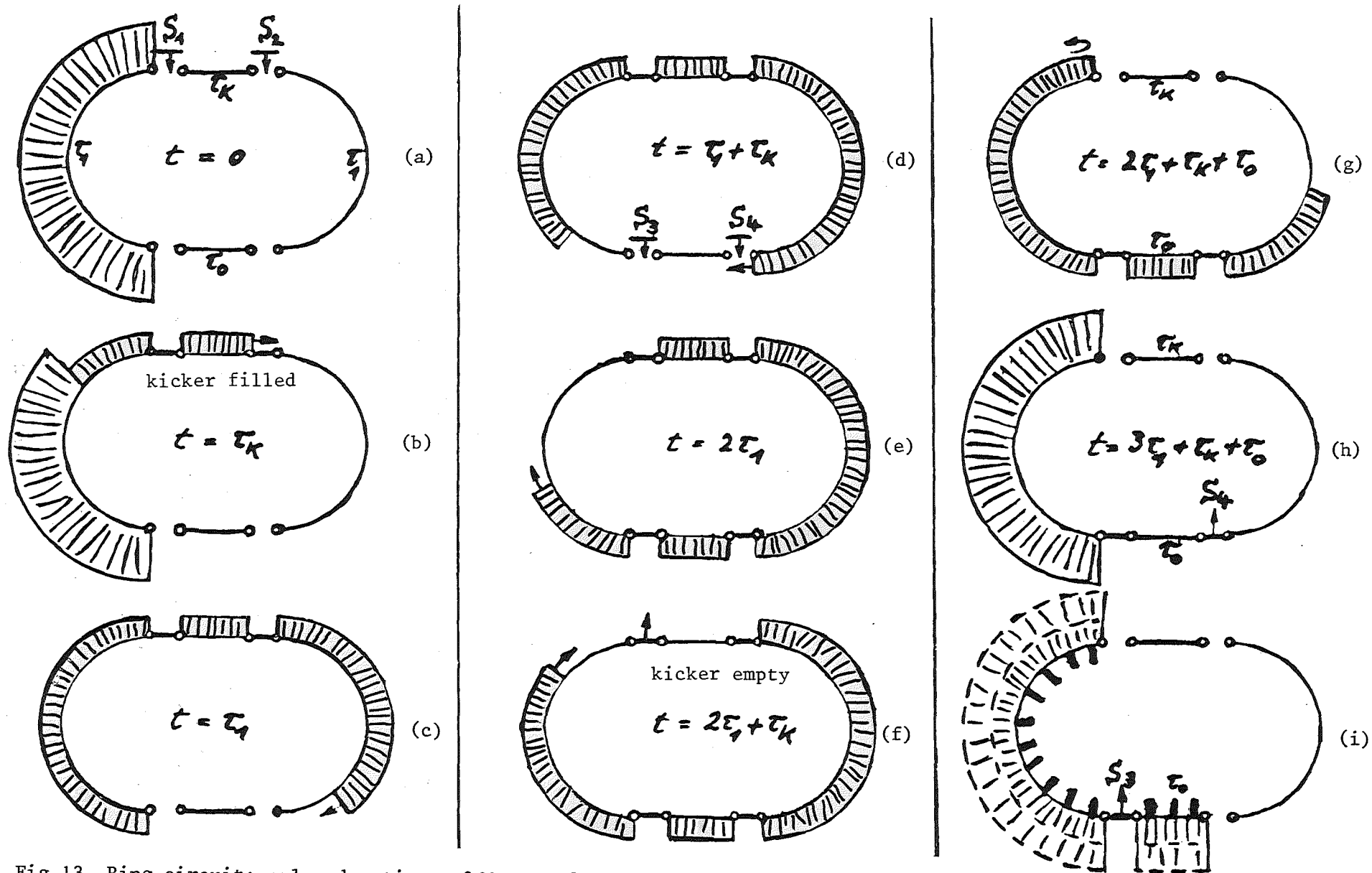


Fig.13 Ring circuit: pulse duration =  $2\tau_1 - \tau_k$  for full excitation of the kicker field. After refilling, smoothing, separation (S3) and discharge of the auxiliary line section ( $\tau_0$ ), the initial condition ( $t=0$ ) is re-established.

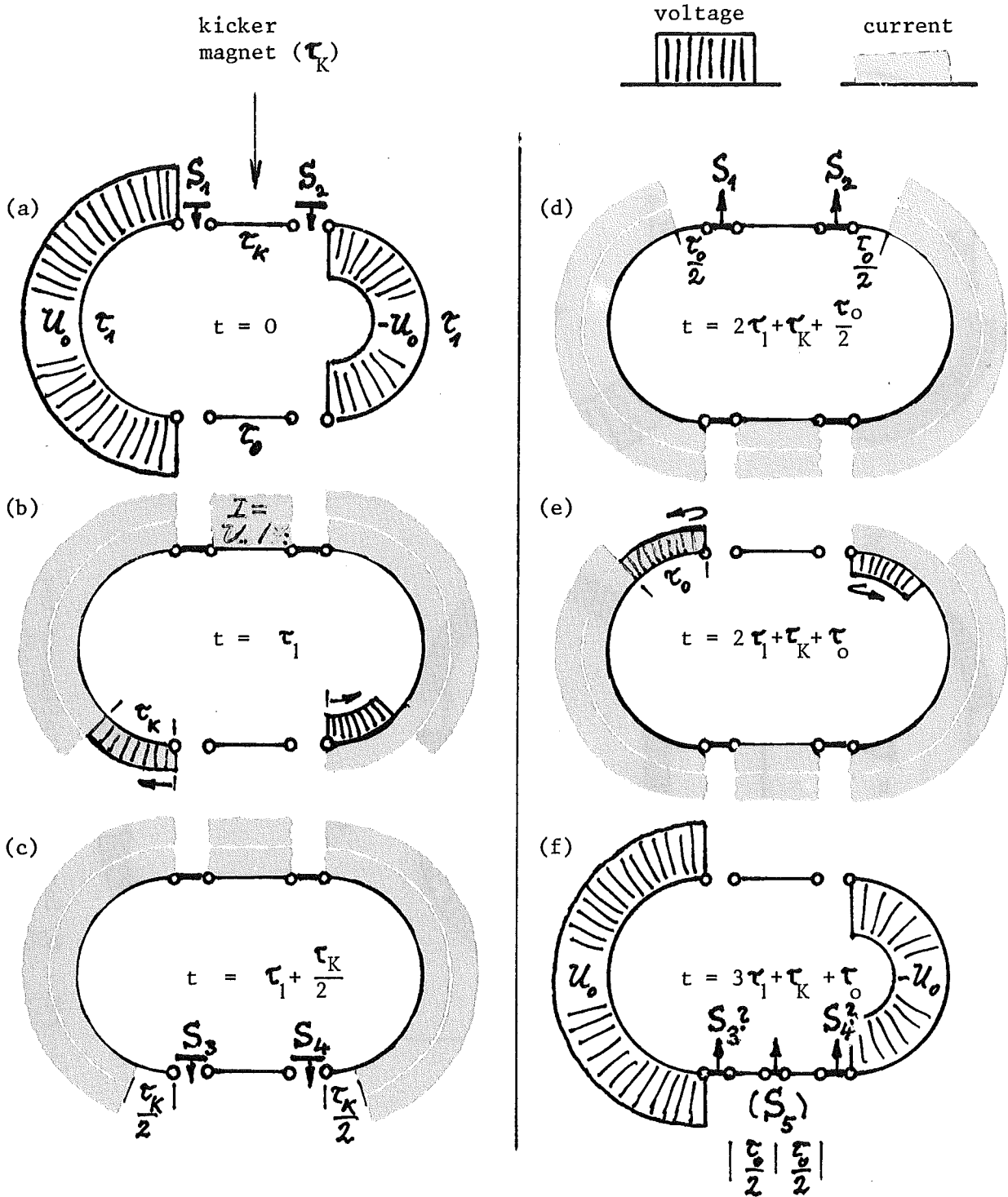


Fig.14 Twin wave ring system:

kicker excitation from both sides by ring waves of opposite polarity. Pulse duration for full excitation =  $2\tau_1 - \tau_K$ . The currents of the counterflowing waves sum up in the kicker magnet, their voltages cancel each other.

The circuit is extended by switch S5 which divides the auxiliary line section ( $\tau_0$ ) into equal parts. S5 can be opened in phase f.

Typical values for SNQ:  $\tau_K = 10 \mu\text{s}$   
 $2\tau_1 = 500 \mu\text{s}$   
 $(\tau_0 = 10 \dots 25 \mu\text{s} = \text{deionization time}).$

### 9. Generation of protective beam voids

The voids within a linac macropulse which are used to protect the septum and the beam transfer channels against beam spill during the rise time of the kicker field, can be generated at the low-energy injection into the rf accelerator /15,36/. The low  $\beta$ -value of the particles suggests chopping by transverse electric fields. An example is shown in Fig.15 (rf chopper for the SNQ linac). Two series of deflecting plates are used, fed by delay lines which are arranged in form of meander-like ribbon lines between watercooled copper sheets as return conductors /35/. The electrical length of each modular section corresponds to the transit time of the particles from plate to plate. Rise and fall times of the deflecting pulses in the nanosecond region can be achieved by an adequate modular structure of the deflection system /15,35/ and by use of linear wideband pulse power amplifiers. Two distributed amplifiers of 10 kW max. output will be required to generate the 100 ns beam voids for compressor ring operation /22/.

The low-energy chopper system may also be used for forming the linac macropulses. The deflected portions of the beam pulse are absorbed by aperture limiting jaws which have to tolerate relatively high average power /37/.

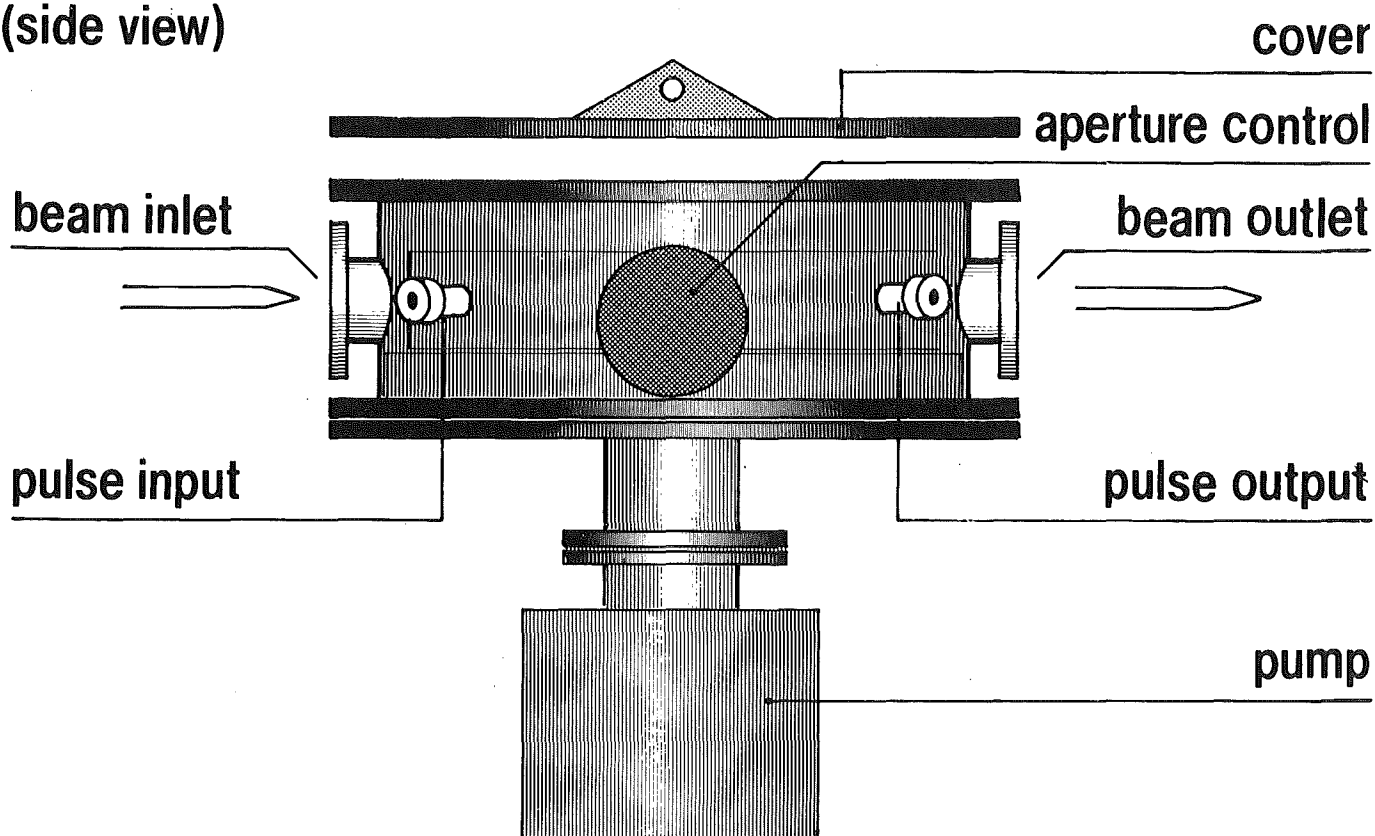
### Acknowledgment

The author wishes to thank Messrs. D. Fiander, G. Nassibian, K. H. Reich, J. C. Schnuriger, G. Schröder, E. Weisse (CERN) and G. Stange (DESY) for many fruitful discussions. He also feels gratefully indebted to J. E. Vetter, H. Willax (†) and to the other members of the SNQ Linac and IKOR Study Groups for their great interest in the subject.

### Discussion:

The fringe fields of the septum magnet are small, but one cannot say how small. More details one can find in the ICOR report.

(side view)



(plane view, cover removed)

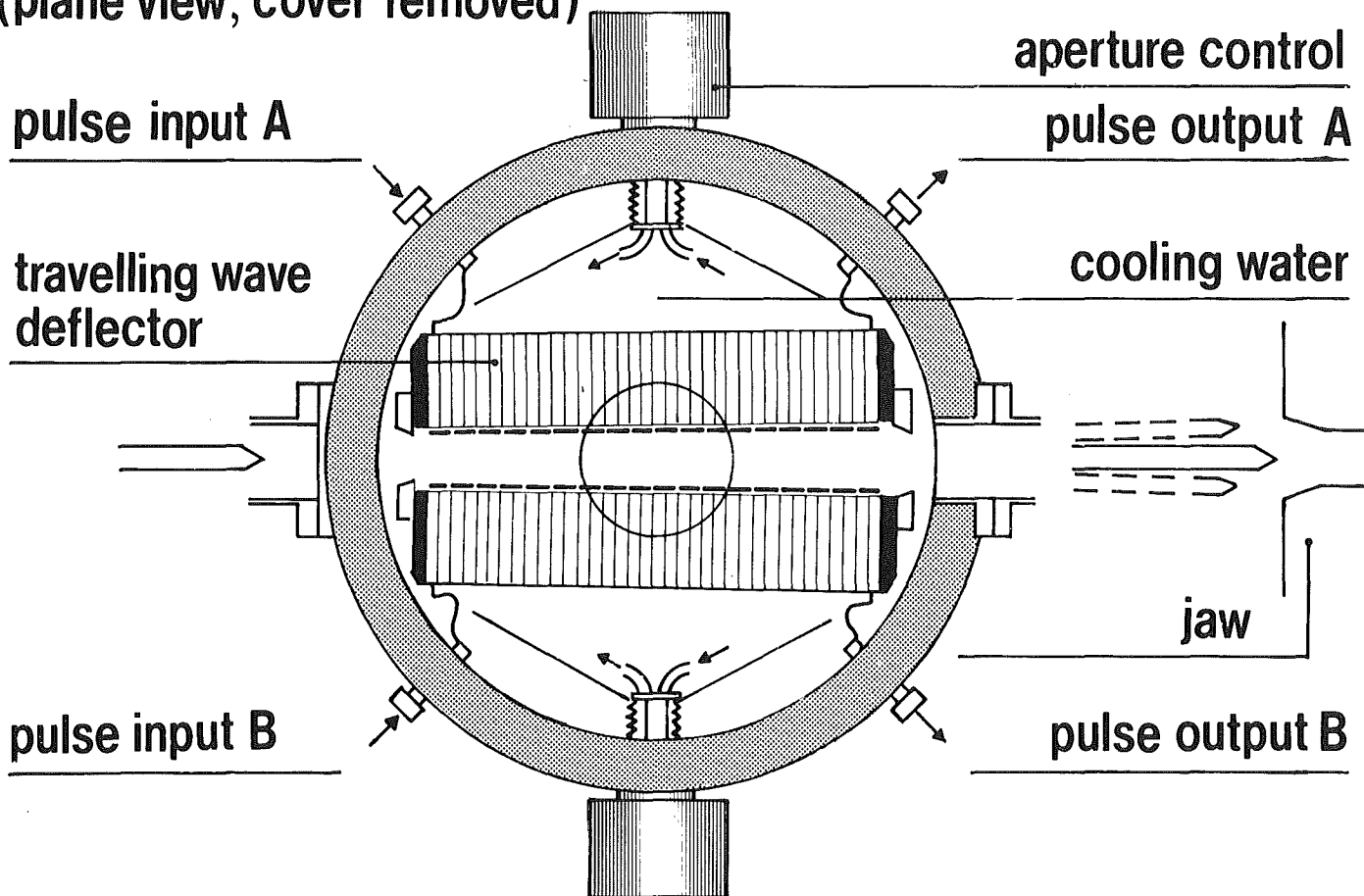


Fig.15. Rf kicker assembly in the low-energy beam transport of the SNQ linac. (450 keV,  $\beta \approx 3\%$ , effective length = 0.4 m, minimum required  $U\ell = 360$  Vm for  $\epsilon = 3\pi$   $\mu$ radm).

References:

- /1/ G.P.Lawrence et al., LASL high-current proton storage ring, Proc. XIth Int.Conf. on High Energy Accelerators, CERN 1980
- /2/ R.K.Cooper, G.Spalek, PSR status report, this meeting
- /3/ D.A.Gray, private communication
- /4/ H.H.Hennies, private communication
- /5/ J.E.Vetter, ed., The basic design concept of the SNQ linear accelerator, Kernforschungszentrum Karlsruhe, KfK 3180 B, Juni 1981
- /6/ The IKOR Study Group, G.Schaffer, ed., IKOR, an isochronous pulse compressor ring for proton beams, private communication
- /7/ K.H.Reich, J.P.Delahaye, this meeting
- /8/ G.K.O'Neill, Storage rings for electrons and protons, Int.Conf. on High Energy Accelerators and Instrumentation, CERN 1959
- /9/ B.Kuiper, G.Plass, Operational experience with the CPS fast ejection system, Proc. Vth Int.Conf. on High Energy Accelerators, Frascati 1965
- /10/ K.H.Reich, Beam extraction techniques for synchrotrons, private communication
- /11/ H.Kuhn et al., The design of the ISR inflector, IEEE Trans.Nucl.Sci. 16, No3, June 1969
- /12/ A.Brückner, Kicking protons, fast and cheap, IEEE Trans.Nucl.Sci. 18, No3, June 1971
- /13/ D.Fiander, Hardware for a full aperture kicker system for the CPS, ibidem
- /14/ J.C.Schnuriger, The 40 kA dumping system for the ISR beams, IEEE Trans.Nucl.Sci. 22, No3, June 1975
- /15/ R.F.Bentley et al., Pulsed beam chopper for LAMPF, ibidem
- /16/ P.E. Faugeras et al., The SPS fast pulsed magnet systems, CERN/SPS/BT/76-1
- /17/ R.K.Cooper, J.R.Faulkner, The LAMPF line D fast deflector system, LASL Report LA-6748-MS, May 1977
- /18/ H.Kuhn, G.H.Schröder, High power pulse generators for fast pulsed magnets, developments and operational experience, CERN-SPS/80-06/ABT, June 1980
- /19/ D.E.Suddeth, G.J.Volk, Intense pulsed neutron source (IPNS-I) accelerator 500 MeV fast kicker, IEEE Trans.Nucl.Sci. 26, No 3, June 1979
- /20/ G.Nassibian, Travelling wave kicker magnets with sharp rise and less overshoot, ibidem
- /21/ D.Fiander et al., The injection kicker of the CERN antiproton accumulator, IEEE Trans.Nucl.Sci. 28, No3, June 1981

- /22/ G.Schaffer, HF-Einrichtungen zur Dunkeltastung des Linacstrahls einer Spallationsneutronenquelle, private communication
- /23/ L.Evans et al., The steel septum magnet for beam splitting at the CERN SPS, CERN-SPS/77-13
- /24/ Y.Baconnier et al., Septum magnets for the extraction channel of the 400 GeV SPS, CERN-SPS/ABT/77-15
- /25/ G.Schaffer, Strahlpulsung und Strahlverteilung am SNQ Linearbeschleuniger, private communication
- /26/ W.C.Nunnally et al., Fast extraction modulator for Los Alamos Scientific Laboratory Storage Ring, LA-UR-80-1510, June 1980
- /27/ G.Stange, A new type of pulsed air core multipoles of extremely simple construction, IEEE Trans.Nucl.Sci. NS-28, No3, June 1981 p.2829
- /28/ M.Ellefsplass and E.Weisse, CERN, private communication  
M.Ellefsplass, Some details on the handling of plug-in magnets, CERN-SPS/RA/TM/76-6, March 1976
- /29/ G.Corazza et al., Remotely controlled vacuum coupling, private communication
- /30/ F.Früngel, High-speed pulse technology, vol.III capacitor discharge engineering, Academic Press 1976
- /31/ P.E.Faugeras, G.Schröder, Generation of high current, long duration rectangular pulses, private communication
- /32/ English Electric Valve Co., Hydrogen Thyatron and Ignitron Product Data
- /33/ W.Kühn, Entwurf einer schnellen Strahlweiche für den hochenergetischen Protonenstrahl des SNQ-Linac, private communication
- /34/ G.Schaffer, Pulsleitungsschaltungen für Laufzeitkickermagnete mit Impulsreflexion, private communication
- /35/ G.Schaffer, Ein robuster Schnellablenker für den UNILAC Injektionsstrahl, GSI Jahresbericht 1978, S.218
- /36/ J.S.Lunsford et al., Versatile H<sup>+</sup> beam chopper at LAMPF, IEEE Trans.Nucl.Sci. NS-26, No3, June 1979
- /37/ G.Schaffer, Auslegung und thermische Belastung von Strahlfängern in der Niederenergie-Strahlführung der Spallationsneutronenquelle, private communication
- /38/ R.J.Macek, this meeting

Rf Power System for SNQ

G. Hochschild

Kernforschungszentrum Karlsruhe, Institut für Kernphysik,  
Postfach 3640, D-7500 Karlsruhe, Federal Republic of Germany

General Requirements

The SNQ linear accelerator<sup>1,2</sup> consists of the alvarez part (up to 105 MeV) operated at 108 MHz and the disk-and-washer part (105 - 1100 MeV) operated at 324 MHz. The requirements for the appropriate rf system are summarized in table 1. The most stringent design parameters are the high pulse power demand and the close rf field tolerances.

Table 1

<b>rf system</b>	<b>general data</b>		
frequency	108	324	MHz
rf pulse power	21	267	MW
<b>amplifier</b>	<b>tetrode</b>	<b>klystron</b>	
peak power output	2 x 1.8	3.5	MW
number (active)	2 x 7	89	
amplitude modulation	rf input	grid	
operational efficiency	39%	52%	
mains power		34	MVA
<b>field stability</b>			
amplitude		± 0.1	%
phase		± 0.2	°
<b>rf pulse</b>			
repetition rate		100	Hz
length	750	600	µs

Additional design informations are derived from the pulse course (fig. 1), which can be divided into a filling period to build up the rf field in the cavity, a control recovery period to stabilize the field within the tolerances and the period of beam transition. Thus, the rf pulse is

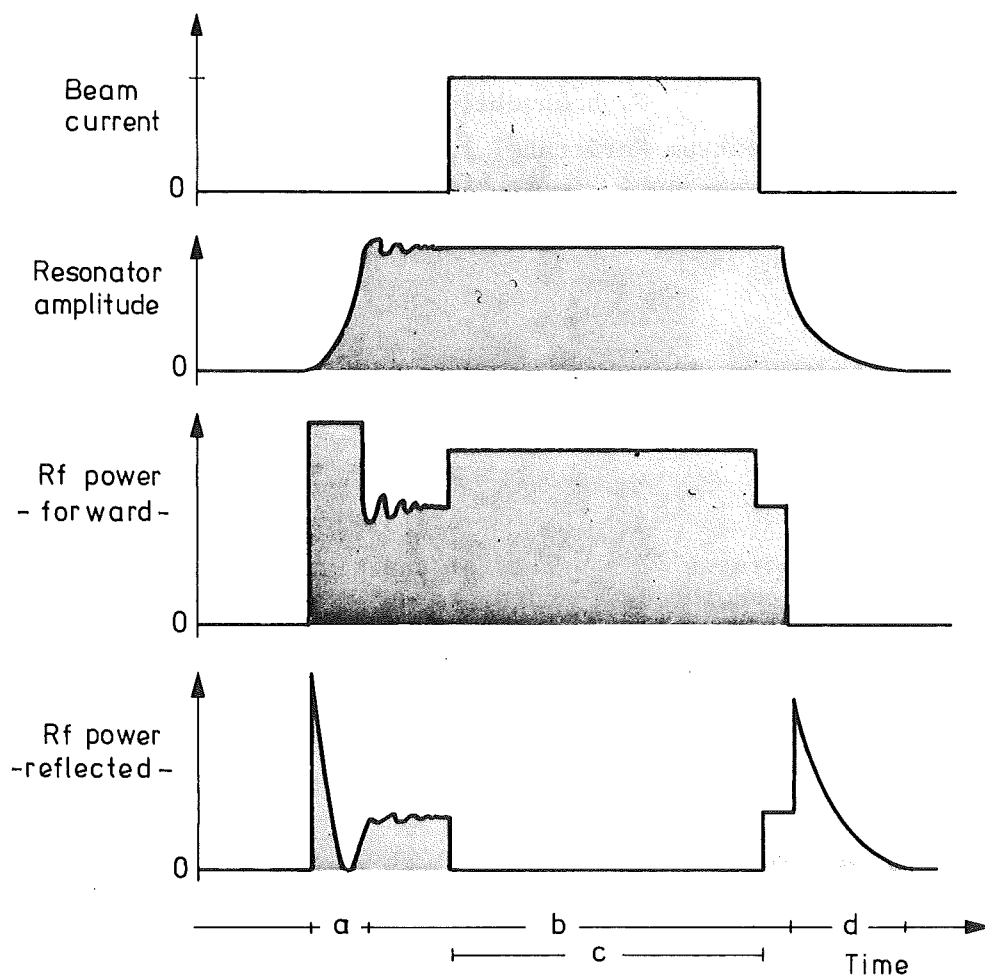


Fig. 1: Pulse course

remarkably longer than the beam pulse. Shortening the filling time, as discussed in <sup>3</sup>, is therefore an effective measure to increase the operational efficiency of the rf system.

Spread over the frequency range of interest for linacs, different technical solutions for rf power amplifiers have been developed, as represented in the graph (fig. 2). The frequencies selected for SNQ (108 and 324 MHz) prove to be well suited from the power generation point of view. With tetrodes and klystrons, respectively, corresponding to the state of the art, the rf power required for SNQ in long pulse operation is certainly achievable. The "exotic triodes" are not considered for this design.

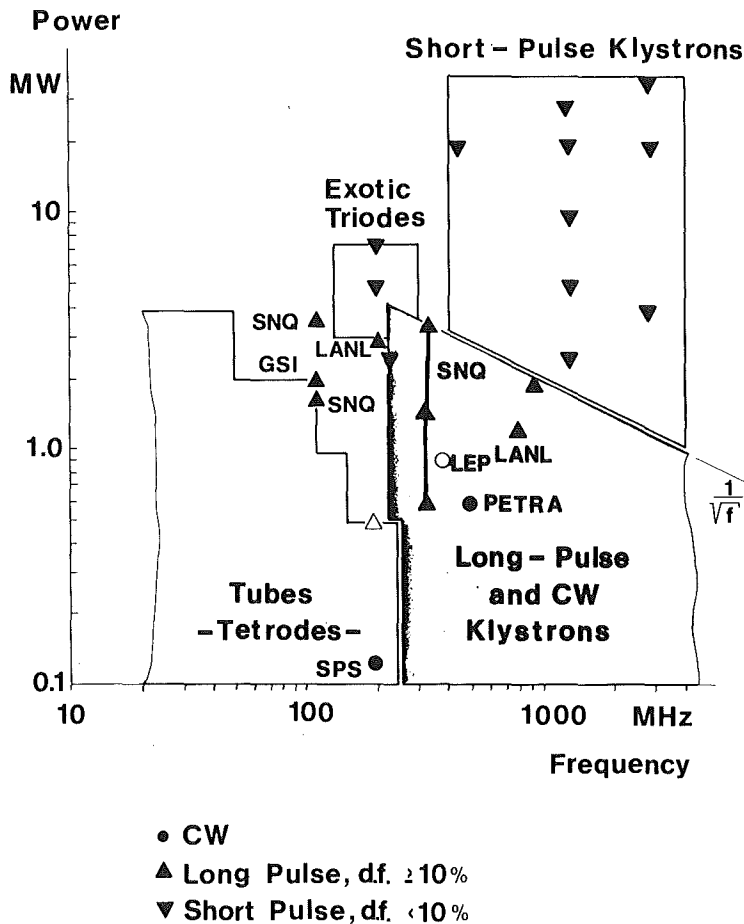


Fig. 2: Power amplifiers: State of the art

### Design Objectives

For the layout of the power amplifiers, the following design objectives are of major concern:

The reliability of each individual power amplifier is an essential condition for the integral beam availability. In contrast to some recent designs (e.g.<sup>4</sup>), where redundant power was provided by coupled amplifiers, only a low power margin was planned for SNQ. The SNQ amplifiers are completely separated on the rf-side. This simplification of the rf system increases the reliability. The modular amplifier design allows for fast replacement even of larger components (e.g. klystrons) and thereby shortens the repair time.

The economy of the rf power system requires optimized operational efficiency, integrated over the different power levels during the pulse course (see fig. 1). Both the advanced grid modulation method for the klystrons (to be

discussed later) and the short filling and control recovery times<sup>3</sup> are outstanding contributions to the optimization of efficiency.

The control behaviour of the power amplifiers must be considered in respect of the close field tolerance requirements (see table 1). Linearity, stability and control response are essential aspects. Short tanks with individual rf feeds and individual control systems are a consequence of the tolerance requirements.

### Tetrode Amplifiers

At 108 MHz, tetrode amplifiers with a nominal rf pulse power of 1.6 MW are commercially available. Long term experience cummulated at GSI/Darmstadt led to a new design<sup>5</sup> (fig. 3).

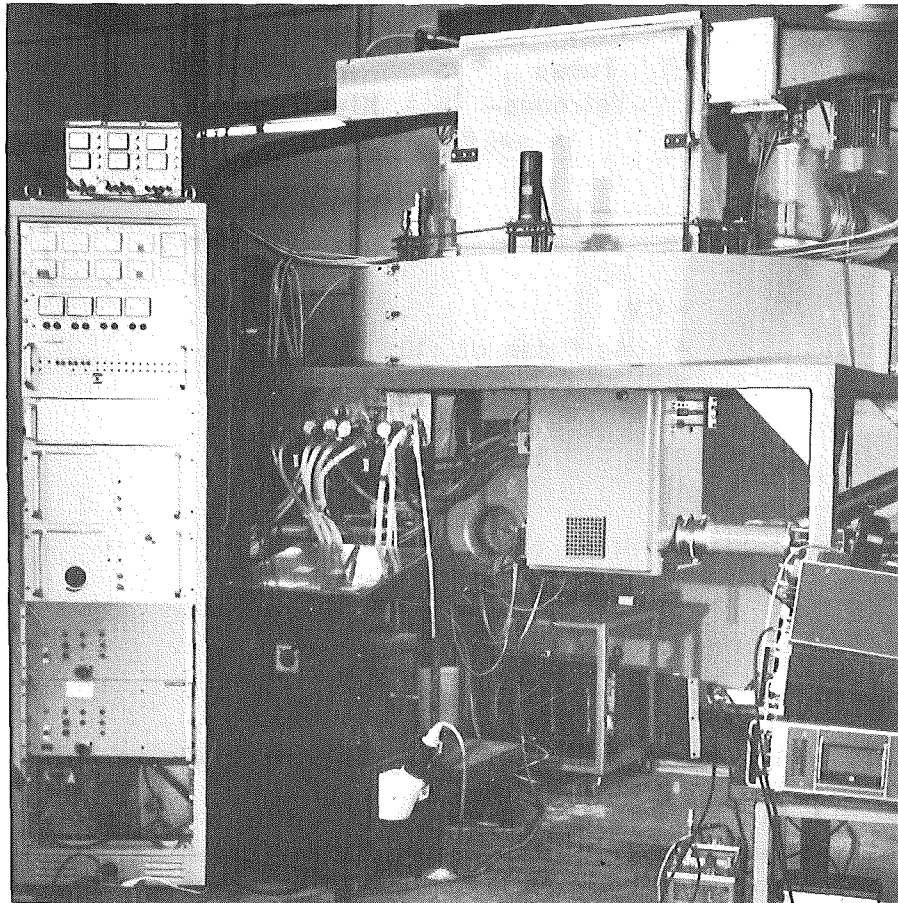


Fig. 3: Tetrode amplifier prototype

The advantage of this amplifier comes from the flat circular anode resonator (fig. 4), which allows for effective damping measures. Thereby parasitic oscillations, the major menace for large rf power tubes, operated at this relatively high frequency, can be eliminated. With this new amplifier, as

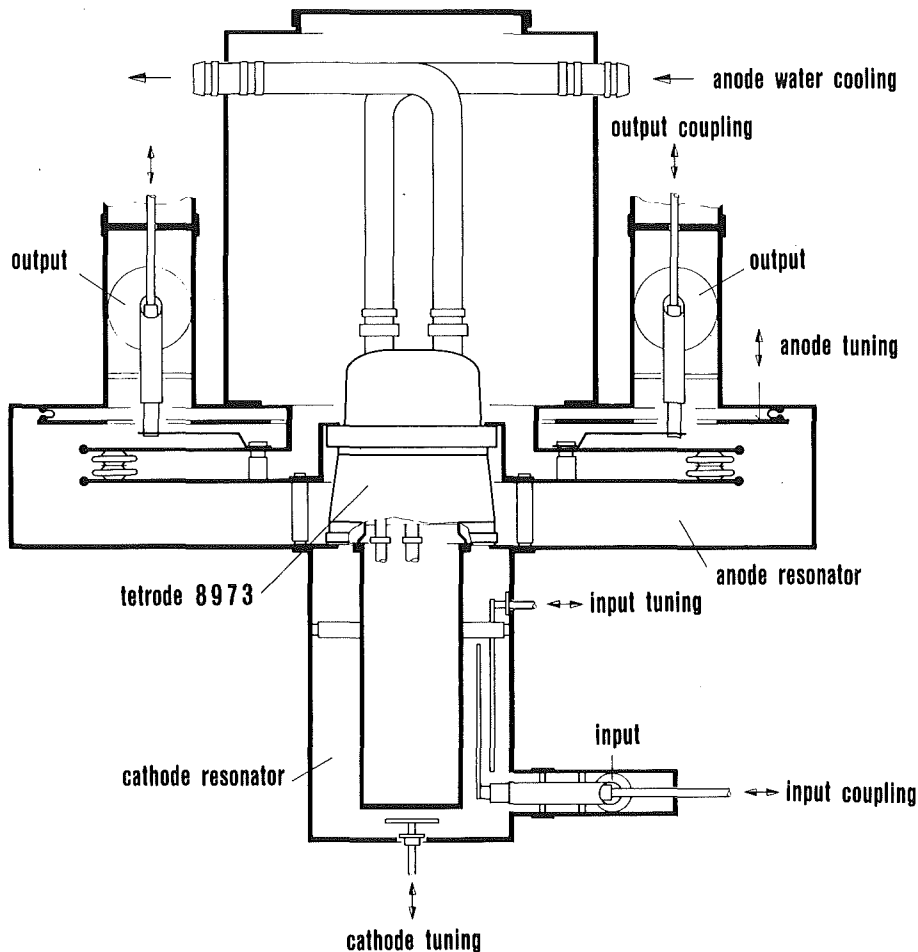


Fig. 4: Schematic cross section at the tetrode amplifier

well as with the improved older GSI equipment, 2 MW of pulse power were achieved<sup>6</sup>.

The power requirement for each 108 MHz power unit is 3.6 MW, thus two tetrode amplifiers must be combined. Therefore a 90° hybrid junction and a symmetry control circuit are provided.

Power tetrodes suitable for the final amplifier are in series production by different manufacturers mainly for shortwave broadcasting applications.

#### Klystron Amplifiers

At 324 MHz, klystron amplifiers are expected to deliver  $\sim 4$  MW of pulse power output (see fig. 1), which perfectly corresponds to the nominal input requirement of 3 MW for the DAW-tanks. A study klystron was built and successfully tested (fig. 5). Details are reported elsewhere<sup>7</sup>. Including the performance of the PETRA-klystron<sup>8</sup>, the following design features have been already demonstrated:

- frequency	324	MHz
- average power	0.6	MW
- efficiency	70	%

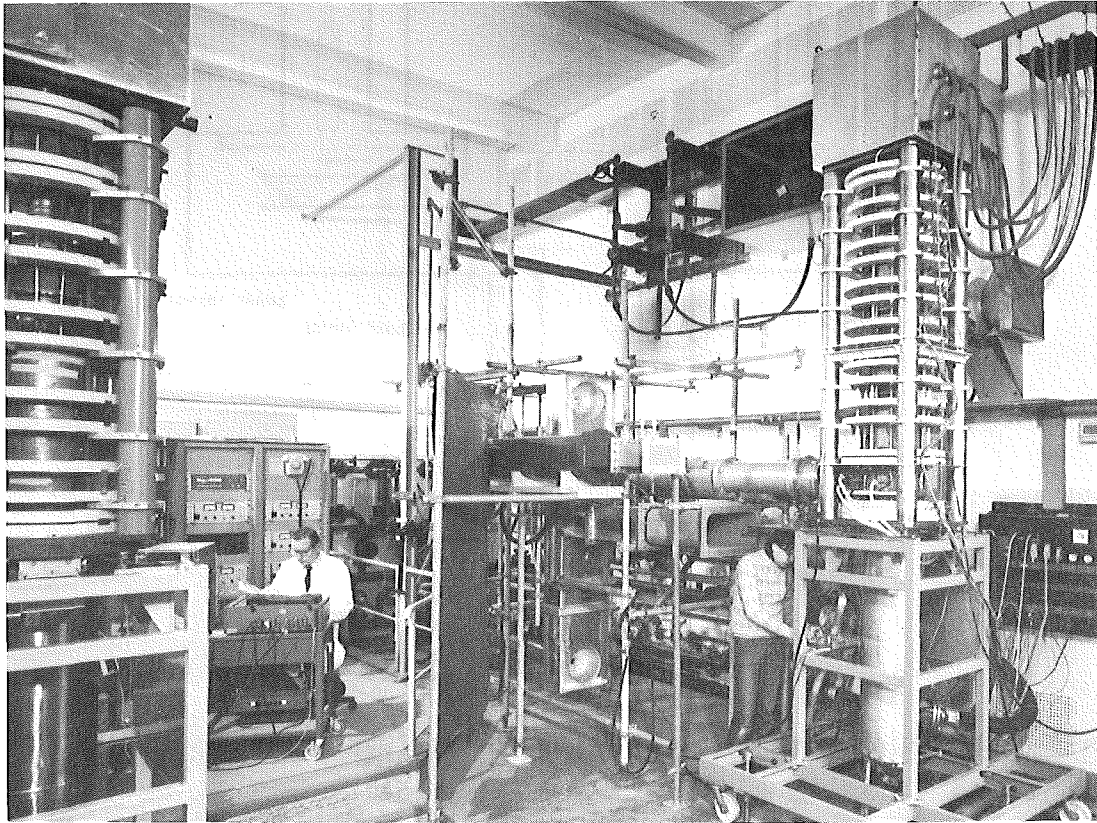


Fig. 5: The study klystron assembled in the test facility

The pulse power required ( $> 3.5$  MW) was not achievable with the present test facility and remains as a future development step.

Amplitude modulation of the klystron amplifier strongly influences the operational efficiency. Alternatively, the following methods may be considered:

- rf drive modulation
- beam current modulation.

In either case, the efficiency depends on the output level as plotted in fig. 6. The highest achievable efficiency results from a combination of both methods. Integrated over the pulse course (fig. 1) with the changing

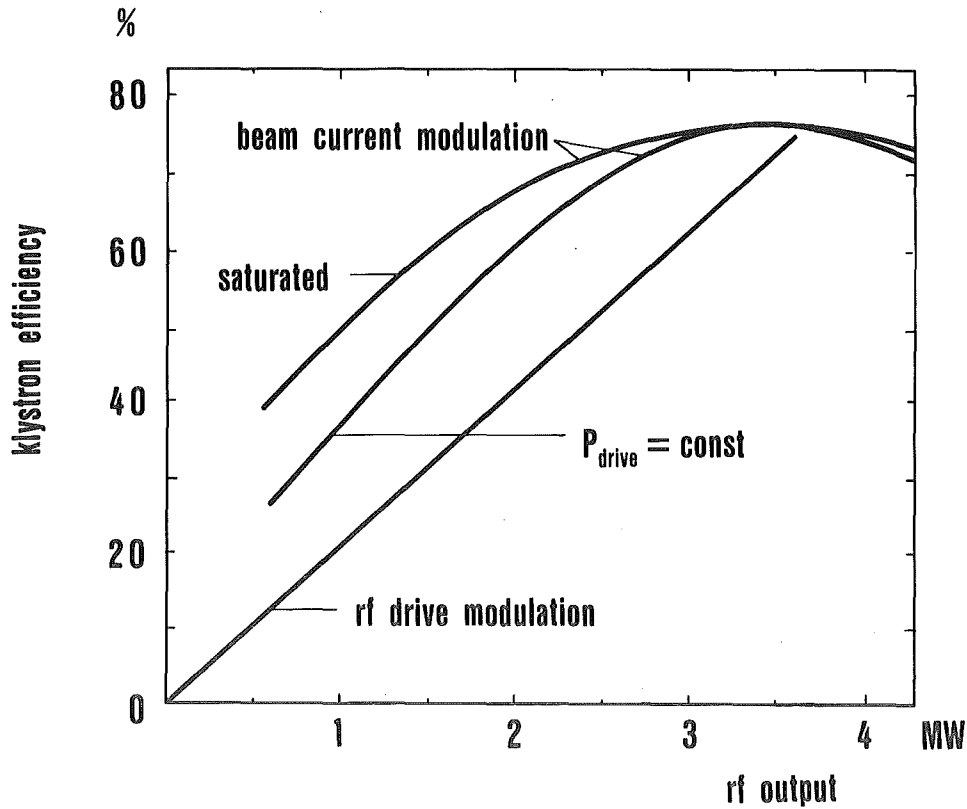


Fig. 6: Klystron efficiency depending on the modulation method

rf power level, an operational efficiency of 45 % for the rf drive modulation and 54 % for the beam current modulation are calculated, which strongly recommends the latter modulation method. In parallel to the efficiency optimization, the control requirements must be accomplished, which includes a fast control response. The control speed achievable with the conventional beam current modulation by a modulation anode is inadequate because of the high voltage swing to be applied.

In order to overcome this control speed problem, grid control of the klystron beam was proposed. Current developments on lower power TV klystrons will be adaptable to high power klystrons. The study klystron (fig. 5) is suitable for modification of the modulation anode controlled electron gun into a grid controlled gun and for subsequent high power tests. In a concluding development step, the construction of the 3.5 MW prototype klystron and integral tests with the prototype amplifier unit (fig. 7) are planned.

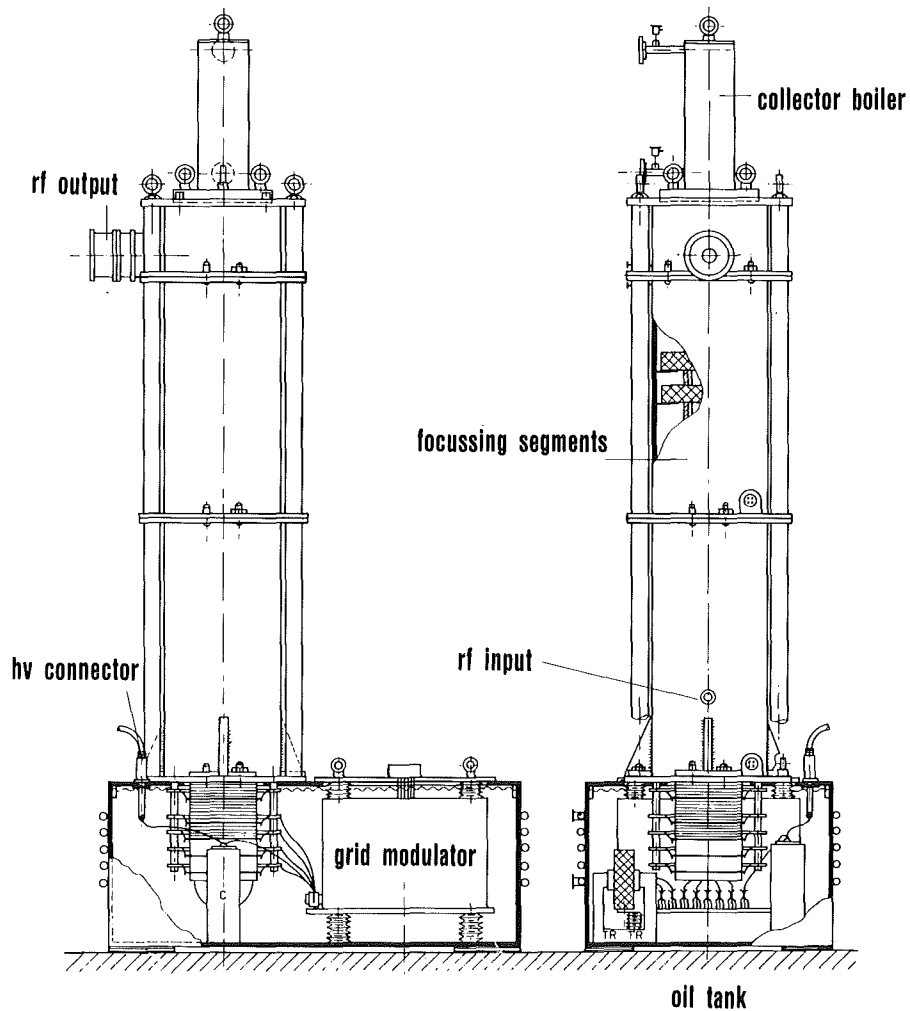


Fig. 7: 3.5 MW klystron amplifier unit

### Conclusions

The rf power system design for SNQ is based on amplifier technologies corresponding to the state of the art, which ensures the feasibility. In particular the development of a grid controlled high power klystron proposed for efficiency optimization still requires some effort.

References:

1. J.E. Vetter ed., "The Basic Concept of the SNQ Accelerator", Kernforschungszentrum Karlsruhe, KfK 3180 B (June 1981)
2. G.S. Bauer et al., ed., "Realisierungsstudie zur Spallations-Neutronenquelle", Jül-Spez-113 and KfK 3175 (June 1981)
3. D. Schulze, "New Methods of RF Control for the SNQ", these proceedings
4. M.V. Fazio et al., "A proposed Rf System for the Fusion Materials Irradiation Test Facility", IEEE Trans. Nucl. Sci. NS-26, No. 3, pp 3018-3020, June 1979
5. K.H. Knobbe, D. Böhne, "A Megawatt Rf Source at 108 MHz", IEEE Trans. Nucl. Sci. NS-28, No. 3, pp. 3010-3011, June 1981
6. G. Hutter, N. Angert, "Improvement of the 108 MHz Rf-Amplifiers for the Unilac Alvarez Structure", IEEE Trans. Nucl. Sci. NS-28, No. 3, pp. 3012-3013, June 1981
7. G. Hochschild, E. Demmel, "Rf Power Source Development for the High Current Linear Accelerator of the Spallation Neutron Source (SNQ)", IEEE Trans. Nucl. Sci. NS-28, No. 3, pp. 2836-2838, June 1981
8. H. Musfeldt, H. Kumpfert, W. Schmidt, "A new Generation of High Power CW-Klystrons for Accelerator and Storage Ring Application, Practical Experience and Aspects for Future Developments", IEEE Trans. Nucl. Sci. NS-28, No. 3, pp. 2833-2835, June 1981

Discussion:

The rise time of the rf is given by the Q-value of the cavities. The control system is designed for a rectangular rf-pulse of the clystrons. This will be discussed in more detail by W. Schulze.

The efficiency of the klystron with more than 70% is the saturated efficiency at power levels of the designed value. At any other power levels the efficiency is lower, but highest with grid control.

The overall efficiencies of the klystron is about 52%. This seems to be optimistic. But the intrinsic efficiency of the designed klystron is higher than usual.

Combining grid-modulation and drive-modulation doesn't increase the efficiency.

The efficiency of 39% for a tetrode is the overall efficiency including the total on time of the tetrode in comparison to the beam transition time.

New Methods of RF-Control for the SNQ

D. Schulze

Kernforschungszentrum Karlsruhe, Institut für Kernphysik,  
Postfach 3640, D-7500 Karlsruhe, Federal Republic of Germany

Summary

The Karlsruhe- Spallations- Source SNQ with 100 mA beam current and 100 Hz repetition rate demands a better rf control accuracy compared with operating proton linear accelerators. Two new methods have been investigated.

The first method applies a phase step during turn-on, which can lead to a shorter filling time and a better efficiency of the pulsed power transfer.

The second method uses a computer model of the amplitude and phase control system for an automatic adjustment of the feedforward beam compensation pulse.

Thereby, the amplitude and the phase control error due to beam transients are reduced and stabilized against long-term parameter fluctuations. This is important for low particle losses.

It is possible to achieve and maintain a field error of  $\pm 0.1\%$  and  $\pm 0.1^\circ$  in the worst case of a sharp pulsed beam.

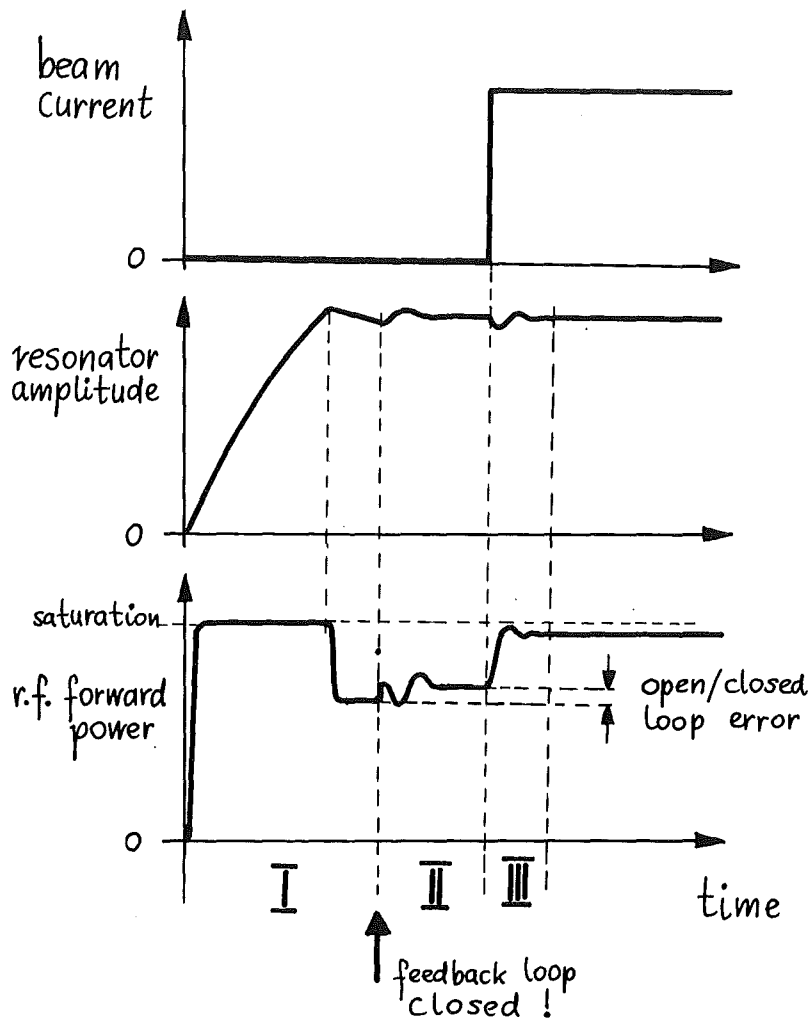


Fig. 1 rf pulses during field build-up and beam turn-on

For a cavity operated in resonance, the answer is well known. But is this right also for the detuned case, if the generator frequency differs from the cavity resonance? And the detuned case is the favorable one in the presence of high beam loading<sup>3</sup>, because the beam produces also reactive power  $I \cdot V \cdot \sin \phi$  ( $\phi$  = phase angle between the beam buckets and the field wave maximum;  $I$  = beam current;  $V$  = voltage drop).

In order to save generator power, this reactive beam power can only be cancelled by detuning the cavity in the unloaded case.

Modern spallation neutron sources based on ion linear accelerators<sup>1</sup> carry an intense beam of hundreds of mA with repetition rates as high as 100 Hz. From the point of view of rf-control two key questions are raised:

1. What is the shortest possible time to transfer the rf field into the steady state?
2. What is the minimum amplitude and phase error due to transient beam loading?

The first question determines the efficiency of pulsed power transfer<sup>2</sup> to the beam. The second question influences the amount of particle losses, a serious question in the presence of high beam intensity and high repetition rate.

Both questions have been analyzed and methods have been developed to minimize both the filling and recovery time and the field error.

#### rf-field and beam turn-on

The two questions are best illustrated by the typical build-up and time-dependencies of the resonator field and the generator forward power, which are shown in Fig. 1. Phase I is the filling of the cavity by applying the maximum available generator power, which is switched back to the nominal value, when the nominal field level is reached. This is done in the open loop state, which provides certainly the fastest way to build up the cavity field.

Phase II is started by closing the amplitude and phase feedback loops. There might be a small error between open and closed loop adjustment. In this case the field and the forward power do need a certain time to recover to the steady state.

Only when the steady state is reached again, the beam is allowed to enter the cavity (phase III). Because the beam represents a complex load on the cavity, both the amplitude and phase feedback loop are forced to restore the nominal amplitude and phase of the resonator. Because of the limited loop gain the forward power can not track exactly the sharp beam transient resulting in a beam induced field error.

#### Dead beat filling of the cavity

Let's turn to the first question and assume that the open/closed loop adjustment error can be avoided. Then the question of the shortest possible filling and recovery time (phase I and phase II) reduces to the question, whether the field phase and amplitude (in the open loop state) is in the steady state immediately after the generator power has switched back to its nominal value.

A theoretical treatment<sup>4,5</sup> shows, that the steady state in the detuned case can only be obtained, if in addition to the generator power step a certain generator phase step is applied.

Mathematically speaking this result means that it is possible to cancel the amplitude step driven beat solution (beat between generator- and eigenfrequency) through a certain phase step.

In analogy to the "dead beat response" of the control theory, this type of cavity filling can be called "dead beat filling".

The theoretical results had been tested by a simple low power rf experiment, which is explained through a series of polaroid photographs in Fig. 2.

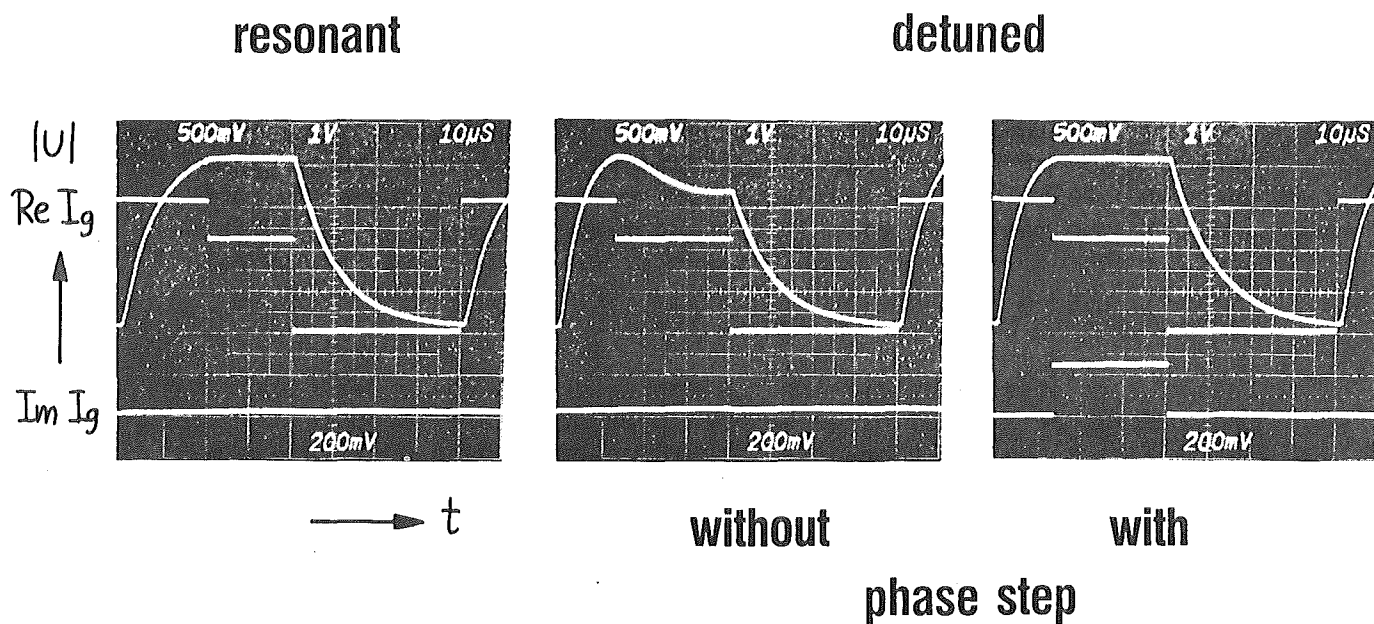


Fig. 2 Dead beat filling of a detuned resonator

The upper step function is the real part of the complex generator amplitude (corresponding to the forward power) and the lower step function is the imaginary part of the complex generator amplitude (corresponding to the generator phase angle).

On the left hand the well-known resonance case is seen. The steady state is obtained only by an amplitude or power step. In the middle one has the detuned case. The cavity field amplitude shows clearly the beat solution and no steady state. Finally, on the right hand one can see the helpful work of the phase step. When the generator is switched off, the phase is returned to zero.

The definition of the phase step  $\Delta\phi$  and the filling time  $T_F$  is illustrated by the hodograph of the complex generator amplitude shown in Fig. 3.

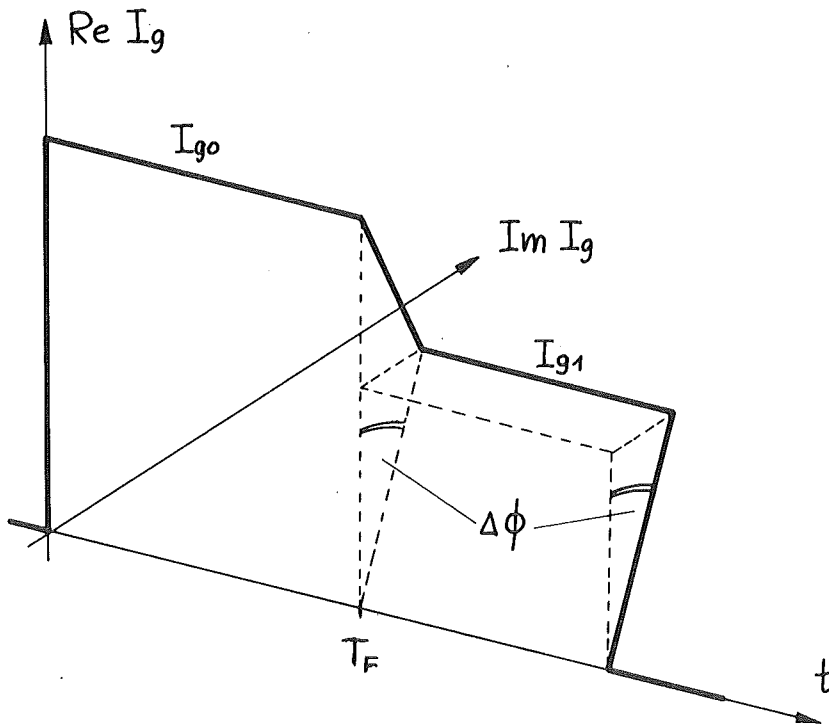


Fig. 3 Hodograph of the complex generator amplitude

The quantitative relation between power and phase step and the resulting filling time  $T_F$  versus beam loading factor is given in Fig. 4. The beam loading factor is defined as ratio of the power extracted by the beam to the cavity loss power. For the disk and washer structure at  $\beta = 0.7$  the beam loading factor becomes  $b = 0.8$  leading to a power step of 1.6 and a phase step of  $4^\circ$ . The filling  $T_F$ , which is normalized on the "loaded" decay time, is in this typical case  $30 \mu\text{sec}$ .

Although the phase step is only  $4^\circ$ , we have certainly to take this into consideration, if we think on the anticipated control accuracy of  $\pm 0.1\%$  and  $\pm 0.1^\circ$ .

A more exact treatment of the turn-on procedure would have to obey the fact, that the source resistance of the klystron or the tetrode power amplifiers differ from the transmission line impedance.

If, in addition, the transmission line length differs slightly from  $n \times \lambda/2$  the dead beat condition does change and so the phase step. This more general case will not be treated here.

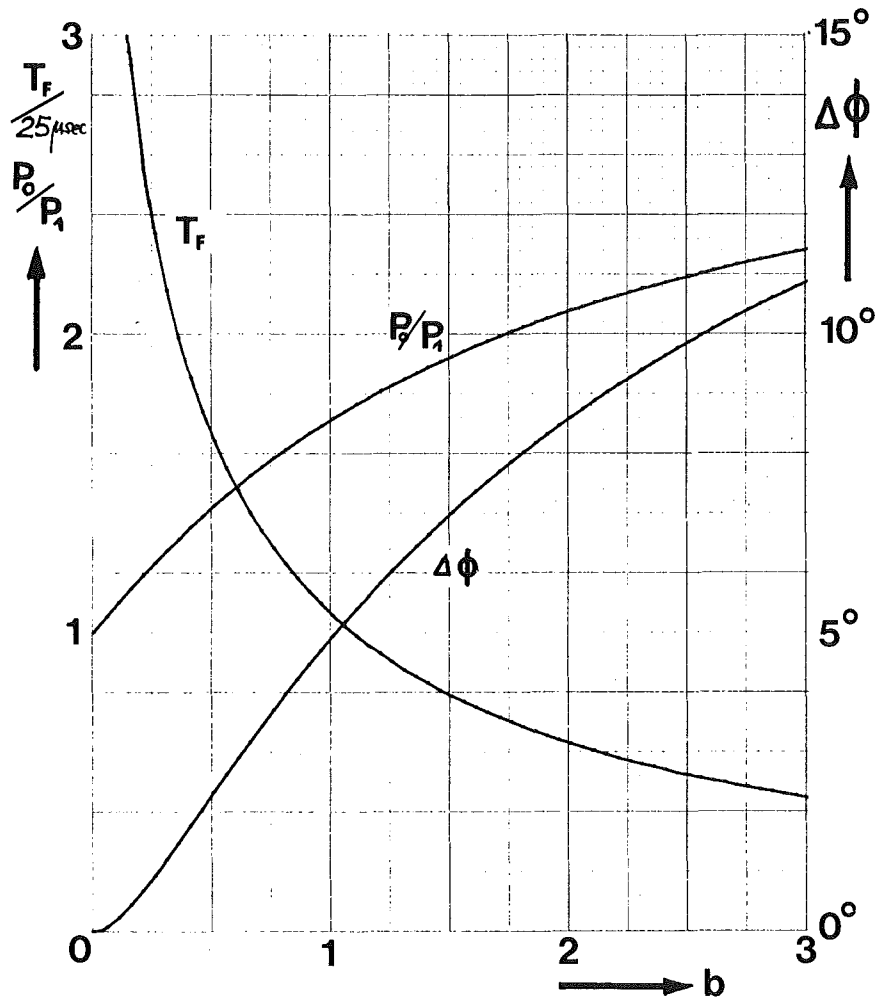


Fig. 4 Phase step  $\Delta\phi$ , power step  $P_0/P_1$  and optimum filling time  $T_F$  versus beam loading factor  $b$

Feedforward control (FFC) due to transient beam loading

Let's now proceed to the second key question, the minimization of the field error caused by beam transients.

The very first measure is an amplitude and phase feedback<sup>6,7,8</sup>. Because the reaction develops with a limited velocity according to the unity gain frequency, which is typical 200 kHz, a field error of typical 3 % can not be avoided.

An improvement can be obtained with an additional feedforward control system. Thereby, usually a signal is created from a beam pick-up and fed to the amplitude (and phase) controller, as it is done i.g. at LAMPF<sup>9,10</sup>.

In our case, most of the experiments that will be done with the Spallation Source, require a sharp pulsed beam. I'll restrict the

the following considerations on this case, namely beam transients, that can be treated as a step function. It is obvious, that the compensating feedforward pulse is also a step function with a certain amplitude and a certain delay time. It then has not necessarily to be derived from the beam. A simple pulse generator will do the same job.

The results of a computer simulation are shown in Fig. 5. The upper curve shows the dynamic field error caused by the beam pulse without feedforward. The maximum field error is 2,5 %.

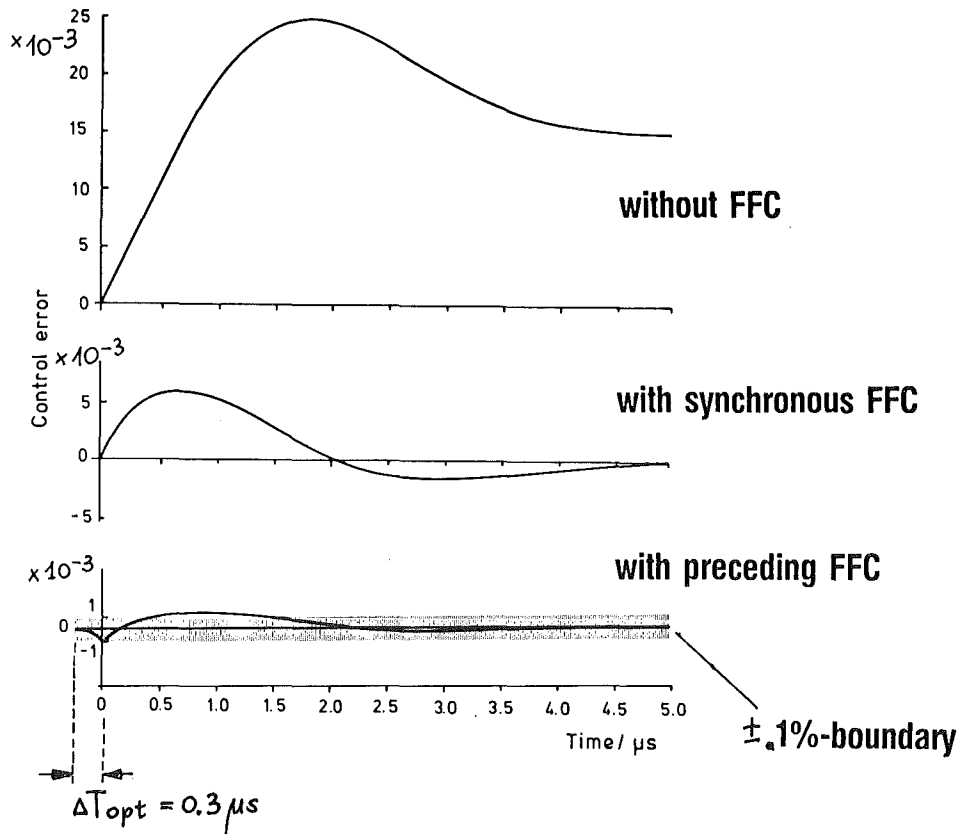


Fig. 5 Control error due to transient beam loading without, with synchronous and with preceding feedforward control (FFC)

The middle curve shows the drastic reduction by a factor of 5, when a FFC pulse synchronous with the beam pulse is added to the amplitude (and phase) modulator. A further reduction can be obtained, when the FFC pulse raises the generator power before the beam enters the cavity; that is the FFC pulse precedes the beam pulse. At an optimum leading time of 0.3  $\mu\text{sec}$  a factor of 4 compared to the synchronous case is gained. A total reduction of the dynamic field error into nearly the desired  $\pm 0.1\%$  boundary is obtained.

From the point of view of a practical accelerator operation the comparison of the middle and the lower curve of Fig. 5 illustrates on the other hand clearly the large sensitivity of the control error against parameter

fluctuations of the delay time. The FFC delay time resolution has to be better than 30 nanosec. In the real accelerator operation an operator would have to correct the delay of the FFC until the desired minimum of the control error is reached again.

One can simply ask: Isn't it possible to replace this human action by an automatic system? We have analyzed this question and we came to a solution, which is outlined in Fig. 6. The most important part is a computer model of the amplitude and phase control system.

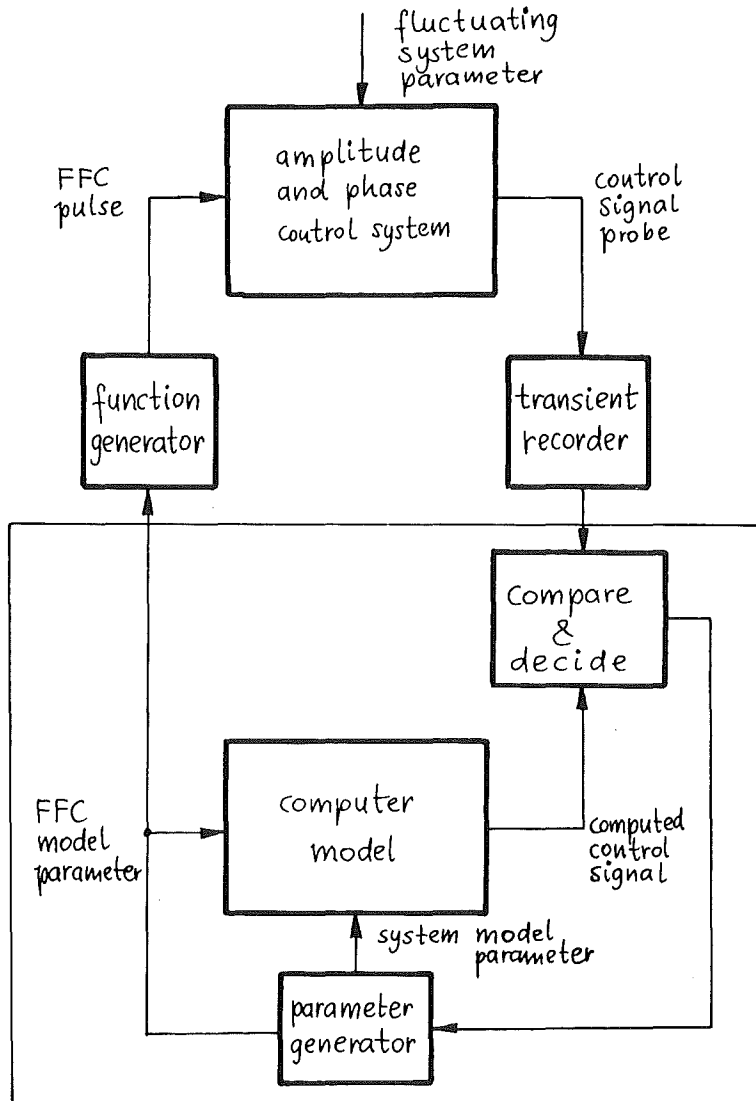


Fig. 6 Basic block diagram of adaptive feedforward parameter adjustment

The parameter adjustment procedure works as follows: A control signal probe is taken from the "real world" through a transient recorder. The

equivalent signal produced by the computer model is varied by means of parameter variations as long as it fits good enough to the probe signal. Then the necessary parameter correction is computed and used to correct the pulse generator parameters. One can call this an adaptive procedure. It will be as good as the computer model of the real world is.

Therefore, we have to look for an appropriate computer model of the feedback loop(s) including the FFC.

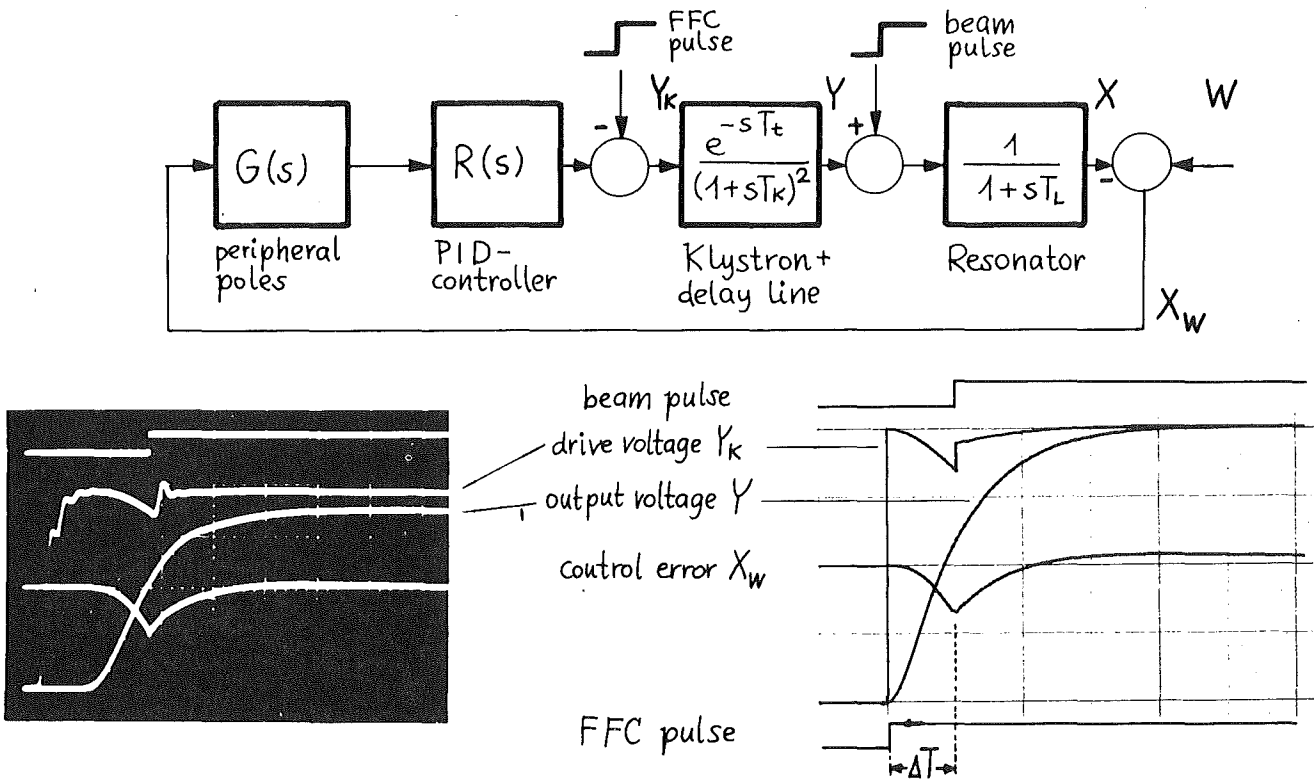


Fig. 7 Control error  $X_w$ , klystron drive voltage  $Y_K$  and klystron output voltage  $Y$  in response to a beam and FFC step

Fig. 7 shows a simplified dynamic model of the amplitude control loop. We have assumed a simple lag behaviour for the resonator with time constant  $T_L$ . The klystron with grid control was assumed to have a double pole with time constant  $T_K$ . For the controller a real PID-controller has been chosen. The transmission line was represented by a delay with time  $T_t$ . Two more poles for the dc-amplifiers have been inserted.

The polaroid photograph on the left was taken from an analog model<sup>12</sup>, which has the advantage that all interesting signals appear in real time and that it is easy to vary the several parameters as pulse delay, pulse height, loop gain etc.

The photograph shows from above the beam pulse, the klystron drive voltage  $Y_K$ , the klystron output voltage  $Y$  and the control error  $X_W$  at optimum delay. One can see, that the klystron drive voltage, which is limited by saturation, at this optimum adjustment shows no overshoot with exception of a little tip. On the right hand side the same signals from a simple computer model are shown. As one can see, there is a fairly good agreement with the results of the analog model.

In order to complete the parameter adjustment loop as shown in Fig. 6 we are developing an algorithm for the parameter generation. The big advantage of the method described above lies in the fact, that only one shot from the "real world" is necessary. The adaption itself takes places in the "computer world".

Summarizing the new methods of control:

1. We have discovered the phase step in detuned operation, which allows to reduce the filling and recovery time.
2. An adaptive feedforward parameter adjustment procedure is developed, which allows to stabilise the field error minimum against parameter fluctuations.

References:

1. J.E. Vetter, editor, The Basic Concept of the SNQ Linear Accelerator, Kernforschungszentrum Karlsruhe, KfK 3180 B (1981)
2. G. Hochschild, RF-Power System at SNQ, this meeting
3. D. Schulze, Zur Wahl der Betriebsparameter für die Resonatoren eines supraleitenden Protonenlinearbeschleunigers, private communication
4. D. Schulze, Dead Beat Filling and Feedforward Control for the Beam Loaded Cavities of the German Spallation Neutron Source, to be published
5. D. Schulze, Zeitoptimales Anfahren der Hf-Resonatoren für eine Spallationsneutronenquelle; private communication
6. R.A. Jameson, Analysis of a Proton Linear Accelerator RF-System and Application to RF Phase Control, LA-3372, Los Alamos, N.M., June 1965
7. B.P. Murin, RF-Field Stabilization and Control for Ion Linear Accelerators (in Russian), Atomisdat, Moscow, 1971
8. J. Cuperus, F. James, W. Pirkel, The RF-System of the CERN New Linac, Proc. 1979 Lin. Acc. Conf., Montauk, N.Y., Sept. 1979, BNL 51 134
9. R.A. Jameson, D.J. Wallace, Feedforward Control of Accelerator RF Fields, IEEE, Trans.Nucl.Sci. NS-18, No. 3, pp. 598-600, June 1971
10. R.J. Macek, Operation Experience with Meson Factories, this meeting
11. D. Schulze, Analyse des SNQ-HF-Regelungssystems und Simulation des zeitlichen Störverhaltens, private communication
12. A. Hornung, Analogmodell der Amplitudenregelung für die 324 MHz-Tanks des SNQ-Beschleunigers, private communication

Discussion.

The calculations are done with a beam current of 100 mAmps. The feed-forward control would work at higher beam loading as well. There is no upper limit .

It is hard to say what the reduction on beam spill can be. It is dependant on the loss mechanism . Most losses seem to be caused by the transients. Measurements done at the new CERN linac showed that only three % of the total loss is caused by the transient. But it is beleaved that for these measurements a big amount of losses in the steady state case is caused by a misalignment of the rf-amplitude and rf - phase. The losses seem to be linear with the deviation from the desired value.

## OPERATING EXPERIENCE WITH THE MESON FACTORIES

Robert J. Macek  
Los Alamos National Laboratory, Los Alamos, NM 87545

### Introduction

It is conventional to define a meson factory as a machine producing protons with energies 500 MeV or higher and currents in excess of 100  $\mu\text{A}$ .<sup>1</sup> I will discuss three operating facilities that meet these criteria, namely LAMPF, SIN and TRIUMF. They are mature facilities that have essentially met or exceeded design goals, are now working reliably, and have active, multifaceted research programs in basic and applied physics. While no really major surprises were encountered in their construction and operation to date, much has been learned from the experience with these machines. They represent a great deal of progress in high intensity accelerator science and technology.

### DESCRIPTION OF LAMPF, SIN AND TRIUMF

Since this is a survey talk and there are non-specialists in attendance, it is appropriate to briefly review the main features of these facilities. An overall view of the LAMPF facility is given in Fig. 1 and a floor plan of the experimental areas is shown in Fig. 2. Protons are injected at 750 keV, accelerated to 100 MeV in a drift-tube Linac and then to the maximum energy of 800 MeV in a side-coupled Linac.  $\text{H}^+$  and  $\text{H}^-$  ions are accelerated simultaneously with a macroscopic duty factor that is now 9%. The experimental areas are extensive and designed to accommodate as many simultaneous users as possible. The intense  $\text{H}^+$  beam is delivered to three targets in series. The primary  $\text{H}^+$  beam line serving these targets is serviced by extensive remote handling systems.

The SIN machine floor plan<sup>2</sup> is shown in Fig. 3. It is a combination of two isochronous cyclotrons. The low energy injector cyclotron operates at 72 MeV and is used for low energy research or as an injector to a ring cyclotron consisting of eight separate sector magnets and four separate main rf cavities. A fifth cavity provides a 3rd harmonic flat top. The main cyclotron accelerates protons to 590 MeV in separated turns. The macroscopic duty factor is 100%. The experimental areas are also extensive and designed to serve many simultaneous users.

The TRIUMF machine, shown in Fig. 4, is a sector-focussed isochronous cyclotron using  $H^-$  ions injected at 300 keV. The  $H^-$  beam is extracted by stripping to  $H^+$  with a foil placed at the appropriate radius in the cyclotron. In this way the energy is continuously variable from 183 to 520 MeV and two or more beams may be extracted simultaneously, and at independently variable energies and intensities with a macroscopic duty factor of 100%. The price paid for these advantages is significant losses due to gas stripping at low energies and electromagnetic stripping at the higher energies. The adjacent experimental areas are extensive and designed to serve several simultaneous users.

A comparison of the high intensity parameters for these machines is given in Table I. LAMPF is presently operating at 600  $\mu$ A while SIN and TRIUMF presently operate somewhat above 100  $\mu$ A.

#### OPERATING EXPERIENCE

There are many interesting topics that could be developed, but I have selected those that seem to be of greatest interest to ICANS participants; in particular, those that relate to limitations on beam intensity and reliability of operation. I will also emphasize what has been learned from operations that might be useful for the design of higher intensity machines.

### A. History of Intensity Buildup

The high intensity phase of LAMPF operations began in 1976 at 10  $\mu\text{A}$ . The intensity rose to 300  $\mu\text{A}$  by 1977 and was over 500  $\mu\text{A}$  in 1979. A graph of the build of intensity for LAMPF is shown in Fig. 5. Activation of the accelerator and switchyard components actually declined as the current went up. This can be attributed, in part, to improved tunes and tuning procedures but more than anything else, to improved brightness of the  $\text{H}^+$  ion source. Through a combination of several detailed improvements, the source brightness was improved by about a factor of two and its reliability significantly enhanced.

A similar intensity buildup is the history at other meson factories. Figure 6 is a histogram taken from the 1979 TRIUMF Annual Report and shows the charge delivered per month over the last several years. During the same period, there was also some increase in the hours of operation per year. They experienced a reduction in the rate of buildup of residual activity in the cyclotron.

One question often asked about the present LAMPF operation is why we run at 600 microamps instead of 1000. Basically the last increment of current is not the major goal of LAMPF operations. Many factors are involved but the main goal is a highly reliable operation optimizing research results from a multi-faceted program utilizing both  $\text{H}^+$  and  $\text{H}^-$  beams. The current will be raised consistent with this goal. The research program needs do not dictate a strong effort to run at 1 ma compared with other desired improvements such as 100 microamps of  $\text{H}^-$  for the PSR.

The Linac will now handle 10-12 mA peak current reliably and we could get 1 mA by running such peak currents at 9% duty factor if we felt comfortable with the ability of the experimental areas handle it reliably. In addition, power costs encourage us to run at low duty factor whenever possible. Moreover, much of the scheduled time is devoted to dual energy operation in which the  $\text{H}^-$  beam runs at a lower energy in a duty factor sharing mode with the 800 MeV  $\text{H}^+$ . Typically the lower energy  $\text{H}^-$  is run at 3% d.f. and the 800 MeV  $\text{H}^+$  at 6%. For 1 mA in this mode, the peak  $\text{H}^+$  current would need to be  $\sim 17$  mA, which

would probably cause problems in the Linac. This will be discussed in more detail later.

#### B. Beam Availability and Reliability

Beam availability in a useful figure of merit for an accelerator operation especially from the viewpoint of users. It is usually taken to be the fraction of the scheduled beam time for which beam is available for the scheduled use. These figures usually improve with operating experience as the weak links in the system are improved and as the management learns to optimize availability through prudent scheduling of preventive maintenance, shutdowns, etc. Each of the meson factories now have operations that yield an enviable 80-90% availability.

It is useful to identify the systems contributing to unscheduled downtime. Table II is data taken from the TRIUMF 1979 Annual Report and lists the systems plus the number of hours each system contributed to downtime in 1979. The ion source and injection system is the single largest contributor (26%) but does not dominate the list. The present LAMPF experience is similar; no single system makes a dominate contribution to unscheduled downtime. Several years ago, LAMPF maintained an extensive data base on component failure, maintenance and repair. It was useful for identifying weaknesses and gauging the cost effectiveness of engineering improvements. The data base has been phase out as an expense that is no longer needed. The operation is now sufficiently reliable that the operational log books provide sufficient information.

#### C. Beam Losses and Activation

One of the key concerns at high intensity accelerators is the beam loss and resultant component activation in areas of hands-on-maintenance. At LAMPF, point spills in the Linac and the beam switchyard are limited by spill monitors and a fast protect system to be less than 50 nanoamps on a short time average (~60 sec). In practice, they run considerably less. Fifty nanoamperes is less than 0.01% loss. Distributed losses in the Linac are about 0.2%. Residual activity in areas of hands-on-maintenance has dropped and stabilized at reasonable values given the present allowed limits on

dose to personnel. On a typical maintenance day one finds Linac readings of  $\sim 10$  mr/hr at a distance 30 cm from the beam axis. In the Switchyard, readings range from 10-100 mr/hr for most components.

Losses at the 0.01% level are presumably due to beam halos from the core of the beam. They are very difficult to measure reliably and nearly impossible to model. With careful work it is possible to model 95 to 98% of the beam in the Linac if good data on beam measurements, magnet calibration and machine parameters are entered into the codes. In the front end where space charge neutralization is a factor, we don't do well at all. Beam halos and beam losses just cannot be predicted.

From experience many of our losses appear to be due to low momentum components. If they are far enough off in momentum, they will show up in the switchyard where the beam is first deflected either on a special phosphor detector or on a nearby spill monitor or both. They can often be tuned away by tuning the r.f. or by correcting the machine set point that has drifted.

Precise control of the r.f. is required to keep beam losses tolerable. One of the commonly held beliefs is that 805 MHz r.f. control tolerance is  $\pm 1\%$  in amplitude or  $\pm 1^\circ$  in phase. In actual practice, the tolerances are closer to  $\pm 0.1\%$  in amplitude or  $\pm 0.2^\circ$  in phase. At the high peak currents (10-12 mA), it is also necessary to slow down the rise time of the beam current pulse to  $\sim 20$   $\mu$ s in order to maintain the required r.f. fields and avoid beam losses.

Our experience has shown that increasing the aperture is very effective in dealing with losses. This can be done by improving the acceptance of the system or by improving the brightness of the beam. I have already mentioned that the factor of two improvement in source brightness was crucial to achieving high intensity at LAMPF. In 1976, revisions to the Switchyard optics improved the acceptance for  $H^+$  beams by a factor of two so as to more nearly match the Linac acceptance. Switchyard activation was greatly reduced even as the intensity increased. Our experience can be summarized by saying that you need six to seven standard deviations for adequate apertures.

Stated another way, this means that the acceptance should be greater than 40 times the r.m.s. emittance of the beam.

Activation of components in the experimental area target cells is no surprise. Fields as high as  $10^5$  R/hr have been measured near the main beam stop. However, one surprise to many people, has been the amount of radioactive gas that can escape from the target cell shielding. It is now necessary to extensively caulk the shielding cracks in order to meet radiation standards. Troublesome Hg isotopes have been identified near the beam stop. It is believed that they came from the Pb neutron reflector, which can reach elevated temperatures through limited cooling. Environmental concerns such as these will become more important if personnel dose limits are lowered significantly.

At the TRIUMF cyclotron, beam losses in the accelerator are considerably larger (~15%) and are due to well-understood causes. Losses at the lower energies are dominated by gas stripping of the  $H^-$  ion (~7%) and at the higher energies (~7%) by electromagnetic stripping. These values are about as expected and imply the need for remote servicing of the cyclotron as was planned for from the beginning.

At SIN, the extraction efficiency was improved by the addition of a third harmonic r.f. cavity to effectively flat top the r.f. and thereby improve the separation of the turns at extraction. A remarkable 99.98% extraction efficiency has been demonstrated in routine operation.<sup>3</sup>

#### D. Tuning and Maintenance of the Tune

LAMPF has a long and complex procedure for turn-on and tuning the accelerator from a cold start. After, say, a two-month shutdown when everything has been turned off, it typically takes 40-50 eight-hour shifts to turn on the facility and establish a production time. It is probably unfair to attribute all of this time to tuning since the accelerator can be completely retuned after startup in a period of about 10 shifts. The set points are not sufficiently reproducible to allow us to just dial up old set points and tweak from there.

Instead, much time is spent at the front end to prepare the correct beam, transport it at 750 keV and match into the Linac.

Part of the nonreproducibility is due to component drift; another important factor is believed to be caused by nonreproducible space charge neutralization that arises when the beam scrapes on jaws or other apertures. The effect of jaws on beam steering and beam phase space parameters is significant but not well understood.

Diagnostics such as the emittance gear are very slow. Those that measure longitudinal (energy and phase) phase space parameters are insufficient resulting in the need to make additional assumptions or indirect inferences as to the longitudinal tune.

Once the beam is tuned into the side coupled Linac, the tuning proceeds more rapidly but still at low duty. It is not complete until the beam has been deflected in the Switchyard and run at full duty into Line A. It is in the process of raising the intensity with a deflected beam that the beam halos and beam losses are encountered and tuned away. If we are unlucky, it may be necessary to completely retune starting at the source.

All of the aforementioned factors contribute to the essentially empirical character of the lengthy and complex startup process. Once in production, however, the tune can be maintained for perhaps three months. Recovery from a scheduled maintenance day typically takes one to one and one-half shifts. Rarely have we had to completely retune in the middle of a cycle. Maintenance of the tune requires dealing with spills that creep in periodically. If only one or two components have drifted, they can usually be found by examining redundant monitors or by inspired tuning.

The other meson factories appear to require less effort to startup from a long shutdown. The TRIUMF machine can be tuned up in a few shifts. The set points are reasonably reproducible except perhaps for the injection line.

#### E. Targeting

Meson producing targets for the LAMPF high intensity beam are made of graphite that is cooled either by radiation or conduction to water-cooled tubes. Radiation-cooled targets rotate to provide a

larger surface for radiating cooling. The water-cooled target is stationary and fabricated from slabs of pyrolytic graphite that has good thermal conductivity in planes normal to the beam. Water-cooled copper tubes are imbedded in and bonded to the graphite by a furnace braze.

LAMPF target designs have evolved since 1972 as the higher intensities exposed problems that were subsequently corrected. The present designs work very well and are highly reliable. They are on assemblies that penetrate the shielding and can be changed out in about a shift without much remote handling.

Earlier version of the radiation-cooled target had problems with bearings that would bind. Present bearings are of two types:

1. Stainless steel ball bearings modified with a 1-2% addition of molybdenum, and
2. A sleeve bearing of molybdenum impregnated with molybdenum disulphide.

Both are working well and are expected to handle 1 ma beams.

The water-cooled target<sup>4</sup> shows evidence of significant radiation damage, i.e., pronounced radiation induced swelling. At the present intensity such targets last three to four months and are replaced because of the swelling. For 1 mA operation, more cooling tubes would be needed and we would expect to replace them more frequently. A lifetime of one to two months is acceptable.

The thick target at SIN is radiation-cooled Be that rotates. At currents approaching 200  $\mu$ A, the bearings bind. Until improved targets are available, they limit the current on the thick target to 100  $\mu$ A.

At TRIUMF, the thick targets are all water cooled and work well at the highest currents that they have achieved. They expect no difficulties at higher currents of 300 to 400  $\mu$ A.

#### F. Target Cell Heating

Beam associated temperatures and vacuum leaks in the target cell are a cause for concern, although to date they are not a dominant cause of downtime. We are very cautious about increasing the risk of

damage to components requiring remote handling because it might result in major unscheduled downtime.

At 600  $\mu$ A, we have 1/2 MW of beam power. At the A-2 target, for example, 15% of the beam interacts and scatters 80 KW of beam power into the target cell. Most nearby components, such as collimators, target boxes and shielding, are water cooled. The maximum temperatures of 200-350°C are not going to melt or weaken components, but the thermal stresses and thermal cycling can and do cause vacuum leaks.

The temperature problems are not fundamental limitations. We know what to do to improve the cooling or to relocate a vacuum seal to a cooler location, but it is costly in time and effort. It will be done gradually as funds become available.

#### G. Remote Handling/Maintenance

Most beam line and shielding components in the target cells and at the beam stop now require remote handling for replacement and servicing. The basic remote handling system at LAMPF is called Monitor<sup>5</sup> and consists of a portable hydraulic crane with an attached bilateral electric master-slave manipulator along with TV cameras, portable lighting and a remote trailer for TV receivers, the slave unit and the operators. A picture of the Monitor is shown in Fig. 7. A view of the setup inside the remote trailer is shown in Fig. 8. In operation, the portable crane is parked at the edge of a target cell while the trailer is parked nearby, but a spot where the radiation field is low. We now have two such systems.

The features of Monitor have been absolutely essential to successful maintenance of the experimental areas. Credit is due Roger Horne of CERN for many contributions to the concept of Monitor. Another implementation of this concept can be seen at CERN.

Remote handling is a major, but totally necessary, complication to target cell maintenance. Such operations take much longer to complete; a factor of 10 or so is typical compared with the same operation done hands-on. Target cell maintenance is further complicated by the fact that most components are water cooled. To

unstack the close-in shielding requires disconnecting waterlines as well as remote rigging.

The overhead for remote servicing in a target cell is high; just to reach the beam line at a target box takes about 10 shifts of setup and unstacking with a comparable amount to close up. For this reason we usually, if we have a choice, wait until we have accumulated several jobs at a given target cell before accessing the beam line remotely.

The jobs requiring remote handling are usually the pacing items for schedule shutdowns. Vacuum leaks and water leaks dominate our shutdowns. Much effort goes into trying to diagnose target cell problems before the shutdown and target cell entry. Advanced preparations of all sorts are necessary to minimize downtime and make most efficient use of remote handling.

Water cooling of target cell components has evolved with operating experience.<sup>6</sup> Much of the cooling was done by TIG welding copper tubes to the component, then flame spraying with copper for good thermal contact. Cracks in the area of the TIG weld cause water leaks. We also have erosion and corrosion problems with the copper tubes and joint brazing. Improved methods use stainless steel tubes either welded or clamped to the components, then flame sprayed with copper.

Remote handling is required at the other meson factories but not quite to the extent that is required at LAMPF. In particular, they are still able to disconnect and replace components without the capabilities of Monitor. The TRIUMF cyclotron, however, does require remote handling. A unique service bridge for remote servicing of r.f. resonators was part of the initial design. Lead shields around the periphery of the vacuum leak can be installed remotely. These have reduced the radiation fields so that people could work inside for longer periods of time. As the activity builds up, more and more maintenance must be done remotely. At SIN, target mechanisms are designed for easy removal and are transported in shielding casks to the nearby reactor facility for repairs in the hot cells. Secondary

beam lines are on rails and can be removed without extensive unstacking of water-cooled radioactive shielding.

Simplicity of operation, easy removal and replacement, long life and extraordinary reliability are important design goals for components that must be handled remotely. Remote handling must be built in as a fundamental design goal and not as an after thought.

#### H. Radiation Damage

Radiation damage has not yet been a major problem. It was thoroughly considered in the design of the experimental areas at LAMPF. Line A downstream of the switchyard is mostly radiation hardened except for some cables to diagnostics at the edges of the target cells. Some of the cable insulation has become brittle and cracked.

I have already mentioned radiation damage to the water-cooled target at A-5. The water-cooled Inconel window that terminates the vacuum in front of the beam stop has been replaced as a precautionary measure after about 0.2 mole of protons passed through it. In the center of this window, perhaps 0.1% of the atoms have been charged by nuclear reactions. It has not yet been analyzed for radiation damage.

The silicon carbide wires of the Line A harps elongate by 1-2% after exposure to about  $10^{20}$  protons/cm<sup>2</sup>. For this reason our harp wires now have springs on them to keep them from sagging after the radiation induced elongation has set in.

#### MAJOR PLANNED IMPROVEMENTS/ENHANCEMENTS

Some additional insight can be gained by looking at improvement plans for the various facilities. At SIN, the main cyclotron works very well, has high extraction efficiency, and appears capable of handling more than 1 mA with a boost of the r.f. power. The present injector is limited to currents of a few hundred  $\mu$ A; therefore, a new high current injector is planned that is expected to have a current capacity beyond 2 mA.

At TRIUMF, they plan improvements to the injector and r.f. systems which, coupled with lowering the extracted beam energy to 450 MeV, would permit reliable operation with beams of 300-400  $\mu\text{A}$ .

The LAMPF intermediate range improvement program centers around providing 100  $\mu\text{A}$  (10 mA peak)  $\text{H}^-$  beams for injection into the PSR now under construction. This requires development of an intense  $\text{H}^-$  ion source, transition region improvements, solution of the dual beam steering problem in the Linac and modifications to the beam switchyard.

### CONCLUSIONS AND RECOMMENDATIONS

In this section I will try to summarize in a list of short statements some conclusions and recommendations supported by the operating experience with the meson factories. The recommendations are tailored for those considering the design of high intensity accelerator facilities more intense than the present generation of meson factories.

1. By most measures, the meson factories have been highly successful.
2. Beam halos in a Linac are very important but have not been measured or modeled successfully. Low momentum components are easily generated and easily spilled in beam lines which have small momentum acceptance.
3. Increased aperture and/or increased beam brightness are probably the best means for reducing spills. At some level of brightness, space charge will be a limit.
4. Precise set point stability and reproducibility are crucial for reliable operation.
5. Beyond 1 ma, the most important limitations to intensity are likely to be targeting, beam stops and other problems in the experimental areas where all of the beam interacts with matter.

6. Remote handling is very expensive and may be the most important design constraint for the components where it is needed.
7. Expect to take several years to reach design intensity.

#### ACKNOWLEDGEMENTS

I am indebted to many people for help in the preparation of this paper. I would especially mention Dr. Ewart Blackmore from TRIUMF, Dr. John Domingo from SIN, and Dr. Donald Hagerman, Dr. Robert Jameson, Dr. Andrew Browman, and Donald Grisham from Los Alamos National Laboratory. In a survey paper of this length, it is impossible to fairly represent the technical achievements of these complicated but highly successful facilities. Any important errors or omissions are unintentional, but nevertheless my responsibility.

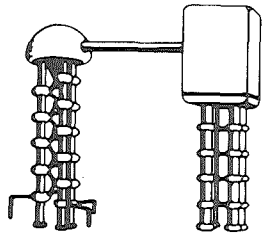
#### REFERENCES

1. Donald C. Hagerman, "Meson Factories-1977," IEEE Trans. Nuc. Sci., Vol. NS-24, No. 3, pp. 1605-1610 (June 1977).
2. Taken from the SIN Jahresbericht 1979.
3. S. Adam et al., "First Operation of a Flattop Accelerating System in an Isochronous Cyclotron," IEEE Trans. Nuc. Sci., Vol. NS-28, No. 3 (June 1981).
4. R. D. Brown and D. L. Grisham, "Design and Operation of Water-Cooled Pyrolytic Graphite Targets at LAMPF," Ibid, pp. 2940-2942.
5. D. L. Grisham et al., "Monitor 1981," Ibid, pp. 3007-3009.
6. D. L. Grisham and J. E. Lambert, "Water-Cooled Beam Line Components at LAMPF," Ibid, pp.2850-2852.

FIGURE CAPTIONS

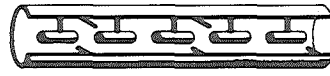
- Fig. 1. Overview of the LAMPF facility.
- Fig. 2. Floor Plan of LAMPF Experimental Areas.
- Fig. 3. SIN Floor Plan (taken from SIN Jahresbericht 1978).
- Fig. 4. TRIUMF Floor Plan.
- Fig. 5. LAMPF Intensity Build-Up.
- Fig. 6. TRIUMF Intensity Build-Up.
- Fig. 7. Monitor.
- Fig. 8. Master Unit.

COCKCROFT-WALTON



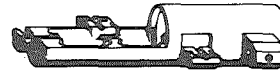
750 keV INJECTOR

DRIFT-TUBE LINAC



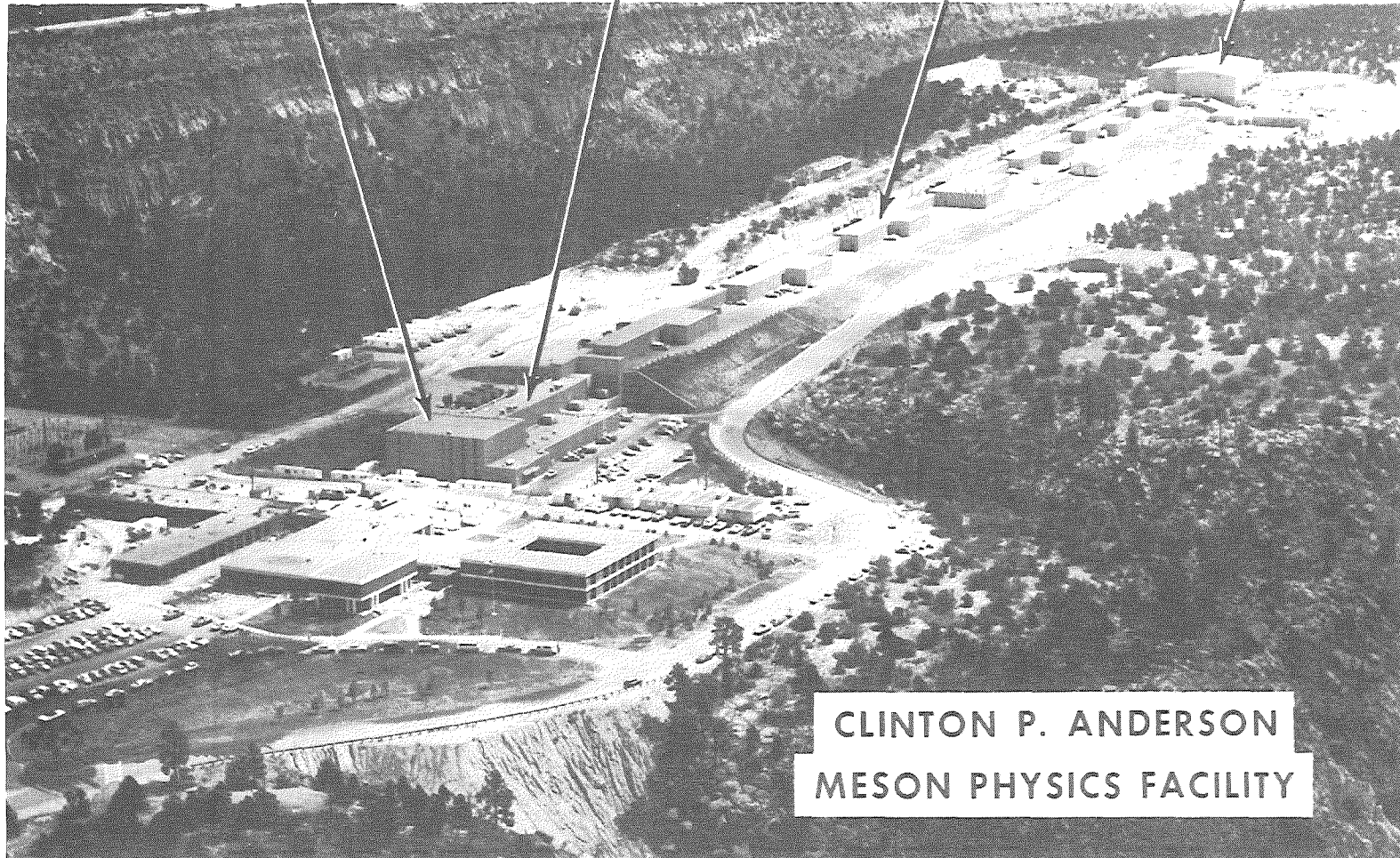
201.25 MHz

SIDE-COUPLED LINAC



805.00 MHz

EXPERIMENTAL AREA



CLINTON P. ANDERSON  
MESON PHYSICS FACILITY

FIG. 1

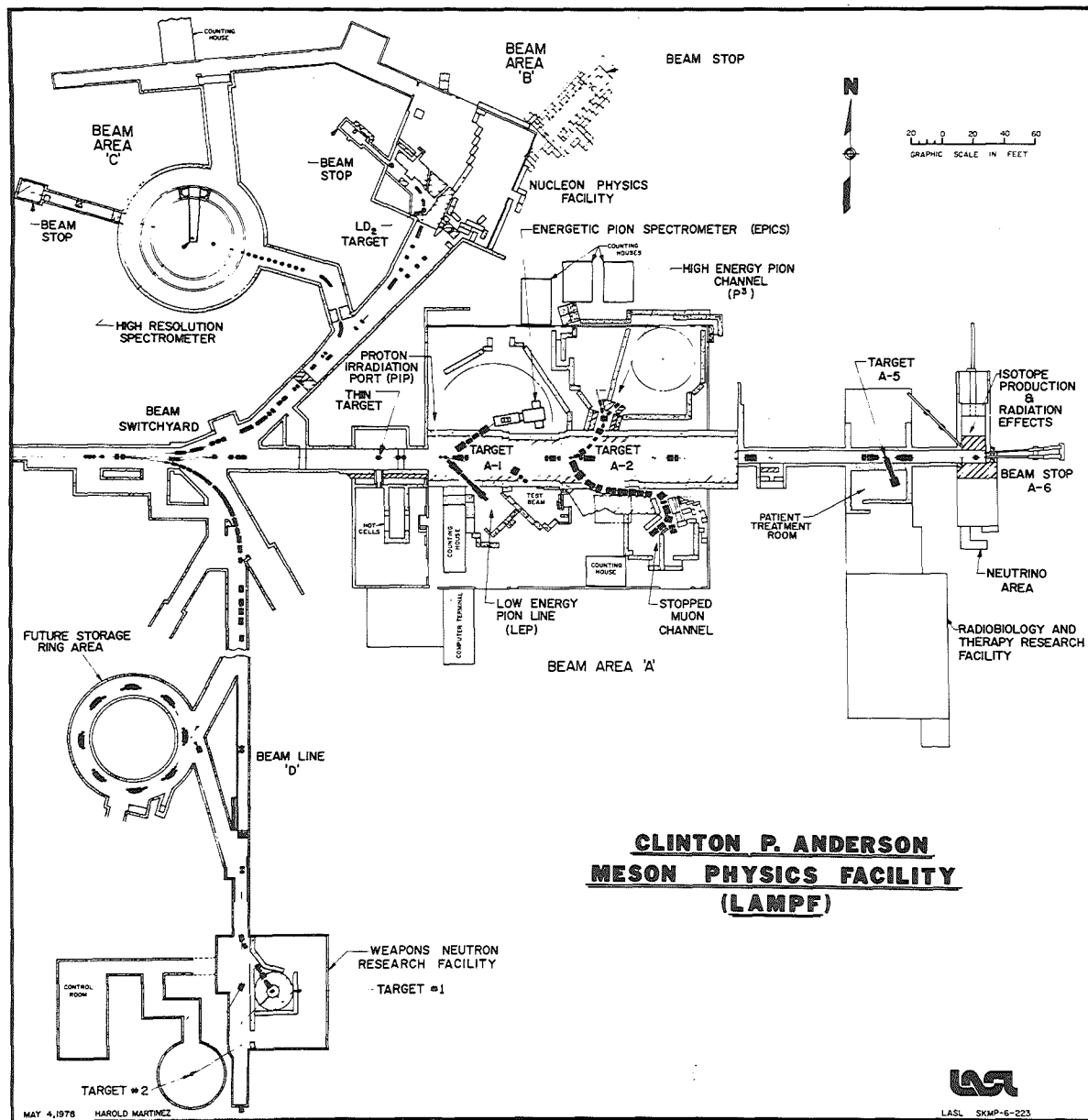


FIG. 2

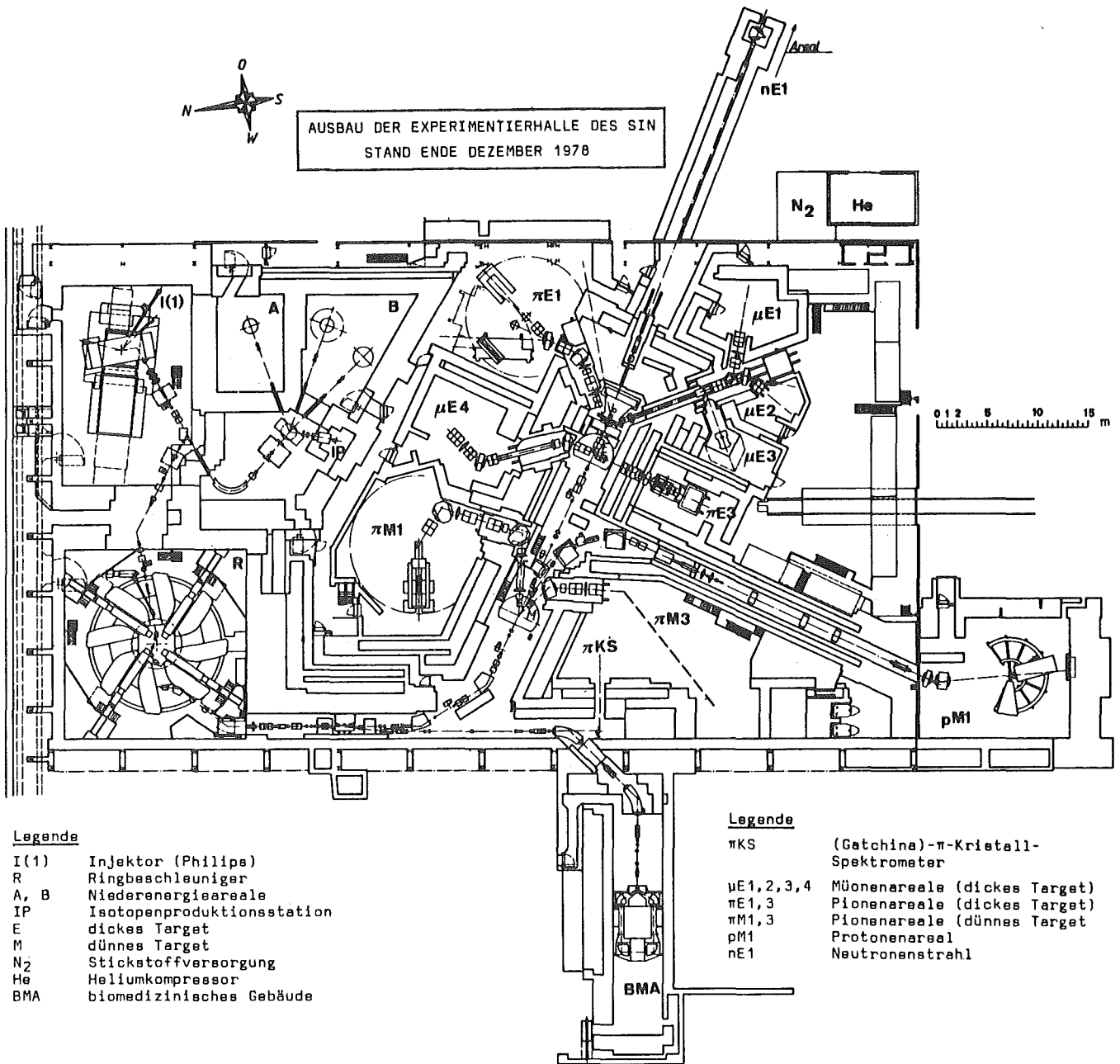


FIG. 3.

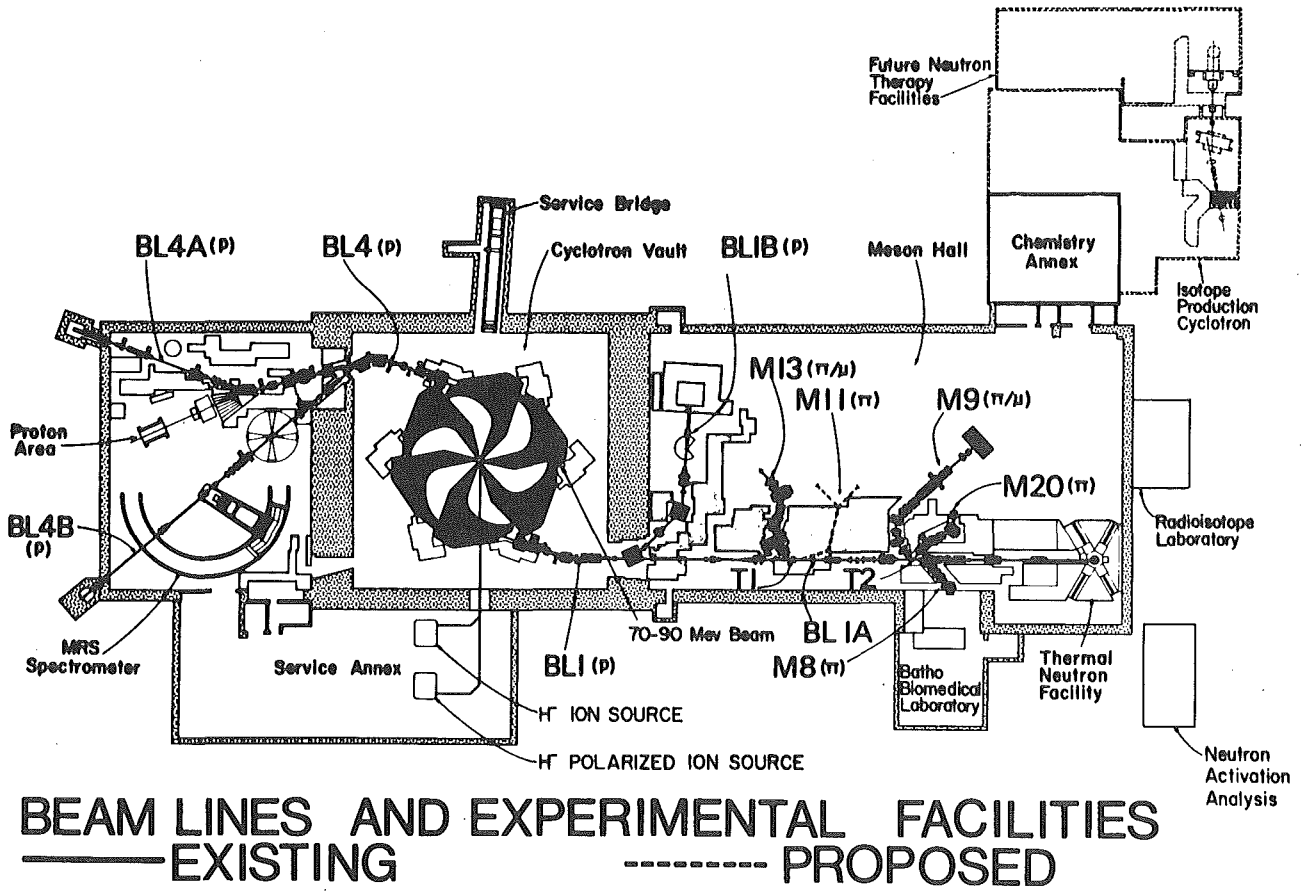


FIG. 4.

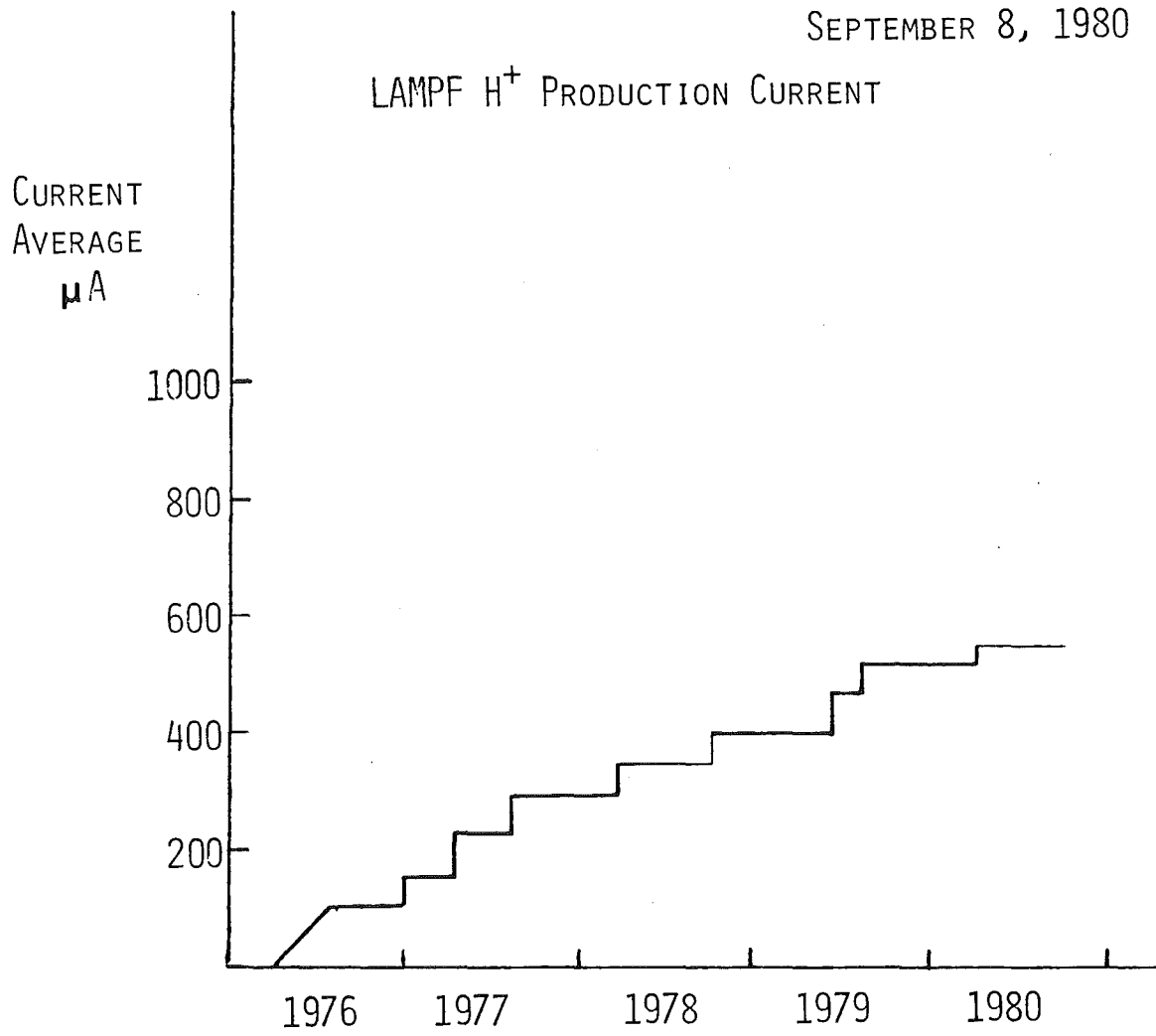


FIG. 5.

During the discussion R.J. Macek answered the corresponding questions: The increase of the intensity at LAMPF is done by raising the repetition rate. To tune the rf the full peak current is used. The peak current is not changed very much. The main difficulties in adjusting are to prepare the proper phase space at the front end of the linac. The reason why it is so difficult to reproduce the properties at the front end is seen in the uncomplete understanding of the space charge neutralization. The tuning of the linac is done for the  $H^+$ -beam only without worrying about the  $H^-$ -beam. Problems may arise when the  $H^-$ -beam will enhanced up to 100  $\mu A$  average.

The capture efficiency of the linac is 75 %, the 25 % are lost up to 5 MeV.

Scrapers and collimators do not work well. The experience at Los Alamos is that one introduces as much halo as one removes.

Status of the New England Nuclear 45 MeV Proton Linac

W. E. Jule

Operations Manager, Accelerator Department

New England Nuclear

601 Treble Cove Road

N. Billerica, MA 01862

Abstract

One of the main product lines of New England Nuclear (NEN) is radioisotopes for diagnostic nuclear medicine. These isotopes are presently produced on cyclotrons at NEN. In order to meet the production requirements for these short lived (3 day half-life) isotopes, NEN decided in 1977 to build a high current (5mA average), 45 MeV proton linear accelerator. By June 1978 we had assembled the core team and began the design of the machine. The building design had begun, with the aid of consultants, in February 1978. We are presently nearing completion of the accelerator with first beam scheduled for late fall of 1981. This paper will briefly describe each major subsystem and discuss its status.

## Introduction

The NEN linac is on schedule to produce a 45 MeV, low current (500 $\mu$ A-1mA average) beam in September/October of 1981. The accelerator is comprised of the following subsystems: pre-accelerator; low energy beam transport; linac; RF power system; high energy beam transport and target facility; and computer control system. Each area will be described briefly with a discussion of its status.

## Pre-Accelerator

A beam of 780 keV protons for injection into the linac is achieved using a Haefely high voltage power supply (HVPS) which is run at 720 kV in conjunction with the ion source extractor voltage of 60 kV. Power is delivered to the dome by an isolation transformer. The ion source was supplied by Culham Laboratory in Abingdon, England and is a bucket type (Cusp Field) source. It is our goal to extract 80-100 mA peak current of protons at a 10% duty factor. The extracted beam is transported around a 90° bend and through a solenoid lens into the high gradient electrostatic accelerating column (20 kV/cm). The 90° bend is used to remove H<sub>2</sub><sup>+</sup> and H<sub>3</sub><sup>+</sup> species from the beam to reduce loading of the accelerating column. The controls of the power supplies in the equipment terminal are micro-processor based and communicate over fiber optics with the main control system.

The pre-accelerator is presently operational. The accelerating column has been conditioned to 760 kV and the ion source extractor has been run at 60 kV with high current operation up to 50 kV.

The bending magnet is designed with  $n=0.5$  to give equal focussing in both planes. The beam optics in the dome transport is operating as designed, but the spot size in LEBT is larger than design. This is at least partially attributable to the fact that we are operating well below the 80mA design current. Emittance measuring equipment is now being used to study the column and LEBT optics.

## Low Energy Beam Transport (LEBT)

The LEBT is made up of three variable strength permanent magnet quadrupole triplets, four electromagnetic quadrupole singlets, a CERN type double frequency buncher, two emittance stations, and diagnostic boxes which are supported on a steel box beam that doubles as a vacuum manifold. The vacuum is maintained by two 1000  $\ell$ /s vacuum ion pumps. All of the components are in house and are being installed. We have run beam through the first triplet to the first emittance station, however, we have not had time to study the beam properties for different magnet settings or different current levels.

## Linac

The accelerator is a single RF cavity made up of six tanks bolted together. The first tank has a diameter of 110 cm, the second and third have a diameter of 106 cm, and the last three have a diameter of 102 cm. The diameter changes are to maintain a low g/L ratio and thus a high transit time factor. The cavity contains 107 drift tubes with an OD of 9 cm, each of which contains a permanent magnet quadrupole for focussing. The quad strengths are fixed in three groups which correspond to the tank diameter changes. The strengths and lengths are: 8.7 kg/cm, 3.81 cm; 6.0 kg/cm, 5.71 cm; and 3.6 kg/cm, 7.62 cm. The bore tube

radius corresponding to these changes is 1.0 cm, 1.25 cm, and 1.5 cm. Post couplers are used for passive stabilization. In the first tank section (.78-5 MeV) we have one post coupler every other drift tube while in the remainder of the machine we have one post coupler per drift tube. The tanks are supported on I-beam sections mounted directly on the tunnel floor. The drift tube stems, post couplers, and RF tuners all penetrate the tank through "choke type" joints with RF spring fingers recessed in the joint. The vacuum is supplied by a roots blower, two turbo-molecular pumps (2000 l/s) and nine vacuum ion pumps (1000 l/s). We plan to run at  $1 \times 10^{-6}$  torr. The tank water cooling system is a channeled shell welded on the outside of the tank. It carries 600 gpm of 75°F water to maintain the tank temperature at 77°F. The RF power is supplied to the tanks through 12 inch coaxial transmission line through feed loops which use magnetic coupling. The loop terminations are just outside the tank circumference. The tank will dissipate approximately 250 kW of average power, while the beam at 5 mA average current will consume 225 kW of average power. The final resonant frequency adjustment will be achieved with a tuning bar attached along the weld seam of the tanks.

All of the major components of the linac are fabricated and in house. The tanks have been installed, aligned, and Q checked. The Q is approximately 85,000 which is 70% of theoretical. The drift tubes are all installed and aligned as are the RF feed loops which have been matched for low power operation. We are planning to have RF power into the tank in late July or early August. At that time, we will do the final high power matching of the RF feed loops. We will not do final bead pulls until after the RF conditioning. The water and vacuum systems have been partially tested. They will of course be completely tested when we RF condition the tanks.

#### RF Power System

The RF power system is based on three transmitters, each of which are capable of 5 MW peak power and 200 kW average power. (The final power amplifier is based on the RCA 7835 tube.) When all three transmitters are in operation at design current of 5 mA, they will each be putting out 1.667 MW peak and 190 kW average power. These transmitters are designed to run at a duty factor of 11.2%. The output of the three RF power amplifiers is combined through a hybrid network, passed through a high power phase shifter, and then through a divider network to give equal amounts of power to be fed in at L/8, 3L/8, 5L/8 and 7L/8.

The power is fed in at the four feed points to provide dynamic compensation for the beam loading compensation pulse.<sup>1,2,3</sup> This also will extend RF window lifetime by reducing the peak and average power levels that a single feed would have had to handle. The RF phase and amplitude set points in the accelerator during beam loading are maintained via servo loops.

In order to improve reliability, the power from the three transmitters is manifolded. The system is designed so that one or two transmitters can be switched out of the system and still allow the system to function. Thus, a transmitter can be off line for tube conditioning or for troubleshooting without affecting operations. The system is designed to accelerate up to 3.5 mA with one amplifier off line.

The RF system is now two thirds installed except for the hard tube (Eimac 8973) modulators. There was an instability in the modulator as originally designed which delayed it well beyond our initial estimates. While this problem has now been solved and the solution is being implemented, we have a temporary

modulator in house. It will function as a switch and thus allow us to RF condition the tanks while we are waiting for the final version.

The system has been factory tested at 5 MW peak and 200 kW average power and operates satisfactorily. The installed systems in house have been tested up to 3 MW at a 2.0% duty factor.

#### High Energy Beam Transport (HEBT) and Target Facility

The HEBT is designed to transport the maximum possible output of the linac to the target without beam loss. However, we have designed a few stations where we can use retractable beam scrapers in locally shielded areas to enable us to modify the transverse phase space of the beam. HEBT will also be used to transform the small linac spot size to a large target spot size. The system uses four electromagnetic singlets and many variable strength permanent magnet singlets. We will use multiple wire scanners to reconstruct the emittance. Later, we may use non destructive beam profile monitors. There is also an energy analysis bend.

The target facility will be either straight ahead or around a 45° bend. In either case, there will be two irradiation chambers to give redundancy as well as an area to develop new targets which is separate from the primary production chamber. These facilities will be equipped with manipulators for remote handling of targets. The targets will be on the face of a removeable shield plug.

The HEBT and target facilities are the area of the facility which have the most remaining work. They have to be complete in September in order to meet our goal of October beam. At this time, we do not see any problems in these areas which will forestall that achievement.

#### Computer Control System

The computer control system uses distributed microprocessors (Motorola 6800) interfaced to a host minicomputer (VAX 11/780). The VAX has proven to be an excellent choice for the main control computer due to the programming environment provided by the virtual memory operating system. This has allowed the development of the system software with a minimum of manpower. This system can handle on the order of 2000 input/output control points.

The communications between the micros and the VAX and the operator's console are over fiber optics cables. This is to avoid RFI/EMI as well as to minimize the amount of cable pulling necessary to interface the equipment. Also, in the high voltage area, it is a solution to the isolation required in this environment.

In order to provide access to the micros on a local basis, we have implemented a mobile console. This device has a keyboard, some local memory, a CRT, and an embedded micro. It can be taken to any micro station and connected via a ribbon cable thus providing a communications interface. This can then be used for local troubleshooting of machine hardware or micro hardware.

The system is partially functional. All of the software to communicate between micros, the VAX, and the operator's console is complete. It is now possible to control the high voltage power supply, ion source, ion source power supply, and all associated equipment through both the mobile and main consoles. Applications programs have been written and are operational which automatically

turn on and bring up the high voltage and the ion source. Other applications programs are in process. The major portion of the remaining hardware for interfacing is in house and in the installation phase. Modifications of power supplies to control equipment is ongoing.

Overall, one can say that the system will be sufficiently in place to be useful during the commissioning phase this fall.

### Conclusion

The project is going well. Most equipment is in house and we have sufficient manpower to keep the work flowing smoothly. We have accelerated a 780 keV, 25 mA beam up to the entrance of LEBT. We are planning to RF condition the tanks in July and have our first 45 MeV beam in October 1981.

### Acknowledgements

Many people have contributed to this project from labs in the U.S. and Europe. I would like to take this occasion to express our appreciation and thank them all for their support. It has made the construction of this accelerator a far less difficult task than it might have been.

Brookhaven: K. Batchelor, N. Fewell, P. Grand, H. Halama, J. Sheehan, R. Witkover.

Los Alamos: E. Bush, J. Farrell, J. Halbig, R. Jameson, E. Knapp, J. Leavitt, J. Potter, R. Stevens, J. Stovall, D. Swenson.

Univ. of Maryland: R. Gluckstern.

LBL: K. Halbach.

SLAC: K. Brown.

AECL, Chalk River: J. Fraser, S. Schreiber.

CERN: E. Boltezar, H. Haseroth, U. Tallgren, D. Warner, M. Weiss.

RHEL: C. Planner, N. West.

SIN: M. Olivo.

Private: R. Fluharty.

### References

1. T. Nishikawa, "Normal Mode Analysis of Standing Wave Linacs-Field Excitation and Beam Loading in Linac Cavities", private communication
2. K. Batchelor, T. Nishikawa, and T. Werntz, "Numerical Analysis of the RF Field in a Drift Tube Loaded Cavity", pg. 295, IEEE Transactions on Nuclear Science, Volume NS-14, Number 3, June 1967.
3. S. Giordano, J. P. Hannwacker, and J. T. Keane, "Studies of Multi-Drive Excitation for Alvarez Structures", pg. 303, IEEE Transactions on Nuclear Science, Volume NS-14, Number 3, June 1967.

Accelerator Development Work at CRNL

(In the context of high current accelerators)

B.G. Chidley

Atomic Energy of Canada Limited  
Research Company  
Chalk River Nuclear Laboratories  
Chalk River, Ontario K0J 1J0

Abstract

This paper describes the accelerator development program at CRNL in support of the long range accelerator breeder program. Development work is discussed which will lead to the construction of "ZEBRA" a Zero Energy Breeder Accelerator which will produce 300 mA of proton at 10 MeV.

The CRNL accelerator breeder program was discussed by G.A. Bartholomew in the plenary session at Jülich and he showed the place of the accelerator development program as a first step of a long range development program. In this paper I will elaborate on the accelerator program related to the development of a high current accelerator suitable for an accelerator breeder. I will not be discussing other aspects of the accelerator breeder program such as the target or whether an accelerator breeder is economically competitive with other systems.

The Accelerator Physics Branch at CRNL consists of 18 professionals and 18 technicians divided into 4 groups as listed in Table 1.

Table 1

1. <u>Proton Beam</u>		
	J.C. Brown	H.F. Campbell
	B.G. Chidley	D.W. Clements
	J.D. Hepburn	K.J. Hohban
	G.E. McMichael	J.C. Jones
	S.O. Schriber	W.L. Michel
	M.R. Shubaly	J.G. Plato
	J. Ungrin	R.A. Vokes
	J.S. Fraser	A.E. Weeden
2. <u>ETA</u>		
	J. McKeown	S.H. Kidner
	K.C.D. Chan	R.T.F. Bird
		M.F. Coulas
3. <u>MEDAC</u>		
	L.W. Funk	B.A. Gillies
	R.M. Hutcheon	P.J. Metivier
4. <u>Heavy Ion Superconducting Cyclotron</u>		
	J.H. Ormrod	L.F. Birney
	J.A. Hulbert	R.J. Burton
	H.R. Schneider	J.E. McGregor
	C.R.J. Hoffmann	R.E. Milks
	E.A. Heighway	J.F. Mouris
	C.B. Bigham	

The proton beam group is working on various aspects of high current proton linear accelerator development and will be discussed in detail.

The Electron Test Accelerator group is using a side coupled cavity linac similar to LAMPF at Los Alamos built to study 100% duty factor operation under heavy beam loading.

The medical accelerator group developed an electron linac therapy machine now being marketed by AECL. The development work at CRNL is completed and the remaining personnel are to be reassigned in the near future.

Structure work in this group has led to acceptance of the on-axis coupled accelerating structure for other groups and laboratories.

The superconducting cyclotron group is building a heavy ion post-accelerator for the tandem Van de Graaff of the Nuclear Physics Branch. (Only the Accelerator Physics Branch personnel is shown in the Table.) The original proposal for this project was made in 1972 and the scheduled date of first beam is 1983. This is a low current machine so it won't be discussed further here.

The ETA program was begun in 1970 as part of a program to examine problems of accelerating currents up to 100 mA in a high  $\beta$  linac at accelerating gradients up to 2 MeV/m. A diagram of the facility is shown in Fig. 1. Because a 100 mA relativistic beam of protons is not available an electron beam is used to load the structure so it is in fact an electron accelerator but used for proton linac structure development.

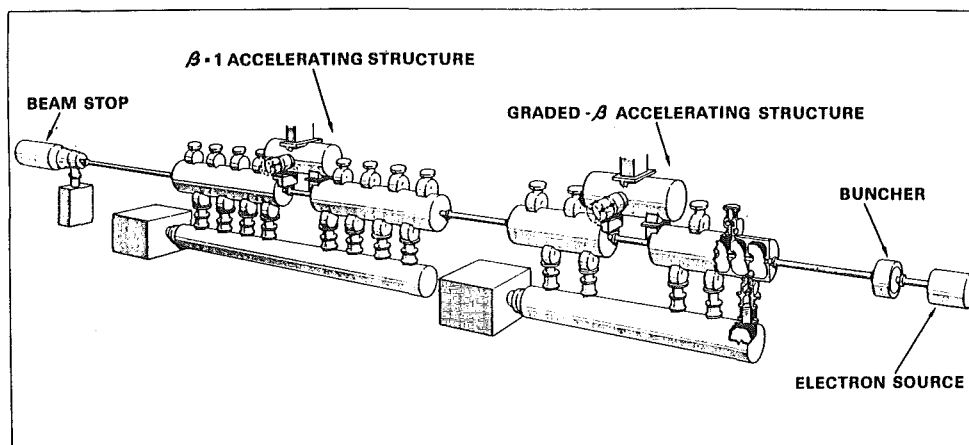


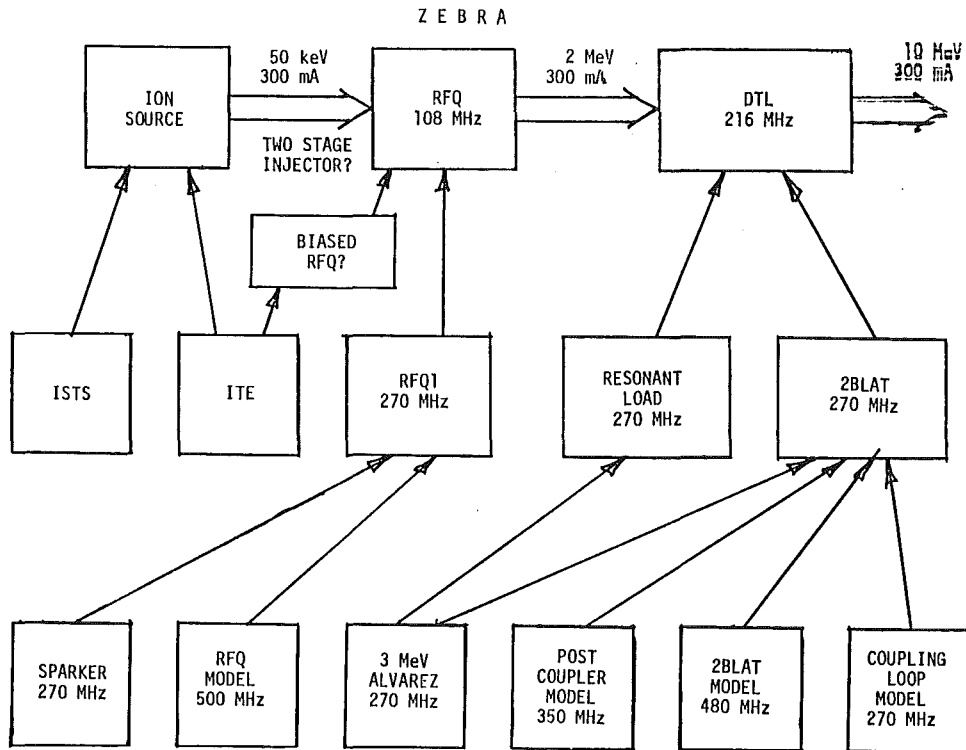
Diagram showing the principal components of the Electron Test Accelerator.

To date the achieved current is 22 mA at a gradient of 0.7 MeV/m (100% duty factor). This represents 40% beam loading (40% of the rf power delivered to the accelerating cavity is transferred to the particle beam, 60% is dissipated in the accelerator structure.) Operation with this beam current at higher gradient in the present structure would require a klystron larger than the present 100 kW ones. The available klystron power also limited the beam loading achievable at 0.7 MeV/m; beam loading of 85% could be achieved in this linac but only at a reduced field of 0.1 MeV/m.

A somewhat shorter on-axis coupled structure is being built which will operate with the present klystrons at 1.7 MeV/m with no beam or 1.1 MeV/m loaded. There are plans to parallel two 100 kW klystrons and this may be done in the next 1-1/2 years but even this will be below the fields and beam loading required in the accelerator breeder.

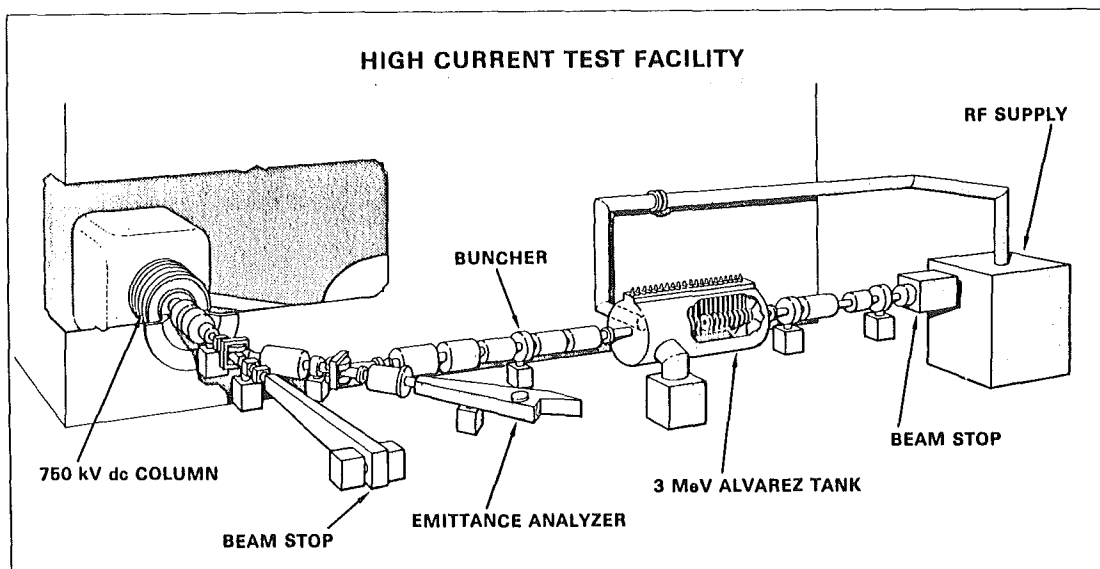
ETA has made contributions to electron accelerators as well - even though this was not the original intention. The accelerating structures in electron-positron storage rings (SPEAR II, PEP, DORIS, PETRA) are very similar to the ETA structure and experiments can be done on ETA which are not possible on the larger machines. Recent work on microtrons has used the Chalk River on-axis coupled structure and further developments are in progress.

The long range plans of the proton beam group are shown in Table 2.



The activities are designed toward the construction of "ZEBRA" a Zero Energy Breeder Accelerator which would produce 300 mA of protons at 10 MeV. This is an experimental prototype designed to study accelerator performance at low energy. It will produce full accelerator breeder beam current but only 1% of the final energy (Zero Energy). Our present view of the accelerator is that it will have dc injection in the 50-100 kv region into a RFQ accelerator operating at 108 MHz and then to a 216 MHz drift tube linac at 10 MeV. This could be the basis of the low energy end of a future spallation breeder. This program is not yet funded but is visualized with a completion date of 1987-89. Before it can be built or even designed there are a number of preliminary experiments to be done, or in some cases more than one generation of preliminary experiments. I will describe these devices starting at the bottom line which are existing devices or equipment now in the machine shop being built.

The 3 MeV Alvarez program, shown in Fig. 2, was begun in 1970 and has been used to study problems associated with operation of a 100% duty factor drift tube linac.



The most serious problem encountered was heating of the bellows of the drift tube stems which restricted tank power to a value well below that necessary for acceleration of beam. After several unsuccessful attempts to protect the bellows, the stems were soft soldered to the tank wall to allow full excitation of the accelerator and further development work is being done on only one drift tube stem (the most easily accessible one). Soldering the stems to the tank wall is very effective at protecting the bellows but is not considered a solution because it allows no adjustment and also could not be used on post couplers or tuning plungers (which although not present in this device will be on the next one).

Low currents were accelerated (up to 2 mA cw) and then it was shut down for further tests of the stem problem.

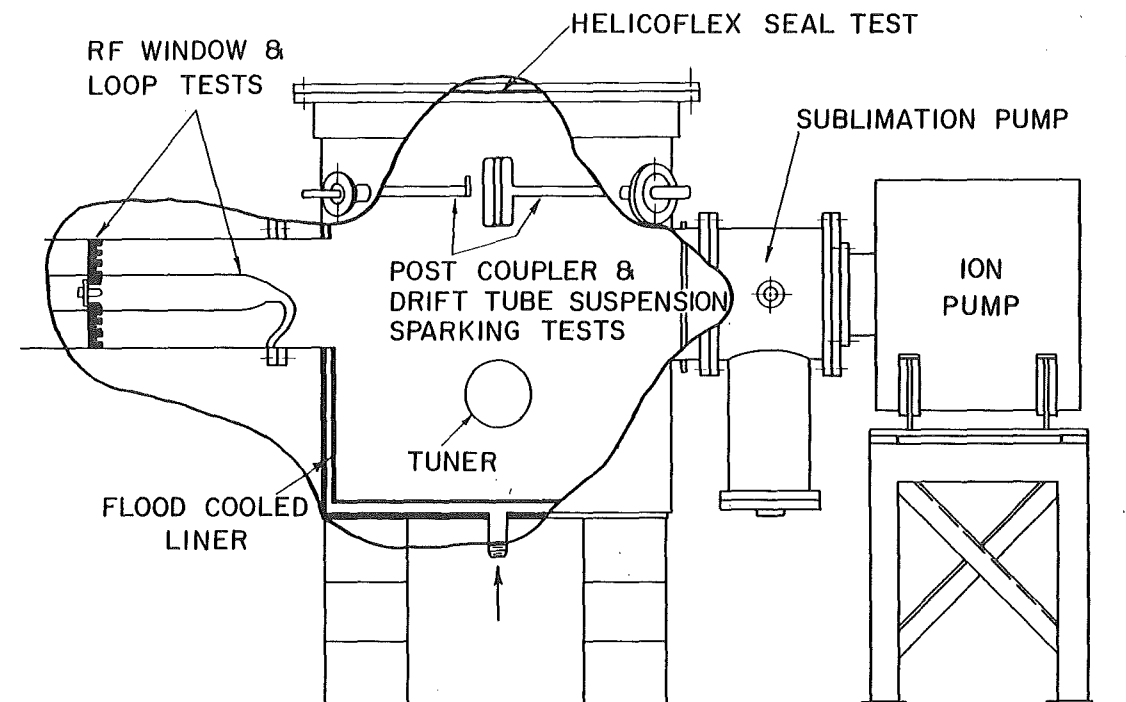
It has been shown that the stem currents and bellows heating can be eliminated by adjusting gaps to an abnormal value. It is inferred that a design could be found with the stems attached asymmetrically which would result in no stem current. This possibility is being investigated.

The rf drive loop is also a source of problems. It works quite well when it works but many of the "tank rf conditioning problems" are thought to be "coupling loop rf conditioning problems" and we have occasional window failures which deposit material on the walls and necessitate a thorough cleaning of the tank.

The 750 kV dc injector works well at a few mA average current but reliability decreases rapidly with increasing current. After a very large amount of conditioning a number of years ago it would run at 50 mA total (unanalyzed) beam current but higher current operation appears impractical. With the advent of the RFQ it appears that a high voltage injector may no longer be required.

There are a number of experiments planned for the 3 MeV accelerator but they should be completed by mid-1982.

The resonant load is shown in Fig. 3. It is an all-purpose test device to test loops, windows, gaskets, etc. It is 83 cm in diameter and



has 11 ports around the circumference to accommodate: drive line, vacuum port, drift tube, post coupler, tuner, field probe, viewing ports, port to test helicoflex and other seals and spares. The resonant frequency is calculated to be 276.5 MHz empty and 273 MHz with a drift tube installed. The load is designed to operate at 400 kW to test rf lines at high power.

The drive line port can take up to a 9" diameter line but may be operated initially with a 6" diameter line similar to the 3 MeV tank.

The shell is expected to be delivered by October but some of the inserts (drift tube, tuner) will be later.

The 2 Beta Lambda Tank (2BLAT) was designed to test a number of concepts for the ZEBRA first Alvarez tank which are not present in the 3 MeV tank. It is designed with a  $2\beta\lambda$  cell length so that cell lengths will be similar to those of a  $1\beta\lambda$  design with a 2.4 MeV input even though it will use a 600 keV input from our existing injector.

The basic design is given in Table 3.

Table 3

2BLAT

Frequency	270 MHz (CW)
Cell Length	$2\beta\lambda$
Length	171.6 cm
Diameter	71.0 cm
Input Energy	600 keV
Output Energy	2.6 MeV
$E_0$	2 MV/m
Q	54000
Power	120 kW
Maximum surface field	21 MV/, (1.5 * Kilpatrick)
Post Couplers	6
Tuners	2
Drift tubes	13 + 2 half drift tubes
OD	13.5 cm
ID	1.5 cm
Face Angle	10° (cells 1-5) 15° (cells 6-14)
Magnets	3.8 cm long 6.0 kG/cm (+--+) permanent magnets (1-5) electromagnets in others
Drive port	9" diameter

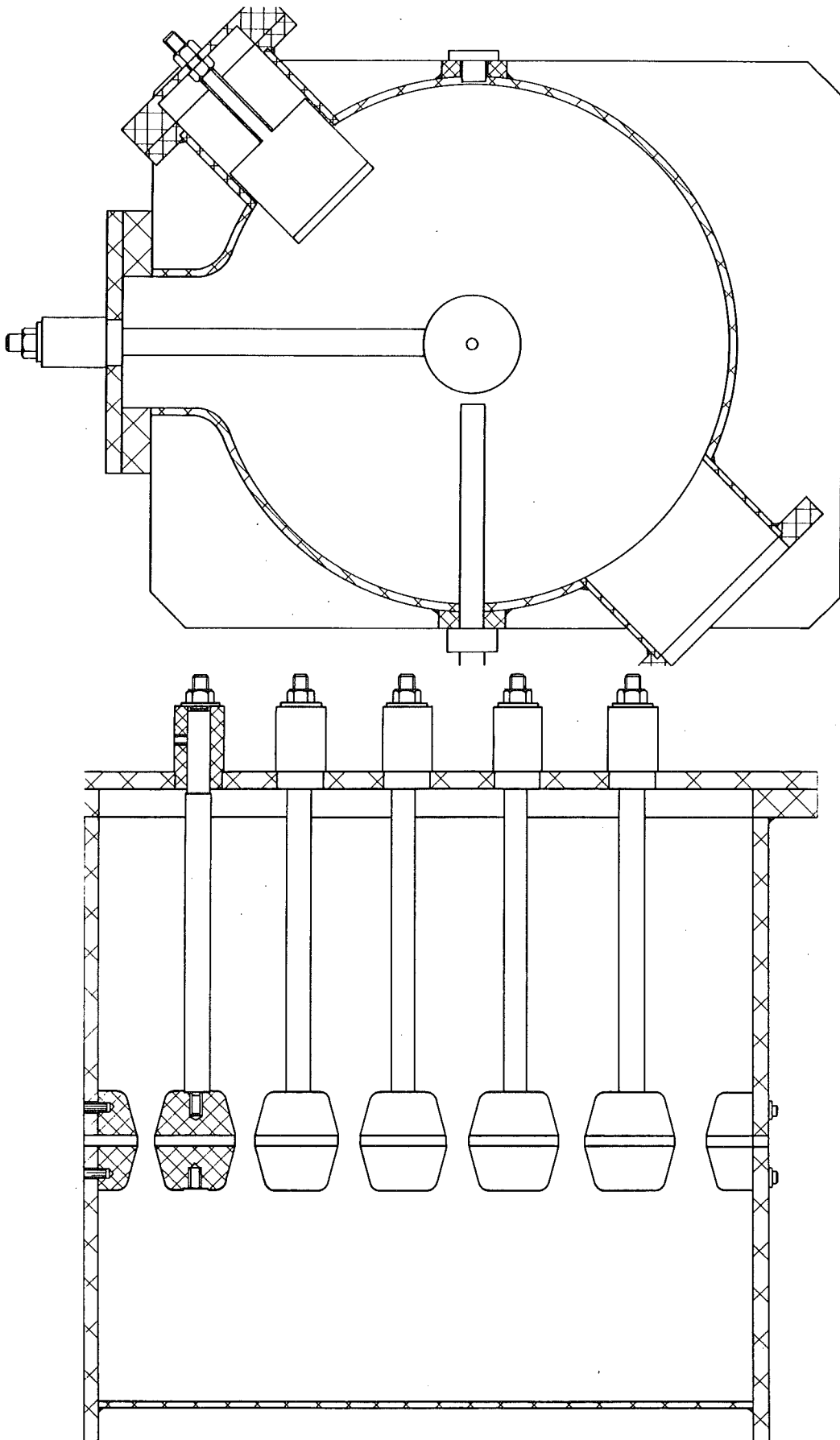
The preliminary design of 2BLAT is as given in the table but there are some details to be settled and to aid in this a 480 MHz aluminum scale model of the last 6 cells is being built. This is shown in Figs. 4 and 5. The frequency shifts produced by the drift tube suspension, coupling loop port and tuners will be measured and the effect of post couplers on stem currents determined. The drift tubes have 4 mounting holes on them so they can be attached to the stem at different points to measure the effect of asymmetric attachment on stem currents.

Design of 2BLAT is to be completed by 1981 December with tests to begin in 1982 June.

RFQ Development

The RFQ accelerator was invented over 10 years ago in the USSR by Kapchinskii and Teplyakov. Considerable further development was done at LANL and in 1980 February a 30 mA beam at low duty factor was accelerated from 100 keV to 600 keV in a small test accelerator. This device worked extremely well and was immediately considered to be a solution to all the problems now facing ion accelerators in the low energy region.

The Los Alamos device was built to test the principle of the RFQ and was not intended to be run at high power, but that is obviously the next step. When it was driven to higher power, damage occurred to rf



finger stock in the coupling manifold and required considerable rebuilding before high power tests could be resumed.

While the RFQ is assumed to be the low energy end of ZEBRA, it is not yet shown that it can operate at 300 mA or that it can operate at 100% duty factor without reducing the peak fields to the point where the current capability is reduced.

To answer the question of field limits under 100% duty factor, a small RFQ is being built called the "sparker". It operates at 270 MHz (using our existing rf supply) and has vanes 36 cm long and an overall length of 90 cm. It requires 35 kW to reach peak fields of 1.0 \* Kilpatrick and will be tested up to 150 kW or twice the Kilpatrick limit. Tests at Los Alamos indicate that pulsed fields up to twice the Kilpatrick are acceptable with suitable surface preparation and rf conditioning, but this must be confirmed for 100% duty factor operation.

This device is under construction and operation is scheduled for the fall 1981.

RFQ1 will be our first operating RFQ accelerator. The preliminary design is given in Table 4.

Table 4

<u>RFQ1</u>	
Frequency	270 MHz
Length	2.8 m
Input Energy	50 keV
Output Energy	1.5 MeV
Beam Current	100 mA
Peak Field	1.0 * Kilpatrick
Power	380 kW

The basic design is similar to the Los Alamos "proof of principle" accelerator.

The construction schedule calls for detailed design to begin 1981 September, construction to begin 1982 March and to be ready for beam tests in 1983 January.

A 500 MHz zero power aluminum model has been built in our shops to provide design data for RFQ1. It has provisions for changing vane tips and end wall positions. Frequency and Q have been measured as a function of end wall position for the TE211, TE212 and TE213 modes. Field measurements are to be made, and various methods of machining pole tip profiles are to be tested.

Ion source and dc accelerating column development will be done on the Ion Source Test Stand and the Injector Test Experiment.

The Ion Source Test Stand has been in operation for many years and most of our ion source development work has been carried out on this

facility. The power supply is rated at 160 kV 500 mA but the ion source will not stand more than 80 kV and it is planned to rewire the supply for 80 kV 1000 mA. A number of high current sources have been tested on this supply up to  $\sim 0.45$  A. At this current a hydrogen source typically gives  $\sim 40\%$   $H^+$  or on rare occasions up to  $45\%$   $H^+$ , so this represents a proton beam current of 200 mA.

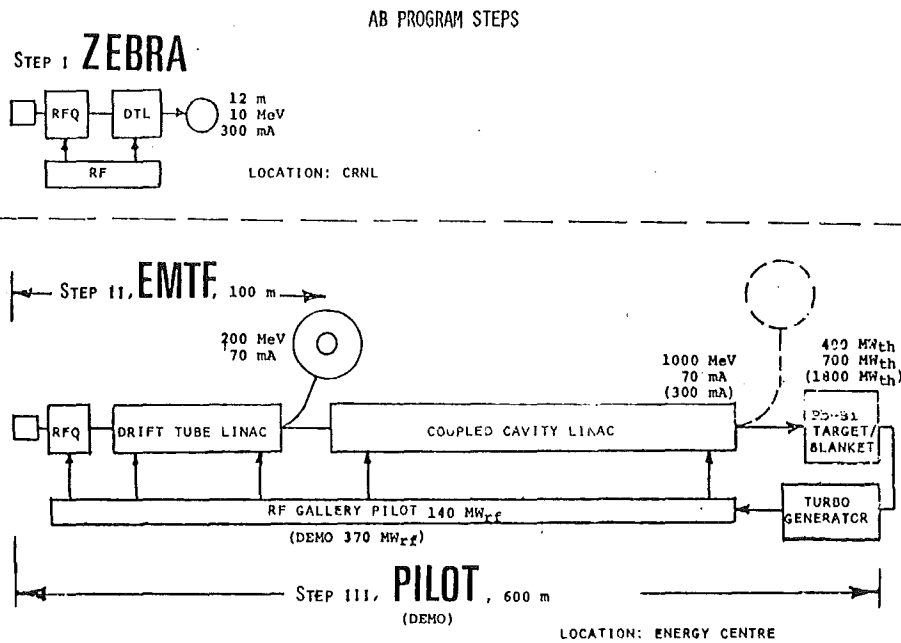
The Injector Test Experiment was begun in 1978. Its aim was to develop a high current ion source such as would be required for a spallation breeder. The facility was originally envisaged as a two stage device consisting of a 50 kV 750 mA pre-accelerator followed by beam analysis to remove molecular ion contamination, followed by a main accelerator column to 250 kV.

The 50 kV stage was built and with the advent of the RFQ accelerator it appears that the second accelerating column may not be necessary, because the RFQ can accept the 50 keV beam without further pre-acceleration. A two stage device may be required in any event to allow variable current operation so that the extraction voltage can be varied without changing the injector output energy, but this would only require a final energy of 75 to 100 keV rather than 250 keV.

Beam was first run in the ITE 1980 August 29. Currents up to 550 mA (total) 42 keV have been run but the facility has been idle recently for the installation of diagnostic equipment.

Its primary purpose is to test an injector "package" or do life-time runs.

I would like to conclude by showing again a figure shown earlier by Dr. Bartholomew of the spallation breeder program and the place occupied by the ZEBRA development program.



HS-RP/062/CF

RADIATION PROBLEMS EXPECTED FOR THE  
GERMAN SPALLATION NEUTRON SOURCE

K. Goebel  
CERN, CH-1211 Geneva 23

A B S T R A C T

The German project for the construction of a Spallation Neutron Source with high proton beam power (5.5 MW) will have to cope with a number of radiation problems. The present report describes these problems and proposes solutions for keeping exposures for the staff and release of activity and radiation into the environment as low as reasonably achievable. It is shown that the strict requirements of the German radiation protection regulations can be met. The main problem will be the exposure of maintenance personnel to remanent gamma radiation, as is the case at existing proton accelerators. Closed ventilation and cooling systems will reduce the release of (mainly short-lived) activity to acceptable levels. Shielding requirements for different sections are discussed, and it is demonstrated by calculations and extrapolations from experiments that fence-post doses well below 150 mrem/y can be obtained at distances of the order of 100 metres from the principal source points. The radiation protection system proposed for the Spallation Neutron Source is discussed, in particular the needs for monitor systems and a central radiation protection data base and alarm system.

RADIATION PROBLEMS EXPECTED FOR THE  
GERMAN SPALLATION NEUTRON SOURCE

1. INTRODUCTION
2. BEAM LOSSES
3. STRAY RADIATION LEVELS OUTSIDE THE SHIELDING ENCLOSURE
  - 3.1 Calculations
  - 2.3 Comparison with measurements
4. ENVIRONMENTAL PROTECTION
  - 4.1 Water activation
  - 4.2 Air activation
5. INDUCED RADIOACTIVITY
6. RADIATION DAMAGE TO COMPONENTS
7. PERSONNEL EXPOSURE
8. THE RADIATION PROTECTION SYSTEM FOR THE SNQ
  - 8.1 Radiation protection personnel
  - 8.2 Rules, procedures and recommendations
  - 8.3 Radiation protection measuring and monitoring systems
9. CONCLUSIONS

RADIATION PROBLEMS EXPECTED FOR THE  
GERMAN SPALLATION NEUTRON SOURCE

1. INTRODUCTION

The spallation neutron source (SNQ) as described in the comprehensive report of the "reference solution" of the German project and discussed at this meeting poses a number of radiation problems. I would like to discuss in this report radiation protection problems for the staff and problems connected with environmental protection, in particular the release of radioactivity. Requirements for low experimental background often are more restrictive than those for radiation protection of experimental teams; this is the case for the low-background requirements for high-energy neutrons in the neutron hall. These requirements as well as some other radiation problems connected with the RF system are not discussed in this report.

Some remarks on radiation damage seem to be appropriate, as the demand for more and more sophisticated equipment and apparatus close to the beam diminishes the reliability of the SNQ facility unless radiation-resistant components are used everywhere.

The most important radiation problems are expected from induced radioactivity in all its forms: activated accelerator components, gaseous nuclides in the air, and activated water and soil in and around the primary-beam tunnels.

Radiation levels in the vicinity of high-energy particle beams depend entirely on the number and distribution of interactions of these particles. These interactions in targets produce the secondary particles needed for the experiments, e.g. the neutrons in the spallation target. If the interactions occur elsewhere we speak of particle or beam losses. These beam losses can occur all along the proton path from the pre-injector to the 1100 GeV targets. The number of protons lost per second in a section of the accelerator or beam line is decisive for all radiation problems. I will therefore first discuss the beam loss assumptions made for the SNQ and accepted as design parameters.

## 2. BEAM LOSSES

Theoretical studies to determine beam losses are very difficult to make as imperfections and influences of the beam-line elements can only be guessed. Empirically, percentage beam losses can be estimated by comparison with existing accelerators. Measurements of global losses, e.g. the difference between the injected protons and the protons arriving at the target depends on the accuracy of the beam monitors and may be of the order of a few percent. In a given sector of a high-current accelerator a "few percent" is a very high beam loss. For existing high-current accelerators the losses are smaller than the error bar of a  $\Delta i$  measurement with beam monitors; in most practical cases beam losses are estimated from the secondary radiation or induced radioactivity they produce.

For the LAMPF accelerator these losses were estimated to be  $< 10^{-3}$  already in 1977 (ref. 1); today  $< 10^{-4}$  per 100 metres of beam line is assumed. At the CERN PS primary-beam line to the West Area the radiation levels near the beam pipe suggest that losses were below  $10^{-4}/100$  m. Experiences with the SIN extracted-beam line confirm these estimates, beam losses are  $\lesssim 10^{-4}$  in the straight part of the SIN primary-beam line (ref. 2). At present intensities (a few hundred  $\mu\text{A}$  average current) beam losses can be controlled to remain below  $10^{-4}$ . For an accelerator of more than 10 times higher proton currents it must be possible to limit beam losses to below  $10^{-3}$  in spite of the possibility that the intensity-related effects may be aggravated.

The beam losses on which we base our calculations for the radiation parameters are limiting operation conditions: the absolute average beam losses must be kept smaller than

$$10^{-3} \times 3 \cdot 10^{-16} \text{ p/s} = 3 \cdot 10^{-13} \text{ protons lost per second}$$

in the different areas; if other measures fail the beam intensity must be reduced. Table 1 gives the maximum acceptable beam losses for the different sections of the SNQ. From these assumed beam losses the secondary radiation level, the induced radioactivity and the local dose to components was estimated by MC calculations and by extrapolation of results from existing measurements. As for all calculations the same loss assumptions were used, the results will be consistent in all radiation aspects.

### 3. STRAY RADIATION LEVELS OUTSIDE THE SHIELDING ENCLOSURE

In order to determine the required shielding thickness one needs, besides the particle interaction rate along the accelerator, the acceptable dose rates outside the shielding. These have been defined as  $< 1$  rem/2000 h of operation outside buildings and where people work permanently\*. Figure 1 gives the acceptable dose rates according to the German radiation protection regulations (ref. 3). The shielding is also determined by the dose rates at large distances, where several loss points contribute to the fence-post dose. Figure 2 shows the SNQ area and the tentative position of the SNQ fence. Everywhere along this fence the radiation level is unlikely to produce dose rates in excess of 150 mrem/6000 h of operation.

#### 3.1 Calculations

The MC codes used for the shielding calculations of the linear accelerator and the primary-beam tunnels are based on simulating the hadron-meson cascade in a simplified shielding structure and on a random choice of the interaction parameters of primary and secondary particles in the cascade. The physical picture is simple: protons are assumed to be "lost" in interactions with the vacuum chamber (number of protons lost from Table 1). The many possible reaction channels and reaction parameters as well as the place of interaction in the "target" are chosen randomly. The interaction is characterised by a vertex, the nucleus hit by the protons, and primary and secondary particles (average number is a function of proton energy) coming out from this vertex (point of interaction). If such an event is observed in nuclear emulsion it is termed a "star". Secondaries which have enough kinetic energy to produce another star are also "followed" by the simulation-calculation, again with random choice of all particles and their interaction parameters. In this way a whole cascade of "events" (= interactions) and particles is generated. The essential results of such calculations are for the relatively simple geometrical configurations used expressed in the following parameters:

- a) The number of stars per unit volume of material throughout the configuration.
- b) The number of secondaries (primaries) escaping from the configuration.

---

\* The maximum yearly operation time of the SNQ is taken as 6000 h.

- c) The energy "left" in each volume element throughout the configuration. This energy comprises
- i) the ionization and excitation energy lost by the particles, and
  - ii) the energy deposited in the vertex of the event (nucleus and heavy fragments and particles).

As nuclei are left mostly in an excited state when the cascade has just passed, many nuclei will "evaporate" neutrons and other particles (MeV energy range) and the residual nuclei are often unstable against  $\beta^\pm$  decay. Some computer programs (HETC) have options to calculate the type of residual nuclei produced in the spallation reactions.

These particle flux densities cannot be calculated for large depths (very thick cylinder) as the statistics become poor. Calculated star densities for smaller depths are therefore extrapolated using well established attenuation lengths. We have mainly used CASIM (ref. 4), a code developed at FNAL to calculate the shielding efficiency and star densities to estimate remanent gamma dose rate and irradiation dose.

### 3.2 Comparison with measurements

A number of shielding measurements were made at 600 MeV proton energy and 10 GeV. Comparisons give reasonable estimates for 1.1 GeV. Table 2 gives some results for the shielding requirements on top of the main tunnel and in sideward direction. With increasing energy the shielding thickness for a given dose rate outside increases with energy up to 500-600 MeV. Particle flux densities outside the shield are obtained by multiplying the star density by 40 (for concrete); the flux density divided by 3 gives the dose at the surface in mrem/h. With 8 m of earth and 1 m of concrete ( $\approx 1900$  g/cm<sup>2</sup>) of side shielding the dose rate outside (for  $3 \cdot 10^{13}$  p/s at 1.1 GeV) remains below 0.50 mrem/h, corresponding to 1 rem/y for 2000 h.

Stray radiation is also escaping from labyrinths and ducts leading to the primary-beam areas. The levels of neutrons in the RF galleries has been estimated using measured and calculated attenuations in tunnels and ducts. Table 3 gives some examples. The total number of particles escaping is of the same order of magnitude as those penetrating the shield.

We can assume that the stray radiation problem can be controlled with the present layout and shielding design (ref. 5), though the details need to be worked out.

For the target station, estimations were made with very large attenuation lengths for steel, which constitutes the bulk shielding material. The shielding here is governed by the required low experimental neutron (hadron) background around the target station.

Stray radiation also escapes from the experimental areas at 350 and 1100 MeV. Here the bulk shielding is mobile (blocks) and the shielding for each beam has to be designed to keep the dose rates in experimenters' control areas below 2.5 mrem/h, in permanently occupied areas below 0.5 rem/h, and in only occasionally accessed places around the shielding below 10-100 mrem/h. The integral of the dose rate  $D$  (in mrem/h) over the insufficiently shielded areas  $S$  (in  $m^2$ ) must obey the inequality:

$$\int_S D_{\text{mrem/h}} \cdot dS_{m^2} < 10^4$$

Secondary-beam areas with more than  $10^6$  interactions/s locally must be shielded all around.

With this limitation for scattered radiation from experimental areas the whole SNQ complex will not release more than  $1-3 \cdot 10^9$  hadrons/sec. This total emission (distributed!) produces dose rates at the fences of the installation below 150 mrem/y (about 100 m from the "source"). Figure 2 gives the estimated fence post doses around the presumed rectangular SNS area.

#### 4. ENVIRONMENTAL PROTECTION

##### Gaseous and aqueous radioactivity outside the shielding enclosure

In addition to stray radiation released from the SNQ installations, radioactive air and water can be transported outside the shielding by cooling and ventilation systems. Radioactivity can also be produced in the soil, rock and water outside the building structure.

##### 4.1 Water activation

The public is most concerned with the radioactivity in drinking water and food. In order to avoid any appreciable activation of soil and ground water, the concrete structure of the primary beam tunnels has been made sufficiently thick so that the radiation penetrating this concrete layer does not produce significant amounts of water and soil activity. Assuming the interaction rates given in Table 1 and a concrete layer of more than 1 m all around the beam line, the total activity expected under

realistic assumptions are given in Table 4. The main radionuclides in soil are  $^{22}\text{Na}$ ,  $^{45}\text{Ca}$ , and  $^3\text{H}$  and  $^7\text{Be}$  in water. The total activity produced must be compared to the water volume which dissolves this activity, the leaching rate, the transport time and the decay of activity. It has been shown that the soil activation (outside 1 m of concrete) and direct water activation will lead to specific water activities well below acceptable drinking-water activities (ref. 6).

The ground water and consequently the drinking-water supply can also be contaminated by release of activated (cooling)water from the installation into the public drains. Therefore all water-cooling circuits for primary-beam areas are conceived as closed systems. Contamination is only possible accidentally, e.g. a sudden discharge (break) of an activated circuit. As a further precaution the internal drains of the tunnels are designed with sufficient volume to act as an "incorporated" retaining tank, which will only be drained to the outside if found "inactive". This drainage system is a barrier against spread of activity. Table 5 gives the total activity expected in the water circuits. It can be seen that only a few Ci are present in the closed circuits of the Linac. A discharge rate of 1-5% per year (incidents) seems to be an upper limit in present installations (CERN). The nuclides in the cooling water of the Linac are spallation products of oxygen (or of impurities in the water), or active corrosion products from the plumbing.

The total interaction rate of high-energy particles in water represents about 1% of all interactions in the accelerator structure and shielding in present installations.

#### 4.2 Air activation

If high-energy particles penetrate air, about 1% interacts within a path length of 6 metres. In accelerator tunnels 6 m of air path is a reasonable average when considering the dimensions, 3-5 m  $\phi$ , and the average particle direction ( $30-80^\circ$  to the beam outside the beam-line elements). However, not more than 10% of all primary and secondary particles escape from the beam line elements. At places where many interactions are expected (targets), the local shielding absorbs even a much higher percentage. As an upper limit about 1 ‰ of all interactions are assumed to take place in air.

With these assumptions one calculates a large amount of mostly short-lived gaseous activity permanently produced and emitted if no special precautions are taken (ref. 7). The ventilation systems of the SNS will therefore be an all closed system for the primary-beam areas. The system will circulate the air during operation and immediately after stop of operation until the gaseous nuclides  $^{15}\text{O}$ ,  $^{13}\text{N}$ ,  $^{11}\text{C}$ ,  $^4\text{A}$  have decayed. For the environment the leakage of active gas is therefore of concern (see Tables 6-8). The residual gaseous activity is released in a vertical jet guaranteeing at least a factor 1000 of dilution. The leaking gas is distributed over a large area and will therefore not give any significant submersion dose. At the point of maximum impact a few mrem/y is the upper limit estimated for the submersion dose. Also the small fraction of activated particulates which could be deposited on the ground are much reduced by using ordinary filters in the exhaust lines. Exposures from this source (internal) are of the order of microrems per year.

In conclusion the environment is well protected against radioactive contamination if:

- a) more than 1 m of concrete is between the beam line elements and the soil and water around the beam tunnel,
- b) the internal drains in the primary beam tunnel have sufficient volume to act as temporary retaining basin,
- c) all water cooling circuits in primary-beam tunnels are closed circuits,
- d) ion exchange beds are installed in the closed circuits to retain long-lived active products,
- e) the ion exchange resins are in easily exchangeable cartridges in order to allow for decay of active products in the resins before regeneration,
- f) all primary beam ventilation systems are closed systems; the venting after decay of gasous nuclides is made via vertical jets (or high chimneys),
- g) the air in the tunnels is filtered at the inlet and outlet,
- h) monitoring is provided for: i) in the drains; ii) in the water release line; and iii) in the ventilation system(s).

## 5. INDUCED RADIOACTIVITY

It has been shown that the activated air and water can present a problem when immediately released from the primary-beam lines even if they represent less than  $10^{-3}$  and  $10^{-2}$  respectively of the activity produced. About 80-90% of all activity is produced in the beam line/accelerator components. High specific activities (order of microcuries per gram) are expected on the outer surface of RF tanks, vacuum pipes and magnets, leading to dose rates of several hundred mrem per hour after 24 hours of cooling at 0.5 m distance from the surface\*.

In the MC simulation of the hadron-meson cascade the star or event density (stars/cm<sup>3</sup>) was calculated per "incoming" (lost) proton. From this star density in the outer layers of the components the dose rates in the vicinity can be estimated using empirical conversion factors. The HETC program permits calculation of the induced radionuclides. A number of conversion factors have been proposed ranging between 4 and  $12 \cdot 10^{-7}$  rem/h for a production rate of 1 star/sec.cm<sup>3</sup> for 30 days of activation and 1 day of cooling time (ref. 8).

Many practical measurements have confirmed these factors. For predictions the more conservative (Oak Ridge) factor of  $1.2 \cdot 10^{-6}$  is used and with this factor and a determination of the star density with the program CASIM for a number of simple configurations the expected dose rates for the SNQ were estimated (ref. 9). Figures 3a and 3b show the results. The only "safety" factors in these estimations are:

- the conversion factor (max. factor 3 too high),
- the beam loss assumptions.

We therefore have to expect that at some locations along the accelerator structure such dose rates might occur. In most places the dose rates from remanent activity will be lower. There is however the problem that with the present beam loss assumptions one cannot predict where the hot spots will be.

The induced radioactivity is in present high-energy proton accelerators to more than 80% responsible for the exposure of the personnel. The accelerator will need maintenance, repair interventions and improvement work. It is to be expected that such work is often needed in the most

---

\* For an infinite surface the surface dose rate from beta and gamma radiation is 1mrem/h for about 1 nCi/g of specific radioactivity produced by spallation processes.

activated areas and therefore costly in dose. In a long-term exposure planning for the accelerator staff the yearly dose should not exceed 1 rem/y. Near highly activated equipment this gives working times of the order of an hour only, for a whole year! Clearly the infrastructure must provide for the (later) use of manipulators and the design of the accelerator must be governed by a number of principles of which some may be mentioned:

- a) The simplest possible design for the accelerator and the beam-tunnel infrastructure must be aimed at (services, communication, safety).
- b) All material and components must be selected to withstand 10 times the yearly radiation doses estimated for these components.
- c) Nothing should be brought into the primary-beam tunnels that is not needed there. The installation must be approved by the chief engineer or commissioner.
- d) All equipment of the tunnel must be designed by specially trained and instructed staff.
- e) The layout of the tunnel and individual components must be such that persons and manipulators have access everywhere.
- f) Modular design where possible. Spare parts are essential to replace modules and to train staff in both maintenance and design.
- g) All active and vulnerable parts of components or systems must be designed to "go with" the removable component or as a separately removable part or module.

Dose saving in the operation is essential for all parts of the SNQ, in particular for the spallation target station. The operation planning should give high priority to dose saving. Long maintenance periods are essential, and indispensable for preventive maintenance.

The kind of interventions and repair envisaged for the active area must be defined and is part of the design criteria. All installations and components in the primary-beam tunnel must be designed to be manipulator-compatible. It is anticipated that in practice the manipulator will mainly be used where and when the beam losses are of the order of magnitude indicated in Table 1. In order to share exposures to ionizing radiation during repair and maintenance it is good practice that all staff of the SNQ are trained to work in the active areas. The designers should also take part in this repair and

maintenance work. If in all stages of the design and construction the requirements for simplicity, easy accessibility, modular construction and fast exchangeability of components as well as of the infrastructure are observed, the operation of the SNQ will not cause collective doses in excess of 100 man-rem per year when judged from experience with present accelerators. Design specifications must be given before individual groups begin to design their particular equipment. The same is necessary for all connections (power, RF, controls, water, etc.) and for general services in the tunnels: power, light, water (fire fighting), telephone, intercom, radiation monitors, warning devices, cranes, rails, transport devices, and the infrastructure for the manipulator, ventilation and airconditioning equipment. It should be easy to keep the tunnel clean and to drain water from possible leaks in the cooling system quickly.

It is highly recommended to appoint a senior engineer to act as a commissioner for the primary-beam tunnels with the right to veto all equipment not designed according to specifications. Lack of experience of the physicists, engineers and designers often results in an "overdesign" or redundancy in the measuring and control equipment, which all need maintenance or at least inspection. All those who have equipment in the primary-beam tunnel must therefore in parallel with the design prepare an inspection and maintenance schedule which defines the persons who will work in the active areas and the time they have to spend in the tunnel. If a manipulator or other handling device must be used, their schedule (including access and transfer to the place of work) must be defined and adapted to the requirements of all manipulator users. It should also be specified who controls the manipulator, whether a central team or the particular group which requires the manipulator.

For high current accelerators it is essential that they can be developed and tuned at low intensity. It is planned that the SNQ is tuned at 1 pulse/s or at 1% of its maximum intensity. It should be kept in mind that beam losses of 10% at this intensity already correspond to the maximum losses in Table 1. Not all tests can be made at this mode of operation. The beam observation equipment must be designed for a large range of intensities.

The induced radioactivity also poses a problem for transport and storage of activated items outside the shielding enclosures. It is

estimated that a shielded storage place corresponding to about a 30-50 meter section of the main tunnel will be needed after an operational period of 10 years. An additional storage area of 300-500 m<sup>2</sup> for slightly activated items is required, of which one half or one third must be roofed. In this estimate it is assumed that active waste and scrap can be handed over to a central waste disposal service and that the target wheels have their own handling and storage facilities in the target building.

## 6. RADIATION DAMAGE TO COMPONENTS

From the MC calculations mentioned and from measurements made at CERN (see ref. 10 for example) and other laboratories one can estimate the dose to components near the primary beam for given beam losses (e.g. Table 1). A production rate of  $2 \cdot 10^6$  stars/sec.cm<sup>3</sup> gives a contact dose rate of about 1 rem/h. A star deposits about 0.5 GeV of energy; in 1 year ( $2 \cdot 10^7$  sec) at this irradiation rate, about  $2 \cdot 10^{13}$  GeV/cm<sup>3</sup>, or  $4 \cdot 10^7$  rad/y are expected for the outer part of these irradiated objects. Close to the beam 10-100 times higher doses can be expected with  $3 \cdot 10^{13}$  p/s lost locally. The doses for a period of 10 years (required life of components) may thus reach values of a few times  $10^{10}$  rad. With a contact remanent dose rate (24 h cooling) of the order of 1 rem/h on the surface of a magnet one must expect an irradiation dose to the coil insulation of  $10^8$ - $10^9$  rad/y. Therefore, when the remanent dose rates are cause for concern for repair and maintenance work, the material of the activated components are exposed to doses that require careful selection; the two problems occur at high irradiation rates simultaneously. Also, materials remote from the beam line must resist  $10^7$ - $10^8$  rad. This is particularly important for electrical installations. It is today possible to find organic materials withstanding  $10^8$  rad for nearly all applications. It is difficult to find organic materials which can be used up to  $10^{10}$  rad, above this dose inorganic materials must be used, but above  $10^{10}$  rad these materials may be affected as well (ferrits, permanent magnets, conductors, etc.).

It is doubly annoying when components fail because of radiation damage: the equipment has to be replaced, and the remanent dose where the damage occurred is particularly high. Table 9 gives some examples of radiation resistivity of common materials taken from ref. 11.

Transistors fail at about  $10^5$ - $10^6$  rad, electronic circuits if not specially designed for working in radiation areas above  $10^5$  rad. Integrated circuits should not be used above  $10^4$  rad and microprocessor memories are

unreliable above  $10^3$  rad if and when strong interactions occur which can produce heavy ionizing particles. If small high-impedance signals have to be transmitted over long distances, the old-fashioned cathode follower may be used up to  $10^7$  rad for adapting impedances.

The radiation damage problems emphasize again the importance of a radiation-proof design. Construction materials as well as design and layout must be carefully studied and meet strict specifications. Compliance with these specifications must also be controlled by a single instance such as the chief engineer or a commissioner.

#### 7. PERSONNEL EXPOSURE

It has already been mentioned that the exposure of personnel to remanent activity in the primary-beam tunnels will be the most important part of all exposures. The prompt radiation can be reduced by shielding, at high cost but efficiently, to acceptable levels. A meter of compact earth shielding reduces the flux density outside by one order of magnitude. Compared to a total thickness of about 10 m, this is 10% in shielding thickness and 20% of the shielding cost for the SNQ. The remanent dose rate on the other hand is directly proportional to the number of interactions and they are a function of the intrinsic losses. According to all experience gained at present accelerators, these losses can be reduced in the first years of operation, but then they remain constant, whereas the beam intensities have a tendency to increase and sometimes offset the gains from reduced relative beam losses. Dose reduction of the personnel is the main purpose of radiation protection. Better planning of interventions and increasing experience lead, at **existing accelerators**, to lower doses for the maintenance staff in spite of the fact that the remanent dose rates have increased. This achievement is nearly always due to better skill of staff, more reliable components (less inspection and maintenance), longer shut-downs, and replacement instead of repair.

The ALARA principle requires keeping doses as low as reasonably achievable. This implies that an optimum solution has to be found for design, construction, operation, modifications and even for improvements. An optimum can only be found if more than one solution is studied in all phases. The evaluation of more than one solution, careful design, and material selection all require

time, in particular for the initial design and construction phase of the SNS. The initial design can already make provisions in the infrastructure for modifications, e.g. by assuming that none of the components are permanent.

Figures 4a and 4b and Table 10 (from ref. 12) show personnel exposure at CERN. More than 80% of all dose is due to exposure to remanent gamma radiation. The groups that receive substantial exposures are fairly constant in number. Also there is a tendency towards "expert exposures", i.e. that those who have high accumulated life doses also receive more dose per year than the average person. We are at CERN conscious of this development and try to react but this has turned out to be difficult as a high degree of specialization is built up in all sectors. It would be a great advantage if for the SNQ this specialization would not be required to maintain and replace specialized equipment.

No internal exposure is associated with the SNQ operation. The activation of dust, aerosols and drinking water is so insignificant that exposures are more than three orders of magnitude lower than the external exposures anticipated (ref. 13). This statement is confirmed by many contamination measurements at the CERN SC and at SIN.

In conclusion, one would expect that a dose planning limit of 1 rem/y and a well controlled design and operation will make it possible to do 90% of all maintenance work "hands on" or by using long tools. It should be possible to keep the total yearly collective dose below 100 man-rem. About 100 persons would be expected to take part in the manual work in active areas. This team should be well trained in radiation work and in (standardized) maintenance and replacement interventions including in the use of manipulators. There should be no need for "specialist" intervention in the tunnel. The team should also include designers of tunnel equipment as well as users of the SNQ, independent of their professional status.

## 8. THE RADIATION PROTECTION SYSTEM OF THE SPALLATION NEUTRON SOURCE

In a broad sense the radiation protection system of the SNQ comprises all measures and precautions and all equipment to prevent or reduce exposure of personnel and of members of the general population to ionizing radiation whilst allowing the operation of the SNQ and its experimental areas (ref. 14). This includes in particular protection against unacceptable exposure to prompt radiation and to remanent gamma and beta radiation, limitation of

emission of radioactivity and radiation to the environment, and prevention of radiation damage to equipment and contamination of areas and installations.

The radiation protection system comprises

- a team of competent persons to initiate or execute all radiation protection measures and to control and check the effect of these measures,
- a set of administrative and technical rules and regulations, procedures and instructions to cope with the regular operation of the SNQ as well as with incidents,
- measuring and ancillary equipment, both mobile and fixed installed, monitoring the radiation situation, controlling and checking the effect of radiation measures and/or operation conditions.

Such a radiation protection system can be independent or part of a more general radiation protection system for a whole research centre. It is difficult to describe at this stage of the project the team of radiation protection personnel and the rules, administrative procedure and instructions, but a few general remarks might be in order.

#### 8.1 Radiation protection personnel

According to the German Strahlenschutzverordnung, radiation protection personnel is already required for the construction phase of the SNQ. These persons have to look after the protection measures and the protection system to be created and installed, in particular in the following areas:

- Design and construction of the SNQ and its installations.
- Shielding design and layout.
- Specifications for remote-handling.
- Selection of materials and equipment with respect to radiation resistivity.
- Planning of interventions and routine work in primary beam areas.
- Participation in training of radiation workers and instruction on radiation protection for all staff.
- Specification of interlock and access systems, of communication and area surveillance systems.

During the construction phase the radiation background monitoring in the surveyed areas has to start and the hardware and software for the complete monitor and surveillance system designed and installed.

Staff requirements for the construction phase:

	Phys./Eng.	Eng./Techn.	Techn.
Planning, specification	1	1	1
Damage tests, material selection	1		1
Instrumentation	1	1	3
Programming, environmental protection		1	1

In the operation phase an additional four technicians for radiation measurements are needed. They must also be trained in instrument development and in programming. An on-call service must be available around the clock for unscheduled access to primary beam areas.

All operators and technical staff of the SNQ will be trained to work in active areas and professional staff will take part in radiation protection courses (shift leaders, engineers in charge, etc.).

## 8.2 Rules, procedures and recommendations

Only some basic specifications for these rules can be given at this stage:

- a) Planning of work for technical staff involving radiation exposure must respect a planning level of 1 rem/y. Intervention times per year multiplied by dose rates expected = 1000 mrem. Dose to auxiliary personnel and users should be kept below 500 mrem/y, in particular if a person only works part time at the SNQ. Hands-on maintenance is excluded above 300 mrem/h.
- b) Access to primary-beam areas must be controlled; this includes
  - planning of work and maximum allowed dose,
  - authorization for access,
  - recording of time, name and dose received,
  - in some areas contamination check when leaving.
- c) Components and items need an authorization for use or installation in the tunnel.

The German Strahlenschutzverordnung will be the basis for the internal rules, which will also define the responsibilities of all those who have to deal with radiation protection, in particular radiation protection personnel, operational staff, and experimentalists.

### 8.3 Radiation protection measuring and monitor systems

This section is restricted to an enumeration of the different systems envisaged at present. The proposed systems have been successfully used in CERN (ref. 15) and other high-energy accelerators. The list is by no means final and specifications are not yet made.

It has however been decided to control all fixed installed measuring devices with a computer-aided RP control system, very probably based on microprocessors. The different monitors conceived for different purposes will all be compatible with the same control device. One control crate can therefore control all types of RP monitors in the "area". The control devices log information and transmit it to a data base and/or a separate alarm system.

The hard-wire alarm system transmits three types of warning:

- a master area alarm,
- an equipment alarm,
- a warning of high levels.

The details on the alarm status are given by the RP computer-based alarm system. If exceptionally an alarm is used to interlock an operation, hard-wire alarm must be used.

#### a) Beam loss monitors

These monitors near the primary beam indicate high instantaneous radiation levels from beam losses (ion chambers, about 100 monitors).

#### b) Activity monitors

During shut-downs they monitor the radiation levels from remanent activity and display the situation outside the active area (ionization chambers, about 100 monitors).

#### c) Area monitors

In radiation controlled areas and radiation surveyed areas, the dose rates are recorded and available in the MCR (main control room), and

warnings are displayed in the areas concerned when appropriate. Most of these monitors are based on ionization chambers, some on neutron counters (about 60-80 monitors depending on the needs in the experimental areas).

d) Air monitors

These are divided into the following groups:

- i) Monitors for measuring the activity in the circulating air to decide when the air can be released (GM tubes or plastic scintillators, about 10 monitors).
- ii) Monitors in the air evacuation ducts to measure the gaseous activity rejected (2-4 monitors).
- iii) Monitors to measure the aerosol activity released from the installations (at four places air filters in the bypass of the air release ducts).
- iv) Portable air monitors for measuring the air leakage rate out of the primary beam tunnels (three monitors).

e) Water monitors

- i) There is an interest to know the activity in the closed circuits (beam loss monitoring, discharge criteria) (10-20 monitors, GM counters).
- ii) Water samplers in the primary beam tunnel draining system (about 4 samplers).
- iii) Sampler and continuous monitor in the water release lines (about 2 monitors).

f) Door and contamination monitors

At the access points to primary beam areas there will be gamma monitors to check activity taken out, at some access points also contamination monitors (5-7 door monitors, 4 contamination monitors).

g) Personal monitors

It is proposed to have for everyone working in primary beam tunnels (coded) personal warning devices indicating the dose rate (acoustically) and transmitting the accumulated dose to the area and access surveillance desk. The person would be warned by intercom when a preset dose is accumulated (e.g. 100 mrem). In addition, quartz-fiber dosimeters will be used.

## 9. CONCLUSIONS

The account given shows that the SNQ has to cope with some radiation protection problems. It might be interesting to compare these with radiation problems at a research reactor like that of Grenoble.

The dose to the personnel for maintenance and repair is lower for the SNQ, the activity produced (2 MCi) about 100 times less than in the reactor. This reduces the radioactive storage problem to finding a few hundred square metres of shielded area for the SNQ. Release of activated air is a factor of 100-1000 less important for gamma activities and even more so for radiotoxic aerosols.

The potential dangers of the SNQ are nil compared to a research reactor, which already represents only a small risk. One can profit from the experience gained at high-energy laboratories for the operation and radiation protection at the SNQ and use the technology available in nuclear centres for handling of active items and for controlling airborne and water activity.

The SNQ is larger and contains more complicated equipment than a research reactor. Simplicity and reliability has to be incorporated into the design of all SNQ components. Designers have to be made aware of the radiation problems involved. The main task is therefore to organize and coordinate the construction work and to impress on all designers of individual equipment that the basic specification of an installation that will become radioactive must be met. If the SNQ is simple, reliable, accessible, radiation-resistant, and almost maintenance-free (at least in the beam tunnel), then it will be possible to operate it at a reasonable cost, both in dose and in money.

REFERENCES

- 1) D.C. Hagerman, LAMPF operations at 500  $\mu$ A, 1979 Linear Accelerator Conference, San Francisco March 1979
- 2) H. Willax, personal communication (1980).
- 3) Verordnung über den Schutz vor Schäden durch ionisierende Strahlen (Strahlenschutzverordnung Strl.Sch.V (13.10.1976), Bundesgesetzblatt Teil I Nr. 125 p. 2905-2999 (20.X.1976).
- 4) M. Höfert, CASIM at CERN, private communication
- 5) K. Goebel, Strahlenschutzprobleme beim Betrieb eines Hochstrom-Linearbeschleunigers, III. Abschirmung des Beschleunigertunnels, private communication
- 6) K. Goebel, Strahlenschutzprobleme beim Betrieb eines Hochstrom-Linearbeschleunigers, I. Aktivierung des Bodens, private communication  
K. Goebel, Radioecological considerations for operating particle accelerators, private communication
- 7) A. Rindi, La radioactivité induite dans l'air de l'accélérateur de protons de 300 GeV du CERN, private communication
- 8) J. Ranft and K. Goebel, Estimation of induced radioactivity around high-energy accelerators from hadronic cascade star densities obtained from MC calculations, private communication
- 9) K. Goebel, Strahlenschutzprobleme beim Betrieb eines Hochstrom-Linearbeschleunigers, II. Aktivierung der Beschleunigerstruktur, private communication
- 10) M. Ellefsplass, K. Goebel, J. Ranft, H. Schönbacher and G. Stevenson, Dose to accelerator components and remanent  $\gamma$ -dose rates in the SPS primary beam areas, private communication
- 11) H. Schönbacher and A. Stolarz-Izycka, Compilation of radiation damage test data, Part I: Cable insulating materials, private communication  
M. Van de Voorde, Effects of radiation on materials and components, private communication
- 12) J. Dutrançois, Contrôle de l'exposition du personnel aux radiations en 1980, 3rd part of the Radiation Protection Group Annual Report for 1980, CERN HS-RP/061 (21.4.80).
- 13) St. Charalambus and A. Rindi, Aerosol and dust radioactivity in the halls of high-energy accelerators, Nucl. Instr. and Meth., 56, 125-135 (1967).
- 14) K. Goebel, Das Strahlenschutzsystem der Spallationsneutronenquelle, private communication

- 15) B. Moy, G. Rau and D. Schwenke, The instrumentation for monitoring the environment around CERN, CERN HS-RP/050 (25.8.80).
- B. Moy, G. Rau, A. Shave and G. Stevenson, The CERN radiation monitor and alarm system for experimental areas, CERN-HS-RP/053 (28.8.80).
- B. Moy, G. Rau and A. Shave, The data acquisition system for radiation measurement at CERN, CERN-HS-RP/057 (6.2.80).

LIST OF TABLES

- Table 1: Assumed maximum average beam losses for linear accelerator and beam transport.
- Table 2: Shielding requirements and dose rates outside the shielding as estimated by using a Moyer model (Absorption) and by calculating the star densities with the program CASIM.
- Table 3: Attenuation of neutrons through the ducts of RF feeder lines. 2 bends, 3 straight ducts and neutron dilution in the service tunnel.
- Table 4: Estimated total activity produced in standard soil by secondaries after penetration of 240 g/cm<sup>2</sup> of concrete from beam losses of  $3 \cdot 10^{13}$  p/s at 200, 400 and 600 MeV (values: Ci produced/year).
- Table 5: Total activity produced in all cooling water circuits. For contamination only long-living nuclides, at least with half lives > 1 h are of interest.
- Table 6: Gaseous activity escaping from the SNQ according to different assumptions. 3% continuous loss with a delay of 4 min. 50 air exchanges per year after 1 hour of decay.
- Table 7: Example of aerosol activation: 1 kW beam loss of the PS target area (20 GeV) ambient dose rate after 2 days of decay is a few mrem/h according to Ref. 13.
- Table 8: Air activation in the 300 GeV SPS accelerator tunnel. According to Ref. 6 the concentration in pCi/cm<sup>3</sup> is given at the outlet of the ventilation system for two ventilation schemes.
- Table 9: Radiation resistivity of different organic material used in the components of high-energy accelerators according to Ref. 14.
- Table 10: Personnel exposure at CERN. The yearly doses versus total accumulated doses of individuals. This is a correlation of high exposure rates to high life doses.

Table 1  
Average maximum beam losses

	Energy MeV	Beam Intensity p/s	%	Beam loss p/s	Lost beam kW
Linear accelerator	0.5-10	$4 \cdot 10^{16}$	25	$1 \cdot 10^{16}$	1-15
	30, 50 100 <u>each</u>	$3 \cdot 10^{16}$	1	$3 \cdot 10^{14}$	1-5
	200, 400, 600 800, 1100 <u>each</u>	$3 \cdot 10^{16}$	0.1	$3 \cdot 10^{13}$	1-5
Switchyard	1100	$3 \cdot 10^{16}$	0.1	$3 \cdot 10^{13}$	5
Beam transfer	1100	$3 \cdot 10^{16}$	0.01	$3 \cdot 10^{12}$	0.5

Table 2

Dose rates outside the shielding

Site	Beam loss p/s	Shielding (m)		Attenuation length g/cm <sup>2</sup>	Method	Dose rate mrem/h
		concrete	earth			
Side-wards 100 MeV	$3 \cdot 10^{13}$	2.80	-	60	Absorption	7
Linac tunnel 400 MeV 600 MeV 800 MeV 1100 MeV	$3 \cdot 10^{13}$	4.80	-	90	"	1
	"	4.80	-	100	{ Absorption CASIM	7 15
	"	5.80	-	115	{ Absorption CASIM	5 6
	"	5.80	-	115	{ Absorption CASIM	7 12
	"	1.00	8.00	115	Absorption	0.2
Top earth shielding 1100 MeV	"	1.00	8.00	115	Absorption	0.2

Table 3

Attenuation through RF-ducts  
Area of ducts < 0.5 m<sup>2</sup>

	Attenuation
First straight duct	100
Neutron dilution in service tunnel	100
Second vertical duct	50
Last bending	10
Third duct into RF gallery	10

}  $5 \cdot 10^7$

Table 4

Radioactivity produced in soil around the Linac  
(200 g/cm<sup>2</sup> of concrete shielding)

Nuclide	Ci saturation	Production Ci/a
T	5	0.2
<sup>7</sup> Be	0.8	2
<sup>22</sup> Na	10	2
<sup>32</sup> P	0.4	3
<sup>35</sup> S	0.3	0.6
<sup>45</sup> Ca	4	4
<sup>48</sup> V	0.3	2
<sup>51</sup> Sr	0.6	2
<sup>54</sup> Mn	1.5	0.8
<sup>55</sup> Fe	15	3
<sup>59</sup> Fe	0.4	1

Table 5

Activity in cooling water (Ci)

Nuclide	Half-life	Time after irradiation		
		0	1 min.	1 hour
<sup>3</sup> H	12.3 y	600	600	600
<sup>7</sup> Be	54 d	1.520	1.520	1.500
<sup>18</sup> F	110 m	20	20	10
<sup>11</sup> C	20 m	3.290	3.140	410
<sup>13</sup> N	10 m	4.300	4.010	70
<sup>15</sup> O	2 m	11.800	8.340	-
<sup>14</sup> O	71 s	2.950	1.650	-
<sup>10</sup> C	20 s	1.350	170	-
<sup>16</sup> N	7 s	8.430	20	-
Total: in all cooling circuits		34000	19.500	2.600
in accelerator 1% <sup>00</sup> :		34	20	3

Table 6

Emission of airborne activity from the linear accelerator

Gaseous nuclides	2% of beam power 100 kW ~ 4 Ci sat. Akt.	
	Leakage 3% Delay 4 min. mCi/a	50 air exch./a after 1 hour mCi/a
<sup>3</sup> H	50	150
<sup>11</sup> C	$3 \cdot 10^5$	$7 \cdot 10^3$
<sup>13</sup> N	$10^5$	$3 \cdot 10^3$
<sup>14</sup> O	$2 \cdot 10^5$	-
<sup>41</sup> A	$5 \cdot 10^4$	$3 \cdot 10^4$
Aerosoles		
<sup>7</sup> Be	400	4000 *)
<sup>22</sup> Na	$<2 \cdot 10^{-3}$	$<2 \cdot 10^{-3}*$ )
<sup>54</sup> Mn	0.02	0.02*)

(Leakage rate: 3% h =  $4 \cdot 10^4$  m<sup>3</sup> in 30 h • 1200 m<sup>3</sup>/h)

\*) Without filters.

Table 7

Aerosol activities in a 25 GeV proton accelerator (Ref. 13)

Nuclide	Decay		Aerosol concentration in the PS target area. Beam loss = 1 kW		
	Mode	T $\frac{1}{2}$	$10^{-12}$ Ci/m <sup>2</sup>	%	(MPC) <sup>a</sup> $10^{-12}$ Ci/m <sup>2</sup>
<sup>54</sup> Mn	EC, $\gamma$	300 d	40	50	40 000
<sup>7</sup> Be	EC, $\gamma$	54 d	20	25	$1 \cdot 10^6$
<sup>51</sup> Cr	EC, $\gamma$	28 d	6	7	$2 \cdot 10^6$
<sup>59</sup> Fe	$\beta^-$ , $\gamma$	45 d	7	9	50 000
<sup>48</sup> V	$\beta^+$ , $\gamma$	16 d	7	9	50 000

Table 8

Air activation in the SPS (300 GeV)  
 Values given: Concentration at outlet (pCi/cm<sup>3</sup>);  
 6 kW beam loss and  $5 \cdot 10^{10}$  cm<sup>3</sup>/h air reject rate

Nuclide	T = 3 min t = 42 min	T = 3 min t = 3 min
<sup>3</sup> H	$6 \times 10^{-5}$	$6 \times 10^{-5}$
<sup>7</sup> Be	$1.4 \times 10^{-3}$	$1.4 \times 10^{-3}$
<sup>11</sup> C	1.5	4.6
<sup>13</sup> N	3.0	28.2
<sup>14</sup> O	$2 \times 10^{-3}$	0.17
<sup>15</sup> O	0.27	18.3
<sup>30</sup> P		$2.6 \times 10^{-2}$
<sup>38</sup> Cl	$8.4 \times 10^{-3}$	$1.5 \times 10^{-2}$
<sup>39</sup> Cl	$1.2 \times 10^{-2}$	$1.8 \times 10^{-2}$
<sup>41</sup> Ar	0.73	0.90
<sup>24</sup> Na	$4.7 \times 10^{-4}$	$4.8 \times 10^{-4}$
Total:	5.4	52

Table 9

Dose limits for **common** materials in radiation areas

<u>Usable up to <math>1-3 \cdot 10^6</math> Gy</u>	
Conventional cable insulations:	PE (Polyolefines) PVC EPR Hypalon Neoprene
Conventional glasses	
Conventional motors	
<u>Usable up to <math>1-3 \cdot 10^7</math> Gy</u>	
Epoxy resins, unfilled, aromatic type hardener (Araldite F)	
Other resins:	Polyurethane Polyimide (Kapton)
Mineral oils	
Special lubricants (Shell APL)	
Special motors	
Paints based on epoxy or PUR resins	
Cerium doped glasses	
<u>Usable up to <math>1 \cdot 10^8</math> Gy</u>	
Inorganic filled resins:	Epoxy (CERN magnet coils) Phenolic Polyester Polyurethane Polyimide Silicone
Ryton (PPS, Phillips)	
Special cables: Kapton, glass fiber (control cables) Mica tape (power cables)	

Materials not recommended or to be used with precaution:  
(dose limit in Gy in brackets): Teflon ( $10^3 - 10^4$ ), Viton ( $10^5$ ), electronic components ( $10^2 - 10^3$ ), optical fibers ( $10^1 - 10^2$ ), silicone oil and silicone rubber ( $5 \cdot 10^5$ ), natural rubber ( $10^5$ ), polyamide ( $5 \cdot 10^5$ ).

Table 10

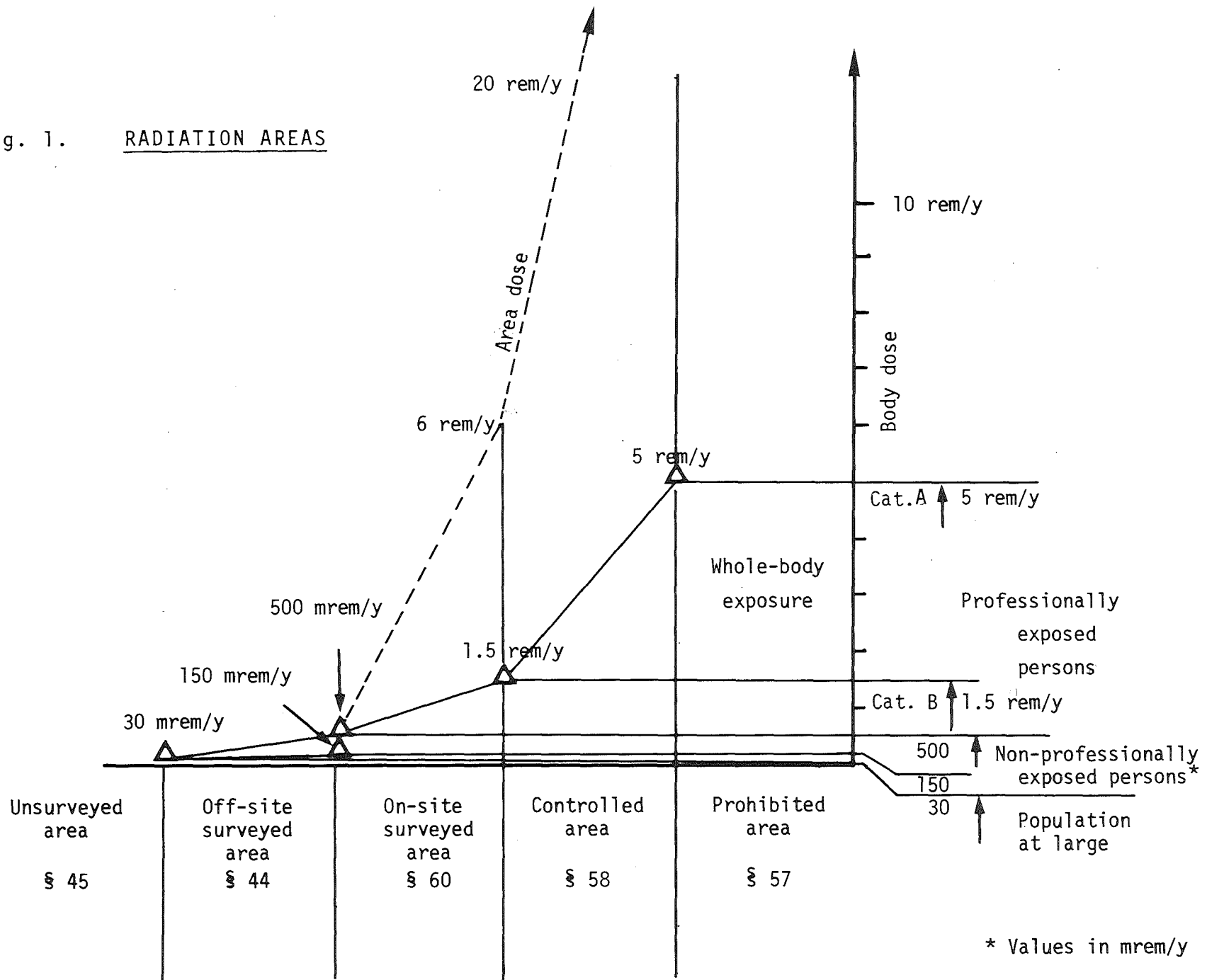
Repartition of the members of the CERN personnel  
 having accumulated more than 10 rems at CERN  
 according to the average annual exposure

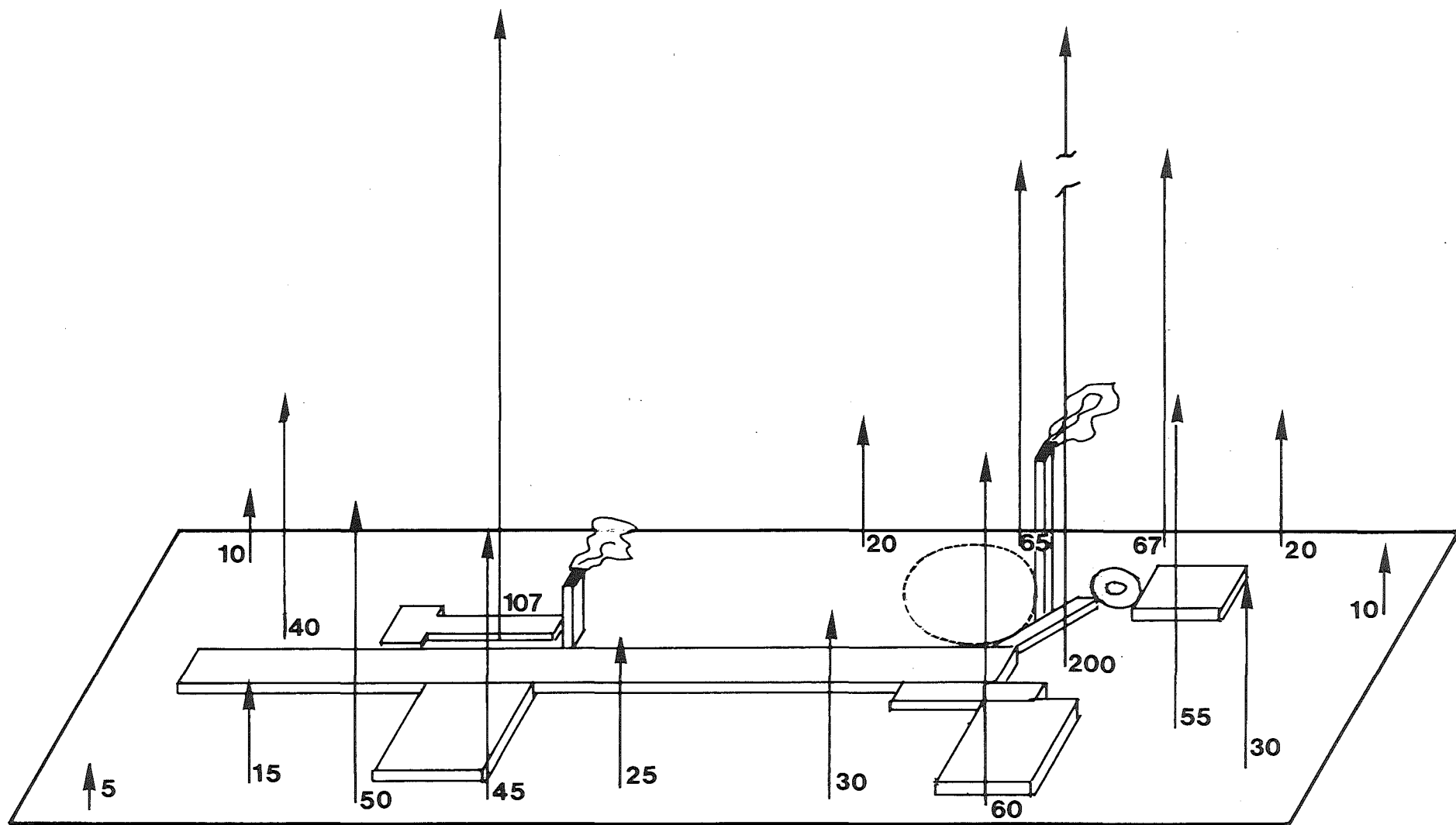
Average annual dose (mrem y <sup>-1</sup> ) Accumulated dose (rem)	0-500	501-1000	1001-1500	1501-2000	2001-2500	2501-3000	Total
10 to 20 rems	4	68	18	1	2	0	93
20 to 30 rems	0	2	26	5	1	0	34
30 to 40 rems	0	0	0	3	1	0	4
plus de 40 rems	0	0	0	1	6	0	7
TOTAL	4	70	44	10	10	0	138

FIGURE CAPTIONS

- Fig. 1. The maximum dose rates according to the German radiation protection regulations (Strahlenschutzverordnung) for the different radiation areas.
- Fig. 2. The area occupied by the SNQ, its experimental areas, target stations and optional compressor ring. The arrows along the fence indicate the yearly expected doses for 6000 h of operation and beam losses according to Table 1.
- Fig. 3a  
and 3b Contours of remanent gamma dose rates after 30 days of continuous operation and 1 day of cooling for a permanent beam loss of  $3 \cdot 10^{13}$  p/s (800 MeV) in the RF accelerating structure (from calculated star densities according to ref. 8, program CASIM).
- Fig. 4a Total yearly dose ( $\gamma+n$ ) and neutron dose for all CERN staff.
- Fig. 4b The number of persons who have been exposed to a yearly dose  $> 500$  mrem and  $> 1500$  mrem respectively at CERN.

Fig. 1. RADIATION AREAS





Radiationlevel at the fence

fig 2

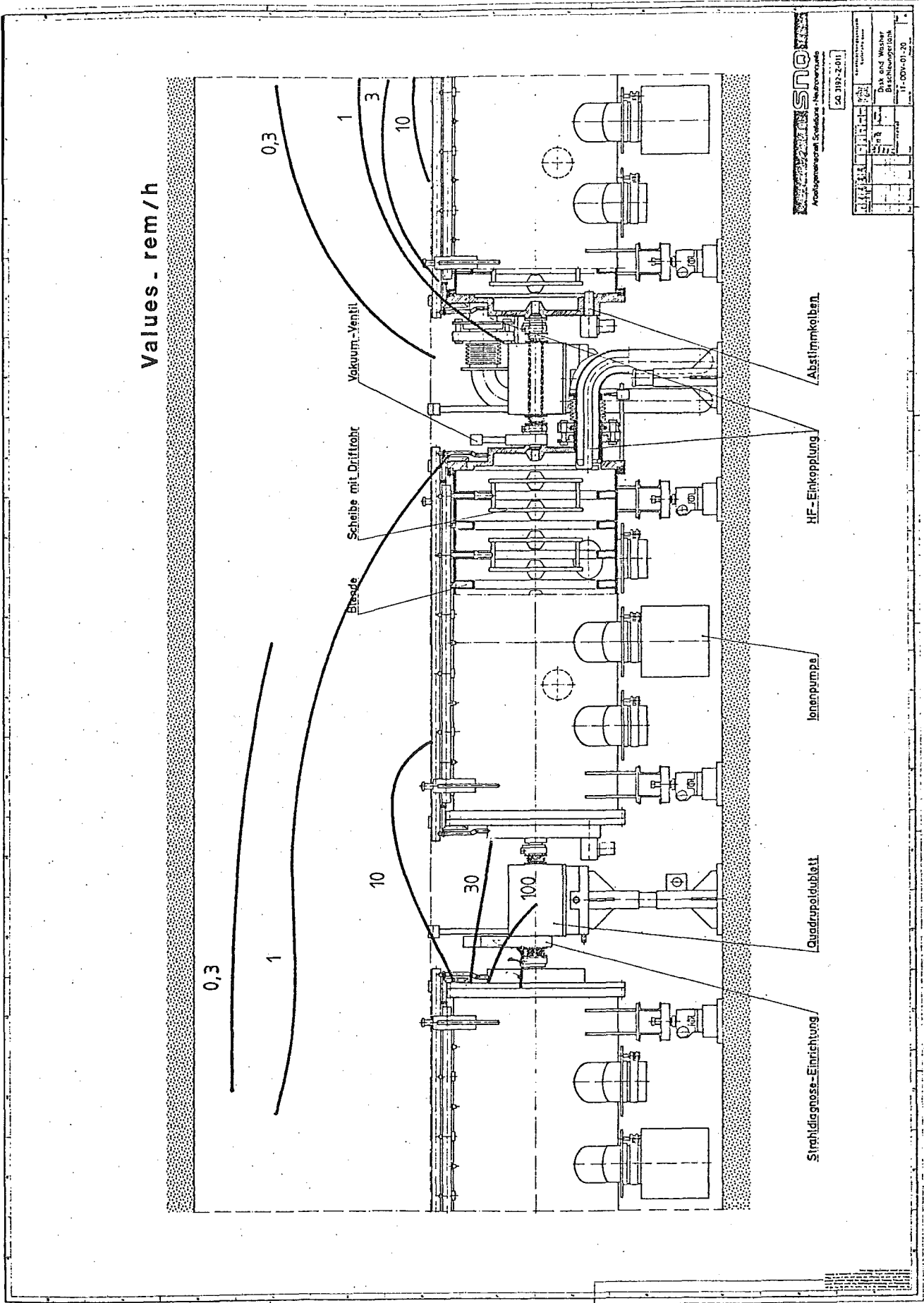


fig - 3a

Values- mrem / h

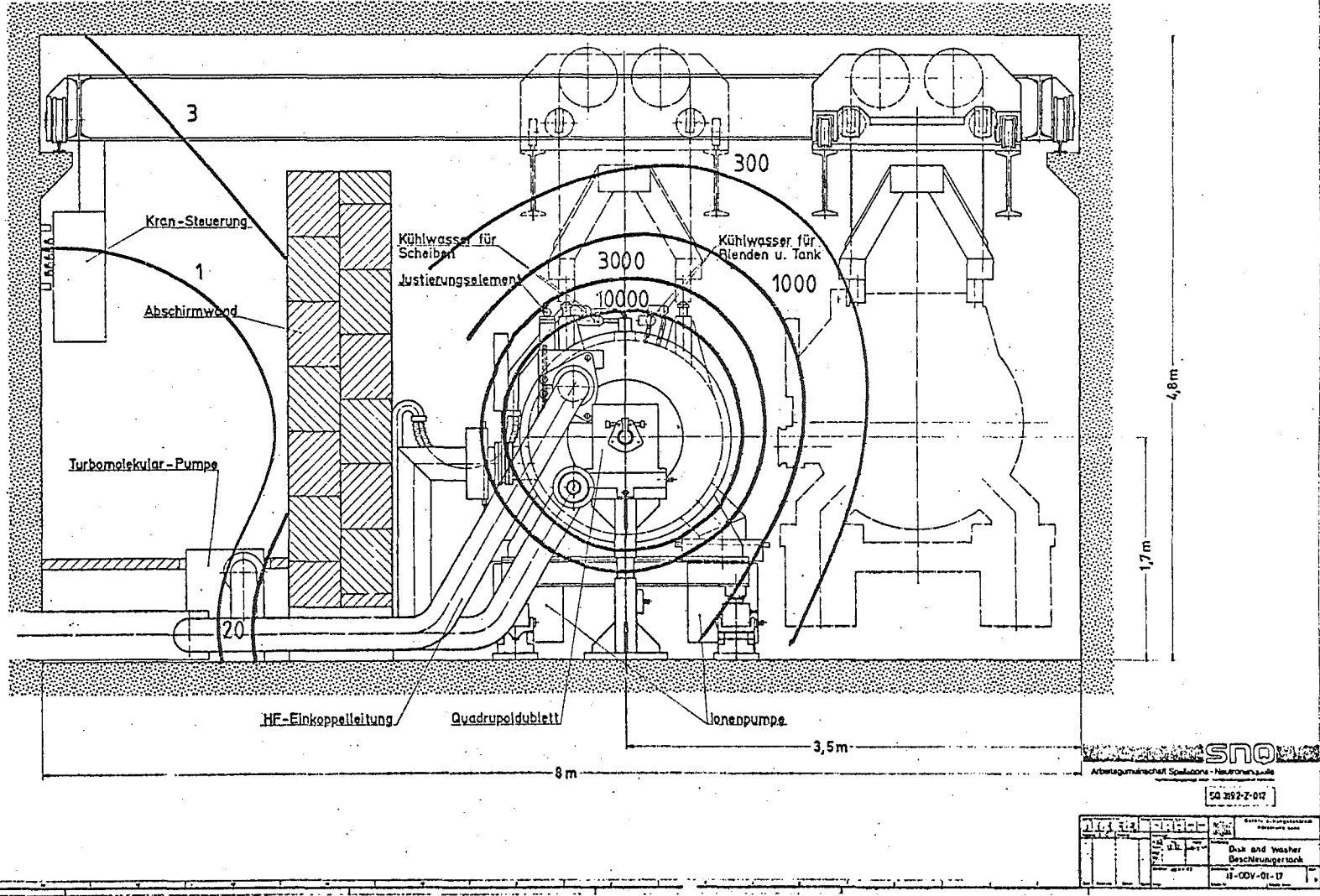


fig-3b

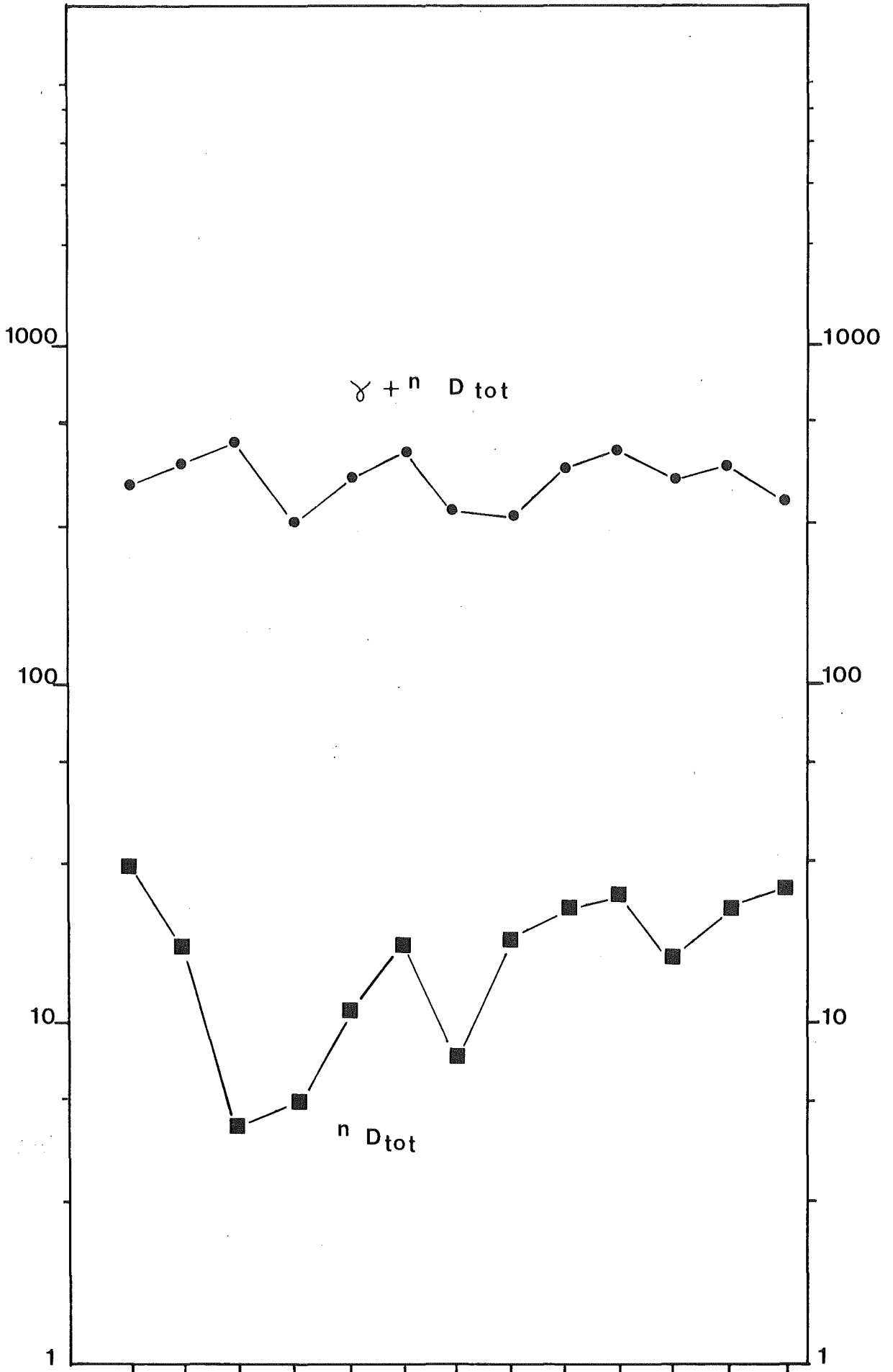


fig.4a

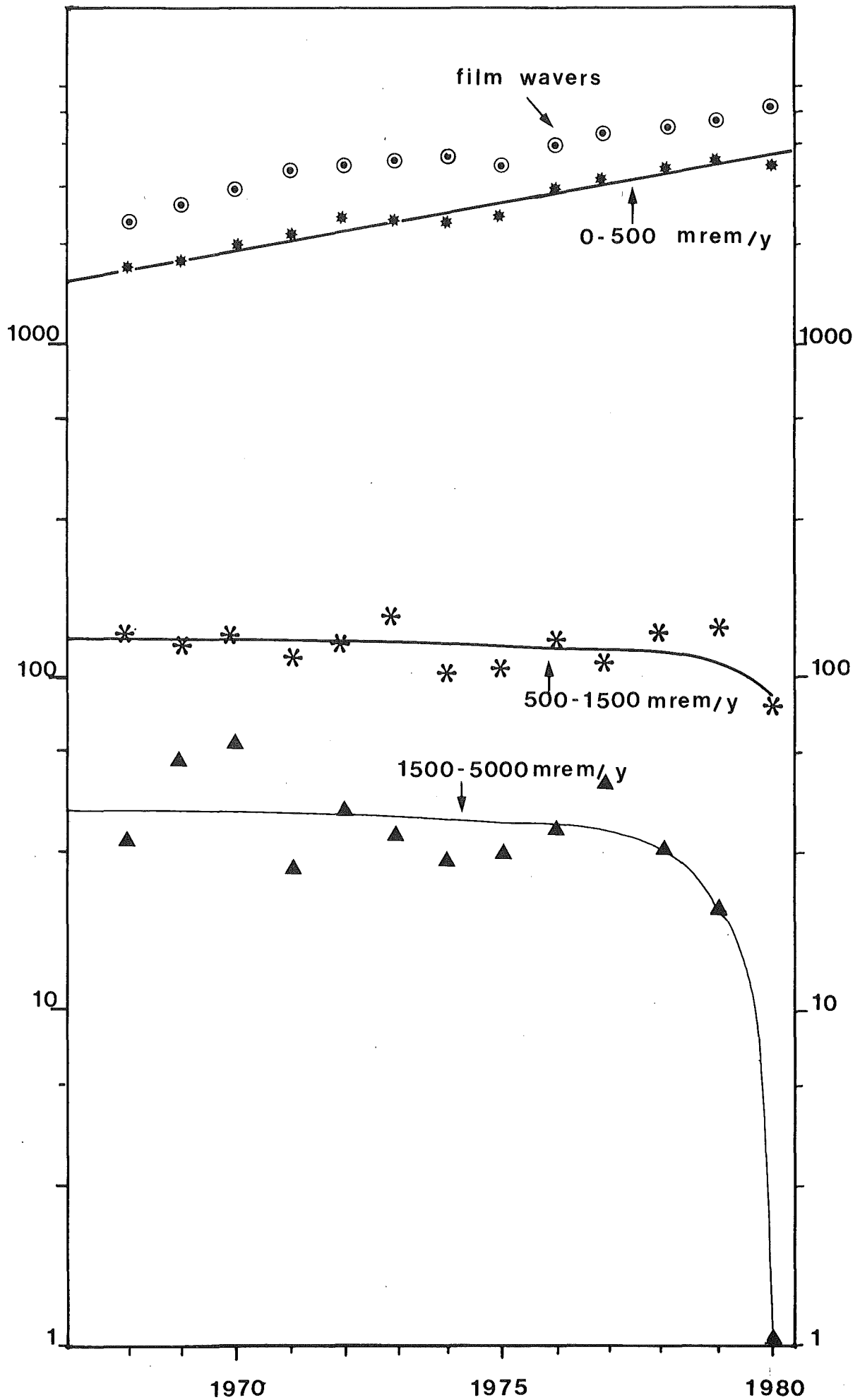


fig. 4b



## Remote Handling Systems

G.W. Köhler

Kernforschungszentrum Karlsruhe, HA Ingenieurtechnik  
Postfach 3640, D-7500 Karlsruhe, Federal Republic of Germany

### 1. Introduction

A variety of handling tasks must be fulfilled as regards mounting during the construction and commissioning phases and in connection with maintenance work. In this paper I shall deal above all with questions of remote handling since in this field in particular new problems must be solved.

Due to beam losses the accelerator structures get increasingly activated in the direction of the beam and with the period of operation getting longer. To the extent and as long as possible, the work is done by staff on the spot. The realistic upper limits of the mean beam losses are considered to be 1 % in the Alvarez accelerator (except for the first tank) and 1 ‰ in the disk-and-washer accelerator /1/. This means that after some time of operation the dose rate at contact on the tank is already as much as 100 mrem/h in the center of the Alvarez accelerator.

If one assumes 10 h per month of working time for the staff employed in the beam tunnel and ten months in total of working time per year, the mean local dose rate must not exceed 10 mrem/h in conformity with the German Radiation Protection Ordinance. Consequently, beginning approximately at the fourth tank of the Alvarez accelerator, first measures must probably be at hand to reduce the radiation impact on the personnel. Beginning in the 105 MeV zone of beam matching, remote handling within the beam tunnel will be required in most cases.

The actual dose rates occurring in the accelerator zones can be predicted within broad limits only. Regarding the expenditure in terms of work (kind and number of incidents and failures as well as duration of specific actions) only coarse estimates can be made for the time being. Therefore, a handling system and related peripherals will be provided which allow remote handling in principle. However, the option for qualitative and quantitative backfitting has been taken into account.

## 2. Handling Equipment

First of all I wish to present to you the handling equipment. Since a variety of tasks must be coped with at widely spread locations and with a relatively low frequency of recurrence and since also unforeseeable cases must be anticipated, a system was designed which consists of multi-purpose and general-purpose remote handling equipment.

Handling objects whose weights vary between many tons and less than 1 kg call for equipment having very dissimilar features.

Fig. 1 shows the remote handling system for the disk-and washer accelerator, which is actually the "backbone" of maintenance work. This system consists of four units which can be displaced on common rails:

- a tank crane of special design
- a pair of electric master-slave manipulators
- a heavy-duty power manipulator and
- a television camera unit.

The tank crane has a load carrying capacity of 30 t and two lifting and load attachment systems similar to that of the usual container cranes. When lifting large components it can automatically engage and release at four lifting heads. The spacing between the front and rear lifting systems with the associated load attachment device can be varied over a large range so that components of very differing lengths can be accommodated. The crane is equipped at its front and rear sides with one television camera each so that it can also be moved independently in a controlled manner.

The electric master-slave manipulators are capable of handling objects weighing up to 24 kg. Seven movements are possible during which the operator feels the forces applied in his hand. These manipulators are particularly suited for complicated and delicate work. Stereo television cameras are used to observe the working place; they are carried on an articulated boom.

The power manipulator has an arm which can perform six movements. Objects up to 250 kg weight can be handled and the load carrying capacity at the sholder hook is 2 t. The power manipulator serves to handle and also to transport rather heavy objects. Stereo television cameras attached on a boom are likewise used as means of observation.

The two manipulator types are supplemented by an assortment of mechanical and electric tools which are carried in magazines and fixtures.

Both manipulator types resemble very much the manipulators developed for the SNR 300 fast breeder nuclear power station.

The safe moving of the manipulators, e.g., close to the sensitive accelerator structures, calls for means of viewing the whole scene in addition. This is achieved by the independently moving television camera unit. Moreover, this unit is equipped with a grip of 2 t load carrying capacity so that it can take over also the function of a component replacement manipulator.

The manipulator units and the television unit have carrier systems equal in design, which consist of a movable bridge, a carriage, a multiple telescope and a swiveling gear. Besides, each unit is equipped with a 1 t hoist.

In all four units the power is supplied via bus bars mounted at the fixed wall of the service tunnel. The commands, information and television pictures are transmitted via radio links. A station has been provided in the high-energy assembly lock for operation of the remote handling equipment in the accelerator.

Fig. 2 shows once more the details of the twin-armed slave unit. The driving boxes are of elongated shape and can be inclined by switch control with respect to an axis on top, thus extending over the range of operation. The boom carrying the television cameras and made as a third arm allows to select the viewing angle required.

The electric master-slave manipulators operate by bilateral position control recording in an indirect manner the acting forces and torques, respectively (Fig. 3). To make the system both sturdy and sensitive, a control was designed with one circuit each for the slave and the master. Both circuits are interconnected by exchange of the position signals and by the velocity signal of the master. This structure allows to compensate for the different dead weights, frictions and moments of inertia of the two arms differing in strength in order to free the operator of avoidable load.

Fig. 4 shows the type EMSM I which is the technical basis for the development of the electric master-slave manipulators to be installed in the accelerator. The figure shows from left to right: the master arm, the control console, the television monitors and the slave unit with stereo television cameras and a variety of tools.

Fig. 5 shows the type SM5-C which would be the basis for the heavy-duty power manipulator. This equipment has the design features preferred in hot cells. It is operated by means of two levers.

To display the stereo pictures the method of polarization was chosen according to test results because it furnished the best quality of the pictures (Fig. 6). Moreover, this method can be implemented with little special auxiliary means. The monitors are arranged at right angles with respect to each other. Filters have been provided in front of the screens, which produce a polarizing effect in the vertical and horizontal directions, respectively. A semi-transparent mirror is placed diagonally between the monitors, which lets pass the image from the monitor in front of the operator and mirrors the image of the other monitor so that it can be viewed by the operator. The operator wears glasses equipped with similar polarizing filters so that his left eye sees only the picture shot with the left camera and the right eye sees only the right picture.

Fig. 7 is a schematic representation of the accelerator tunnel with its peripherals and the complete handling system. Approximately in the center the four movable system units already mentioned for the disk-and-washer accelerator have been indicated.

The rails leave the disk-and-washer accelerator and run to the left up to the front side of the Alvarez accelerator and to the right up to the end of the high-energy distribution tunnel. In this way, the system is capable of performing also work within the Alvarez accelerator (with one exception), in the zones of beam matching, 350 MeV beam deflection and beam diagnostics and (in part) in the high-energy distribution tunnel.

On account of the overhead clearance required in the Alvarez accelerator an additional 3 t crane is necessary to remove and remount the girders with the drift tubes.

In order to be able to work also in the 6 m. wide section of the high-energy distribution tunnel on the left side in the beam direction, three shorter bridges will be provided in which the carriages with the two manipulators and the television unit of the disk-and-washer system can be installed. Heavy components are conveyed by means of a 30 t crane extending over the whole high-energy distribution tunnel.

For interventions in the beam transport tunnels leading to the 350 MeV and 1100 MeV experimental halls and to the target, three bridges with little span will be provided which, if required, can be placed on the rails of one or the other tunnel. This is performed by means of the 30 t cranes of the accelerator and the high-energy distribution tunnel, respectively, and with a device provided for this purpose. The carriages with the manipulators and the television unit of the disk-and-washer system can likewise be transferred to these narrow bridges.

A system equipped with small remotely controlled manipulator units has been given preference over a movable shielded and manned cabin with manipulators because in this way the tunnel cross section can be kept much smaller (Fig. 8).

In case the radiation dose rates in the accelerator zones are not excessively high, also mobile shielding walls with radiation shielding windows and simple remote handling equipment can be conveniently used in addition as a stage half-way between work done by staff on the spot and remote operation (Fig. 9).

Another eligible means are portable remotely handled tongs with which a distance can be kept from a radiation emitting object (Fig. 10).

The use of heavier tools calls for a support, e.g., a movable frame with a ball pivot (Fig. 11).

The cranes in the accelerator zones are also used for work performed by staff on the spot and in this case they are controlled from portable operating boxes. Likewise, power manipulators can be used.

In the inspection, maintenance and repair cell of the target station mainly the conventional hot cell technique is applied (Fig. 12). Shielding windows and master-slave manipulators with mechanical power transmission are installed in the shielding walls. They are supplemented by a power manipulator with a load carrying capacity on the arm of 500 kg and a bridge crane with 25 t of load carrying capacity. In the front part of the cell which can be compartmentalized and where the power manipulator may be used as well monitoring is by television.

### 3. Passive Handling System

Remotely operated work is greatly facilitated in case specific parts of plant components are designed for remote operation capability. This is true above all for connecting elements, controls and supporting elements. Besides, components, clutches as well as gripping points for manipulators, if applicable are reasonably given a specific shape to facilitate fitting.

There should be provided in addition, e.g.:

- devices preventing that components, e.g., the ion pumps, get displaced after the connections have been removed, and which also allow to deposit the components in the course of remounting and to move them, if applicable, into their final positions.

Moreover, the working time required can be considerably shortened while handling if a number of design principles are taken into account. For Examples:

- Minimizing the number of components and assemblies as well as individual parts, respectively, from which the assemblies are made.
- Avoiding as far as possible small parts such as nuts and bolts or secure them so that they cannot get lost.

Let me quote as an example of a typical design suitable for remote handling compared to a conventional design of a pipe coupling as will be provided for ion pumps (Fig. 13).

The pipe ends are equipped with flanges with a usual metal seal in-between. Whilst a conventional flange connection, with a nominal width of 350 mm and for nominal pressures from 1 to 6 bar, requires as much as 12 bolts, nuts, washers and elements for bolt securing each, the advanced design suitable for remote handling constitutes a device with three articulated clamping jaws which are tightened or loosened by twisting one single captive (!) "screw", one thread pin with right and left thread on both halves.

To facilitate work, the variety of different electric plug-in couplings have a receptacle at the socket into which the plug is deposited and a lever by which the two parts of the couplings are subsequently fitted (Fig. 14).

#### 4. Sequence of Handling Processes

To ensure full-scope maintenance quite a number of activities must be performed within the accelerator tunnel and outside in a hot cell, respectively.

Fig. 15 shows the overall sequence of repair work with alternative sequences, their interconnection and order of succession. The alternatives are in situ repair, replacement of components, repair outside of the tunnel and provision of new components. Minor work and the adjustment of tank internals are completed on the spot. The same would be aimed at for tank-side installations and connections, which makes considerable requirements on the handling system as regards the flexibility and skillness to be realized.

To attain the highest possible plant availability, standardized components are replaced because this is by far the quickest method in case couplings and connecting elements suitable for remote handling are used.

If the repair within the tunnel fails or replacement is not feasible, the tank (or similiary large-scale magnets) would have to be withdrawn.

Let me indicate as an example of a major operation the remotely operated removal, the repair outside the tunnel and the reinstallation of a disk-and-washer twin tank. Fig. 16 is a schematical representation of the sequence of working steps.

The tank is connected by about 15 to 20 couplings for media, power supply and electrical signals with the adjacent plant components and its operating systems (Fig. 17). These couplings are to be seen in the middle of this diagram.

Fig. 18 shows the sequence of work of tank removal: first the couplings are disconnected by means of manipulators and a screwer. Then, the tank is lifted off from the V-ways anchored in the bottom of the tunnel, using the tank crane; it is then transported to the high-energy distribution tunnel through the corridor of the beam tunnel. The expenditure in terms of time is estimated at the order of only 12 h since none of the individual working steps causes any problems.

The sequences of operations and the type of work to be completed are similar for removal and reinstallation of the Alvarez tanks, the disk-and-washer single tanks, the intermediate tank sections and the magnets as well as for the replacement of ion pumps. The number of working steps to be performed are in the individual cases slightly more or also considerably less. By contrast, the girder with the drift tubes call for a markedly higher expenditure in terms of time because due to the length of sealing about 60 individual bolts have to be unfastened and tightened again.

The active components are repaired in the high-energy assembly lock (Fig. 19). There, a cell open on top of up to 14 m length can be erected from concrete blocks; it can be equipped with 2 to 10 working stations with one shielding window and one pair of mechanical master-slave manipulators each.

A number of steps are necessary to convey a tank further from the end of the disk-and-washer tunnel into the assembly lock. The tank is first taken over by the crane of the high-energy distribution tunnel, then deposited on a platform carriage which conveys it through a door opening in the shielding wall into the assembly lock; at last it is deposited in the hot cell by the crane of the assembly lock.

Remounting after repair work goes in the reverse order with an additional leakage test and tank adjustment at the end of the operations (Fig. 20).

Should there be indications that the activation has attained values no longer permitting application of the method described before, the following backfitting work is planned: Within the assembly lock a large hot cell is erected with ceiling and a new assembly lock is attached to the existing building. Moreover, shielding doors are installed so that the crane of the high-energy distribution tunnel can be moved into the hot cell.

A low-energy assembly lock is located in the front part of the Alvarez accelerator, where a crane similar to that in the high-energy assembly lock has been installed and from which the accelerator tunnel is accessible after the lids of the hatches have been withdrawn.

In the low-energy assembly lock the Alvarez tanks and their components are repaired which have suffered from little activation only. If necessary, a cell open on top can be erected similar to that in the high-energy assembly lock.

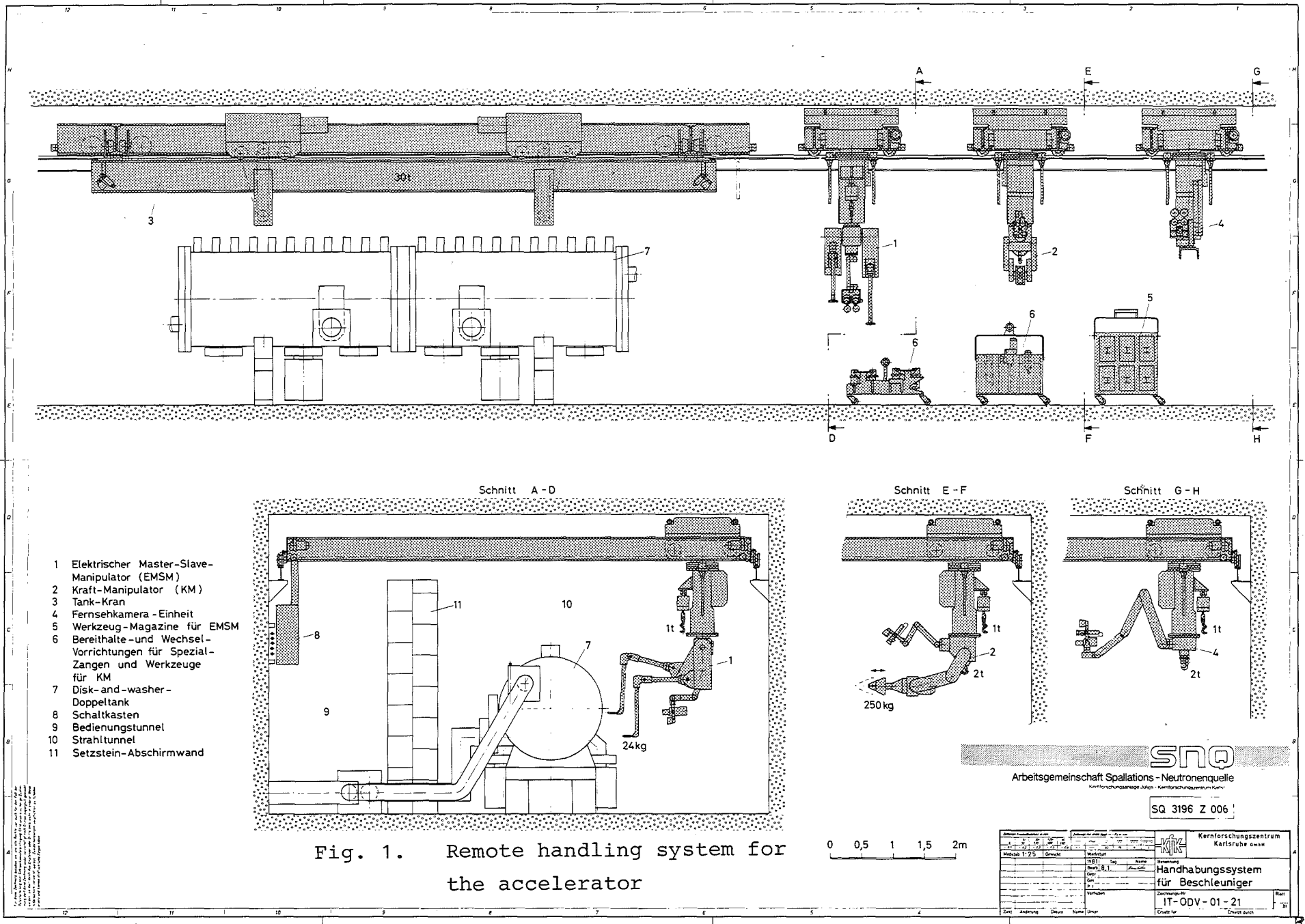
The tank crane is posted in and out from the tunnel, respectively, within the low-energy assembly lock. Quick maintenance of the movable, remote handling equipment can be performed in the zone of intervention of the high-energy distribution tunnel.

In conclusion the following statements should be made:

If the planned multi-purpose remote handling system will be realized and in addition the components will be so designed that they are suitable for remote handling, and if good possibilities of access to the active zones and possibilities of adjustment will be provided, maintenance of the accelerator can be guaranteed.

#### Reference

- /1/ K. Goebel  
Problems of radiation protection operating a high current linear accelerator; 2. activation of the accelerator structures, private communication



- 1 Elektrischer Master-Slave-Manipulator (EMSM)
- 2 Kraft-Manipulator (KM)
- 3 Tank-Kran
- 4 Fernsehkamera - Einheit
- 5 Werkzeug - Magazine für EMSM
- 6 Bereithalte- und Wechsel-Vorrichtungen für Spezial-Zangen und Werkzeuge für KM
- 7 Disk- and -washer- Doppeltank
- 8 Schaltkasten
- 9 Bedienungstunnel
- 10 Strahlentunnel
- 11 Setzstein-Abschirmwand

Fig. 1. Remote handling system for the accelerator

0 0,5 1 1,5 2m

**SNO**  
 Arbeitsgemeinschaft Spallations - Neutronenquelle  
Kernforschungsanlage Jülich - Kernforschungszentrum Karlsruhe g.w.m.b.H.

SQ 3196 Z 006

Abmessungen: 1.25m x 1.25m Gewicht: 8.1t		Hersteller: IRT Baujahr: 1981		Kernforschungszentrum Karlsruhe g.w.m.b.H.	
Zeichnungs-Nr.: IT-ODV-01-21				Blatt: 1/1	
Zeichnungs-Nr.: IT-ODV-01-21		Blatt: 1/1		Gezeichnet durch:	

# Electric Master-Slave Manipulator EMSM

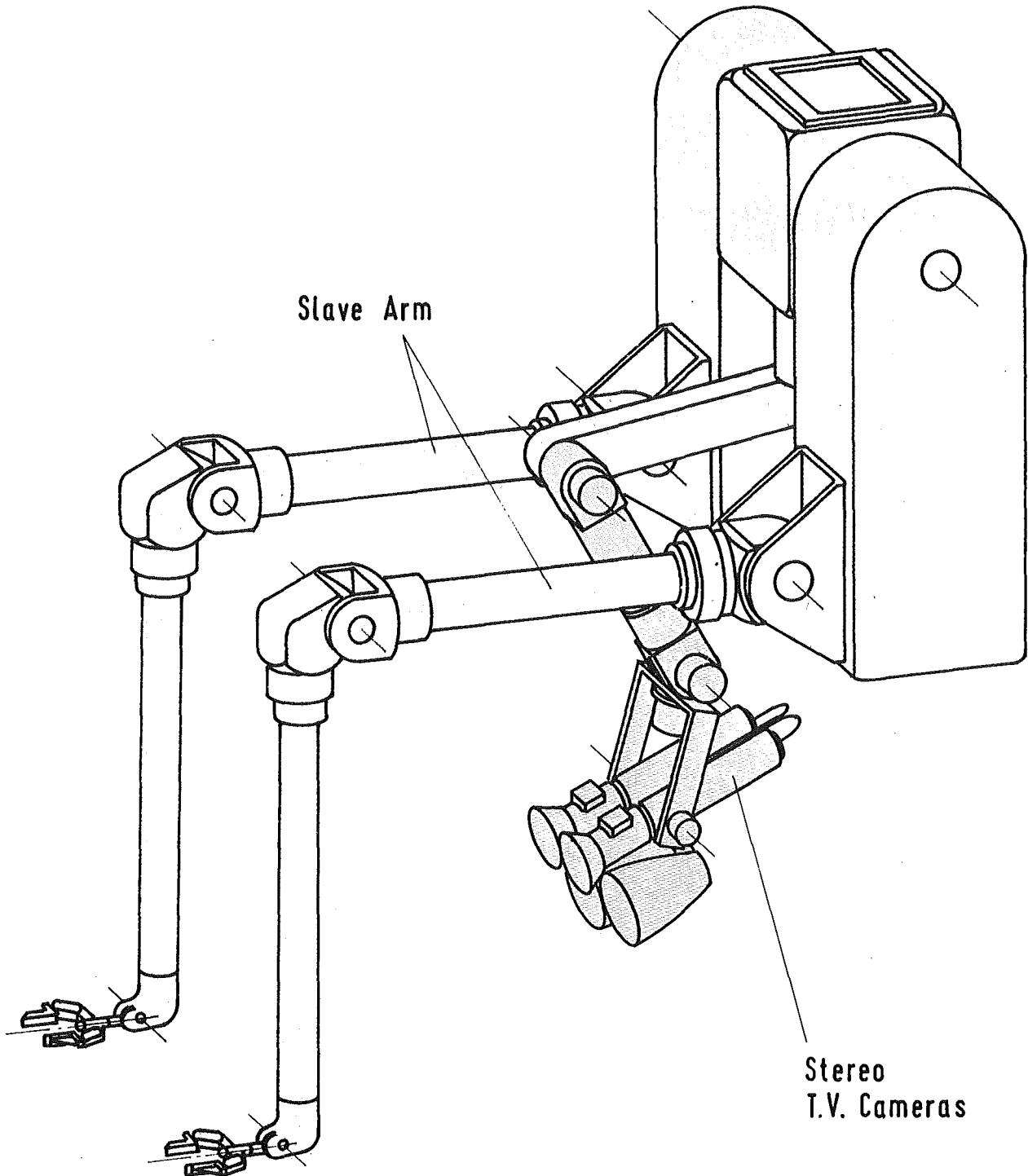


Fig. 2

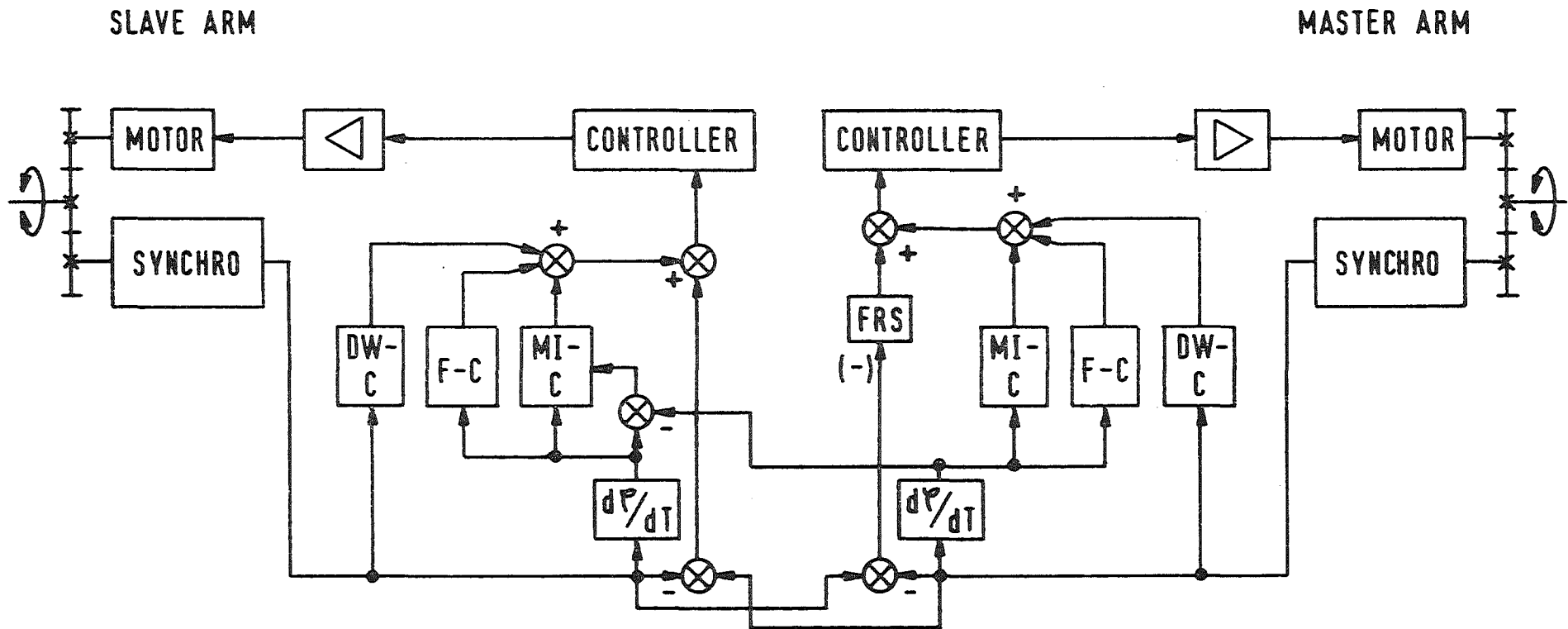


Fig.3. BILATERAL SERVO SYSTEM WITH TWO-CIRCUIT POSITION CONTROL WITH COMPENSATIONS, FOR ELECTRIC MASTER-SLAVE MANIPULATOR

DW = DEAD WEIGHT  
 F = FRICTION  
 MI = MASS INERTIA

C = COMPENSATION  
 FRS = MASTER TO SLAVE  
 FORCE RATIO SELECTOR

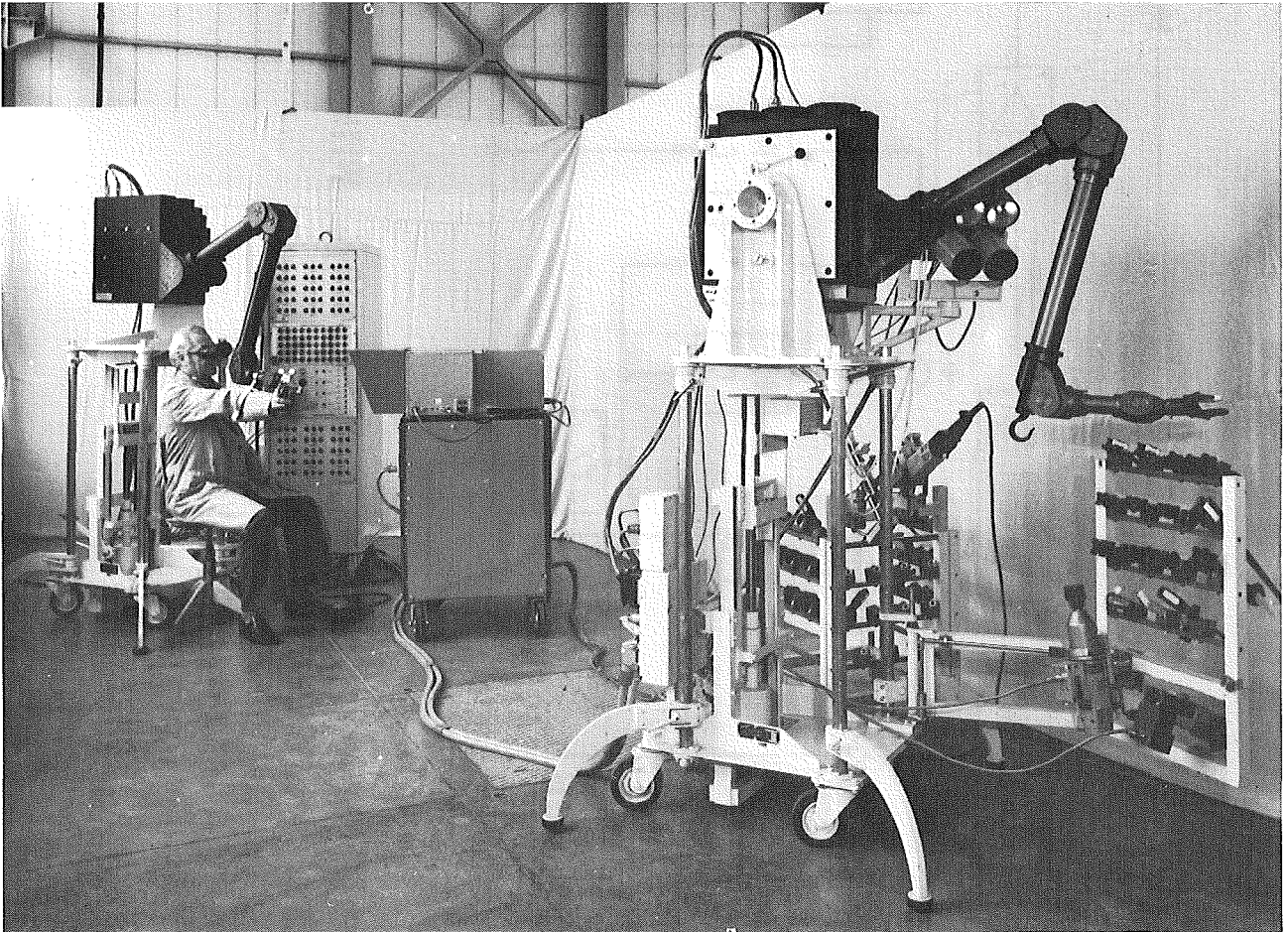


Fig. 4 EMSM 1 Electric Master-Slave Manipulator,  
Handling Capacity 25 kg, 9 Motions

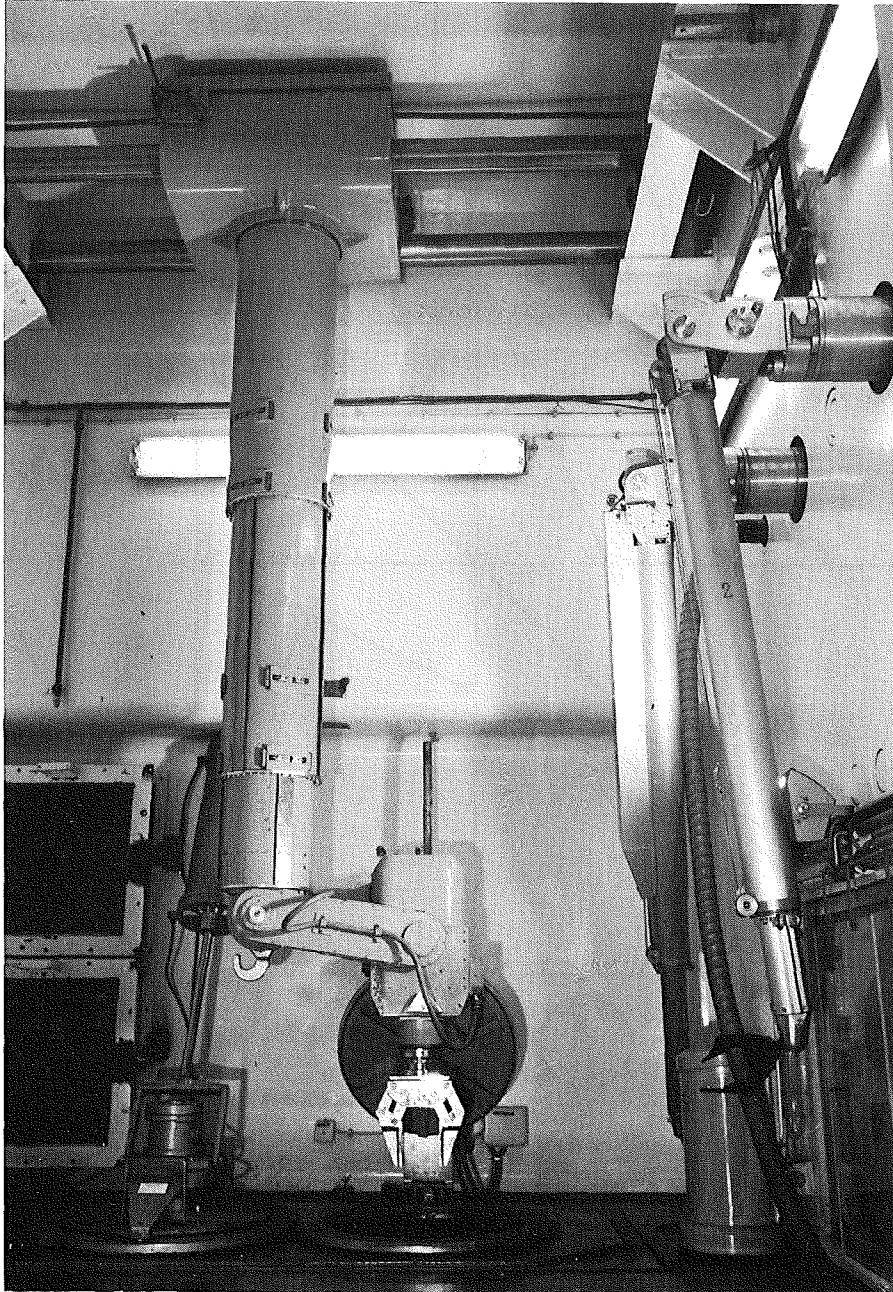


Fig. 5 SM5-C Power Manipulator,  
Handling Capacity 300 kg,  
Lifting Capacity on the Hook 2000 kg,  
8 Motions

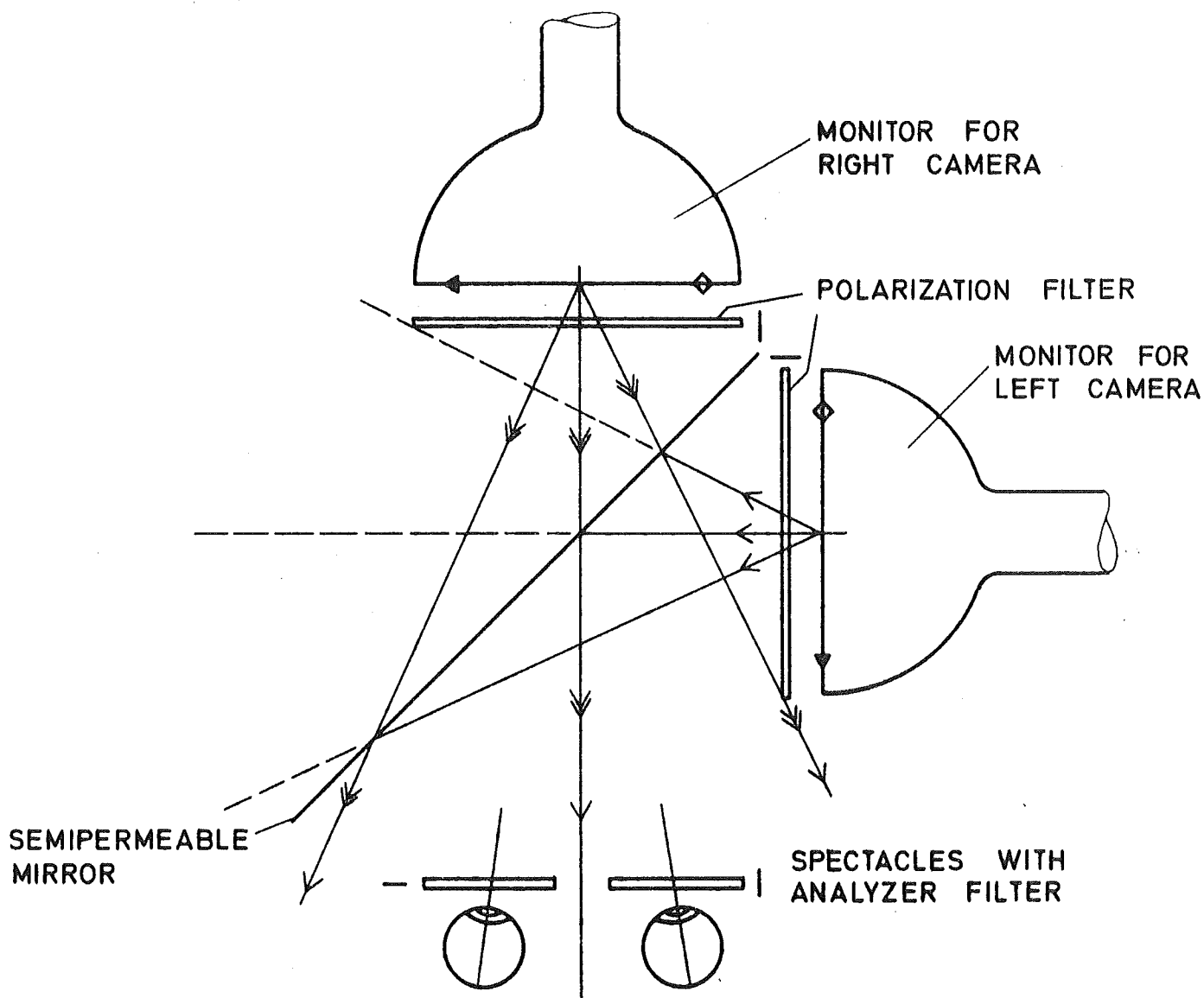
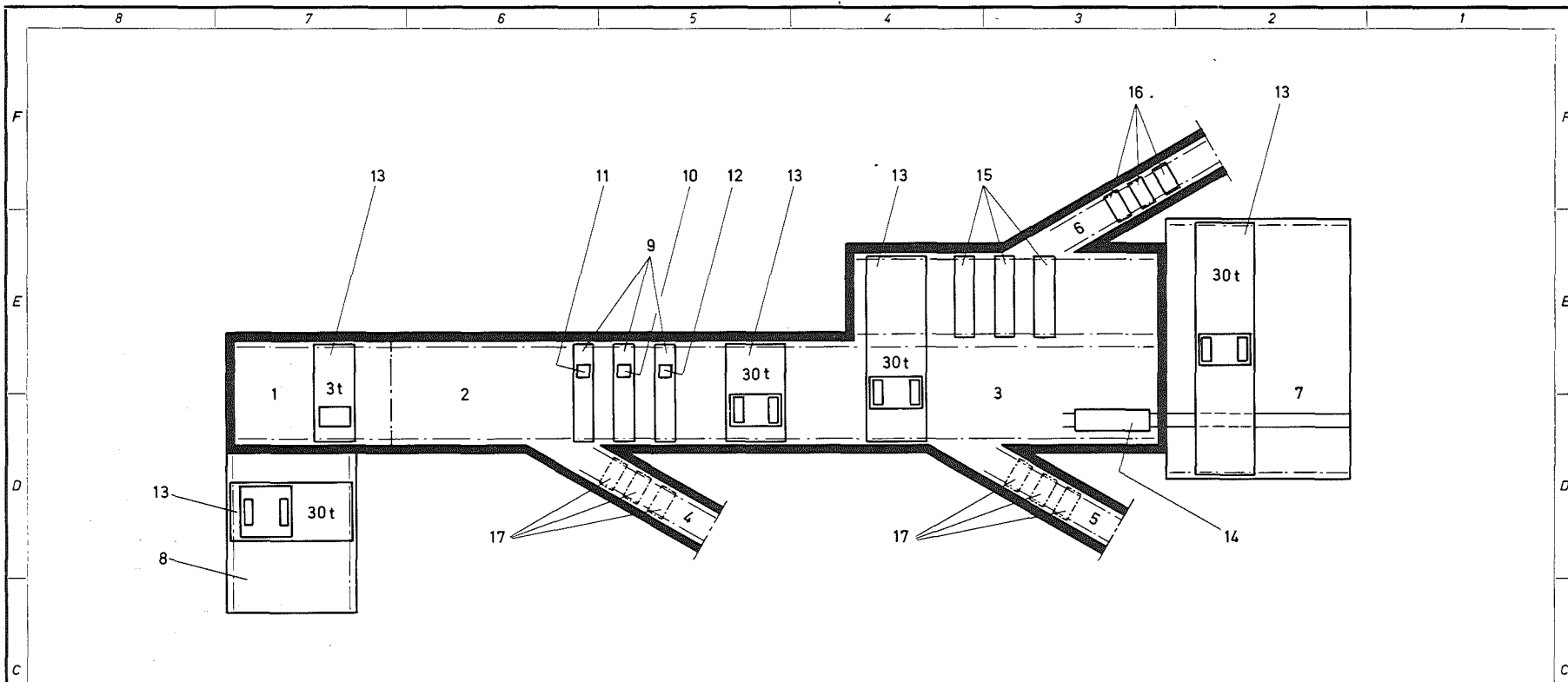


Fig. 6. Viewing equipment for stereo television



- |  |   |
|--|---|
| 1 Alvarez-Beschleuniger                                | 9 3 Brücken mit 7,5 m Spannweite                              |
| 2 Disk-and-washer-Beschleuniger                        | 10 1 Paar Elektrische Master-Slave-Manipulatoren              |
| 3 Hochenergie-Verteilungstunnel                        |   |
| 4 Strahlführungstunnel zur 350 MeV-Experimentierhalle  | 11 Schwerer Kraft-Manipulator                                 |
| 5 Strahlführungstunnel zur 1100 MeV-Experimentierhalle | 12 Fernsehkamera-Einheit und Komponentenaustausch-Manipulator |
| 6 Strahlführungstunnel zum Target                      | 13 Kran   |
| 7 Hochenergie-Montageschleuse                          | 14 Wagen  |
| 8 Niederenergie-Montageschleuse                        | 15 3 Brücken mit 5,5 m Spannweite, Nr. 10 bis 12 aufsetzbar   |
|  | 16 3 Brücken mit 2,7 m Spannweite, Nr. 10 bis 12 aufsetzbar   |
|  | 17 Nr. 16 einsetzbar  |



Arbeitsgemeinschaft Spallations - Neutronenquelle  
Kernforschungsanlage Jülich - Kernforschungszentrum Karlsruhe

SQ 3196 Z 008

Fig. 7. Scheme of the handling system in the accelerator

Teil	Stück	Benennung	Werkstoff	Abmessung	Zeichngs. Nr. Norm	Bemerkung				
Oberflächenzeichen	~	□	□	□	□	□				
Rauhtiefe max. in H	1000	40	10	4	1,6					
				Freiabtoleranz	bis 6 bis 30	über 30 bis 120	über 120 bis 400	über 400 bis 1000	über 1000 bis 2000	
					- 0,1	- 0,2	0,3	- 0,5	- 0,8	- 1,2
1981	Tag	Name	Werkstoff	Kernforschungszentrum Karlsruhe GmbH Postfach 36 40 7500 Karlsruhe 1		Zugeh. Zeichng.				
gez.	B.1.	%				Ersatz für				
gepr.						Ersatz durch				
ges.						Zeichnungs Nr.				
Maßstab	Benennung Schema					Handhabungssystem für Beschleuniger	IT-ODV-01-23			

Paßmaß	Abmaß
--------	-------

Buchstabe	Kommt vor	Änderung	Tag	Name
-----------	-----------	----------	-----	------

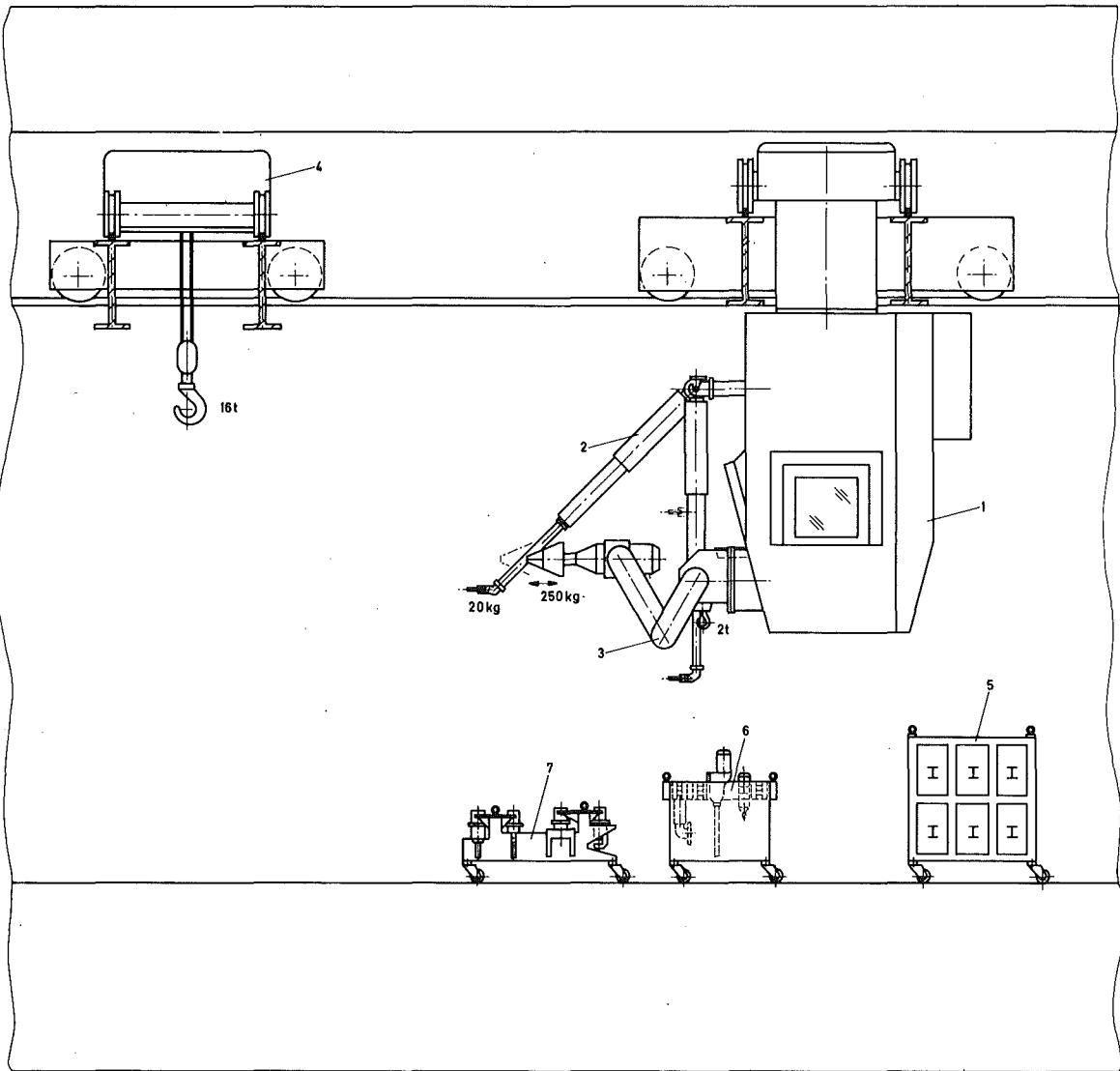


Fig. 8. Movable shielded and manned cabin  
with manipulators

- 1 Abgeschirmte Kabine
- 2 Mechanischer Master-Slave-Manipulator (mMSM)
- 3 Kraft-Manipulator (KM)
- 4 Kran
- 5 Werkzeug-Magazine für mMSM
- 6 Bereithalte-Vorrichtung für Elektrowerkzeuge für KM
- 7 Wechsellvorrichtung für Spezial-Zangen und mechanische Werkzeuge für KM

Die hier beschriebene Vorrichtung ist ein Modell für die Entwicklung einer mobilen, abgeschirmten und besetzten Kabine mit Manipulatoren. Die Kabine ist für die Aufnahme von zwei Personen vorgesehen. Die Manipulatoren sind für die Handhabung von schweren Lasten geeignet. Die Vorrichtung ist für die Verwendung in der Atomenergie vorgesehen.

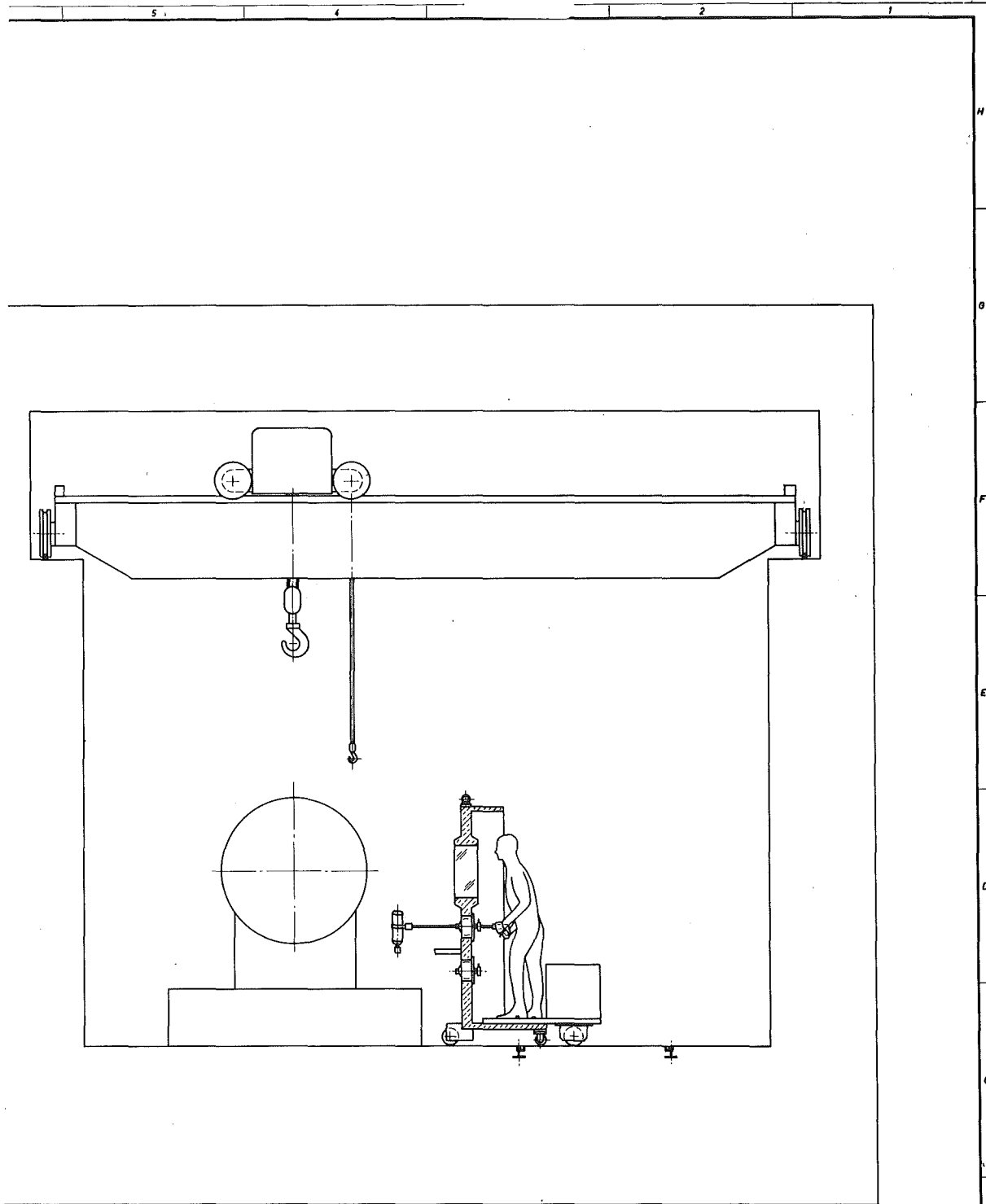


Fig. 9. Mobile shielding wall with shielding window and simple remote handling equipment

Mit auf dem Boden selbstfahrender Abschirmwand

Ref	Stück	Dimension					Werkstoff	Abmessung		Zulassung: Hi Norm					Bemerkung		
Übermaßabweichung	~	□	▽	▽▽	▽▽▽	▽▽▽▽	Fräseblech	± 0,1	± 0,2	± 0,3	± 0,4	± 0,5	± 0,6	± 0,7	± 0,8	± 0,9	± 1,0
Positiv max. in $\mu$	300	60	70	1	1,8												
1378	1	Name		Werkstoff			Gesellschaft für Kernforschung in G.H.		Zugab. Zeich.								
gr.	15.11.	[Signature]					7500 Karlsruhe		Erstellt für								
gr.							Postfach 3640		Erstellt durch								
Maßstab	1:25	Benennung Manipulier-System für Beschleuniger-Tunnel					Version 4		Zulassung Nr.					IT-ODV-01-4			

Bezeichnung	Änderung	gr.	Name



Fig. 10 Portable Remotely Handled Tong

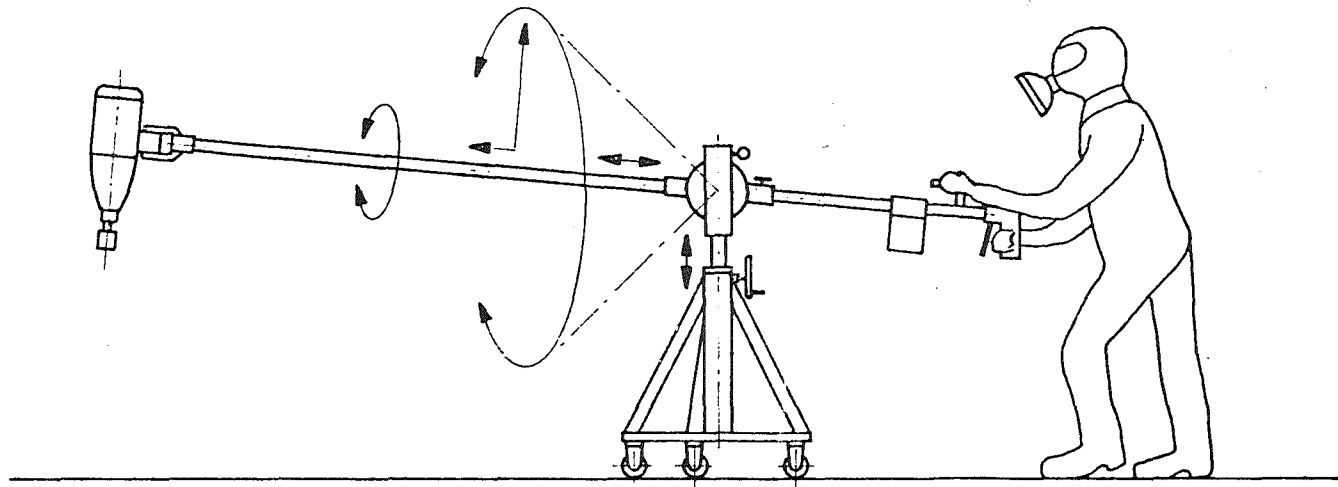
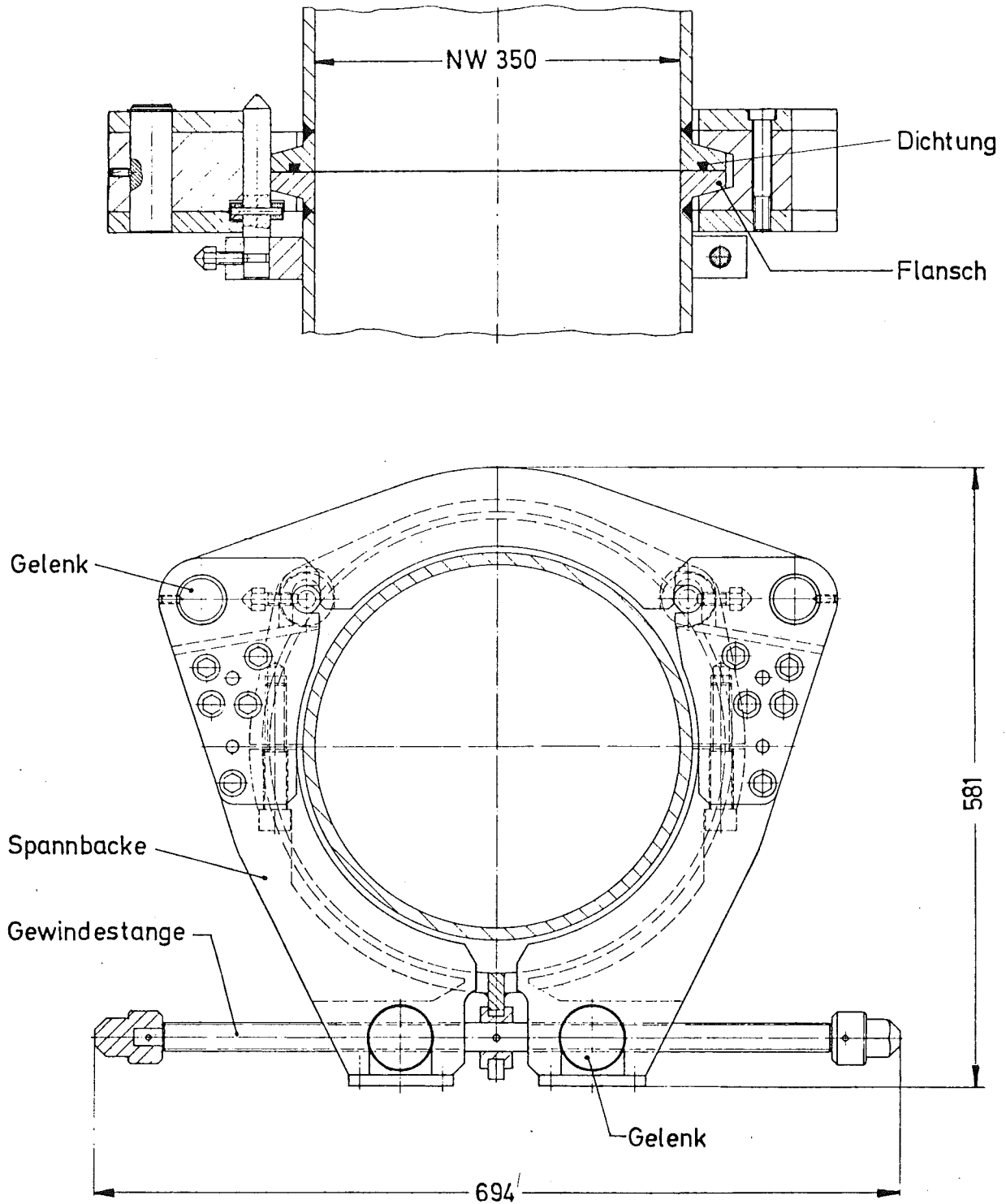


Fig. 11. Supported remotely handled tool  
(e.g. an impact wrench)



Fig. 12 Operating Area of a Hot Cell Plant,  
with Slave Arms of Mechanical Master-Slave  
Manipulators and Shielding Windows  
Installed in Concrete Shielding Walls



SNQ

Arbeitsgemeinschaft Spallation - Neutronenquelle Kernforschungsanlage Jülich - Kernforschungszentrum Karlsruhe

Fig. 13. Pipe coupling for ion pumps of the accelerator tanks, suitable for remote handling

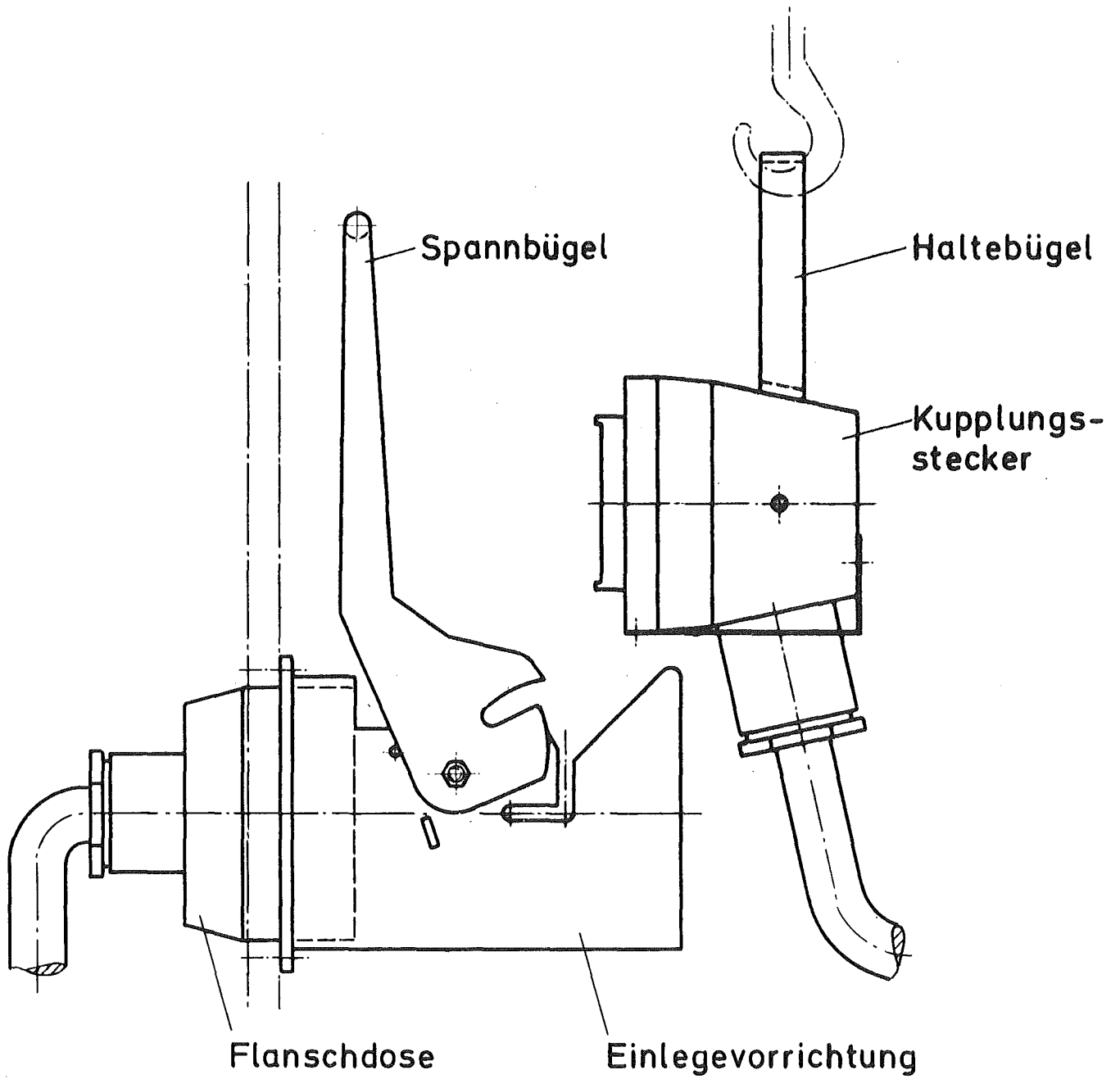


Fig. 14. Electric plug-in coupling, suitable for remote handling

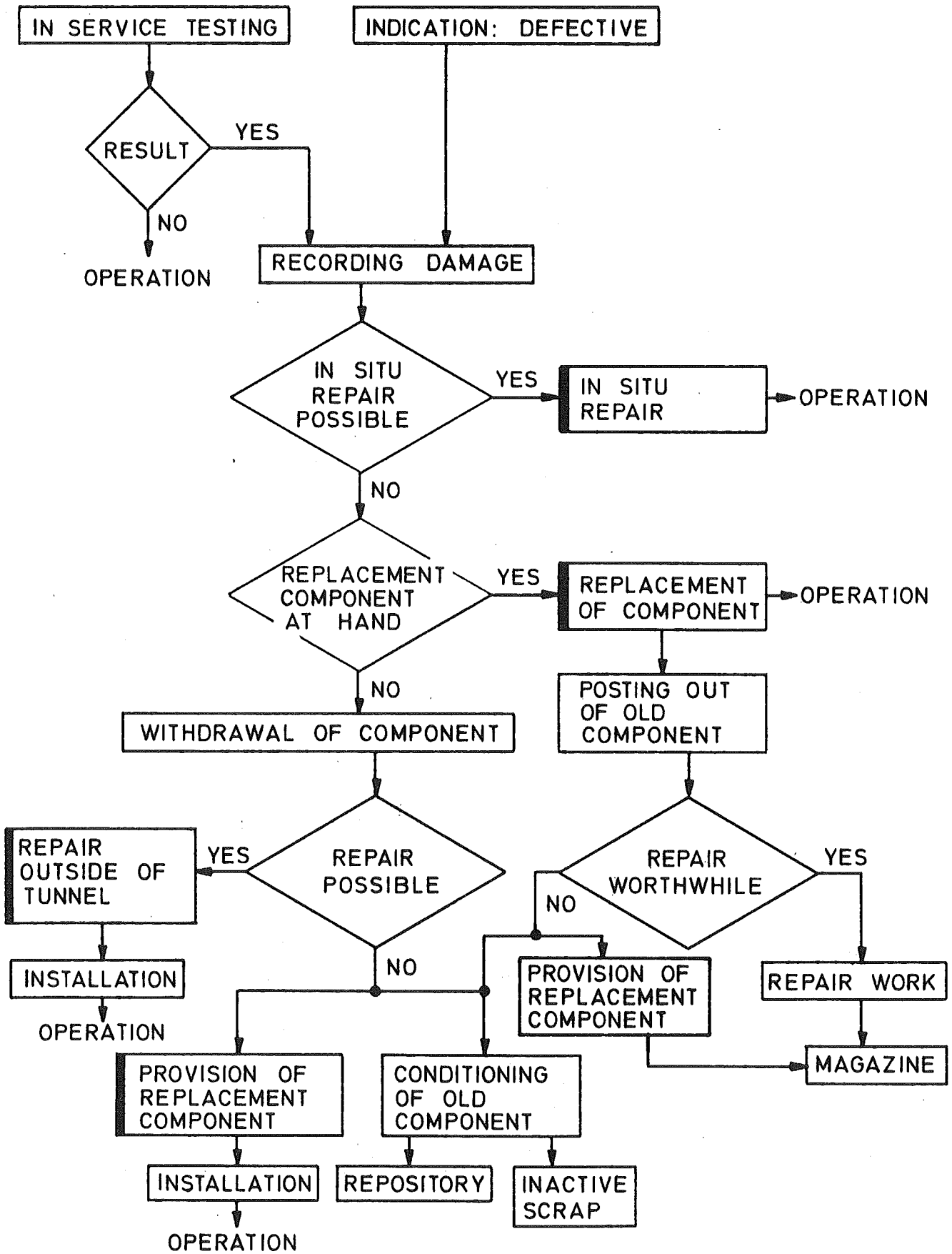


Fig.15. Flow diagram and alternatives of repair.

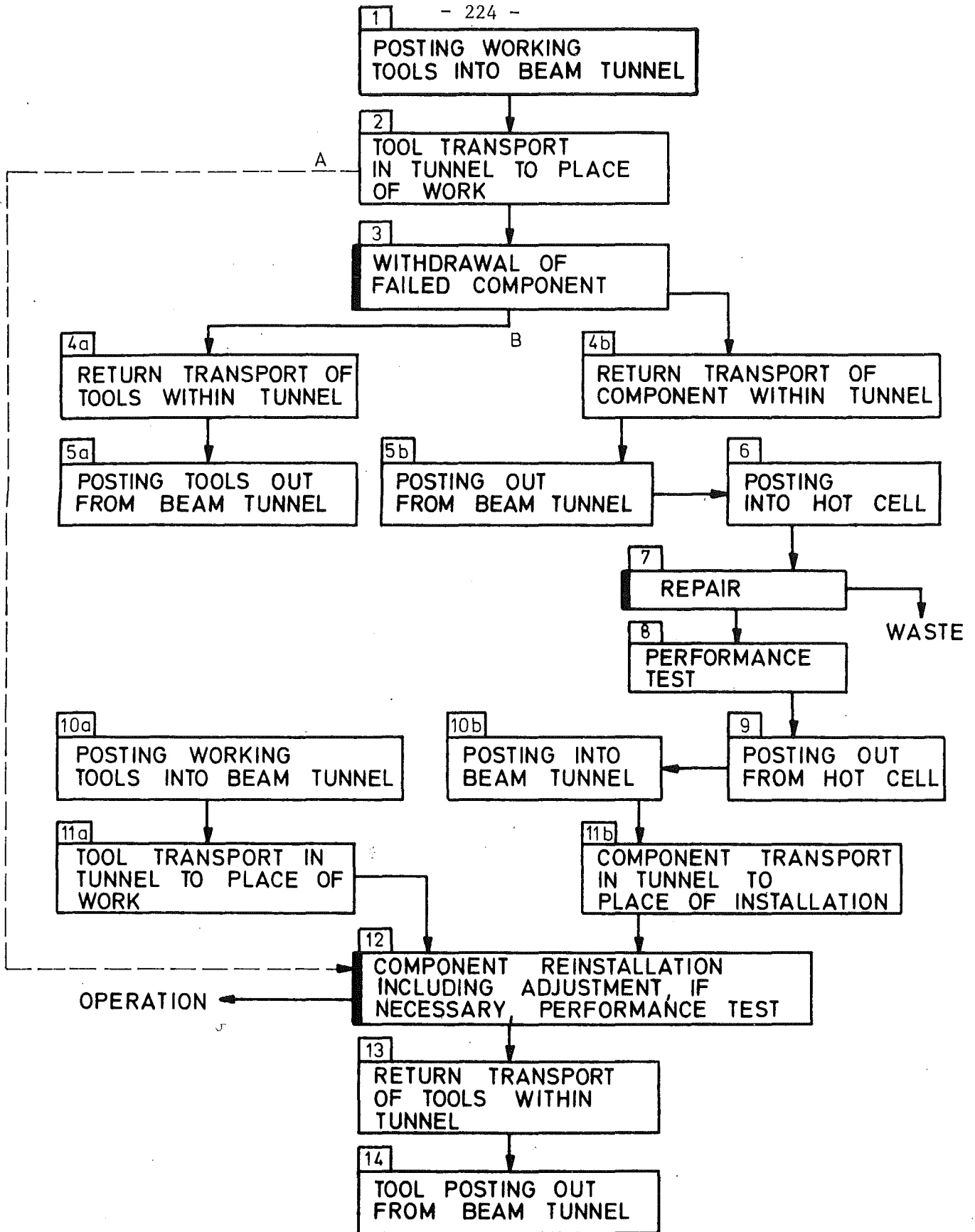


Fig.16. Basic flow diagram of repair work on withdrawn components

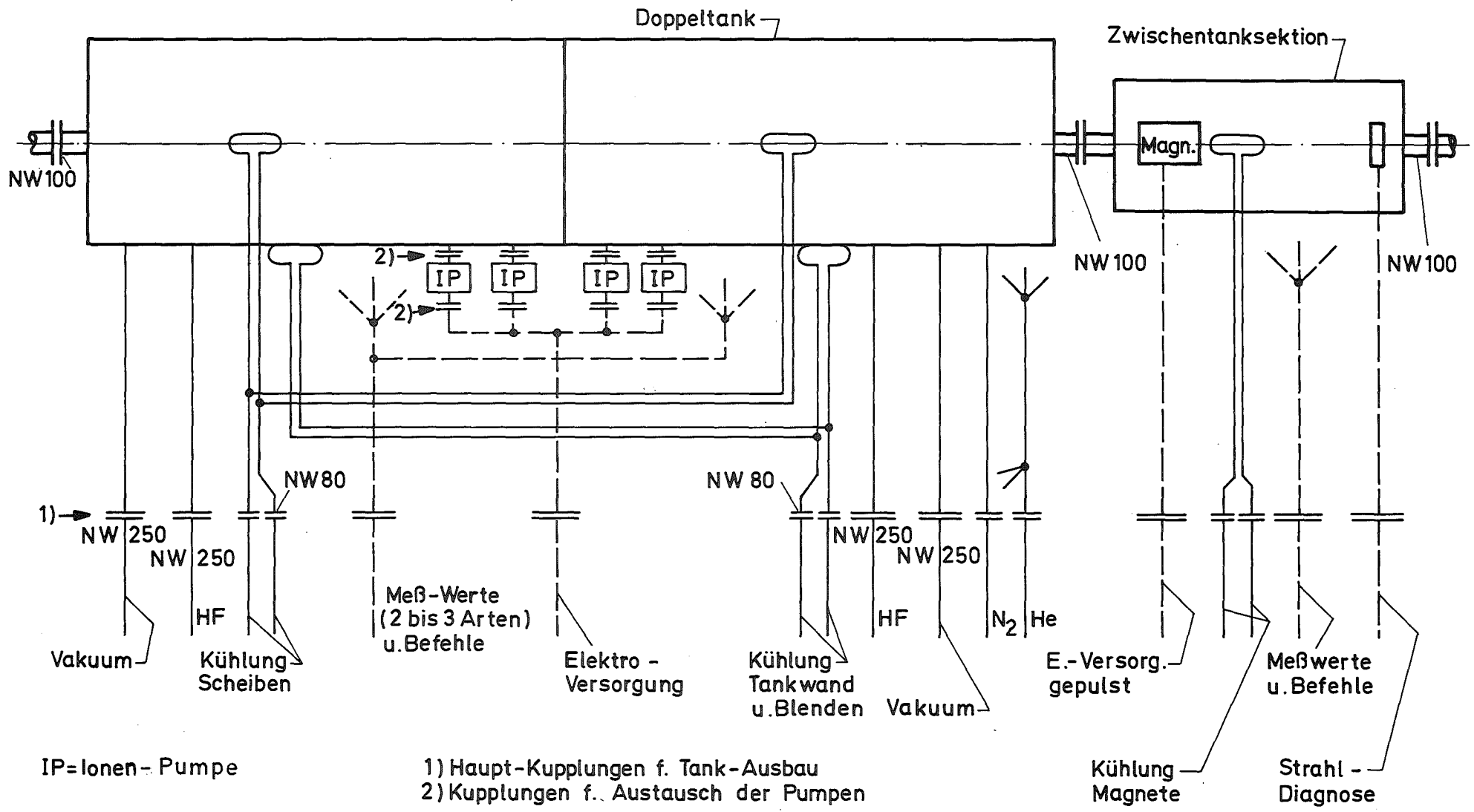
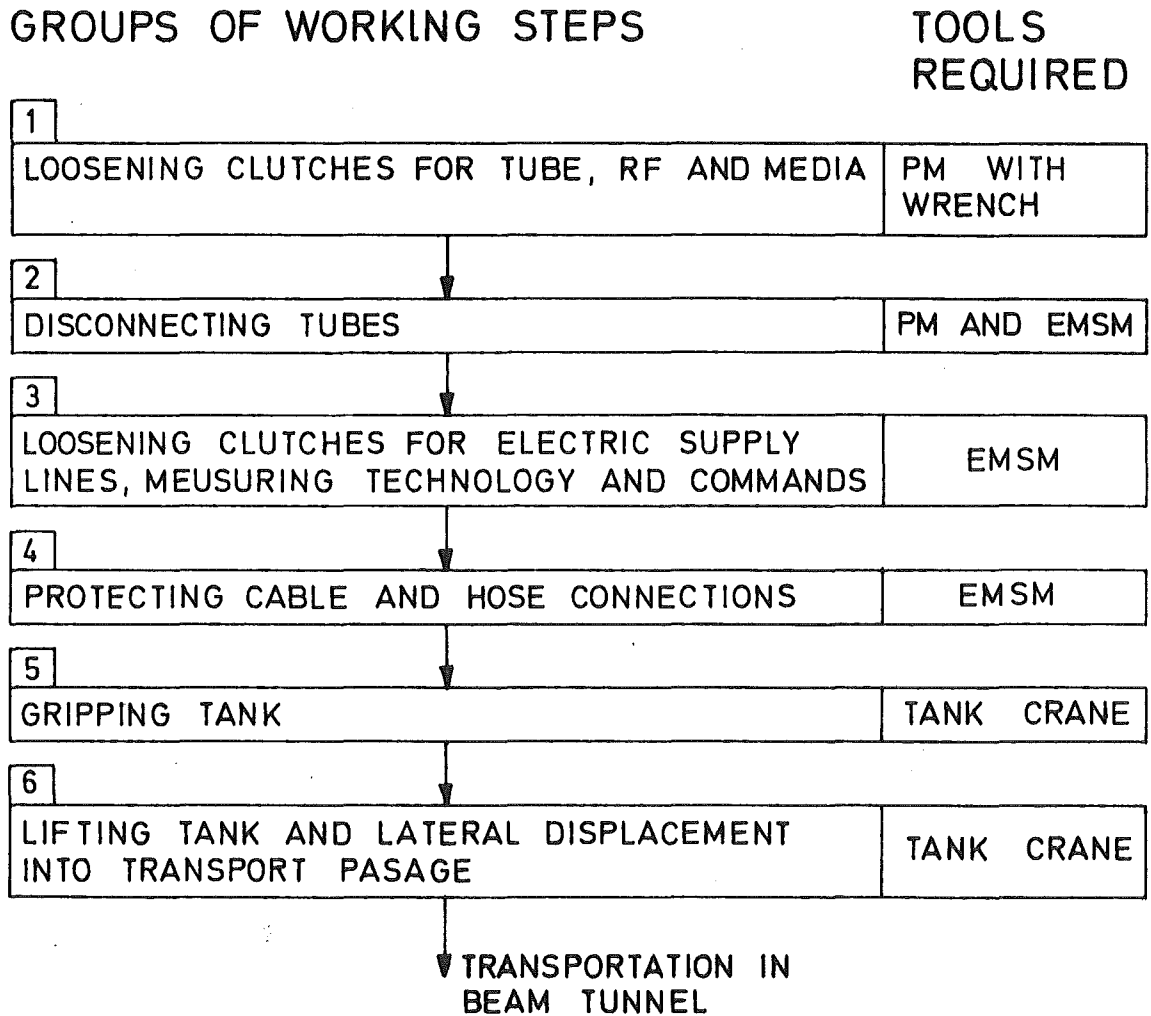


Fig. 17. Disk-and-washer accelerator, coupling diagram

### INITIAL CONDITION

ACCELERATOR SHUT DOWN, SECTION ACCOMODATING FAULTY TANK ISOLATED, TANK FLOODED WITH N<sub>2</sub>, WORKING TOOLS, DISPLAY UNITS AND AUXILIARIES IN PLACE



PM = Power Manipulator

EMSM = Electric Master - Slave Manipulator

Fig.18. Sequence of tank removal  
(Alvarez, D+W double tank and D+W single tank).

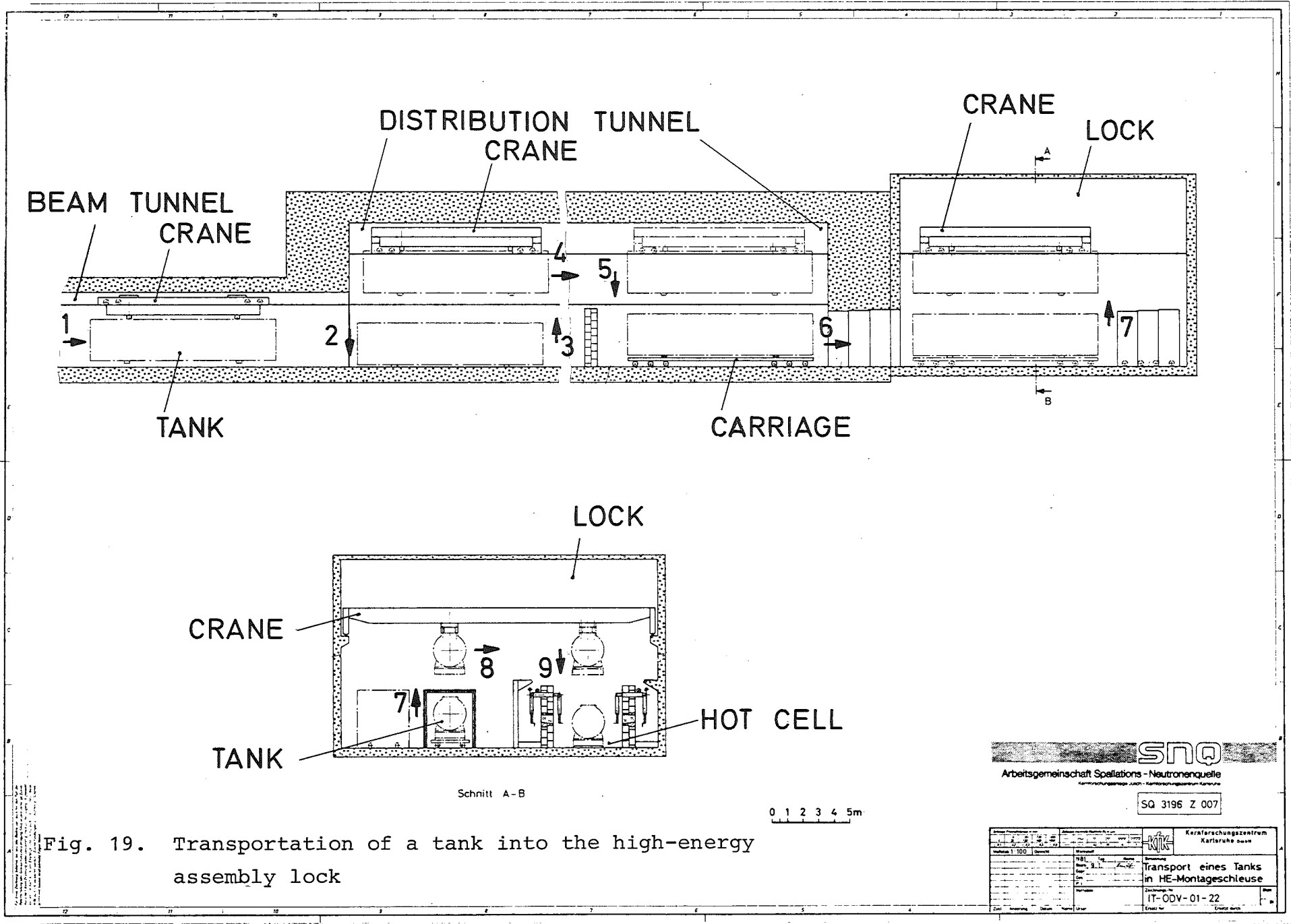


Fig. 19. Transportation of a tank into the high-energy assembly lock

**SNQ**  
 Arbeitsgemeinschaft Spallations - Neutronenquelle  
 Kernforschungszentrum Jülich - Kernforschungszentrum Karlsruhe

SQ 3196 Z 007

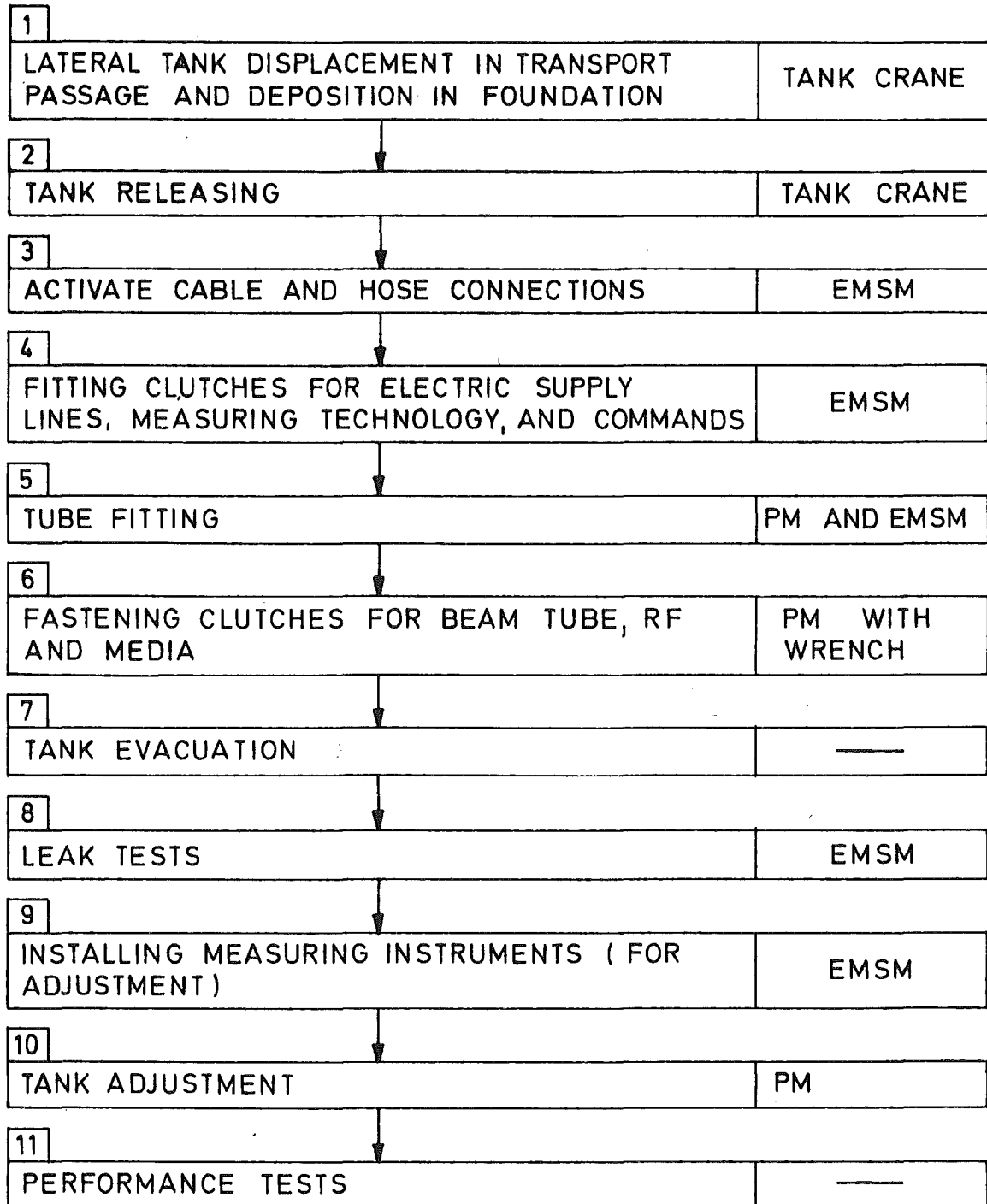
Kernforschungszentrum Karlsruhe 6900	
Maßstab 1:100 Blatt 11 Datum 11.11.72 Zeichnung Nr. IT-ODV-01-22 Ersteller	Beschreibung <b>Transport eines Tanks in HE-Montageschleuse</b> Blatt 11

INITIAL CONDITION

WORKING TOOLS, DISPLAY UNITS AND AUXILIARIES IN PLACE,  
REPAIRED TANK TRANSPORTED TO PLACE OF INSTALLATION

GROUPS OF WORKING STEPS

TOOLS  
REQUIRED



PM = Power Manipulator      OPERATION  
EMSM = Electric Master-Slave Manipulator



Fig. 20. Sequence of Tank Remounting  
( Alvarez, D+W double tank and D+W single tank ).

Appendix: Papers from the poster session

Self Field Effects on the Beam in Storage Rings

K. Mika, L. Stanco\*, V.G. Vaccaro\*\*, G. Wüstefeld

KFA Jülich, W.-Germany

Abstract

A high intensity beam (protons) moving in a storage ring creates sizable fields which act back on the particles. The influence of these self and mirror fields, excluding any additional RF fields, is taken into account to discuss the changing of a linear charge distribution. We describe the spatial deforming of the bunch in a first order approximation by a differential equation which is independent of any ring parameter. By a simple scaling law we can apply the solution to special ring dimensions. For a parabolic charge distribution we found an analytical solution for the time- and position-dependence of the charge density  $\lambda(z,t)$  and of the particle momentum  $\Delta p/p(z,t)$ .

\* Guest scientist from the University Padua, Italy

\*\* University Napoli, Italy

Theory

The longitudinal particle distribution is given by the line density  $\lambda(z,t)$ . The z-coordinate-system is defined in the longitudinal direction and moves with the particle bunch. We define  $z = 0$  at the center of the bunch.

For the line density we can apply the one dimensional continuity equation

$$\frac{\partial \lambda}{\partial t} = - \frac{\partial}{\partial z} (\lambda v_z) ,$$

where the relative particle velocity  $v_z$  is given as

$$v_z = \frac{dz}{dt} = \Delta \omega R_o = \beta_o c \eta \frac{\Delta p}{p_o} .$$

As usual,  $\omega$  is the angular frequency, R is the radial position and  $\eta$  is defined by

$$\frac{\Delta \omega}{\omega_o} = \eta \frac{\Delta p}{p_o} .$$

The index o indicates parameters which are related to particles with zero momentum deviation ( $\Delta p = 0$ ).

The effects of the electric self- and mirror-fields on the particles are described via the particle momentum. The change of the momentum is given (/1/, /2/) as

$$\frac{\partial}{\partial t} \frac{\Delta p}{p_o} = - \frac{2Xc^2}{k\pi\beta_o\gamma_o^3} \frac{\partial \lambda}{\partial z} , \tag{1}$$

where X is the reactance of a perfectly conducting wall and  $k = 4 m_o c^2/e = 4 \cdot 0.938 \cdot 10^9$  V (for protons).

This relation holds as long as the characteristic bunch length  $\ell$  is large compared to the radius of the ring chamber ( $\ell^2 \gg b^2/\gamma^2$ ,  $\gamma$  is the relativistic energy parameter of the particles and b is the radius of the chamber).

By using the fundamental relation

$$\frac{\overline{\Delta R}}{R_o} = \alpha \frac{\Delta p}{p_o}$$

and approximating the reactance by

$$X = X_o [1 - \left(\frac{\overline{\Delta R}}{b}\right)^2]$$

we are able to integrate equation (1) which gives

$$\frac{\Delta p}{p_0} = \frac{-b}{R_0 \alpha} \tanh \left[ \frac{R_0 A \alpha}{b} \frac{\partial}{\partial z} \int \rho dt \right]$$

with

$$A = \frac{2X_0 c^2 Q}{k\pi\beta_0 \gamma_0^3} .$$

Here we separated the charge density  $\lambda$  in the total charge  $Q$  and a density function with the relation

$$\int \lambda dz = Q \int \rho dz = Q .$$

Introducing  $\Gamma(z, t)$  by

$$\Gamma(z, t) = \int_0^t \rho(z, t') dt' ,$$

we have  $\rho(z, t) = \partial\Gamma / \partial t$ , and finally for the continuity equation

$$\frac{\partial^2 \Gamma}{\partial t^2} = \frac{\partial}{\partial z} \left\{ \frac{\partial \Gamma}{\partial t} \beta_0 c \frac{b\eta}{R_0 \alpha} \tanh \left[ \frac{R_0 A \alpha}{b} \frac{\partial \Gamma}{\partial z} \right] \right\}$$

By scaling  $z$ ,  $\Gamma$  and  $t$  in

$$z = \bar{z} z_0$$

$$\Gamma = \bar{\Gamma} \frac{bz_0}{R_0 A \alpha}$$

$$t = \bar{t} \frac{R_0 z_0 \alpha}{b\beta_0 c\eta}$$

where  $2z_0$  is the initial bunch length,  
it is possible to simplify this equation:

$$\frac{\partial^2 \bar{\Gamma}}{\partial \bar{t}^2} = \frac{\partial}{\partial \bar{z}} \left\{ \frac{\partial \bar{\Gamma}}{\partial \bar{t}} \tanh \frac{\partial \bar{\Gamma}}{\partial \bar{z}} \right\} .$$

The relation between the scaled variables and the momentum and the density is given as

$$\rho(z,t) = \frac{b^2 \beta_o c \eta}{R_o^2 A \alpha^2} \frac{\partial \bar{\Gamma}}{\partial \bar{t}}$$

$$\frac{\Delta p}{p_o}(z,t) = \frac{-b}{\alpha R_o} \tanh \frac{\partial \bar{\Gamma}}{\partial \bar{z}}$$

To summarize, we can say, to the first order approximation the bunching or respectively the debunching of the particle cloud follows a scaling law, where the scaled equation is independent of any special ring parameter.

A further mathematical description of the differential equation will be given in /3/.

Examples:

1. A parabolic density distribution

We choose a further approximation ( $\tanh \frac{\partial \bar{\Gamma}}{\partial \bar{z}} \approx \frac{\partial \bar{\Gamma}}{\partial \bar{z}}$ ) which is acceptable for  $\frac{b/2}{R_o} \gg \alpha \frac{\Delta p}{p_o}$  and solve the new equation

$$\frac{\partial^2 \bar{\Gamma}}{\partial \bar{t}^2} = \frac{\partial}{\partial \bar{z}} \left( \frac{\partial \bar{\Gamma}}{\partial \bar{z}} \frac{\partial \bar{\Gamma}}{\partial \bar{t}} \right)$$

for an initial parabolic density distribution (and  $\frac{\partial \bar{\Gamma}}{\partial \bar{z}}(z,t=0)=0$ )

$$\rho(z,t=0) = \frac{3}{4z_o} \left[ 1 - \left( \frac{z}{z_o} \right)^2 \right], \quad |z| \leq z_o$$

The function

$$\bar{\Gamma}(\bar{z}, \bar{t}) = T_1 - T_2 \bar{z}^2, \quad \left( \frac{\partial \bar{\Gamma}}{\partial \bar{t}} \geq 0 \right)$$

with 
$$T_1 = \int_0^{T_2} (1 - 3 T^2 / T_o)^{-\frac{2}{3}} dT$$

$$T_2 = \sqrt{T_o/3} \tanh \bar{t} \sqrt{3T_o}$$

$$T_o = \frac{3}{4z_o} \frac{R_o^2 \alpha^2 A}{b^2 \beta_o c \eta}$$

satisfies the differential equation and the initial conditions.

For the density and the momentum follows then:

$$\rho(z,t) = \frac{\partial \Gamma}{\partial t} = \frac{3}{4z_0} \left[ \cosh \frac{2}{3} \tau - \left( \frac{z/z_0}{\cosh \tau} \right)^2 \right],$$

$$\frac{\Delta p}{p}(z,t) = -A \frac{\partial \Gamma}{\partial z} = \frac{2b}{R_0 \alpha} \sqrt{T_0/3} \frac{z}{z_0} \tanh \tau$$

with

$$\tau = \frac{3}{2} t \sqrt{\frac{A\beta_0 c \eta}{z_0^3}}$$

## 2. A Gaussian density distribution:

A numerical calculation of the equation

$$\frac{\partial^2 \bar{\Gamma}}{\partial \bar{t}^2} = \frac{\partial}{\partial \bar{z}} \left( \frac{\partial \bar{\Gamma}}{\partial \bar{t}} \frac{\partial \bar{\Gamma}}{\partial \bar{z}} \right)$$

with a computer program for the density distribution as an initial condition

$$\rho(z,t=0) = \frac{1}{\sqrt{2\pi}z_0} \exp \left[ -\frac{1}{2} \left( \frac{z}{z_0} \right)^2 \right]$$

gives a development of the density distribution as shown in fig. 1. Different from the parabolic case, we have here a build up of a shock wave ( $\frac{\partial \rho}{\partial z} \rightarrow \infty$ ) at  $\bar{t} \approx 4.7$ .

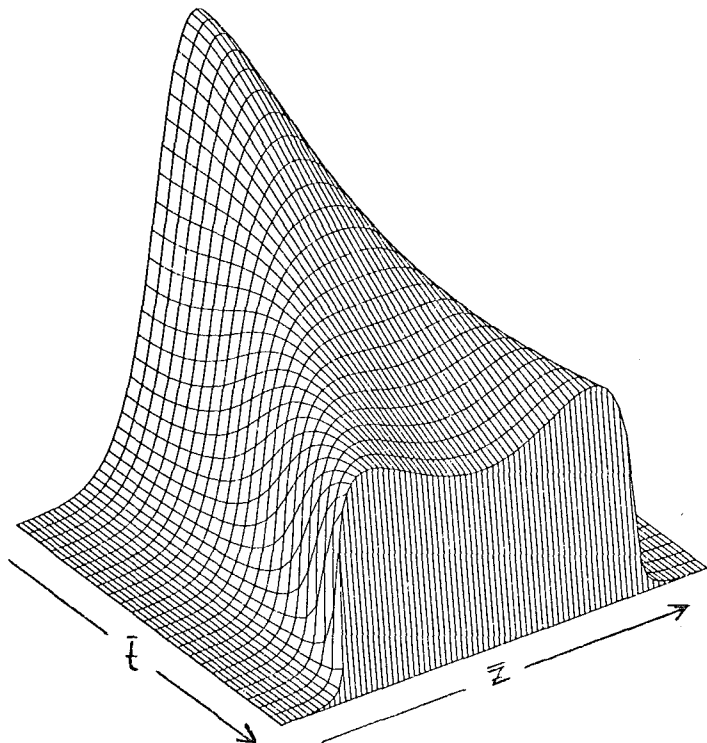


Fig. 1:

Development of a shock-wave in a Gaussian distribution. The calculation stops at  $t=4.6$ . The figure shows the density  $\rho=\rho(z,t)$ .

Final Comment:

A sufficient spread in the angular velocity, which should be compared with the longitudinal electric field induced by the charge cloud, may damp the discussed effect. However, this effect is still ignored at the present level of calculation. By this reason the theory pointed out here is of special interest if we work close to transition energy with a high intensity beam.

References:

- /1/ Blewett, M.H. (Editor), Johnsen, K., Zichichi, A.; "Theoretical aspects of the behaviour of beams in accelerators and storage rings", private communication
- /2/ L. Palumbo, V. Vaccaro, G. Wüstefeld; "Coherent space charge phenomena", SNQ project study, private communication
- /3/ K. Mika et al., to be published

## PRESENT STATUS OF THE RUTHERFORD AND APPLETON LABORATORIES' H<sup>-</sup> ION SOURCE

P. E. Gear and R. Sidlow  
Science and Engineering Research Council, Rutherford and Appleton Laboratories,  
Chilton, Didcot, Oxon, UK.

### ABSTRACT

A surface conversion ion source of the Penning type is being developed at the Rutherford and Appleton Laboratories for use with the pulsed spallation neutron source (SNS) currently under construction. The ion source is required to deliver 40 mA of H<sup>-</sup> ions at a duty factor of 2½% (50 Hz x 500 μsec). At the present time 30 mA of H<sup>-</sup> ions have been extracted with the source operating at a duty factor of 2.1%.

### INTRODUCTION

The Rutherford and Appleton Laboratories are currently building a high intensity pulsed spallation neutron source (SNS). Neutrons will be produced by bombarding a heavy metal target with protons accelerated to 800 MeV by a synchrotron pulsing at 50 Hz. An accelerated beam intensity of  $2.7 \times 10^{13}$  protons per pulse is required in order to produce the required neutron flux of  $4 \times 10^{16}$  neutrons sec<sup>-1</sup>. This corresponds, at the injection energy of 70 MeV, to a circulating current of 2.9 A. To accumulate such a large current H<sup>-</sup> stripping injection will be used. This method of charge exchange at injection by using stripping foils removes the acceptance limitation of normal multiturn injection. The accumulated beam is then limited only by space charge and instability effects in the magnet ring.

Ion sources capable of producing many tens or hundreds of mA of H<sup>-</sup> ions have, during the past decade, undergone considerable improvement with the development of the surface conversion sources. These sources operate with a mixture of hydrogen gas and caesium vapour, the H<sup>-</sup> ions being formed predominantly at caesiated surfaces when bombarded with positive ions and neutrals from a hydrogen discharge. The mechanism for H<sup>-</sup> production is discussed by Hiskes and Schneider<sup>1)</sup>.

A surface conversion source is at present in operation at Fermi National Accelerator Laboratory producing 40-50 mA of H<sup>-</sup> ions for acceleration in the linac and charge exchange in the booster. The duty factor is of the order of 0.1%<sup>2)</sup>. The requirement for a 40 mA H<sup>-</sup> ion source of 2½% duty factor therefore represents a significant advance on present H<sup>-</sup> sources used for particle accelerators.

## SOURCE ASSEMBLY

The overall ion source assembly, shown in Fig 1, consists of a removable discharge chamber and extractor assembly with a sector magnet and cold box assembly permanently attached to the main flange. Details of these and of the test rig have been described elsewhere<sup>3)</sup>.

Under normal operation it is expected that approximately 60 A of pulsed arc current at about 100 V with a resulting mean discharge power of approximately 150 W will be required to produce 40 mA of H<sup>-</sup> ions. It has been shown<sup>4)</sup>, that the ratio of cathode to anode power is approximately 2 at a discharge voltage of 100 V. Hence of the order of 100 W of discharge power flows into the cathode. The method of cooling the cathode, described earlier, by heat transference across a mica insulator, was found to be insufficient to keep the cathode temperature below approximately 600°C, desirable in preventing localised low voltage discharges, when operating with power inputs above approximately 75 W. It has therefore been replaced by a "cold finger" consisting of a metallised alumina ring to which is brazed a copper disc. This cold finger is clamped to the base plate on assembly of the source components, Fig 2. A silicon 'O' ring, which will withstand temperatures of 200°C, is used to provide the necessary vacuum seal. The coolant, either air or water, is passed via small bore pipework across the underside of the copper disc. Other modifications made to the source box include large radii on edges and corners close to the extractor and cold box, which is at extraction potential, and the removal of the caesium inlet support pipe. This pipe was thought to block up periodically and prevent the proper flow of caesium vapour into the source. The heated caesium transfer line is now inserted directly into the source box via a small ceramic bead which prevents excessive cooling of the end of the transfer line by the source box.

## ELECTRONICS

There have been some changes in the source electronics described previously<sup>3)</sup>. The pulsed arc power supply has been replaced by a 200 V, 100 A unit with a much faster rise time, 10 μsec compared with the earlier 50 μsec. In order to stabilise the flow of hydrogen into the source a servo system has been developed utilising a pressure gauge, the PV-10 pulse gas valve and a Veeco APC-100 pressure controller. A bistable pulse generator, controlled by the APC-100, varies the voltage pulse amplitude to the valve and hence varies its throughput. Pulse width is controlled manually.

The biggest change has been to the extraction power supply. Previously the extraction potential had been provided by a 30 kV, 5 mA dc power supply charging a 0.5  $\mu$ F capacitor via a 100 k $\Omega$  resistor. However, achieving the desired extraction potential of 18 kV had proved difficult during source operation due to a discharge, seen as a pale blue glow, occurring in the extraction gap and running between the magnet pole tips. This discharge would give a drain current  $> 4$  mA at a few kV sufficient to trip off the supply. It was initially thought to be due to a Penning type discharge, with favourable conditions for such a discharge being set up by the shape of the magnetic and electric field lines. Attempts were made, by the use of shields and plates, to change the shape of the electric field lines and eliminate the discharge. This was not successful. Another possible explanation, was that electrons emerged from the arc and travelled along the magnetic field lines to the pole tips ionising the residual gas. An attempt was made to reduce this electron flow by moving the arc discharge volume away from the anode slit plate. To be extracted, electrons have to pass down a longer extraction canal in the anode. This canal acts as an electron (and  $H^-$  ion) filter and so a reduction in the parasitic discharge was expected. This was not entirely successful, the loading on the dc extraction supply still being too great for the necessary extraction voltage to be attained. This discharge has been seen by other workers using this type of source. It has been overcome in the main by the use of a pulsed extraction power supply which is more able to handle the additional pulsed drain current.

A pulsed extraction power supply using a 25 kV, 100 joule capacitor charging unit, charging a 0.1  $\mu$ F capacitor, followed by a series regulating valve (Eimac 4PR 1000 pulse beam tetrode) was built. The requirement was to be able to operate at a potential of 18 kV with a stability of 0.3% (approximately 50 V) and to be capable of providing of the order of 200 mA per 500  $\mu$ sec pulse at 50 Hz. It was found however that the parasitic discharge, which only occurs when the arc pulse is on, plus loadings due to  $H^-$  ion current, electron current and a 100 mA bleed in the power supply for feedback purposes was of the order of 300 mA. The extractor could not therefore be operated at 50 Hz. Hence with most of the results described later the extraction power supply was only operated every third arc pulse. Used in this way the power supply was able to maintain the required potential.

Plans are well underway to increase the size of the capacitor charging unit to 600 joules and to increase the capacitor to 0.6  $\mu$ F. This will enable the power supply to handle well in excess of 500 mA of total drain current during each pulse.

## OPERATION

The arc power supply is in two parts, a 700 V, 2 A dc supply for the high impedance mode and the pulse supply for normal use in the low impedance caesium mode. A typical run up of the source is as follows:- using the dc power supply and with hydrogen gas flowing via the pulse valve, an arc is struck at approximately 400 V. There is usually some internal arcing with a new or cleaned source which can last up to 15 minutes. After this discharge cleaning process a low current discharge is obtained at approximately 650 V, the corresponding time average current being of the order of 30-40 mA. The indicated time average pressure is usually between  $3 - 6 \times 10^{-4}$  torr. This is measured in the volume around the source and gives an indication of hydrogen gas flow. When the anode and cathode temperatures have reached about 200°C the caesium transfer line is heated to 300°C followed by switching on of the caesium boiler to a temperature between 205-215°C. Evidence of caesium flowing into the source is seen by a fall in arc impedance to approximately 400  $\Omega$ , which occurs between  $\frac{1}{2}$  to 1 hour after caesium boiler switch on. The pulsed power supply is switched on at this point and there is a transition period where both power supplies run together. When the arc impedance has fallen to approximately 1.5  $\Omega$  pulsed currents of up to 100 A can be drawn and it is sometimes possible to switch the dc power supply off. It is usually necessary to "assist" the source impedance to fall to its correct operating impedance. This is normally done by reducing the gas pressure suddenly by a factor of 3 or 4. Other adjustments include manipulation of the dc arc current level, which will change cathode temperature, as it is found that the impedance is more likely to fall if the cathode temperature is rising. It is difficult to quantify such adjustments as each run up can be different and hands-on operation at this stage is essential. It is possible to see a reflection of the arc discharge and it has been found that a deep reddish glow between extractor and anode slit gives a better indication of "correct" source operation than simply monitoring the arc pulse waveforms.

There is often some degradation of the first 50-100  $\mu$ sec of arc pulse waveforms, visible as hash. It often appears if attempts at reducing, for example, gas pressure are made too soon after correct running has been achieved. This degradation is also seen on the H<sup>-</sup> ion beam. It can be reduced but not eliminated by a slight reduction in magnetic field.

Up to the earlier part of this year it had been usual to condition the extractor to 18 kV after correct source operation had been achieved. This would sometimes

take several hours. Recently, however, the extractor has been conditioned before the source has been run up, the extractor then being left at 18 kV during the run up period. This method has proved very successful, with very little extractor source breakdown being observed and on occasions no sign of the parasitic discharge.

It has been found possible on several occasions to restart an ion source discharge after the source assembly has cooled down to ambient temperatures. On one such occasion, over a weekend, the source was cold for almost 60 hrs. On all occasions the caesium boiler, which is at present not switched off by the loss of the arc discharge, remained on and hence caesium vapour continued to flow into the source assembly.

## RESULTS

For ease of source handling and to simulate conditions that will apply on installation into the accelerator column, all source components on the test rig were at ground potential. The magnet/cold box assembly, collector and all diagnostic equipment were therefore at extraction potential with all currents being detected by toroidal isolating transformers in the high voltage feeds.

In the most successful (highest duty factor and  $H^-$  output) run to date a temporary cold finger was used to cool the cathode. With an arc current of 55 A a 30 mA  $H^-$  ion beam was extracted, this at a time average pressure of  $4.5 \times 10^{-5}$  torr. The duty factor was 2.1% (50 Hz x 420  $\mu$ sec). The output was pressure dependent, at  $5.7 \times 10^{-5}$  torr the  $H^-$  ion output fell to 21 mA. Cooling of the cathode via the cold finger was very successful and it was found possible to use compressed air as the coolant. A needle valve was used to control the flow of air and gave some control over the cathode temperature. Unfortunately this cold finger developed a vacuum leak after the run described above which proved impossible to repair. While waiting for further such cold fingers to be manufactured a number of successful runs were made by reverting to the use of cathode cooling via the mica disc. During these runs the extractor was held at extraction potential during the source run up period. No problems in holding off extraction volts were encountered and  $H^-$  ion beam was seen as soon as the arc impedance was low enough for an arc pulse to be obtained. Due to inefficient cooling via the mica disc the power into the source was halved by reducing the repetition rate to 25 Hz. Figure 3 shows an  $H^-$  pulse of 33 mA and the accompanying extractor pulse, due to electrons, negative ions of other species and incorrectly focussed  $H^-$  ions, of approximately 120 mA. The pulse width is 500  $\mu$ sec and the arc current is 45 A. Degradation of the first

100  $\mu\text{sec}$  is evident and is due to hash on the arc pulse over this period. The ratio of  $\text{H}^-$  ion current to arc current  $I_{\text{H}^-} \text{ A} / I_{\text{arc}} \text{ A} = 0.73 \times 10^{-3}$ . No higher value than  $0.75 \times 10^{-3}$  has been seen.

Typical source operating parameters for a 30 mA beam (using cold finger):

Repetition rate	50 Hz
Arc pulse width	420 $\mu\text{sec}$
Arc voltage	80 V
Arc current	55 A
Arc power (mean)	92.5 W
Cathode temperature	575-625 $^{\circ}\text{C}$
Anode temperature	450-500 $^{\circ}\text{C}$
Source magnetic field	$\sim 0.18 \text{ T}$
Bending magnetic field	0.24 T
Extraction voltage	18 kV
Caesium boiler temperature	210 $^{\circ}\text{C}$
Extracted $\text{H}^-$ current density (for 30 mA)	0.6 $\text{A cm}^{-2}$
* $\text{H}_2$ gas flow at 50 Hz	0.17 $\text{TLS}^{-1}$
*(estimated from knowledge of pumping speeds and pressure changes)	

### $\text{H}^-$ BEAM EMITTANCE

The method used to measure the extracted beam emittance consists of stopping the  $\text{H}^-$  beam on a thin plate which has a series of thin parallel slits 0.2 mm wide and 2.0 mm apart. The beam after passing through the slits impinges after a short distance on sensitive copy paper which gives a visible image after exposure to the beam. The copy paper is on a roller so that several emittance measurements can be carried out without breaking the vacuum. The position of a particular slit on the plate gives the transverse co-ordinate on the emittance diagram and the width of the corresponding image measured with a travelling microscope is then converted into a measure of the divergence.

The normalised emittance for a 20 mA beam at 18 keV was measured as

$$E_{nh} = 0.08 \pi \text{ mm mrad}$$

$$E_{nv} = 2.2 \pi \text{ mm mrad}$$

for the horizontal and vertical planes respectively (vertical being parallel to the anode slit). There was evidence of some misteering of the beam during these

measurements due to instability of the extraction power supply. The resultant vertical motion of the beam caused a smearing of the images especially when the slits were horizontal. The vertical emittance given is therefore a maximum and it is anticipated that a lower value will be obtained when the stability of the extraction power supply has been improved.

The maximum divergence of the beam was  $\pm 30$  mrad.

Calculations have been carried out using computer codes PLOT Ø3, which provides electric field distributions and WALSH 1, which gives the variation of beam radius with distance as it moves under the influence of accelerating fields, space charge and emittance. These show that a 2 cm diameter 50 mA beam with the above emittance and initial divergence will easily be transmitted by the 665 keV accelerator column.

#### ACCELERATOR COLUMN

Commissioned as a preinjector for the 70 MeV linac injector for Nimrod, the column operates at approximately  $15 \text{ kV cm}^{-1}$  and has successfully accelerated 200 mA pulsed beams of protons<sup>5)</sup>.

Figure 4 shows how the  $\text{H}^-$  ion source assembly will be mounted into the preinjector. An insulated diaphragm of source extraction potential is situated close to the cold box and helps to decouple the source from the main vacuum system. An orifice in the diaphragm allows the extracted beam to pass down the column. The source will be evacuated by a  $270 \text{ LS}^{-1}$  turbomolecular pump which will remove almost half the hydrogen emitted from the source. The preinjector column is evacuated by two  $1100 \text{ LS}^{-1}$  turbomolecular pumps. With an expected throughput down the column of  $0.09 \text{ TLS}^{-1}$  the pressure in the column varies between 1 and  $3 \times 10^{-4}$  torr at the ion source or high voltage end to  $9 \times 10^{-5}$  torr at the earthy end. The  $\text{H}^-$  beam will be partially stripped by the residual gas, the dominant process being single stripping to  $\text{H}^0$  with the release of a single electron. The greatest stripping will occur at the ion source end of the column and it has been calculated that an electron current of  $20 \mu\text{A}$  at an energy of 665 keV will be produced. These electrons will reach a quadrupole triplet situated at the earthy end of the column. A graphite sleeve is to be inserted on the inside bore of the triplet vacuum tube to prevent excessive X-ray levels being produced by the deflected electrons.

## DISCUSSION

An  $H^-$  ion source has been developed that will produce 30 mA of  $H^-$  ions at a 2.1% duty factor. Further work is necessary in order to reach the requirements of the SNS. The effect of different caesium coverage has not yet been fully investigated neither has maximum cooling been applied. It is expected that with further development the required output will be attained with the existing arc power levels.

The source is not easy to operate. It will on some occasions run up quickly to the desired levels, then on repeating the run with apparently identical parameters there is difficulty in reaching the correct mode of operation. In general however, recent runs have proved easier to control.

A new magnet assembly has been manufactured and is undergoing test prior to installation into the accelerator column. New power supplies are being manufactured and will permit local control as well as remote control via a light guide system.

It is expected that tests to accelerate an  $H^-$  beam to 665 keV will commence later this year.

## ACKNOWLEDGEMENTS

We wish to acknowledge the work of K Bellinger and G Allen for design and commissioning of source power supplies, P W Gregory and S Hancock for mechanical design and procurement, and Dr N D West for helpful discussions.

## REFERENCES

1. Hiskes J R and Schneider P J, 1980, Proc 2nd Symp Production and Neutralisation of Negative Hydrogen Ions and Beams, Brookhaven National Laboratory, 1980, p15.
2. Schmidt C W, 1980, above Symp, p189.
3. Gear P E and Sidlow R, 1980, Proc 2nd Int Conf Low-energy Ion Beams, Bath 1980: Inst Phys Conf Ser No 54, p284.
4. Bel'chenko Yu I and Dudnikov V G, Conf Interactions of Atomic Particles in Solid Bodies, Kharkov, 1976.
5. Fowler R G, Sidlow R and West N D, Rutherford Laboratory Report RL-76-070, 1976.

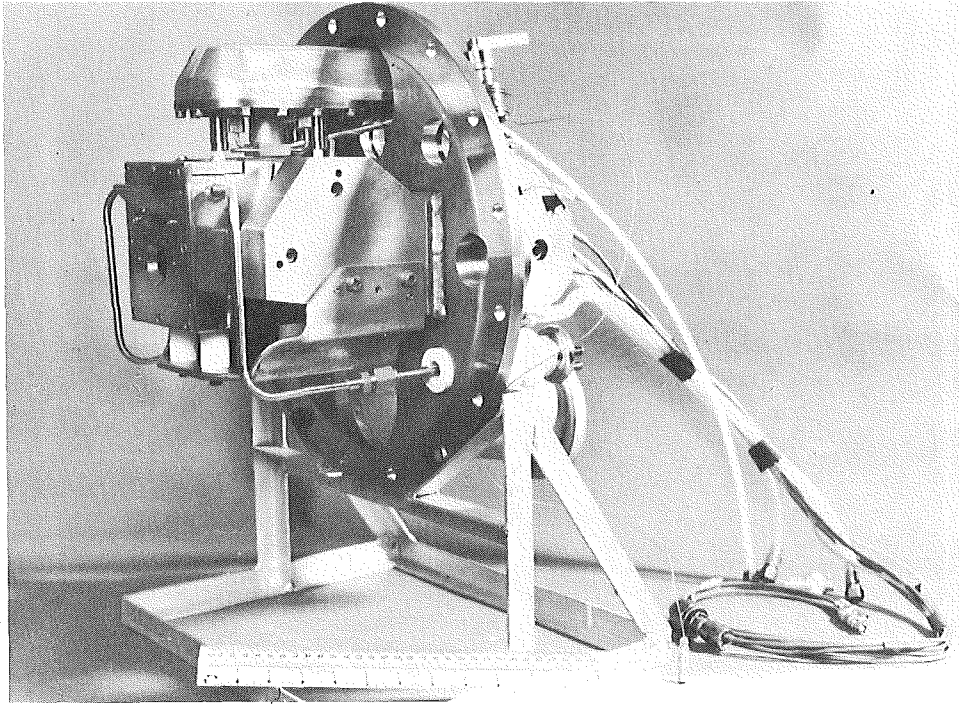


Figure 1. Ion Source Assembly

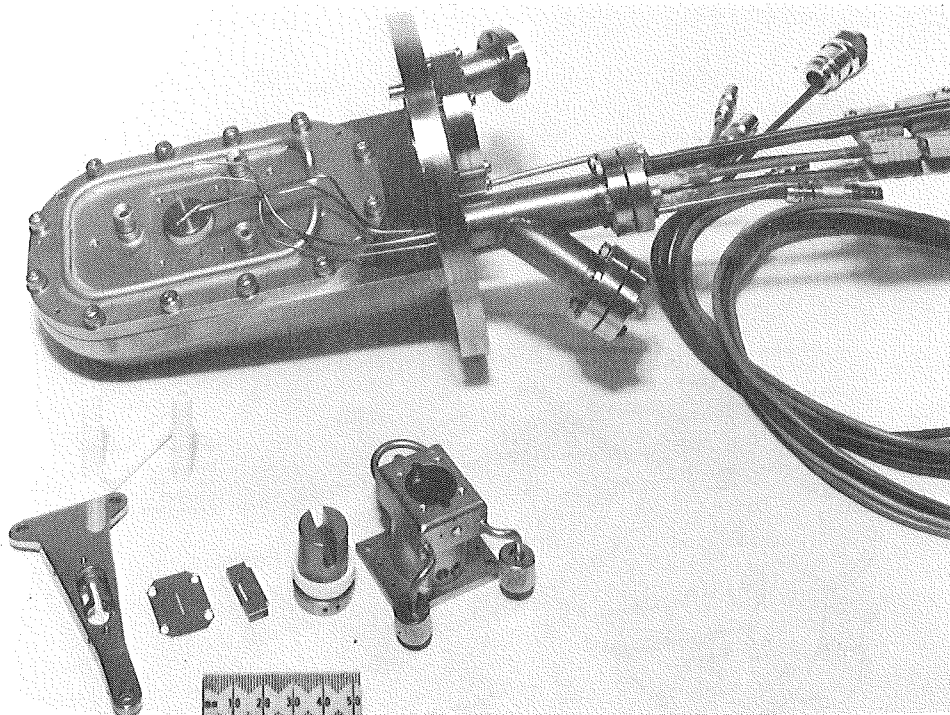


Figure 2. Discharge Chamber and Extractor Assembly

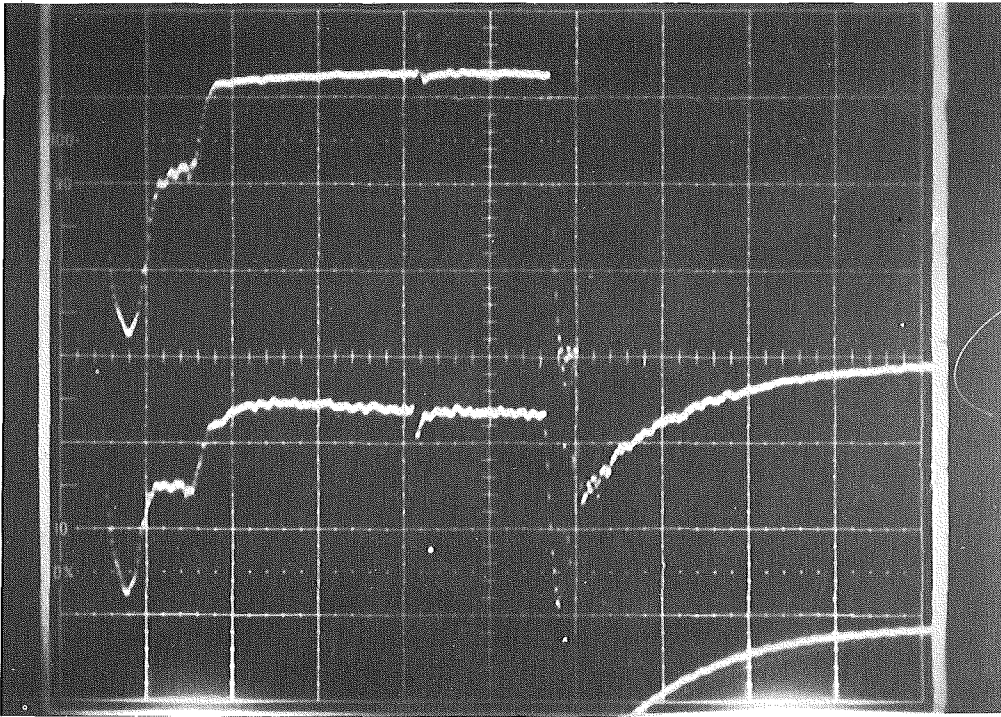


Figure 3. Top,  $H^-$  Ion Pulse  $10 \text{ mA div}^{-1}$   
Bottom, Extractor pulse  $50 \text{ mA div}^{-1}$   
Horizontal  $100 \mu\text{sec div}^{-1}$

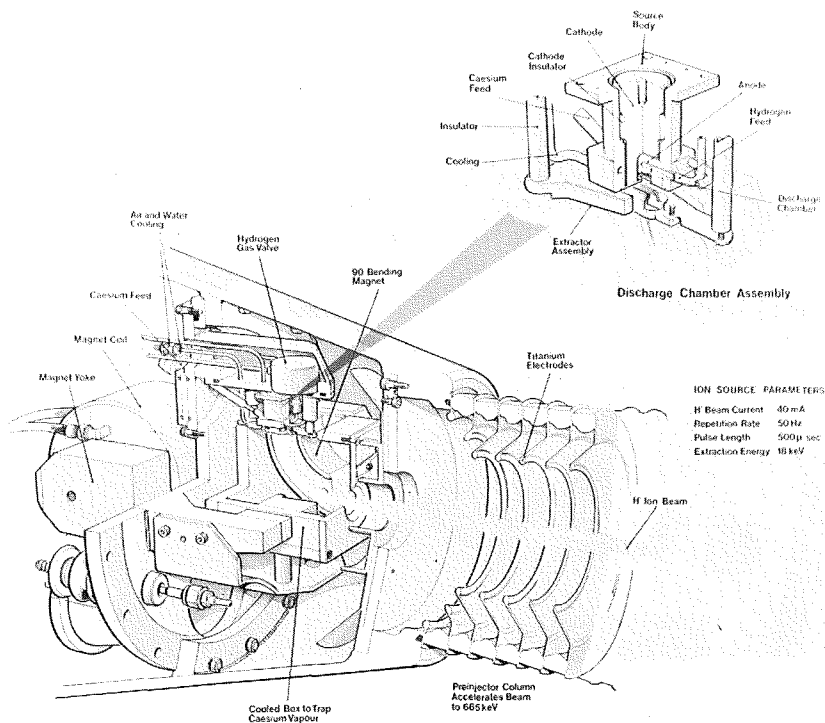


Figure 4. Ion Source and Accelerator Column

The control of  $\gamma_{tr}$  by sextupole magnets in IKOR

C.J.A. Corsten

Eindhoven University of Technology

Eindhoven, The Netherlands

Abstract

As IKOR is proposed to operate very close to transition energy the variation of  $\gamma_{tr}$  with momentum is of interest. Analytical expressions which describe the dependence of  $\gamma_{tr}$  on the momentum are derived.

Some of these expressions contain one or more terms which do not appear in for example a paper of Faugeras (ref.1). The approximations made in this theory may not be used for IKOR.

Sextupole strengths for the control of  $\gamma_{tr}$  are calculated analytically and are compared with numerical results obtained with the AGS program (refs. 2 and 3).

### Introduction

The idea to operate IKOR close to  $\gamma_{tr}$  has several advantages (see refs. 4 and 5). From the point of stability all protons in the beam should have values on one side of  $\gamma_{tr}$ . It is preferable to operate below  $\gamma_{tr}$  (ref.5). To optimize operation at highest intensity the lattice should ensure that  $\gamma_{tr}$  is independent of the radial position (= momentum). Furthermore, experiments at the CERN PS showed that it could be interesting to satisfy the condition  $(1/\gamma_{tr}^2 - 1/\gamma^2) = \text{constant}$  across the beam (see ref. 6). The compressor ring is planned to be operated at a value of 0.01 .

Sextupole magnets can be used to control the behaviour of  $\gamma_{tr}$  with momentum. Analytical formulas which describe this behaviour are derived in a same way as already done by Faugeras (ref.1). However, some of these relations are extended in this paper, which is necessary to use them for IKOR (see ref.7).

### Chromatic effects on $\gamma_{tr}$

Working at 'transition energy' means that the revolution frequency  $\omega$  of the particles do not depend on their momentum  $p$ :  $(d\omega/\omega)/(dp/p) = 0$ . In general the dependence of  $\omega$  on the momentum  $p$  consists of two contributions:

$$-\frac{d\omega/\omega}{dp/p} = \frac{dL/L}{dp/p} - \frac{d\beta/\beta}{dp/p} = \alpha - 1/\gamma^2 \quad (1)$$

where  $L$  is the orbit length,  $\beta=v/c$ ,  $\alpha$  is the momentum compaction factor and  $\gamma$  is the ratio of the total energy and the rest energy of the particle.

Assuming the reference particle with momentum  $p_0$  moving along the orbit  $L_0$ , the difference in orbit length due to a momentum deviation  $\Delta p$  can be written as

$$\frac{\Delta L}{L_0} = \alpha_1 \frac{\Delta p}{p_0} ( 1 + \alpha_2 \frac{\Delta p}{p_0} + \dots ) \quad (2)$$

Considering now the lengthening of the orbit with respect to the particle with momentum  $p_0 + \Delta p$ , one gets after some calculations (see ref. 7)

$$\frac{dL/L}{dp/p} \approx \alpha_1 ( 1 + ( 1 - \alpha_1 + 2\alpha_2 ) \frac{\Delta p}{p_0} ) \quad (3)$$

where we omitted terms of second degree in  $\Delta p/p_0$  and  $dp/p$ .

Because

$$\frac{dL/L}{dp/p} = \frac{1}{\gamma_{tr}^2} \quad (4)$$

we can write for the momentum dependence of  $\gamma_{tr}$

$$\gamma_{tr} = \gamma_{tr_0} ( 1 - (\alpha_2 - \frac{1}{2}\alpha_1 + \frac{1}{2}) \frac{\Delta p}{p_0} ) \quad (5)$$

$$\text{where } \gamma_{tr_0}^2 = \alpha_1^{-1} \quad (6)$$

In literature the term  $\alpha_1$  is often neglected in the r.h.s. of eq.(5).

As

$$\gamma \approx \gamma_0 ( 1 + \beta_0^2 \frac{\Delta p}{p_0} ) \quad (7)$$

where index "o" refers to the reference particle with momentum  $p_0$ , we get for the momentum dependence of the quantity  $( 1/\gamma_{tr}^2 - 1/\gamma^2 )$  :

$$\frac{1}{\gamma_{tr}^2} - \frac{1}{\gamma^2} = \left( \frac{1}{\gamma_{tr_o}^2} - \frac{1}{\gamma_o^2} \right) + \left( \frac{2\beta_o^2}{\gamma_o^2} + \frac{2\alpha_2^{-\alpha_1+1}}{\gamma_{tr}^2} \right) \frac{\Delta p}{p_o} \quad (8)$$

When the quantity  $\alpha_2$  is known eqs.(5) and (8) give the relevant behaviour with momentum.

The quantity  $\alpha_2$

In this section we have to find an analytical expression for the quantity  $\alpha_2$ , which is defined in eq.(2). The change in length of the closed orbit of a particle with a momentum deviation is given by (ref.1)

$$\Delta L = \left( \int_0^{L_o} \frac{\eta_1}{\rho} ds \right) \frac{\Delta p}{p_o} + \left( \int_0^{L_o} \left( \frac{\eta_2}{\rho} + \frac{1}{2} \left( \frac{d\eta_1}{ds} \right)^2 \right) ds \right) \left( \frac{\Delta p}{p_o} \right)^2 \quad (9)$$

where  $\rho$  is the radius of curvature in the bending magnets. The radial position due to a momentum error is defined by

$$x = \eta_1 \frac{\Delta p}{p_o} + \eta_2 \left( \frac{\Delta p}{p_o} \right)^2 + \dots \quad (10)$$

The quantities  $\eta_1$  and  $\eta_2$  are determined and the quantity  $\alpha_1$  can be written as

$$\alpha_1 = \frac{1}{L_o} \int_0^{L_o} \left( \frac{\eta_1}{\rho} \right) ds = \frac{Q^3}{R} \sum_n \frac{F_n^{(1)} F_n^{(1)}}{Q^2 - n^2} \quad (11)$$

with

$$F_n^{(1)} = \frac{\beta_x^{3/2}}{\rho} = \sum_n F_n^{(1)} e^{in\phi} \quad \text{and} \quad d\phi = \frac{ds}{Q\beta_x}$$

R is the 'mean radius' of the machine ( $=L/2\pi$ ), Q is the horizontal tune and  $\beta_x$  is the horizontal amplitude function. For the quantity  $\alpha_2$  we find (ref.7),

$$\alpha_2 = -1 + \frac{Q^3}{\alpha_1 R} \sum_n \frac{F_n^{(1)} F_n^{(2)}}{Q^2 - n^2} + \frac{1}{2\alpha_1 L_o} \int_0^{L_o} \left( \frac{d\eta_1}{ds} \right)^2 ds \quad (12)$$

with

$$F_n^{(2)} = \beta_x^{3/2} \frac{B'}{B_o \rho} \eta_1 - \frac{1}{2} \beta_x^{3/2} \frac{B''}{B_o \rho} \eta_1^2 + \frac{\beta_x^{3/2}}{\rho^2} \eta_1 + \frac{1}{2} \frac{\beta_x^{3/2}}{\rho} \left( \frac{d\eta_1}{ds} \right)^2 - \frac{\beta_x^{3/2}}{\rho^3} \eta_1^2 = \sum_n F_n^{(2)} e^{in\phi} \quad (13)$$

The last three terms in this equation for  $F_n^{(2)}$  are of the second or higher degree in  $1/\rho$  and can therefore be neglected for very large machines. In the theory of Faugeras for example (ref.1) these third, fourth and fifth term in the r.h.s. of eq.(13) do not appear. However, since the bending radius is not so large for IKOR all terms of eq(13) have to be taken into account in order to determine  $\alpha_2$ .

Furthermore

$B' = (\partial B_x / \partial x)$  represents the strengths of the quadrupole magnet and  $B'' = (\partial^2 B / \partial x^2)$  represents the sextupole strength.

The influence of a sextupole magnet with strength  $B''$  on  $\gamma_{tr}$  now becomes quite clear from the eqs. (5), (12) and (13). It appears that a sextupole magnet at a position with a large horizontal amplitude function  $\beta_x$  has a maximum influence on the quantity  $\alpha_2$ .

The results obtained from these analytical formulas will be compared with numerical results in the next paragraph.

Calculations for IKOR. Comparison with AGS results (see refs. 2 and 3)

We will illustrate the influence of sextupole magnets on  $\gamma_{tr}$  for IKOR. A list of the needed data of this ring is given in table 1. For controlling  $\gamma_{tr}$  it is planned to use a sextupole magnet of 40 cm length in each cell, placed between the quadrupoles QF and QD1 (see fig.1 and ref.2)

$\gamma_o$	= 2.172	Q	= 3.25
$\beta_o^2$	= 0.788	R	= 32.18 m
$\gamma_{tr_o}$	= 2.224	$B_o$	= 1.3 T
$\alpha_1$	= 0.202	$\rho$	= 4.64 m

Table 1. Relevant data of IKOR

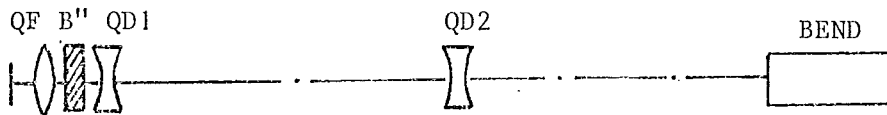


Figure 1. Unit cell of IKOR with position of sextupole magnet B'' (periodicity of the machine N=11).

The Fouriercomponents needed for the calculation of  $\alpha_2$  are given in ref.7. The 'wiggling factor'  $(1/2\alpha_1 L_o) \int (dn_1/ds)^2 ds$  is computed using a matrixcode (see also ref.7). For IKOR the value is 0.35 and for the quantity  $\alpha_2$  we finally get(see ref.7):

$$\alpha_2 = 1.8 - 2.6 B'' \tag{14}$$

The behaviour of  $\gamma_{tr}$  for a particle with a relative momentum deviation  $\Delta p/p_o = 0.01$ , is given in fig.2 as a function of the sextupole strength  $B''$ . The result is compared with the result from AGS computations done by Reich (ref.2) and Faugas (ref.3)

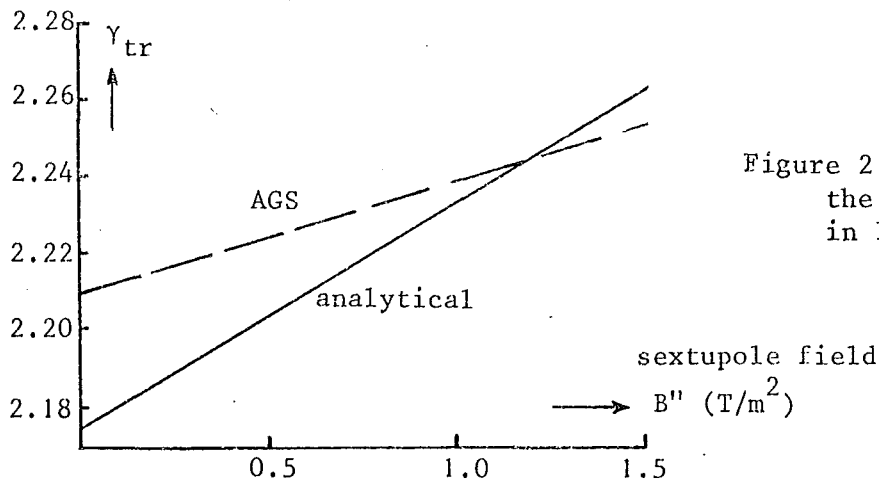


Figure 2.  $\gamma_{tr}$  versus the sextupole strength in IKOR for  $\Delta p/p_o = 0.01$

As mentioned before, it could be interesting to satisfy the relation  $(1/\gamma_{tr}^2 - 1/\gamma^2) = \text{constant}$ . The variation of this quantity as a function of the sextupole strength is shown in fig. 3 for a particle with  $\Delta p/p_0 = 0.01$

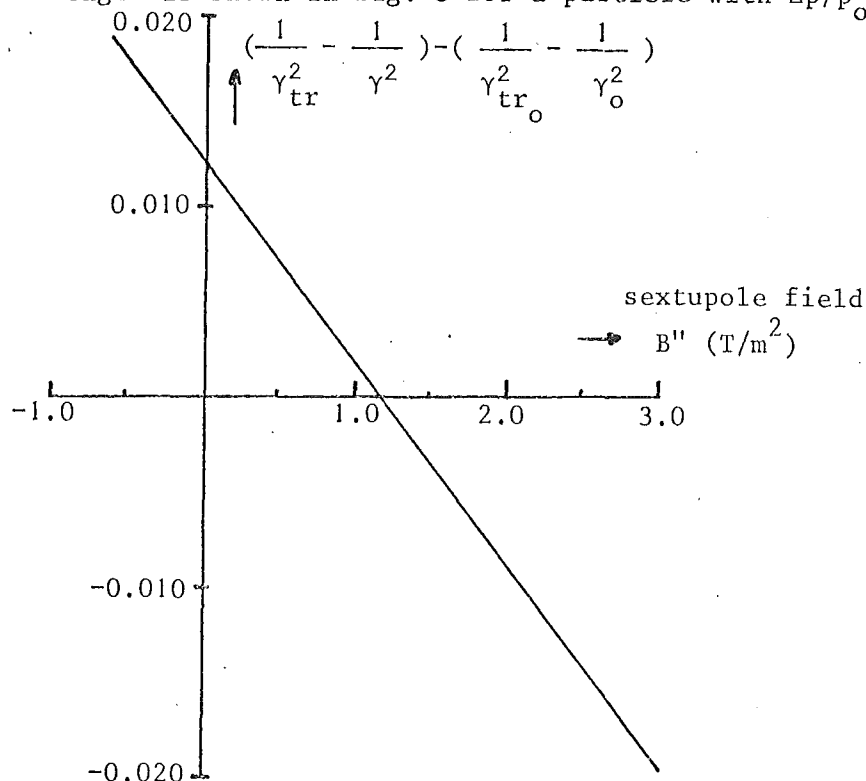


Figure 3.  $(1/\gamma_{tr}^2 - 1/\gamma^2)$  versus the sextupole strength in IKOR for  $\Delta p/p_0 = 0.01$  (analytical calculations)

From this figure we see that a sextupole strength  $B'' = 1.16 \text{ T/m}^2$  is required in order to keep  $(1/\gamma_{tr}^2 - 1/\gamma^2) = \text{constant}$ . This value is in good agreement with the value obtained from the AGS program by Reich (see ref.2):  $B'' = 1.2 \text{ T/m}^2$ .

#### Concluding remarks

The variation of  $\gamma_{tr}$  with momentum is deduced analytically. The existing theory is extended in order to get 'good' results for IKOR. The influence of the sextupole strength on  $\gamma_{tr}$  calculated from the analytical formulas differs somewhat from results obtained by the AGS program. In near future we will look for the source of this discrepancy.

Acknowledgements. I would like to thank dr. Reich and dr. Faugeras for their helpful communications and their AGS computations.

#### References

1. P.Faugeras et al., Second order effects in the sextupole-corrected SPS lattice. IEEE NS-26 (1979) p3577.
2. K.H.Reich, Some considerations on the correction elements for the SNQ Compressor Ring private communication
3. P.Faugeras, private communication.
4. K.H.Reich, Proton beam dynamics in the SNQ Compressor Ring including collective effects and implications for the reference design (1980) private communication

5. H.Fischer and K.H.Reich, Notes on the meeting with H.G.Hereward on 5th February, 1980, at the KfK Karlsruhe private communication
6. R.Cappi et al. PS beam measurements at flat-top fields near transition energy. IEEE NS-28 (June 1981) p2389.
7. C.J.A.Corsten, Control of  $\gamma$  by using sextupoles for the SNQ Compressor Ring. private communication

WORKSHOP SUMMARY

A. Citron  
Kernforschungszentrum Karlsruhe GmbH  
Postfach 3640  
7500 Karlsruhe 1  
Federal Republic of Germany

From a conference summary you expect perhaps an overview by somebody, who is far above all the topics treated and distributes praise in an impartial way. I am afraid that I am, by no means, such a person. On the contrary, I am involved in one of the projects presented, namely the German Spallation Source and I cannot help wondering, when listening to the various contributions, what relevance they could have for this project.

Some contributions, namely those on linear accelerators were dealing directly with comparable machines. Here it is gratifying to see the progress made on existing machines, such as LAMPF and the confidence that some groups have in extrapolating to very high current machines, such as the Canadian project. It shows at least that other groups are even more optimistic on the prospect of handling high average currents.

Quite a number of contributions were dealing with circular machines or accumulator rings. Here, many problems are in common, e.g. the 'beam stacking' and the 'fast ejection'. It is fortunate that the time schedule on several of these devices are such that the validity of the solutions proposed will have been proved by

the time, where the German Spallation Source will have to freeze its design of the accumulator ring. So we will be able to profit from other people's experience for this crowning piece of our installation.

Finally I should mention the contribution on the induction linac. This is clearly a very interesting proposal, but which needs considerable development before it can be compared seriously to the accelerator types just mentioned. It gave rise at the conference dinner to a lively discussion on the ethics of accelerator building. Some had the view that accelerator builders should mainly serve the community of prospective users, whereas others thought their prime duty was the advancement of new methods and technologies. Needless to say that no agreement could be reached. So I propose it as a suitable topic for the common lunch, which is now waiting for us.



List of Participants

1.	N. Angert	GSI	Darmstadt
2.	J. Bedau	Bruker Physik	Karlsruhe
3.	K. Blasche	GSI	Darmstadt
4.	D. Böhne	GSI	Darmstadt
5.	E. Boltezar	CERN	Genf
6.	K. Bongardt	KfK	Karlsruhe
7.	B. Chidley	CRNL	Chalk River
8.	Y. Cho	ANL	Argonne
9.	A. Citron	KfK	Karlsruhe
10.	R.K. Cooper	LANL	Los Alamos
11.	C.J.A. Corsten	Univ.	Eindhoven
12.	G. Dammertz	KfK	Karlsruhe
13.	H. Deyda	BMFT	Bonn
14.	S. Fukumoto	KEK	Tsukuba
15.	P.E. Gear	Rutherford	Chilton
16.	K. Goebel	CERN	Genf
17.	P. Grand	BNL	Brookhaven
18.	D.A. Gray	Rutherford	Chilton
19.	H. Hecker	KFA	Jülich
20.	J. Heil	BMFT	Bonn
21.	H.G. Hereward	Univ.	Dorchester
22.	R. Hietschold	KfK	Karlsruhe
23.	G. Hochschild	KfK	Karlsruhe
24.	A.J. Jason	LANL	Los Alamos
25.	W.E. Jule	NEN	Billerica
26.	W. Karbstein	KfK	Karlsruhe
27.	D. Keefe	LBL	Berkeley
28.	J. Klabunde	GSI	Darmstadt
29.	W. Klose	KfK	Karlsruhe
30.	W. Knobbe	Fa. Herfurth	Hamburg
31.	W. Köhler	KfK	Karlsruhe
32.	M. Korschinek	TU	München
33.	W. Kühn	KfK	Karlsruhe
34.	M. Kuntze	KfK	Karlsruhe
35.	R. Lehm	KfK	Karlsruhe
36.	R. Lehmann	KfK	Karlsruhe
37.	R.J. Macek	LANL	Los Alamos

38.	K. Mittag	KfK	Karlsruhe
39.	K.R. Müller	KfK	Karlsruhe
40.	H. Nöldge	Fa. Herfurth	Hamburg
41.	M. Olivo	SIN	Villigen
42.	B. Piosczyk	KfK	Karlsruhe
43.	C.W. Planner	Rutherford	Chilton
44.	W. Porschen	KFA	Jülich
45.	C.W. Potts	ANL	Argonne
46.	H. Prange	GSI	Darmstadt
47.	V.T. Pugh	Rutherford	Chilton
48.	K.H. Reich	CERN	Genf
49.	G. zu Putlitz	GSI	Darmstadt
50.	G.H. Rees	Rutherford	Chilton
51.	M. Reiser	Univ.	Maryland
52.	G. Schaffer	KfK	Karlsruhe
53.	U. Schmidt-Rohr	MPI	Heidelberg
54.	D. Schulze	KfK	Karlsruhe
55.	H. Schweickert	KfK	Karlsruhe
56.	H. Sebening	KfK	Karlsruhe
57.	L. Stanco	KFA	Jülich
58.	P. Strehl	GSI	Darmstadt
59.	H. Uhlhorn	BMFT	Bonn
60.	J.E. Vetter	KfK	Karlsruhe
61.	D.J. Warner	CERN	Genf
62.	G. Wüstefeld	KFA	Jülich